Fen Bilimleri & Matematikte

Güncel Araştırmalar

Academic Studies in

Science and Mathematics

EDİTÖRLER /EDITORS

Prof. Dr. Alpaslan DAYANGAÇ
Prof. Dr. Hasan AKGÜL
Doç. Dr. Zafer ÖZOMAY
Dr. Öğr. Üyesi Meral ÖZOMAY

gece kitaplığı

İmtiyaz Sahibi / Publisher • Yaşar Hız
Genel Yayın Yönetmeni / Editor in Chief • Eda Altunel
Kapak & İç Tasarım / Cover & Interior Design • Gece Kitaplığı
Editörler / Edıtors •Prof. Dr. Alpaslan DAYANGAÇ
Prof. Dr. Hasan AKGÜL
Doç. Dr. Zafer ÖZOMAY
Dr. Öğr. Üyesi Meral ÖZOMAY
Birinci Basım / First Edition • © Haziran 2023
ISBN • 978-625-430-853-6

Gece Kitaplığı / Gece Publishing
Türkiye Adres / Turkey Address: Kızılay Mah. Fevzi Çakmak 1. Sokak Ümit Apt. No: 22/A Çankaya / Ankara / TR
Telefon / Phone: +90 312 384 80 40
web: www.gecekitapligi.com
e-mail: gecekitapligi@gmail.com

Baskı & Cilt / Printing & Volume
Sertifika / Certificate No: 47083

Fen Bilimleri & Matematikte Güncel Araştırmalar

Academic Studies in Science and Mathematics

Haziran 2023 / 2023 June

Editörler

Prof. Dr. Alpaslan DAYANGAÇ
Prof. Dr. Hasan AKGÜL
Doç. Dr. Zafer ÖZOMAY
Dr. Öğr. Üyesi Meral ÖZOMAY

İÇİNDEKİLER

BÖLÜM 1

CHAPTER 1

BİTKİ BİYOÇEŞİTLİLİĞİNİN DNA TABANLI TANIMLAMA SİSTEMİ İLE KORUNMASI

Asiye ULUĞ[1]

1 Dr. Öğr. Üyesi Kafkas üniversitesi, Fen Edebiyat Fakültesi, Biyoloji Bölümü ORCID ID: https://orcid.org/0000-0001-5524-8431

1. Bitki biyoçeşitliliği

Ekosistemlerin dengeli bir şekilde işleyişi tür zenginliği, tür bileşimi, genetik çeşitlilik ve türler arasındaki fonksiyonel ilişkilere bağlıdır. Bu yüzden, biyoçeşitlilikteki mevcut değişiklikler ekosistemlerin işleyişinde de değişikliklere yol açmaktadır. Ekosistemleri dengede tutarak yaşanabilir hale getiren biyoçeşitlilik, artan dünya nüfusunun beraberinde getirdiği kirlilik, habitat kaybı, avlanma, iklim değişikliği ve doğal afetler gibi stres faktörleri nedeniyle günden güne azalmaktadır. Bir ekosistemde yaşayan herhangi bir türün neslinin tükenmesi, canlıların beslenme ilişkilerini, madde döngülerinin sürdürülebilirliğini, doğal kaynakların kullanımını ve yenilenebilirliğini de önemli ölçüde etkilemektedir.

Doğal bitki kaynaklarını korumak; tozlaşma, besin geri dönüşümü, gıda ve orman ürünleri gibi canlılığın devamını sağlayan temel ekosistem hizmetlerini sağlamak adına kritik öneme sahiptir. Biyoçeşitliliği şekillendiren türler ve bu türlere ait popülasyonları korumak için popülasyonlarda meydana gelen değişikliklerin ekolojik ve moleküler düzeyde izlenmesi gerekmektedir. Küresel ısınmanın eşlik ettiği yüksek çevresel baskı, özellikle artan buharlaşma oranı ve yüksek irtifalarda sert iklim koşulları nedeniyle kendilerini stabil olmayan ekosistemlerde bulunan türlerin değişen çevre koşullarına karşı evrimsel potansiyel sağlayan genetik çeşitliliklerinin açığa çıkarılması ve korunması gerekmektedir (Dobson, 1997a; Khan vd., 2013). Uluslararası Doğanın Korunması Birliği (IUCN) ve Kırmızı Liste kategorileri (IUCN Red List of Threatened Species, 2022) başta endemik türler olmak üzere türlerin dağılımı ve popülasyon durumunu değerlendirmek için envanterlerin çıkarılması gerekliliğini vurgulamıştır (BakshComeau vd., 2016). IUCN kriterlerine göre son derece nadir, tehlikede veya kritik derecede tehlikede olan endemik türlerin moleküler tanımlamasının yapılarak bu endemik türlerin evrimsel ilişkilerinin açığa çıkarılması ve popülasyonlarının korunması için gerekli bilimsel çalışmaların yapılması ülkelerin biyoçeşitliliğini korumak açısından büyük önem arz etmektedir.

2. DNA barkodlama ve biyoçeşitliliğin korunması

Biyoçeşitliliğin korunması için yapılan taksonomik değerlendirmeler, popülasyon büyüklüğünün ve floranın dağılımının belirlenmesi moleküler çalışmalardan önce, genellikle herbaryumlar tarafından geliştirilen morfolojik tanımlayıcıların değerlendirmesine dayanıyordu (Godfray, 2002; Li vd., 2015). Mevcut örnekler karmaşık bir cinse aitse veya alt türleri içeriyorsa, morfolojik belirteçlerle doğru tür tanımlama yapmak mümkün olmamaktadır (Ortega vd., 2007). Bir türün doğru tanımlanması ve genetik kaynaklarının analizi biyolojik çeşitliliğin korunması ve sürdürülebilir kullanımı için önem arz etmektedir. Son yirmi yıldır klasik morfoloji ve fizyolojinin yanı sıra filogenetik çalışmalarla genetik çeşitlilik değerlendirme

stratejileri geliştirilmektedir. Morfolojik taksonomi için tamamlayıcı bir yöntem olarak, her tür için spesifik olan kısa ve standartlaştırılmış evrensel DNA gen bölgeleri (rbc*L*, mat*K*, trn*H*-psb*A*, nrDNA ITS DNA) kullanılarak yapılan DNA barkodlama; tür tanımlama ve keşfi için etkili bir yöntem haline gelmiştir (Hebert vd., 2003; Barrett ve Hebert, 2005; Hollingsworth, 2011). Tür tanımlamasının yanı sıra, DNA barkodlama ve genomik yaklaşımlar yeni taksonların tespiti (Bell vd., 2012), türlerin korunması ve bitki ekolojisine yönelik çalışmalarda dahil olmak üzere biyoçeşitlilik araştırmalarında kullanılmaktadır (Savolainen ve Karhu, 2000; Hollingsworth, 2008; Hosein vd., 2017). Bir türün yayılımının doğru bir şekilde sınırlandırılması ve tanımlanması, genetik çeşitlilik analizi için önem arz etmektedir. Herbaryumlarda muhafaza edilen tanımlanmış materyaller, bitki florası için DNA barkod kütüphanesi oluşturmak adına referans olarak kullanılabilir zengin bir kaynak sağlamaktadır. Bitki biyoçeşitlilik analizi ve DNA barkod kitaplığı oluşturmak için herbaryum koleksiyouna dayalı bitki evrimsel genetiği ve genomik çalışmaları dünya çapında yürütülmektedir. Ülke florası için DNA barkod kütüphaneleri oluşturmak ve bu verileri kullanılabilir hale getirmek biyoçeşitliliği daha iyi anlamak, korumak ve kullanmak için önemli bir role sahiptir.

3. DNA barkodlama metodolojisi

DNA barkodlama, kısa, standardize edilmiş DNA fragmentlerini kullanarak canlı bir organizmayı moleküler olarak tanımlama yöntemidir. İnsandaki parmak izine benzer şekilde, her türün de kendine ait bir DNA barkodu bulunmaktadır. DNA barkodlama araştırması için kullanılan teknolojiler büyümeye ve gelişmeye devam ederken, temel metodoloji değişmeden kalmıştır. Barkodlama için gerekli olan DNA bitkinin yaprak, meyve, kök, tohum gibi herhangi bir dokusundan alınacak küçük bir parça numuneden izole edilir. Genellikle yaprak örneklerinden DNA izolasyonu, bitkilerde standart olarak kullanılan CTAB (Cetyl Trimethyl Ammonium Bromide) (Doyle, 1991) metodu ile başarılı bir şekilde gerçekleştirilmektedir. Standartlaştırılmış evrensel DNA barkodları tasarlanan uygun primerler ile polimeraz zincir reaksiyonu (PCR) kullanılarak çoğaltılır. Hızlı evrimleşme özelliği, küçük boyutu ve her hücrede yüksek oranda kopya sayısı içermesi sebebiyle filogenenetik çalışmalarda yaygın olarak kullanılan 26S rDNA (ribozomal DNA) gen dizisi (Kuzoff vd., 1998) çalışılacak türlerin yakın akrabalarıyla aralarında gerçekleşen genetik yapı değişimlerinin belirlenmesi amacıyla kullanılmaktadır. Yaşam Barkodu Konsorsiyumu (The Consortium for the Barcode of Life (CBOL)) (2009), bitki sistematiği çalışmalarında tür ve cins ayırımı için evrensel olmaları, kolay amplifiye edilebilmeleri ve yüksek oranda değişim göstermelerinden dolayı temel barkod bölgeleri olarak kloroplast DNA'sından *rbc*L (ribuloz 1,5 bisfosfat büyük alt birimi) ve *mat*K (Maturase K)'ya ek olarak intergenik

dizi trn*H*-psb*A* ve nükleer ribozomal ITS1 ve ITS2 (Internal Transcribed Spacer) gen bölgelerini belirlemiştir (Tablo 1). mat*K*, kloroplast lizin tRNA (trn*K*) genindeki intron bölgesinde tek kopya olarak bulunan, 1500bç uzunluğunda sistematik ve evrimsel botanik çalışmalarında yaygın olarak kullanılan gen bölgelerinden biridir (Kang vd., 2017). Kloroplast kökenli barkodlama bölgeleri arasında en hızlı değişim gösteren bölgedir (Chase vd., 2007). Ribulose-1,5-bis-phosphate carboxylase / oxygenase (RuBisCO)genini kodlayan kloroplast kökenli rbc*L* geni cins üstü taksonomik seviyelerdeki filogenetik çalışmalar için yaygın bir şekilde kullanılmaktadır (Li vd., 2015). Kloroplast DNA'sında trn*H* ve psb*A* genleri arasında kalan bölge hem psb*A* geninin transkripsiyon sonrası regülasyonu için önemli 3'UTR bölgesini hem de kodlanmayan trn*H*-psb*A* intergenik boşluk bölgesini içermektedir. Bu bölge trn*H*-psb*A* dizisinin evrensel primerler olarak tasarlanmasını kolaylaştırır. Bitkilerde birçok grupta yüksek oranda çeşitlilik içerdiği için filogenetik çalışmalarda rbc*L* bölgesi ile birlikte kullanıldığında cins ve tür bazında yüksek oranda ayırım gücüne sahiptir (Kress ve Erickson., 2007; Dong vd., 2012). Yüksek kopya sayısına sahip nükleer ribozomal ITS bölgesi ise; ITS1, ITS2 ve 5.8 S'yi bölgelerini içermektedir ve karasal bitki türlerini cins düzeyinde ayırma gücüne sahiptir (Chase vd., 2007; Kang vd., 2017). ITS bölgesi farklı bitki gruplarının evrimsel ve sistematik çalışmalarında en çok kullanılan DNA barkod bölgesi olmasının yanı sıra plastid DNA barkod bölgeleri ile karşılaştırıldığında türler arası ayrım yapma gücü daha fazladır (Alvarez, 2003). ITS2 bölgesi, tür ve familya seviyesindeki filogenetik çalışmalarda yüksek oranda ayrım yapma gücüne sahiptir (Alvarez, 2003; Bailey, 2003).

Tablo 1 *DNA tabanlı tanılama sistemi için evrensel olarak kullanılan DNA barkod bölgeleri*

Barkod primer	Primer sekansı	Primer yönü	Ürün uzunluğu (bç)	Referans
26S rDNA	TTCCCAAACAACCCGACTC GCCGTCCGAATTGTAGTCTG	İleri Geri	704	Alvarez ve Wendel (2003)
rbcL	ATGTCACCACAAACAGAGACTAAAGC GTAAAATCAAGTCCACCRCG	İleri Geri	704	CBOL Bitki Çalışma Grubu (2009)
matK	CGTACAGTACTTTTGTGTTTACGAG ACCCAGTCCATCTGGAAATCTTGGTTC	İleri Geri	794	CBOL Bitki Çalışma Grubu (2009)
trnH-psbA	CGCGCATGGTGGATTCACAATCC GTTATGCATGAACGTAATGCTC	İleri Geri	340-600	Hebert vd. (2003)
ITS4 **ITS3**	TCCTCCGCTTATTGATATGC GCATCGATGAAGAACGCAGC	Geri İleri	310	White vd. (1990)
ITS2	GCTGCGTTCTTCATCGATGC	Geri	208	White vd. (1990)
ITS5	GGAAGTAAAAGTCGTAACAAGG	İleri		White vd. (1990)

PCR da barkod bölgeleri amplifiye edildikten sonra Sanger Dizileme gibi yeni nesil dizileme metotları kullanılarak ilgili DNA bölgelerinin nükleotid dizileri elde edilir. Elde edilen diziler NCBI Genbak ve Barcode of Life gibi veri tabanlarında depolanan DNA referans kütüphanesindeki verilerle karşılaştırılarak bitkilerin familya, cins ve tür bazında tanımlamaları yapılmaktadır. Ayrıca genetik barkodlaması yapılan bitki türlerinin veri tabanında bulunan yakın türlerle olan filogenetik ilişkileri de barkod sekansları kullanılarak açığa çıkarılmaktadır.

4. Dünyada yapılan bitki DNA barkodlama çalışmaları

DNA Barkodlama yöntemi ile biyoçeşitliliğin ve genetik kaynakların çeşitliliğinin açığa çıkarılması ve korunması alanında dünya çapında önemli çalışmalar yapılmaktadır. Ülkeler DNA barkodlama yoluyla az miktarda bitki dokusu kullanarak biyolojik çeşitliliklerine katkı sağlayan bitki ve hayvanlara moleküler kimlik vererek kendi ülkelerine ait olduğu bilgisini ülke envanterlerine ve literatüre eklemekte ve sahip olduğu genetik kaynaklar ve gen havuzu üzerinde hak sahibi olmaktadır. Hashim vd.

(2021) Sina yarımadasına endemik olan dokuz medikal bitkinin her birine 19 genetik barkod vermişlerdir. Hosein vd. (2017) Atlantik Okyanusu ve Karayip Denizi'ndeki adalarda bulunan tehdit altındaki 14 endemik bitki türünü barkodlamışlardır. Srivastava ve Manjunath (2020) 35 orkide türünü genetik barkod vererek tanımlamışlardır. Mishra vd. (2017) barkodlama çalışmasını Hindistan'da tehdit altındaki *Decalepis* türlerini korumak için yapmışlardır. Chen vd. (2022) Çinde yayılış gösteren tıbbi açıdan önemli kullanım alanlarına sahip 21 *Fritillaria* türünün tüm kloroplast genomunu barkodlamışlardır. Uluslararası Yaşam Barkodu Projesi (IBOL, International Barcode of Life) (The International Barcode of Life Consortium, 2022), ulusal ve uluslararası biyoçeşitliliğin keşfini ve korunmasını destekleyen önemli kuruluşların önde gelen araştırmacılarından ve temsilcilerinden oluşan bir platformdur. Projenin amacı kapsamlı bir biyoçeşitlilik envanteri oluşturmak ve biyo-gözetim kapasitesini geliştirerek ekonomik, sosyal veya çevresel açıdan önemli türler için bir tanımlama sistemi ve tüm yaşam için barkod referans kitaplığı oluşturmaktır. Yaşam Barkodu Konsorsiyomu Bitki Çalışma Grubu (The Consortium for the Barcode of Life (CBOL) Plant Working Group) (2009), 550 bitki türünü temsil eden 907 örneği yedi DNA barkod bölgesi ile çalışmışlardır. Ülkemizin de içerisinde yer aldığı, 47 ülkenin üye olduğu, araştırma alanı DNA barkodlama olan veya bunu destekleyen araştırmacı ve organizasyonların oluşturduğu uluslarası bir ağ olan IBOL, bilinen türleri tanımlamak ve yenilerini keşfetmek için, standartlaştırılmış gen bölgelerindeki dizi çeşitliliğini kullanarak, coğrafi ve taksonomik kapsamda detaylı bir barkod referans kitaplığı oluşturmaktadır. Elde edilen barkod kayıtları, uluslararası erişime açık olan Barcode of Life Veri Sistemleri (BOLD) tabanında depolanmaktadır. Bu veri tabanında çalışılan türlere ait lokalite bilgileri, morfolojik görüntüleri, DNA barkod dizileri gibi çok sayıda bilgiye ulaşılmaktadır. DNA barkod veri tabanları kullanılarak morfolojik tanımlamalarında zorluk yaşanan türler veya alttürler kısa sürede ve etkin bir şekilde tanımlanabilmektedir.

5. Türkiye'de yapılan bitki DNA barkodlama çalışmaları

Ülkemizde tatlı su balıkları üzerinde gerçekleştirilen DNA barkodlama çalışmaları dışında barkodlama alanında yeterli sayıda çalışma bulunmamaktadır (Keskin ve Atar, 2013a,b). Bitkilerde barkodlama çalışmaları dünyada yaklaşık 15 yıldır gerçekleştirilmesine rağmen, ülkemizde bir kaç çalışma dışında kapsamlı bir çalışma bulunmamaktadır (Çabuk Şahin, 2016; Dönmez vd., 2017; İnal ve Karaca, 2019; Hürkan, 2020; Şapçı Selamoğlu, 2022). Tarımsal Araştırmalar ve Politikalar Genel Müdürlüğü'nün (TAGEM) desteklediği Türkiye Tohum Gen Bankası' nın 2017' de başlattığı "Ulusal DNA Barkodlama Projesi" kapsamında; başta endemik türlerimiz olmak üzere, genetik kaynaklarımız moleküler düzeyde karakterize edilip "BarkodTürk" adı verilen veri tabanında kayıt altına alınmaya

başlanmıştır. Veri tabanına aktarılan bilgiler, uluslararası veri tabanlarındaki verilerle karşılaştırılarak, ülkemize özgü genetik kaynakların doğru bir şekilde tespit edilip biyokaçakçılık ile etkin bir şekilde mücadele edilmesine katkı sağlayacaktır.

6. Türkiye'de ki bitki çeşitliliğini korumak

Türkiye; Akdeniz, İran-Turan ve Avrupa-Sibirya floristik bölgelerini içermesi nedeniyle bitki örtüsü bakımından dünyanın en zengin ülkelerinden biridir (Davis, 1988). Ülkemizin yedi bölgesinde görülen iklim farklılıkları, topoğrafik, jeolojik ve jeomorfolojik çeşitlilik, deniz, göl ve akarsu gibi su ekosistem çeşitliliği zengin bir floraya sahip olmamıza katkı sağlamaktadır (Güneş ve Özba 2014). Türkiye, yaklaşık on binden fazla bitki türü ile floristik zenginliği en fazla olan ülkelerden biri olmasının yanı sıra sahip olduğu türlerin 3035'inin endemik olmasıyla da çok önemli bir biyoçeşitlilik merkezidir (Yılmaz, 2012). Türkiyede doğa korumada öncelikli alanlar olarak uluslararası Önemli Bitki Alanları (ÖBA) kriterleri ile belirlenen 144 ÖBA bulunmaktadır (Özhatay vd., 2005; Özhatay, 2006).

Ülkemizde yayılış gösteren başta endemik bitki türleri olmak üzere biyoçeşitliliğe katkı sağlayan bitki türlerine genetik barkod ile moleküler kimlik verilmesi ve bu türlerin korunma durumlarının belirlenerek yerinde korunmaya alınması için çalışmaların yapılması gerekmektedir. DNA tabanlı tanımlama sistemi ile elde edilecek genetik veriler küresel ısınma ve küresel kıtlık konularının ülke gündemlerini meşgul ettiği bu günlerde toplumun biyoçeşitlilik ile etkileşimde bulunduğu gıda üretimi ve güvenliği, kaynak yönetimi, koruma, araştırma, eğitim ve rekreasyon gibi alanlarda önemli çalışmalar yapılmasına katkı sağlayacaktır. Floristik zenginliğimizi oluşturan bitki türlerine moleküler kimlik verilmesi bitkilerin tanınması ve yerinde korunmasının (in-sitü) yanı sıra sahip olduğumuz biyoçeşitliliğin evrensel standartlarda kayıt altına alınarak korunmasına olanak sağlayacaktır.

Kaynakça

Alvarez, I., Wendel, J.F. (2003), Ribosomal ITS sequences and plant phylogenetic inference, *Mol Phylogenet Evolut*, 29(3), 417–434.

Amirahmadi, A., Osaloo, S.K., Mozaffar, M.K., Charkhchian, M.M. (2014), A new species of Onobrychis sect. Onobrychis (Fabaceae) from Iran, *Turkish Journal of Botany*, 38 (4), 658-664.

Bailey, C. (2003), Characterization of angiosperm nrDNA polymorphism, paralogy, and pseudogenes, *Molecular Phylogenetics and Evolution*, 29(3), 435–455.

BakshComeau, Y.S., Maharaj, S.S., Adams, C.D., Harris, S.A.,Hawthorne, W.D. (2016), An annotated checklist of the vascular plants of *Trinidad* and *Tobago* with analysis of vegetation types and botanical "hotspots", *Phytotaxa*, 250: 1–431

Barrett, R.D.H., Hebert, P.D.N. (2005), Identifying spiders through DNA barcodes, *Canadian Journal of Zoology*, 83, 481–491.

Bell, D., Long, D.G., Forrest, A.D., Hollingsworth, M.L., Blom, H.H., Hollingsworth, P.M. (2012), DNA barcoding of European *Herbertus* (Marchantiopsida, Herbertaceae) and the discovery and description of a new species: DNA BARCODING HERBERTUS, *Molecular Ecology Resources*, 12, 36–47.

Bendiksby, M., Brysting, A.K., Thorbek,L., Gussarova,G. and Ryding,O. (2011), Molecular phylogeny and taxonomy of the genus Lamium L. (Lamiaceae): Disentangling origins of presumed allotetraploids, *Taxon*, 60 (4), 986-1000.

Çabuk Şahin, E. (2016), Identification of Colchicum L. genus belong to Turkey's flora by morphological parameters and DNA barcoding system, *Dissertation*, Marmara University, İstanbul, Türkiye.

CBOLPlantWordingGroup.(2009),DNAbarcodeforlandplants,*PNAS,*106:12794–12797.

Chase, MW., Cowan, R.S., Hollingsworth, P.M., van den Berg, C., Madriñán, S., Petersen, G. (2007), A proposal for a standardised protocol to barcode all land plants, *Taxon*, 56(2), 295–299.

Chen, Q., Hu, H., Zhang, D. (2022), DNA Barcoding and phylogenomic analysis of the genus *Fritillaria* in China based on complete chloroplast genomes, *Frontiers in Plant Sciences*, 13:764255.

Davis, P.H., Mill, R.R., Tan, K. (1988), *Flora of Turkey and East Aegean Islands*, 10, (Supplement 1), Edinburgh University Press.

Dobson, A.P., Bradshaw, A.D., Baker, A.J.M. (1997a), Hopes for the future: Restoration ecology and conservation biology, *Science*, 277, 515-521.

Dong, W., Liu, J., Yu, J., Wang, L., Zhou, S. (2012), Highly variable chloroplast

markers for evaluating plant phylogeny at low taxonomic levels and for DNA barcoding, *PLoS One*, 7: E35071.

Doyle, J. (1991), DNA Protocols for Plants. Molecular Techniques in Taxonomy, NATO ASI Series Series H: *Cell Biology*, vol 57. Editörler: Hewitt, G.M., Johnston, A.W.B., Young, J.P.W. Berlin, Heidelberg: Springer.

Dönmez, A., Aydın, Z.U., Koca, A.D. (2017). Can DNA Barcoding provide any help for conservation of the Turkish geophytes? *XIX International Botanical Congress.*

Godfray, C. (2002), Challenges for taxonomy-The discipline will have to reinvent itself if it is to survive and flourish, *Nature*, 417, 17-19.

Güneş, F., Özba, B. (2014), *Kars çiçekleri (1. Baskı)*, Kars, Kafkas Üniversitesi Yayınları.

Hashim, A.M., Alatawi, A., Altaf, F.M., Qari, S.H., Elhady, M.E., Osman, G.H., Abouseadaa, H.H. (2021), Phylogenetic relationships and DNA barcoding of nine endangered medicinal plant species endemic to Saint Katherine protectorate, *Saudi Journal of Biological Sciences*, 28, 1919–1930.

Hebert, P.D.N., Cywinska, A., Ball, S.L., deWaard, J.R. (2003), Biological identifications through DNA barcodes, *Proceedings of the Royal Society of London B: Biological Sciences,* 270, 313–321.

Hollingsworth, P.M. (2008), DNA barcoding plants in biodiversity hot spots: Progress and outstanding questions, *Heredity*, 101, 1–2.

Hollingsworth, P.M., Graham, S.W., Little, D.P. (2011), Choosing and using a plant DNA barcode, *PLoS ONE*, 6, e19254. 668.

Hosein, F.N., Austin, N., Maharaj, S., Johnson, W., Rostant, L., Ramdass, A.C., Rampersad, S.N. (2017), Utility of DNA barcoding to identify rare endemic vascular plant species s in Trinidad, *Ecology and Evolution*, 7, 7311–7333.

Hürkan, K. (2020), Analysis of various DNA barcodes on the Turkish protected designation of origin apricot "Iğdır Kayısısı" (*Prunus armeniaca* cv. Şalak), *Turkish Journal of Agriculture-Food Science and Technology,* 8(9):1982-1987.

International Union for Conservation of Nature, IUCN (2022), https://www.iucn.org/.

Inal B., Karaca M. (2019), matK ve trnH-psbA barkot genleri kullanilarak bazi bitki taksonlarinin moleküler olarak siniflandirilmasi, *Türkiye Tarımsal Araştırmalar Dergisi*, 6(1): 87-93.

Kang, Y., Deng, Z., Zang, R., Long, W. (2017), DNA barcoding analysis and phylogenetic relationships of tree species in tropical cloud forests, *Sci Rep* 7, 12564.

Katz-Downie, D.S., Valiejo-Roman, C.M., Terentieva, E.I. et al. (1999), Towards a molecular phylogeny of *Apiaceae* subfamily *Apioideae*: Additional information from nuclear ribosomal DNA ITS sequences, *Plant Systematic and*

Evolution, 216, 167–195.

Keskin, E., Atar, H.H. (2013a), DNA barcoding commercially important aquatic invertebrates of Turkey, *Mitochondrial DNA*, 24(4): 440-450.

Keskin, E., Atar H.H. (2013b), DNA barcoding commercially important fish species of Turkey, *Molecular Ecology Resources*, 13(5): 788-797.

Khan, S.M., Page, S.E., Ahmad, H., Harper, D.M. (2013), Sustainable utilization and conservation of plant biodiversity in montane ecosystems: the western Himalayas as a case study, *Annals of Botany,* 112: 3, 479–501.

Kress, W.J., Erickson, D.L. (2007), A two locus global DNA barcode for land plants: the coding rbcL gene complements the non-coding trnH-psbA spacer region, *PLoS ONE*, 2(6), e508.

Kuzoff, R.K., Sweere, J.A., Soltis, D.E., Soltis, P.S., Zimme, E.A. (1998), The phylogenetic potential of entire 26S rDNA sequences in plants, *Mol Biol Evolut*, 15(3):251–263.

Li, X., Yang, Y., Henry, R. J., Rossetto, M., Wang, Y., Chen, S. (2015), Plant DNA barcoding: from geneto genome, *Biological Reviews*, 90(1), 157–166.

Mishra, P., Kumar, A., Sivaraman, G., Shukla, A.K., Kaliamoorthy, R., Slater, A., Velusamy, S. (2017), Character-based DNA barcoding for authentication and conservation of IUCN Red listed threatened species of genus Decalepis (Apocynaceae), *Scientific Reports*, 7: 14910.

Mavrodiev, A.S, Tancig, M., Sherwood, A.M. et al. (2005), Phylogeny of Tragopogon L. (Asteraceae) based on ınternal and external transcribed spacer sequence data, 2005, *International Journal of Plant Sciences*, 166(1):117-133.

Ortega, J.F., Valentin, E.S., Acevedo, P., Lewis, C., Pipoly J., Meerow, A.W., Maunder, M. (2007), Seed plant genera endemic to the Caribbean Island Biodiversity Hotspot: A review and a molecular phylogenetic perspective, *The Botanical Review*, 73(3):183-234.

Oskoueiyan, R., and Kazempour S., Amirahmadi, A. (2014), Molecular phylogeny of the genus Lathyrus (Fabaceae-Fabeae) based on cpDNA matK Sequence in Iran, *Iranian Journal of Biotechnology*, 12, 41-48.

Özhatay, N. (2006), *Türkiye'nin BTC boru hattı boyunca önemli bitki alanları*, İstanbul.

Özhatay, N., Byfield A., Atay, S. (2005), *Türkiye'nin 122 önemli bitki alanı*, WWF Türkiye, İstanbul.

Piwczyński M., Puchałka, R., Spalik, K. (2015), The infrageneric taxonomy of *Chaerophyllum* (Apiaceae) revisited: new evidence from nuclear ribosomal DNA ITS sequences and fruit anatomy, *Botanical Journal of the Linnean Society*, 178: 2, 298–313.

Şapcı Selamoğlu, H. (2022), DNA barcoding of two narrow endemic plants; *Astragalus argaeus* and *Astragalus stenosemioides* from Mount Erciyes, Tur-

key, *Conservation of Genetic Resources*, 14, 81–84.

Savolainen, O., Karhu, A. (2000). Assessment of Biodiversity with Molecular Tools in Forest Trees. In: Jain, S.M., Minocha, S.C. (Eds.), Molecular Biology of Woody Plants: Volume 1, *Forestry Sciences*. Springer, Netherlands, Dordrecht, pp. 395– 406.

Srivastava, D., Manjunath, K. (2020), DNA barcoding of endemic and endangered orchids of India: A molecular method of species identification, *Pharmacognosy Magasine*,16: S290-9.

The International Barcode of Life Consortium (2022). International Barcode of Life project (IBOL). Occurrence dataset https://doi.org/10.15468/inygc6 accessed via GBIF.org on 2023-03-30.

The IUCN Red List as follows: IUCN. 2022. The IUCN Red List of Threatened Species.

White, T.J., Bruns, T., Lee, S.H., Taylor, J.W. (1990), *PCR protocols: aguide to methods and application*, San Diego, 315−322.

Wilson, C.A. (2009), Phylogenetic relationships among the recognized series in Iris Section Limniris, *Systematic Botany*, 34 (2), 277-284.

Yılmaz, M.N. (2012), Kafkas Üniversitesi Kampüs Florası, (*Yüksek Lisans Tezi*), Dumlupınar Üniversitesi, Fen Bilimleri Enstitüsü, Kütahya.

BÖLÜM 2

CHAPTER 2

ANTİK BİTKİ DNA ÇALIŞMALARI

Funda ÖZDEMİR DEĞİRMENCİ[1]

1 Dr. Öğr. Üyesi , Ahi Evran Üniversitesi, Ziraat Fakültesi, Tarla Bitkileri Bölümü ORCID ID: https://orcid.org/0000-0002-8875-0273

1. Tarımın ortaya çıkışı ve yayılışı

Tarımsal ekonomiye dayalı yerleşik hayata geçiş olarak adlandırılan 'Neolitik dönüşüm' süreci dünyanın farklı bölgelerinde birbirinden bağımsız olarak farklı zamanlarda başlamış ve zaman içinde tüm kıtalara yayılmıştır (Diamond vd., 2003; Gepts, 2004). Arkeolojik, antropolojik ve genetik çalışmalar, Neolitik dönüşümün günümüzden yaklaşık 13 bin yıl önce Doğu Akdeniz'in kıyı bölgesi (Güney Levant), İran ve Irak'ın Toros-Zagros sınırları, Kuzey Mezopotamya, Güneydoğu Anadolu ve Orta Anadolu'yu içeren Bereketli Hilal olarak adlandırılan bölgede gerçekleştiğini göstermektedir (Özdoğan, 2011; Riehl vd., 2013; Broushaki vd., 2016). Her ne kadar tarımın ve hayvan evcilleştirilmesinin ilk olarak Bereketli Hilal bölgesinde başladığı kabul edilsede, son yıllarda yapılan arkeolojik, antropolojik ve genetik veriler ışığında tarımın Yakın Doğu'da tek bir noktada başlamadığı, birden fazla çekirdek bölgede farklı toplumlar tarafından yapıldığı açığa çıkarılmıştır (Salamini vd., 2002; Gebel, 2004; Fuller vd., 2011; Özbaşaran, 2011; Stiner vd., 2014; Hodder, 2014). Fuller vd. (2011) Bereketli Hilal'de yer alan Neolitik yerleşim yerlerinde yapılan kazı çalışmalarında bulunan darı, arpa, buğday, burçak ve keten gibi tarımsal ürünlerin ve bunların yabanıl atalarının dağılımını arkeobotanik verileri kullanarak göstermişlerdir. Elde edilen veriler bu tarım ürünlerinin tek bir merkezde değilde birden fazla bölgede bulunduğunu ve kültüre alındığını göstermektedir. Ayrıca Levant, İran ve Orta Anadolu Neolitik insanlarının arkeogenomik incelemeleri de yerel avcı toplayıcıların farklı bölgelerde tarımı başlattığı ve birbirleri ile genetik etkileşim içinde olmadıklarını göstermiştir (Lazaridis vd., 2016).

Orta Anadolu bölgesinde açığa çıkarılan 11 Neolitik yerleşim merkezinin 5 tanesinde tarım uygulamalarının izlerine rastlanmıştır (Baird, 2009, 2012a). Bu toplumların birbirleriyle ve Bereketli Hilal'de bulunan Neolitik topluluklarla bölgesel ve bölgeler arası sosyal ve ekonomik etkileşimlerinin olduğu bulunmuştur (Gerard ve Thissen, 2002; Özbaşaran, 2011). Orta Anadolu Hitit devletinin liderleri, Batı Anadolu'daki ticaret yollarına erişimi olan toprakların kontrolü ve diplomatik bağlantıları için Ege, Levant ve Mısır'ın stratejik bölgelerinde yaşayarak bu bölgeler arasındaki sosyal ve ticari ilişkilerini devam ettirmişlerdir (Bryce, 2005). Günümüzden yaklaşık 13 bin yıl önce Yakın Doğu'da başlayan tarımsal faaliyetlerin (Özdoğan ve Başgelen, 1999), aşamalı olarak hem Akdeniz hem de Ege kıyıları ve kuzey batı Anadolu üzerinden 6 bin yıl önce Avrupa'ya yayıldığı, yapılan arkeolojik kazılardan elde edilen bulgularla desteklenmektedir (Özdoğan, 2011; Fort vd., 2012). Radyokarbon (C^{14}) tarihlendirmesi, seramik analizleri ve iklim verileri, Batı Anadolu ve güney Avrupa Neolitik toplumları arasında çeşitli dinamik ilişkilerin olduğunu göstermiştir. Evcil hayvanların kalıntılarıyla yapılan antik DNA (aDNA) çalışmaları da bu

kültürel etkileşimin ve tarımın Batı Anadolu'dan Avrupa'ya yayılışını kanıtlamaktadır (Fernandez vd., 2006; Beja-Pereira vd., 2006; Larson vd., 2007; Haak vd., 2010; Weninger vd., 2014). Ayrıca Kılınç vd. (2016) en erken Neolitik dönem Anadolu çiftçilerinin Avrupa'ya yayılan ilk Neolitik göçmenler ile aynı gen havuzunu paylaştıklarını ortaya koymuştur.

2. Genetik tabanlı arkeobotanik çalışmalar

Tarım bitkileri, yüzyıllar boyunca kültüre alınma ve ıslah sürecinde insan müdahalesi, değişen çevresel koşullara yönelik, seçilim ve adaptasyon sonucunda sürekli olarak genetik değişimlere uğramıştır. Tarımın ilerlemesiyle bu ürünler yeni coğrafik bölgelerde farklı seçilim koşullarında gelişmeye ve yayılmaya başlamıştır. Bu yayılım çok sayıda istenilen agronomik özelliklere sahip yerel tohumların gelişmesini sağlamıştır. Tarım tarihi konusunda en doğru bilgilere ulaşmak, tarım bitkilerinin yayılımını, zaman içinde geçirdiği değişimleri ve ürünlerin yeni ortamlara uyum sağlama yeteneğini daha detaylı bir şekilde inceleyebilmek için modern tohumlar, onların yabanil formları, herbaryum ve müze koleksiyonlarında bulunan diğer bitki materyallerinin morfolojik ve genetik analizleri yapılmaktadır. Çalışılan örneklerin referans genomları kullanılarak ortak atalarının sahip olduğu genom dizisi ve yapısı uzun bir zaman dilimini içerecek şekilde ortaya çıkarılmaktadır. Arkeobotanik alanının gelişmesiyle, arkeolojik kazılar sırasında elde edilen antik bitki örnekleriyle yapılan makro ölçekteki analizler, tarımın çıkışı ve gelişmesiyle ilgili belli sorulara cevap verse de tarım ürünlerinin geçirdiği değişiklikler ve yayılışı hakkında daha kesin bilgilere ulaşmak için genetik analizlerden yararlanmak zorunlu hale gelmiştir (Leino vd., 2013; Kistler vd., 2017). Optimum şartlarda kömürleşmiş tohum ve odun gibi biyolojik örneklerde DNA ve biyokimyasal moleküllerin varlığını binlerce yıl sürdürebildiği yapılan çalışmalarla ortaya konmaktadır (Parducci ve Remy, 2004; Gugerli vd., 2005; Rogers ve Kaya, 2006). Paleogenetik, moleküler biyoloji tekniklerinin kullanılarak arkeolojik kaynaklardan elde edilen biyolojik kalıntıların genetik yapılarının açığa çıkarıldığı disiplinlerarası bir araştırma alanıdır ve arkeolojik kalıntılarda korunan aDNA'yı yeni nesil dizileme metotları kullanarak açığa çıkan genomik değişikliklerin daha kısa bir zaman diliminde doğrudan tanımlanmasına odaklanır. Spesifik genomik bölgeleri hedefleyerek DNA parçalarının çoğaltılmasını sağlayan gerçek zamanlı Polimeraz Zincir Reaksiyon (PZR) teknikleri, geliştirilen yüksek kapasiteli dizileme teknolojileri ve biyoinformatik yöntemler düşük yoğunlukta ve bozunuma uğramış DNA ile çalışmanın zorluklarını aşarak paleogenetik alanının gelişmesine olanak sağlamaktadır (Mullis vd., 1986; Paabo vd., 2004).

DNA'nın arkeolojik bitki kalıntılarında iyi bir şekilde muhafaza edildiğini saptayan ve DNA'yı çoğaltarak paleogenetik analizlerin yapıldığı

az sayıda çalışma bulunmaktadır. Allaby vd. (1997) ve Brown vd. (1998), Brown (1999)Avrupa'daki değişik kazı alanlarından çıkarılan kömürleşmiş buğday tohumlarından DNA izole ederek PZR çalışmaları ile çoğaltmışlardır. Çin'in Sincan bölgesinde erken Tunç Çağı'na tarihlenen buğday tanelerinden çok iyi durumda DNA izole edilmiştir. Nükleer ribozomal DNA bölgeleri (ITS) ve intergenik (IGS) ara bölgelerden elde edilen sonuçlar çalışılan buğdayların hekzaploid ekmeklik buğdayla yakın genetik benzerlik gösterdiğini açığa çıkarmıştır (Li vd., 2011). Oliviera vd. (2012) Gran Canaria bölgesinde İspanya dönemi öncesine ait kurumuş buğday tohumlarından DNA izole ederek ribozomal DNA bölgelerinden ITS ve IGS, gluten lokusunun üst bölgesi ve tek lokus nükleer mikrosatellit bölgelerini başarılı bir şekilde çoğaltmışlardır. IGS lokusu, tetraploid (AABB) ve hexaploid (AABBDD) buğdayların belirlenmesine yardımcı olmuştur. Ayrıca çalışılan çekirdek DNA bölgeleri ekmeklik ve durum buğdaylarını da birbirinden ayırmıştır. Mascher vd. (2016) Ölü Denize yakın Judean çölündeki bir mağaradan elde edilen kazıdan çıkarılan 6000 yıllık arpa tohumlarının genom dizi analizini yapmışlardır. Antik örneklerin ekzom dizilerinin modern arpa çeşitleriyle karşılaştırılması bu örnekler ile güney Levant ve Mısır daki çeşitler arasında yüksek oranda benzerlik olduğunu göstermiştir. Palmer vd. (2009) Qasr Ibrim bölgesinden elde edilen antik tohumlardan DNA izole ederek, arpada başak sayısını belirleyen VRS1 geninin dizi analizini gerçekleştirmişlerdir. Bütün başakların altı sıralı genotip yapısına sahip olduğu bulunmuştur. Baklagil türleri için bildirilen ilk başarılı aDNA izolasyonu güneydoğu Sırbistan da bulunan Hissar kasabasındaki M.Ö. 1.350-1.000 tarihli bir tepeden çıkarılan bezelye (*Pisum sativum*) ve burçak (*Vicia ervilia*) tohumlarına aittir. Her iki türden elde edilen DNA'nın tüm genom çoğaltımı yapılarak, ribozomal DNA geni olan 26S rDNA bölgesi çoğaltılmıştır (Mikic, 2015). Smykal vd. (2014) aynı bölgeden çıkarılan bezelye tohumlarından elde edilen aDNA'yı kullanarak dört kloroplast DNA bölgesini (trnSG, trnK, matK ve rbcL) çoğaltarak antik, kültüre alınmış ve yabani bezelye tohumları arasındaki farkı ayırt etmeye çalışmışlardır. Antik DNA analizi kömürleşmiş bezelye tohumlarını kültüre alınmış *Pisum sativum* ile yabani form olan P. *sativum* subsp. *elatius* arasına yerleştirmiştir. Literatürde karbonlaşmış/kömürleşmiş antik *Vitis vinifera* tohum örnekleri ile yapılmış çalışmalarda, bu örneklerin coğrafik orjinlerini belirlemek ve modern çeşitlerle ilişkilendirmek amacıyla mikrosatelit markörleri kullanılmıştır (Manen vd., 2003; Cappellini vd., 2010; Gismondi vd., 2016; Bacilieri vd., 2017). Cappellini vd. (2010)'nin çalışması kuru üzüm ticareti ile ilgili tarihsel verileri ortaya çıkarmıştır. Bunlara ek olarak çok kopyalı olması sebebiyle kloroplast RuBisCO büyük ünite geni (rbcL) (Malenica vd., 2011), yine kloroplast DNA'sında bulunan matüraz kinaz (matK) ve trnH-psbA bölgeleri türün belirlenmesi ve modern çeşitlerle karşılaştırma çalışmalarında kullanılmıştır (Gismondi

vd., 2016).

3. Sediment DNA çalışmaları

Son yıllarda göllerden sondajlarla çıkarılan sediment örnekleriyle yapılan sedaDNA çalışmaları ile kazı yapılan bölgelerin jeolojik ve paleocoğrafik özellikleri daha kapsamlı bir şekilde açığa çıkarılmaktadır. Sediment örnekleri üzerinde gerçekleştirilen detaylı genetik, sedimantolojik, jeokimyasal ve kronolojik analizler ile elde edilen bitki örneklerinin ait oldukları jeolojik dönemlerde nasıl bir coğrafyayla temsil edildikleri ve ne gibi değişimler geçirdikleri açığa çıkarılabilmektedir. Göller, kıyıları farklı noktalardan gelen çökeltiler ile sürekli beslendiğinden eski tarihlerden bu yana anoksik koşullarda korunan su ve karasal çevresel bileşenler içeren tortu kaynaklarıdır. Göl sedimentleri, geçmiş zamanların bitki örtüsünü içeren ve bu bitki türlerinin ve popülasyonlarının köken, yayılış ve zaman içinde geçirdikleri değişimleri anlamaya olanak sağlayacak moleküler kayıtların oluşturulması açısından zengin bir kaynaktır. Metabarkodlama yöntemi kullanılarak, göllerden alınan sedimentlerden izole edilen aDNA (*seda*DNA) ile yapılan genetik analizlerde tekli numunelerden çoklu organizma grupları kolaylıkla tanımlanmıştır ve buna ek olarak klasik polen ve makrofosil çalışmalarında belirlenemeyen bitkilerin cins ve tür seviyesi açığa çıkarılmıştır (Lydolph vd., 2005; Willerslev vd., 2007; Anderson-Carpenter vd., 2011; Taberlet vd., 2012b; Boessenkool vd., 2013; Alsos vd., 2015, 2016). Farklı çalışma grupları tarafından gerçekleştirilen *seda*DNA çalışmalarında göllerdeki sedimentlerden izole edilen DNA'nın polenlerden daha çok makrofosillerin DNA'sına benzediği açığa çıkarılmıştır. Elde edilen sonuçlar *seda*DNA analizlerinde açığa çıkarılan taksonların çoğunluğunun mevcut bölgedeki florayı temsil ettiğini göstermiştir. Sediment örnekleriyle metabarkod ve metagenomik analizlerin yapılması geçmiş zamanlarda yerel vejetasyonu temsil eden türlerin açığa çıkarılması ve bitki örtüsünün, özellikle de kültüre alınmış bitki türlerinin, geçmişteki farklı zaman dilimlerinden günümüze kültürel, çevresel ve iklimsel değişiklikler sonucu geçirdiği değişimlerin anlaşılmasına çok büyük bir katkı sağlamıştır (Boessenkool vd., 2013; Parducci vd. 2015; Alsos vd., 2015).

4. Türkiye'de antik bitki DNA çalışmaları

Türkiye, antik DNA (aDNA) çalışmaları için bol miktarda hayvan ve bitki materyali sağlayan arkeolojik sit alanları bakımından oldukca zengin bir ülkedir. Farklı kazı alanlarından elde edilen arkeobotanik kayıtlar, Anadolu'da hangi bitki türlerin kültüre alındığıyla ilgili ipuçları vermektedir. Türkiye'de çok sayıda gerçekleştirilen arkeolojik kazılardan elde edilen bitki örnekleri arkeobotanik alanında yapılacak olan araştırmalar için önemli bir kaynak sağlasada çalışmaların çoğu yabancı bilim insanlarının

oluşturduğu gruplar tarafından yapılmaktadır. Bilgiç vd. (2016) Çatalhöyük ve Türkiye'nin diğer arkeolojik bölgelerinden çıkarılan kömürleşmiş buğday tohumlarından DNA izole edip, gluten protein lokuslarını çoğaltarak antik buğday tanelerini modern akrabalarıyla karşılaştırmışlardır. Bu tohumlar genetik olarak çalışılan en yaşlı antik tohumlar olup (yaklaşık olarak 8400 yaşında) hexaploid buğday türlerine (*T. aestivum, T. spelta*) benzerlik göstermişlerdir. Anadolu'da Diyarbakır Karacadağ bölgesinin siyez buğdayının yaklaşık 10500 yıl önce kültüre alındığı ilk bölge olduğu yapılan arkeobotanik ve genetik çalışmalarla açığa çıkarılmıştır (Nesbitt, 1998b; Özkan vd., 2002). Çiftçi vd., (2019) Kaymakçı kazı alanından çıkarılan ve morfolojik olarak buğday, arpa, nohut, burçak, üzüm olarak tanımlanan kömürleşmiş beş tohumdan DNA izole ederek oldukça polimorfik ve iyi korunmuş 26S rDNA bölgesini çoğaltmıştır. Elde edilen dizi analizi ile morfolojik olarak tanımlanan türlerin genetik olarakta aynı türler olduğu belirlenmiş ve çağdaş akrabalarıyla yüksek düzeyde benzerlik gösterdiği ve türe göre farklılaşan DNA baz değişimlerinin olduğu ortaya konmuştur.

Değirmenci vd. (2022) Mersin Yumuktepe ve İstanbul Yenikapı kazı alanlarından çıkarılan yaklaşık 8000 yıllık kömürleşmiş buğday tohumlarından antik DNA izole ederek bu tohumların intergenik (IGS) lokuslarını çoğaltmışlardır. IGS lokusunun dizi verileri çalışılan antik tohumların hexaploid (AABBDD) ekmeklik buğday olan *Triticum aestivum* türüne ait olduğunu ve Neolitik dönemde bu buğday türünün tarımının yapıldığını açığa çıkarmıştır. Kazı alanlarımızdan çıkarılan arkeobotanik kalıntılardan (fosiller, kömürleşmiş tohumlar, sediment) yüksek oranda, kaliteli ve çoğaltılabilir aDNA izole ederek palegoenetik araştırmaların yapılması açığa çıkarılan türlerin orjini, ilk kültüre alınması, yayılması ve günümüz populasyonlarıyla olan benzerlik ya da farklılıklarıyla ilgili çok önemli sorulara cevap verecektir. Arkeolojik materyallerden elde edilen aDNA tür içi ve türler arası ilişkileri çalışmak, paleobotanik, etnobotanik, populasyon genetiği ve filogenetik çalışmalar için çok önemli veriler sunacaktır. Ayrıca ülkemizdeki yerleşimlerin ve kültürel geçmişin üzerinde doğal ortamın etkisinin ve bu yerleşimlerin ve kültürlerin varlığından doğal çevrenin ne şekilde etkilendiğinin anlaşılması bölgesel anlamda arkeolojik, tarihsel, tarımsal, biyolojik ve jeolojik birçok konuya katkı sağlayacaktır. Ayrıca, arkeolojik alanlardan çıkarılan antik materyallerde DNA'nın korunmasına yol açan çevresel, biyolojik ve fiziksel koşulların anlaşılması, bitki DNA bankalarında bulunan genetik mirasımızı en iyi şekilde korumak için stratejiler geliştirmemize yardımcı olacaktır.

Kaynakça

Allaby, R.G., O'Donoghue, K., Sallares, R., Jones, M.K., Brown, T.A. (1997). Evidence for the survival of ancient DNA in charred wheat seeds from European archaeological sites. *Ancient Biomolecule*s, 1, 119-129.

Alsos, I.G., Coissac, E., Edwards, M.E., Merkel, M., Gielly, L. (2015). Plant DNA in sediments: to which degree do they represent the flora? *Genome*, 58, 163–303.

Alsos, I.G., Sj€ogren, P., Edwards, M.E., Landvik, J.Y., Gielly, L., Forwick, M., Coissac, E., Brown, A.G., Jakobsen, L.V., Føreid, M.K. et al. (2016). Sedimentary ancient DNA from Lake Skartjørna, Svalbard: assessing the resilience of arctic flora to Holocene climate change. *The Holocene*, 26, 1–16.

Anderson-Carpenter, L., Mclachlan, J., Jackson, S., Kuch, M., Lumibao, C., Poinar, H. (2011). Ancient DNA from lake sediments: bridging the gap between paleoecology and genetics. *BMC Evolutionary Biology*, 11, 1–15.

Bacilieri, R., Bouby L., Figueiral I. vd. (2017). Potential of combining morphometry and ancient DNA information to investigate grapevine domestication. *Vegetation History and Archaeobotany*, 26, 345.

Baird, D. (2009). The Boncuklu Project: Investigating the Beginnings of Agriculture, Sedentism and Herding in Central Anatolia, *Anatolian Archaeology*. 15, 9-10.

Baird, D. (2012a). Pınarbaşı: From Epi-Paleolithic Camp-Site to Sedentarising Village in Central Anatolia, in: Özdoğan, M., Başgelen, N. and Kuniholm, P. (eds.) The Neolithic in Turkey, Vol 3 (Central Turkey), pp. 181-218. *Archaeology and Art Publications*, Istanbul.

Beja-Pereira, A. et al. (2006). The origin of European cattle: evidence from modern and ancient DNA. *PNAS,* 103:21, 8113-8118.

Bilgic¸ H., Hakki, E.E., Pandey, A., Khan, M.K., Akkaya, M.S. (2016). Ancient DNA from 8400year-old Çatalhöyük wheat: implications for the origin of Neolithic agriculture. *PLoS One*, 11:3, e0151974.

Boessenkool, S., McGlynn, G., Epp, L.S., Taylor, D., Pimentel, M., Gizaw, A., Memomissa, S., Brochmann C, Popp, M. (2013). Use of ancient sedimentary DNA as a novel conservation tool for high-altitude tropical biodiversity. *Conservation Biology*, 28, 446–455.

Broushaki, F. et al. (2016). Early Neolithic genomes from the eastern Fertile Crescent. *Science*, 353, 499-503.

Brown, T.A. (1999). How ancient DNA may help in understanding the origin and spread of agriculture. *Philosophical Transaction of the Royal Society London Biological Sciences*, 354, 89–98.

Brown, T.A., Allaby, R.G., Sallares, R., Jones, G. (1998). Ancient DNA in charred wheats: taxonomic identification of mixed and single grains. *Ancient Bio-*

molecules, 2, 185-193.

Cappellini, E., Gilbert, M.T., Geuna, F. vd. (2010). A multidisciplinary study of archaeological grape seeds. *Naturwissenschaften*, 97, 205-217.

China Plant CBOL Group, Li, D.Z., Gao, L.M., vd. (2011). Comparative analysis of a large dataset indicates that internal transcribed spacer ITS should be incorporated into the core barcode for seed plants. *Proc. Nat. Acad. Sci*. U.S.A., 108, 19641-19646.

Çiftci, A., Değirmenci, F.O., Luke, C., vd. (2019). aDNA extraction and amplification from 3500-year-old charred economic crop seeds from Kaymakçı in Western Turkey: comparative sequence analysis using the 26S rDNA gene. *Genetic Resources and Crop Evolution*, 66, 1279.

Diamond, J. et al. (2003). Farmers and Their Languages: The First Expansions. *Science*, 300, 597-603.

Fernandez, H., Hughes, S., Vigne, J.D., Helmer, D., Hodgins, G., Miquel, C., Hänni, C., Luikart, G., Taberlet, P. (2006). Divergent mtDNA lineages of goats in an Early Neolithic site, far from the initial domestication areas. *PNAS,* 103 :42, 15375-15379.

Fort et al. (2012). Modelling The Neolithic Transition In The Near East And Europe. *American Antiquity*, 77, 203-219.

Fuller, D.Q., Willcox, G. and Allaby, R.G. (2011). Cultivation and domestication had multiple origins: arguments against the core area hypothesis for the origins of agriculture in the Near East. *World Archaeology*. 43, 628-652.

Gebel H.G. (2004). There was no centre: The polycentric evolution of the Near Eastern Neolithic. *Neolithics,* 1: 28.

Gepts, P. (2004). Domestication as a long-term selection experiment*. Plant Breeding Reviews*, 24:2, 1–44.

Gerard, F. and Thissen, L. (ed.) (2002). The Neolithic of Central Anatolia: Internal development and external relations during the 9th-6th millennium BC, Proceeding of the International CANeW Table Ronde, Istanbul, 23-24 November 2001. *Ege Yayınları*, İstanbul.

Gismondi, A., Di Marco, G., Martini, F., Sarti, L., Crespan, M., Martínez-Labarga, C., Rickards, O., Canini, A. (2016). Grapevine carpological remains revealed the existence of a Neolithic domesticated Vitis vinifera L. specimen containing ancient DNA partially preserved in modern ecotypes. *Journal of Archaeological Sciences*, 69, 75-84.

Gugerli, F., Parducci, L., Petit, R.J. (2005). Ancient plant DNA: review and prospects. *New Phytologist*, 166:2, 409–418.

Haak, W. et al. (2010). Ancient DNA from European early Neolithic farmers reveals their Near Eastern affinities. *PLoS Biology*. 8, e1000536.

Hodder, I. (2014). Çatalhöyük: The leopard changes its spots. A summary of recent work. *Anatolian Studies*, 64, 1–22.

Kılınc¸ G.M et al. (2016). The demographic development of the first farmers in Anatolia. *Current Biology*, 26:19, 2659–2666.

Kistler, L., Ware, R., Smith, O., Collins, M. and Allaby, R. G. (2017). A new model for ancient DNA decay based on paleogenomic meta-analysis. *Nucleic Acids Researches*, 45, 6310-6320.

Larson, G. et al. (2007). Ancient DNA, pig domestication, and the spread of the Neolithic into Europe. *PNAS*, 104 (39), 152-176.

Lazaridis I. et al. (2016). Genomic insights into the origin of farming in the ancient Near East. *Nature*, 536, 419-424.

Leino, M. W., Boström, E. and Hagenblad, J. (2013). Twentieth-century changes in the genetic composition of Swedish field pea metapopulations. *Heredity*, 110, 338-346.

Li, C., Lister, D.L., Li, H., Xu, Y., Cui, Y., Bower, M.A., Jones, M.K., Zhou, H. (2011). Ancient DNA analysis of desiccated wheat grains excavated from a Bronze Age cemetery in Xinjian. *Journal of Archaeological Sciences*, 38(1), 115–119.

Lydolph, M.C., Jacobsen, J., Arctander, P., Gilbert, M.T.P., Gilichinsky, D.A., Hansen, A.J., Willerslev, E., Lange, L. (2005). Beringian paleoecology inferred from permafrostpreserved fungal DNA. *Applied and Environmental Microbiology*, 71, 1012–1017.

Malenica, N., Ŝimon, S., Besendorfer, V., Matelić, E., Kontić, J.K., Pejić, I. (2011). Whole genome amplification and microsatellite genotyping of herbarium DNA, revealed the identiy of an ancient grapevine cultivar. *Naturwissenschaften*, 98, 763–772.

Manen, J., Bouby, L., Dalnoki, O., Marinval, P., Turgay, M., Schlumbaum, A. (2003). Microsatellites from Archaeological Vitis vinifera Seeds Allow a Tentative Assignment of the Geographical Origin of Ancient Cultivars. *Journal of Archaeological Science,* 30, 721-729.

Mascher, M., Schuenemann, V.J., Davidovich, U., Marom, N., Himmelbach, A., Hubner, S., Korol, A., David, M., Reiter, E., Riehl, S., Schreiber, M., Vohr, S.H., Green, R.E., Dawson, I.K., Russell, J., Kilian, B., Muehlbauer, G.J., Waugh, R., Fahima, T., Krause J., Weiss, E., Stein, N. (2016). Genomic analysis of 6,000-year-old cultivated grain illuminates the domestication history of barley. *Nature Genetics.*, 48:9, 1089-93.

Mikic, A., Medovic, A., Jovanovic, Z., Stanisavljevic, N. (2015). A note on the earliest distribution, cultivation and genetic changes in bitter vetch (*Vicia ervilia*) in ancient Europe. *Genetika*, 47:1, 1–11.

Mullis, K., Faloona, F., Scharf, S., Saiki, R., Horn, G. and Erlich, H. (1986). Specific enzymatic amplification of DNA in vitro: the polymerase chain reaction, Cold Spring Harbor symposia on quantitative biology. *Cold Spring Harbor Laboratory Press*, 263-273.

Nesbitt, M., Samuel, D. (1998). Wheat domestication: archaeobotanical evidence. *Science*, 279: 1431–1431.

Oliveira, H. R., Civáň, P., Morales, J., Rodríguez-Rodríguez, A., Lister, D. L., Jones, M. K. (2012). Ancient DNA in archaeological wheat grains: Preservation conditions and the study of pre-Hispanic agriculture on the island of Gran Canaria Spain. *Journal of Archaeological Sciences*, 39 (4), 828–835.

Özbaşaran, M. (2011). The Neolithic on the Plateau‟, in S. Steadmann & G. McMahon (ed.) The Oxford Handbook of Ancient Anatolia: (10.000-323 B. C.E.). *Oxford University Press*, 99-124.

Özdoğan, M., Başgelen, N. (1999). Neolithic in Turkey, the Cradle of Civilization: New Discoveries, İstanbul. *Arkeoloji ve Sanat Yayınları*.

Özdoğan, M. (2011). Archaeological Evidence on the Westward Expansion of Farming Communities from Eastern Anatolia to the Aegean and the Balkans. *Cur. Anthology*, 52 :4, 415-S430.

Özkan, H. et al. (2002). AFLP analysis of a collection of tetraploid wheats indicates the origin of emmer and hard wheat in southeast Turkey. *Molecular Biology and Evolution*, 19, 1797–1801.

Paabo, S., Poinar, H., Serre, D., Jaenicke-Despres, V., Hebler, J., Rohland, N., Kuch, M., Krause- Vigilant, L., Hofreiter, M. (2004). Genetic analyses from ancient DNA. *Annual Review of Genetics*, 38, 645–647.

Palmer, S.A., Moore, J.D., Clapham, A.J., Rose, P., Allaby, R.G. (2009). Archaeogenetic evidence of ancient nubian barley evolution from six to two-row indicates local adaptation. *PLoS One*, 4:7, e6301, doi:10.1371/journal.pone.0006301.

Parducci, L., Remy, P. (2004). Ancient DNA - Unlocking plants'fossil secrets. *New Phytologist*, 161:2, 335–339.

Parducci, L., V€aliranta, M., Salonen, J.S., Ronkainen, T., Matetovici, I., Fontana, S.L., Eskola, T., Sarala, P., Suyama, Y. (2015). Proxy comparison in ancient peat sediments: pollen, macrofossil and plant DNA. *Philosophical Transactions of the Royal Society B: Biological Sciences*, 370, 20130382.

Riehl, et al. (2013). Emergence of Agriculture in the Foothills of the Zagros Mountains of Iran. *Science*, 341: 65-67.

Rogers, S.O., Kaya, Z. (2006). DNA from ancient cedar wood from King Midas Tomb, Turkey, and Al-Aksa Mosque, Israel. *Silvae Genetica*, 55(1–6):54–62.

Salamini, F., Özkan, H., Brandolini, A., Schäfer-Pregl. R., Martin. W. (2002). Genetics and geography of wild cereal domestication in the Near East. *Nature Reviews Genetics*, 3: 429–441.

Smýkal, P., Jovanović, Ž., Stanisavljević, N. vd. (2014). A comparative study of ancient DNA isolated from charred pea (Pisum sativum L.) seeds from an Early Iron Age settlement in southeast Serbia: inference for pea domestica-

tion. *Genetic Resources and Crop Evolution*, 61, 1533–1544.

Stiner, M. C., Buıtenhuıs, H., Duru, G., Kuhn, S. L., Mentzer, S., Munro, N. D., Pöllath, N., Quade, J., Tsartsıdou, G. and Özbaşaran, M. (2014). A Forager-Herder Trade-Off, from Broad-Spectrum Hunting to Sheep Management at Aşıklı Höyük, Turkey. *PNAS* 111/23: 8404-8409.

Taberlet, P., Coissac, E., Pompanon, F., Brochmann, C., Willerslev, E. (2012b). Towards next-generation biodiversity assessment using DNA metabarcoding. *Molecular Ecology*, 21, 2045–2050.

Weninger, B., Clare, L., Gerritsen, F., Horejs, B., Krauß, R., Linstädter, J., Özbal, R., & Rohling, E. J. (2014). Neolithisation of the Aegean and Southeast Europe during the 6600–6000 calBC period of Rapid Climate Change. *Documenta Praehistorica*, 41, 1-31. https://doi.org/10.4312/dp.41.1.

Willerslev, E., Cappellini, E., Boomsma, W., Nielsen, R., Hebsgaard, M.B., Brand, T.B., Hofreiter, M., Bunce, M., Poinar, H.N., Johnsen, S. et al. (2007). Ancient biomolecules from deep ice cores reveal a forested southern Greenland. *Science*, 317: 111–114.

BÖLÜM 3

CHAPTER 3

BİYOAKTİF PEPTİDLERİN TERAPÖTİK UYGULAMALARI

Özden CANLI TAŞAR[1]

1 Öğr. Gör. Dr. , Erzurum Teknik Üniversitesi, Yüksek Teknoloji Uygulama ve AraştırmaMerkezi, Erzurum, Türkiye, e-mail: ozden.tasar@erzurum.edu.tr, ORCID: 000-0002-4313-5373

Giriş

İnsan sağlığı ve gelişimi üzerine etki eden çeşitli faktörler mevcuttur. Çevresel faktörler ve hayat tarzının yanında, beslenme şekli ve alışkanlıklar insanların yaşam kalitesini belirler. Mikroorganizmaların diyetle alınması ve simbiyotik mikroorganizmaların sindirim sisteminde gösterdiği faaliyetler sonucunda hastalıkların etki mekanizmaları değişiklik gösterir. Günümüzde, mikrobiyata ile insan sağlığı arasındaki ilişkinin aydınlatılması amacıyla yapılan çalışmalar artmaktadır (Levy et al., 2017). Son yıllarda yapılan çalışmalarda, insan vücudunda bulunan mikrobiyotanın çeşitli hastalıklardaki rolleri araştırılmaktadır. Klinik olarak bilinen tek rutin tedavi, *Clostridium difficile* enfeksiyonlarına karşı yapılmaktadır. Kommensal bakterilerin direkt olarak insan vücudunda fonksiyonel olarak aktif olması ve bununla birlikte, salgıladıkları moleküllerin vücut döngüsüne karışarak insan fizyolojisi ve hastalık oluşturulması üzerine etkileri nedeniyle, mikroorganizmalar tarafından oluşturulan moleküllerin terapötik özellikleri merak konusu olmuştur (Thaiss & Elinav, 2017). Bu metabolitler bakteriyel metabolizma ürünü oldukları gibi, diyetle alınan besinlerin, sindirim sisteminde bulunan mikroorganizmalar tarafından işlenmesi sonucu ortaya çıkmaktadır. Mikrobiyomun endokrin aktivitesi ve çok sayıda karmaşık hastalığa dahil olması, mikrobiyomun modüle ettiği metabolitleri yeni tedavilerin geliştirilmesi için çekici bir hedef haline getirmiştir. Bu bağlamda, geniş bir konsantrasyon aralığında doğal olarak meydana gelme, fonksiyonel pleiotropi, uygulama kolaylığı ve doku biyoyararlanımı gibi bazı özelliklerden dolayı metabolit bazlı tedavi çeşitlerinde mikrobiyom uygulamaları artmaktadır (Descamps et al., 2019).

Peptidler, proteinlerin sindirimi sonucu doğal olarak oluşan moleküller olup, enzimatik sindirimle oluştuğu gibi, kimyasal maddelerin kullanımları sonucunda sentetik olarak elde edilebilmektedir. Antibiyotiğe dirençli mikroorganizmaların çoğalması nedeniyle antimikrobiyal peptidlerin üzerine yapılan araştırmalar artış göstermektedir. Elde edilen peptidlerin, zararlı mikroorganizmaların zarlarına ve hücre duvarlarına zarar vermek suretiyle etki ettikleri tespit edilmiştir. Bu biyoaktif peptidlerin ayrıca biyofilm oluşumunun engellenmesinde rol oynadıkları bilinmektedir (Souza et al., 2020). Biyoaktif peptidlerin insan sağlığı ve hastalıkların iyileştirilmesi amacıyla kullanılabilirlikleri üzerine yapılan çalışmalar umut vericidir. Peptidlerin fonksiyonlarını yapısal olarak içerdiği amino asitlerin dizilimi etkiler. Çoğunlukla 2-20 amino asit uzunluğunda olan peptidlerin güncel çalışmalar sonucunda daha uzun yapıya sahip oldukları da belirlenmiştir (Yada 2017). Enzimatik olarak hidroliz olan peptidler aktif hale gelir ve çeşitli fizyolojik fonksiyonlarda görev alırken, sentetik olarak üretilen peptidler eş sekansı ile birlikte iken normal şartlar altında inaktif halde bulunurlar (Okasha, 2020).

Biyoaktif peptidler sentetik ve doğal peptidler olmak üzere iki gruba ayrılır. Sentetik peptidler (ribozomal olmayan, nonribozomal) kapsamlı bir şekilde modifiye edilir ve esas olarak glikopeptidler, gramisidinler, basitrasinler ve polimiksinler içeren bakteri suşları tarafından üretilir. Doğal (ribozomal) peptidler, tüm mantar ve bakteri türleri tarafından üretilir ve bu organizmaların birincil savunma hattında önemli bir rol oynar (Saleem et al., 2007). Sentetik antimikrobiyal peptidler, sentetik biyoaktif peptidlere örnek olarak gösterilebilir. Antibiyotik kullanımının yaygınlaşması ve gereğinden fazla kullanımı sonucunda, dirençli bakterilerin gelişmesi nedeniyle daha etkin ve spesifik yapıya sahip antimikrobiyal ilaçlar araştırılmaktadır (Souza et al. 2020).

Biyoaktif peptidler canlıların fonksiyonları üzerine olumlu etkileri bulunan protein parçalarıdır. Antimikrobiyal, antiviral ve antitümör etkileri bulunmakla birlikte, hemen hemen tüm yaşam türleri tarafından sentezlenmektedir. Peptidler kolaylıkla sentezlenebildikleri gibi, pek çok hastalık karşısında istenen şekilde iyileştirici etkiyi elde etmek amacıyla optimize edilebilirler. Daha saf formda ve büyük miktarlarda üretim imkânı olduğundan, ticari üretimlerine olan ilgi artmaktadır. Bunun yanında, gıda paketleme tekniklerinde bozulmanın önlenmesi amacıyla peptidlerden faydalanılmaktadır (Perez et al. 2012).

Bilim insanları uzun süredir yaptıkları çalışmalarda, önemli vücut fonksiyonlarının yerine getirilmesinde görevli olan hormonların üzerinde peptidlerin düzenleyici etkilerinin bulunduğunu bildirmişlerdir. Antioksidan, antienflamatuar, antihipertansif, sitomoldülatör, antiobezite gibi önemli etkileri sebebiyle peptidlerin etki mekanizmaları araştırılmaktadır (Sánchez & Vázquez, 2017). Peptidler pek çok hastalığa karşı, kimyasal terapötiklerle kıyas edildiğinde daha efektif, seçici, güvenilir ve istenen terapötik etkilere sahip olarak sentezlenebilmektedir. Denizel organizmalardan özellikle alglerden elde edilen bazı peptidler Dünya Gıda ve Tarım Örgütü tarafından onaylanmıştır. Doğa, yaşayan türlerin çoğunda ifade edilen çeşitli peptidler sağlar. Evrimsel baskı ve doğal seçilim, bu peptitleri yüksek afiniteli reseptörlere bağlanmak üzere değişikliğe uğratmış ve optimize etmiştir. Deniz kökenli peptidler, basit solvent ekstraksiyon teknikleriyle ekstrakte edilebilir. Analitik tekniklerin ilerlemesi, doğal kaynaklardan saf peptidlerin elde edilmesine olanak sunmuştur. Ekstrakte edilen peptidler, antibakteriyel, antifungal, antidiyabetik ve antikanser aktivitenin yanı sıra, kardiyovasküler ve nörotoksin aktivite dahil olmak üzere çok çeşitli hastalıklar için olası terapötik ajanlar olarak değerlendirilmektedir. Deniz kökenli kaynaklar çok sayıda muhtemel peptid sağlamasına rağmen, elde edilen sadece birkaç deniz kökenli peptid farmasötik pazarına ulaşmıştır (Sable et al., 2017). Bu özelliklerinden dolayı terapötik amaçlı kullanılan peptidler üzerinde yapılan çalışmalar ve ticari üretimleri

artış göstermektedir (Mandal et al., 2023).

Biyoaktif Peptid Kaynakları

Biyoaktif peptidler, protein kaynaklarının enzimatik hidrolizi ile veya mikrobiyal kültürlerle kombinasyonlarının starter kültür olarak kullanıldığı fermentasyon yöntemi ile üretilebilmektedir (Korhonen and Pihlanto 2006). Biyoaktif peptidler bitkiler, hayvanlar ve mikroorganizmalardan elde edilebilmekte ve kaynağına göre farklı fonksiyonlar gösterebilmektedir. *İn-vivo* ve *in-vitro* çalışmalarda hayvansal veya bitkisel biyoaktif peptidlerin regülatör fonksiyonlarına sahip olduğu bilinmektedir. Kan basıncını düşürücü (Angiotensin Converting Enzyme, ACE inhibitörü), kolesterol düşürücü, antitrombotik, antioksidan ve antimikrobiyal etkiye sahip, mineral emilimini ve dolayısıyla biyoyararlanımı artıran, sitomodülatör ve immunomodülatör özellikte pek çok gıda kaynaklı biyoaktif peptid bulunmaktadır. Hipertansiyon, dünya nüfusunun büyük bir bölümünde görülen, kardiyovasküler hastalıklara sebep olan bir rahatsızlıktır. Anjiyotensin dönüştürücü enzim (ACE), dipeptid yapıda bir karboksipeptidazdır ve anjiyotensinin vazokonsrüktör anjiyotensine dönüşümünü katalizler. Bu işlevi ile kan basıncının ayarlanması ve memelilerde tuz dengesinin sağlanmasında görev alır. İlk olarak yılan zehrinde tespit edilen ACE inhibitörü peptidler, daha sonra çeşitli gıdaların özellikle süt, balık ve etten izole edilmiştir. ACE inhibitörü peptidler genellikle kısa zincirli yapıya sahiptir (Ondetti et al. 1977; Fuglsang et al. 2003). Gıda kaynaklı ticari üretimi olan peptidlerin başında süt ve süt ürünlerinden elde edilen peptidler gelmektedir. (Hartmann & Meisel, 2007). En çok çalışılan peptidler laktoferrisinlerdir ve sığır ve insan laktoferrinlerinden türevlenirler. Antimikrobiyal peptidler Gram pozitif ve Gram negatif bakteriler üzerine, mayalar ve funguslar üzerinde etkilidirler (Rizzello et al. 2005; McCann et al. 2006).

Normal büyüme ve bakım için mevcut protein içeriğini etkileyen beslenme gereksinimlerinin ötesinde fizyolojik öneme sahip, biyolojik olarak aktif gıda proteinlerinin birçok örneği bulunmaktadır. Çeşitli gıda protein kaynaklarından proteaz aktivitesi ile türetilen birçok fizyolojik olarak aktif peptid vardır; ancak yapısal özellikler ile fonksiyonel aktiviteler arasındaki ilişkiler tam olarak açıklanamamıştır. Birçok biyoaktif peptid, prolin, lizin veya arginin gruplarına ek olarak hidrofobik amino asit gruplarına sahip olan nispeten kısa bir peptit kalıntı uzunluğu (örneğin 2-9 amino asit) içeren ortak yapısal özelliklere sahiptir (Kitts and Weiler 2003). Aşağıdaki tabloda gıdalardan elde edilen biyoaktif peptidlerden bazıları verilmiştir (Tablo 1).

Tablo 1. *Gıda türevli bazı biyoaktif peptidler (Hartmann & Meisel, 2007)*

Etki şekli	Kökeni	Yazdırılan proteinler	Referans
ACE inhibitörü	Soya	Soya proteini	Kodera and Nio (2006)
	Balık	Balık kas proteini	Nagai et al. (2006)
	Et	Et kas proteini	Vercruysse et al. (2005)
	Süt	α-LA, β-LG, α-, β-CN	Murray and FitzGerald (2007)
	Yumurta	Ovotransferrin	
		Ovalbumin	Mizushima et al. (2004)
			Lee et al. (2005)
Sitomodülatör	Süt	α-, β-CN	Kampa et al. (1997)
Antimikrobiyal	Yumurta	Ovotransferrin	Mine and Kovac-Nolan (2006)
		Lizozim	
	Süt	Laktoferrin	McCann et al. (2006)
Antitrombotik	Süt	α-CN	Chabance et al. (1995)
Mineral bağlama	Süt	α-, β-CN	Walker et al. (2006)
Immunomodülatör	Pirinç	Pirinç albümini	Takahashi et al. (1994)
	Yumurta	Ovalbumin	Mine and Kovac-Nolan (2006)
	Süt	α-LA, β-LG, α-, β-CN	
	Buğday	Buğday gluteni	Meisel (2005)
			Horiguchi et al. (2005)
Hipokolesterolemik	Soya	Glisinin	Wang and de Mejia (2005)
	Süt	β-LG	Nagaoka et al. (2001)
Antioksidan	Balık	Sardin kası	Erdmann et al. (2006)
	Buğday	Buğday germ proteini	Zhu et al. (2006)
	Süt	α-LA, β-LG	Hernandez-Ledesma et al. (2005)

Hayvansal kaynaklardan sonra bitkisel biyoaktif peptidler başlıca peptid kaynakları olarak bilinmektedir. Buğday (Kumagai 2010), soya (Meinschmidt et al. 2016), pirinç (Selamassakul et al. 2016), kabak, sorgum (Moller et al. 2008) gibi bitkilerle birlikte deniz bitkileri de bitkisel biyoaktif peptid üretiminde kullanılmaktadır (Zhang et al. 2021).

Kronik böbrek sorunlarının sonucunda oluşan diyabet, hipertansiyon gibi kronik rahatsızlıkların yol açtığı komplikasyonlar sonucunda yüksek oranda ölümler gerçekleşmektedir. İnsan sindirim sisteminde bulunan mikrobiyotanın patojenik değişimler geçirmesi nedeniyle üremik toksinlerin ki, başlıca olarak indoksil sülfat, p-kresol sülfat ve trimetilamin-N-oksit oluşur. Diyetle birlikte alınan lifler (oligosakkaritler ve polisakkaritler), polifenoller (kurkumin, antosiyaninler, kateşinler ve resveratrol vb.) ve biyoaktif peptidler sindirim sisteminde ve bağırsaklarda bulunan mikrobiyota için iyileştirici etki göstererek, bağırsak-böbrek ekseninde kronik böbrek yetmezliğinin önlenmesinde veya rehabilitasyonunda olumlu etki gösterir (Jian et al., 2023).

Denizde ve tatlı sularda yaşayan balıklar üzerine yapılan çalışmalarda, terapötik ve medikal uygulamalarda sentetik biyoaktif peptidlerin elde edi-

lebilmesi amacıyla bu canlıların moleküler yapıları araştırılmıştır. Balıklardan, kronik rahatsızlıklardan olan obezite, yüksek tansiyon ve diyabet için iyileştirici etkileri bulunan biyoaktif peptidler elde edilmiştir (Prakash Nirmal et al., 2023).

Bir diğer biyoaktif peptid kaynağı böceklerdir. Son yıllarda yapılan araştırmalar sonucunda biyoaktif peptidlerin insanlar, çiftlik hayvanları ve bitkilerin gelişimleri üzerine faydalı etkilere sebep oldukları tespit edilmiştir. Çiftlik hayvanlarının ve ticari değeri olan bitkilerin, patojen organizmalar karşısında biyoaktif peptidlerin koruyucu etki sağladıkları tespit edilmiştir ve böceklerin sahip oldukları peptidler üzerine çalışmalar yapılmaktadır. Yenilebilir böcek türlerinden biyoaktif peptid tanılanması üzerine yapılan araştırmalar, antioksidan, anti anjiyotensin, antilipoksijenaz, anti obezite gibi karakteristiklere sahip peptidlerin elde edildiğini göstermektedir (Quah et al., 2023). Artan dünya nüfusuna karşı mevcut besin kaynaklarının yetersiz kalması ve pandemi, kuraklık, küresel ısınma gibi çevresel kısıtlayıcı şartların oluşması nedeniyle alternatif besin kaynaklarına ilgi artmıştır (Taşar ve Canlı Taşar, 2022). Protein içeriği bakımından yüksek seviyeli besleyici özelliği bulunan yenilebilir böcekler, dünyanın farklı bölgelerinde, özellikle Asya kıtasında bulunan ülkelerde uzun yıllardan beri gıda katkı maddesi, çerez veya sokak yemekleri şeklinde yaygın olarak tüketilmektedir (Canli et al., 2013; Canlı Taşar & Taşar, 2023; Taşar, 2022a). Bununla birlikte yapılan çalışmalarda, farklı türlerden elde edilen proteinlerin insan diyetine uygunluğu, toksisite, alerjik etki gibi biyolojik olarak uyumlulukları araştırılmaktadır (Pan et al., 2022). Ülkemizin çeşitli illerinden toplanan bazı sucul böcek türlerinin de (Aykut et al., 2016, 2018, 2021; Aykut & Taşar 2018; Erman et al., 2018; Taşar, 2022b; Taşar, 2018a,b,c; Taşar, 2017a,b; Taşar, 2014a,b,c; Taşar & Mascagni 2014) yüksek protein ve değerli peptid içeriğine sahip olup-olmadığına dair çalışmaların yapılması düşünülmektedir.

Opioid peptidler

Bu grupta bulunan peptidler 1970'li yılların sonlarına doğru ilk olarak bulunan gıda türevli, "ekzorfinler" olarak adlandırılan peptidlerdir (Ziodrou et al. 1979). Yapısal olarak endorfinler ve enkefalinlerle benzerlik göstererek, opioid reseptörlerle iletişim kurarlar. Farmakolojik etki alanları morfin ve diğer uyuşturucu etkiye sahip agonist ilaçlara benzemektedir. Memelilerde boldur (Beaumont 1983, Lewis et al. 1983). Opioid peptidler, endorfinler, enkefalinler ve dinorfinler olmak üzere üç gruba ayrılır (Çakıcı ve ark. 1987).

Opioid peptidlerin hipertansiyon üzerine etkileri araştırılmaktadır. Kronik hipertansif durumlarda feokromasitoma olgularında opioid peptidlerin düşük miktarda olduğu, nadiren hipertansif krizi geçiren hastalarda

ise bu peptidlerin miktarının yüksek olduğu tespit edilmiştir (Petersdorff et al. 1984). Biyoaktif peptitler ayrıca sindirim peptidazlarının etkisine karşı dirençlidir. Anjiyotensin I dönüştürücü enzim (ACE) inhibitörleri olarak bilinen antihipertansif peptidler süt, mısır ve balık protein kaynaklarından elde edilmiştir. Opioid aktiviteleri olan peptitler, pepsin ile sindirimin ardından buğday glüteninden veya kazeinden elde edilir. Buğday ve süt gibi gıda proteinlerinden türetilen ekzorfinler veya opioid peptidler (örn. eksojen kaynaklar), amino terminalinde veya biyoaktif bölgede bulunan bir tirozin kalıntısı ile endojen opioid peptidlere benzer bir yapıya sahiptir. Pirinç ve soya fasulyesi proteinlerinin triptik hidrolizatlarından türetilen immünomodülatör peptidler, spesifik olmayan bağışıklık savunma sistemlerini tetikleyen süperoksit anyonlarını (reaktif oksijen türleri, ROS) uyarma görevi görür. Esansiyel yağ asitlerinin peroksidasyonunu önleyen antioksidan özellikler, süt proteinlerinden türetilen peptidler için de gösterilmiştir. Biyoaktif peptitleri izole etmek ve saflaştırmak için tuzla ayırma veya çözücü ekstraksiyonu kullanma yöntemlerinin yerini alabilecek seçici kolon kromatografisi yöntemleri geliştirmek için çok çaba sarf edilmiştir. Buradaki gelişmeler, biyoaktif peptidlerin minimum yıkımla geri kazanılmasını sağlayacak ve böylece bu aktif peptidlerin fonksiyonel gıdaya veya spesifik nutrasötik uygulamalara geri döndürülerek kullanılmasına olanak sağlayacaktır (Kitts and Weiler 2003).

Peptid Üretiminde Kullanılan Yöntemler ve Karşılaşılan Problemler

Peptidlerin üretimi biyolojik aktivite sonucunda başlayan enzimatik sindirim ile başlar. Sonuçta oluşan peptidler hidrolizat şeklinde olabildiği gibi saf olarak da sentezlenebilirler (Lafarga et al. 2016). Saflaştırma teknikleri, zaman alıcı, biyoinformatik içeren, kantitatif yapı tabanlı ve biyoaktif peptidlerin miktarının tahmin edildiği uzun bir seri işlemi içermektedir (Gu et al. 2011).

Biyoaktif peptidlerin hazırlanması esnasında proteinin kapsamı önemlidir. Enzimatik reaksiyonlar sonucunda oluşan uzun süreli hidrolizasyon aşamaları, biyoaktivite fonksiyonlarında azalmaya veya kayıplara neden olur. Yabanil suşlarla yapılan çalışmalarda yeniden üretim durumu garanti edilemeyeceği için biyoaktif peptidlerin miktarlarının önceden belirlenmesi pek mümkün değildir (Daliri et al. 2018). Hidroliz üzerine, ağırlıklı olarak lösin, prolin, fenilalanin ve tirozin gibi hidrofobik amino asitler içeren düşük moleküler ağırlıklı peptitlerin oluşumu nedeniyle nihai ürüne acı bir tat verilir ve bu acılığın giderilmesi için farklı teknikler geliştirilmiştir (Meinlschmidt et al. 2016). Diğer yandan yüksek basınçlı pişirme yönteminin ekzo ve endo peptidazların kombinasyonu yardımıyla, esansiyel amino asitlerin kaybının önlendiği bildirilmiştir (Nishiwaki et al. 2002;

Hou et al. 2011).

Yüksek kimyasal yapıya sahip olan protein sentezi kompleks, zaman alıcı ve pahalı bir süreçtir (Gogineni and Hamann 2018). Kısa yarı ömürleri (<2 saat) ve düşük maksimum plazma konsantrasyonları nedeniyle, terapötik peptitlerin oral alımdan sonra insan kanındaki biyoyararlanımını test etmek büyük bir zorluk teşkil etmekte ve bu nedenle bu peptitlerin artan biyoyararlanımı ile etkili taşınımasını geliştirmek için yeni stratejiler gerektirmektedir. Bu nedenle yapılan *in vitro* çalışmalar artış göstermektedir (Uhlig et al. 2014). Yapılan araştırmalar sonucunda peptidlerin korunması amacıyla prob kuyruk kullanımı (Kaspar and Reichert 2013), laktam köprüleri (Houston et al. 1996) ile veya peptid sekanslarının sabitlenmesi veya kesilmesi yolları kullanılmaktadır (Timmerman et al. 2007).

Öte yandan, peptidlerin uzun ömürlü olmalarını sağlamak amacıyla albümin bağlayıcı peptit elemanlarının peptit omurgasına eklenmesi, albümin bağlayıcı antikor fragmanlarına konjugasyonu gibi yöntemler kullanılmaktadır (Knudsen 2010). Karşılaşılan diğer bir zorluk da işleyiş şeklidir. Sindirim enzimlerinin oral formülasyonlar yoluyla parçalanması her zaman mümkün olmamaktadır. Sindirim enzimleri kümelenme eğilimindedirler ve aynı zamanda düşük zar geçirgenliğine sahiptirler. Nazal sprey, pulmoner, intradermal enjeksiyon ve topikal uygulamalar gibi alternatif sistemler ve ayrıca implante edilebilir cihazlar yoluyla uygulama, peptitlerin daha yüksek etkinlik ve kabul edilebilir uyum ile uygun bir ilaç formu elde etmesine yardımcı olabilir (Mandal et al. 2023).

Enzimatik Hidroliz ve Mikrobiyal Fermantasyon Yoluyla Peptid Üretimi

Mikrobiyal peptidlerin üretiminde fermantasyon yöntemi uygulanır. Bu amaçla, mikroorganizmaların üretim ortamının optimizasyonun gerçekleştirilebilmesi için, besiyeri pH değeri, yetişme sıcaklığı, havalandırma, çalkalama hızı gibi parametreler kullanılarak kısa sürede yüksek verimli ürün üretimi amaçlanır. Proteaz A, pepsin, tripsin, papin, pankreatin gibi sindirimde kullanılan enzimlerden yararlanılarak peptidlerin üretimleri gerçekleştirilir (Lassoued et al. 2015).

Proteolizisin yanı sıra, enzimler veya kimyasal parçalama ile mikrobiyal suşların salgıladığı proteazlar protein içeren substratları parçalarlar. Fermentasyon tekniği, kimyasal olarak gerçekleştirilen asit/baz tepkimelerine göre daha tercih edilebilir özelliktedir. Esansiyel amino asitlerin kaybı ve çevre kirliliği kimyasal parçalanmanın sebep olduğu başlıca dezavantajlardır Tadesse and Emire 2020). Fermantasyon tekniği, farklı protein kaynaklarından, özellikle sınırlı tüketime sahip olanlardan ve/veya biyolojik atıklardan biyoaktif peptidler hazırlamak için umut verici bir yöntem-

dir. Bakteriler, farklı katalitik proteolitik enzim türlerinin potansiyel üretim kaynağı olarak hizmet eder. Fermantasyon yoluyla biyoaktif peptidler elde etmek için kullanılan en yaygın cins *Lactobacillus* sp. ile *Bacillus* sp.'dir. Mikrobiyal çeşitlilik üzerine kapsamlı araştırmalar, kendine özgü biyokimyasal özelliklere sahip çeşitli farklı peptidazların keşfedilmesiyle sonuçlanmıştır (Elfahri et al. 2016, Rai et al. 2016, Sanjukta and Rai 2016).

Özellikle bakteriler, filamentöz funguslar ve mayalar biyoaktif peptidlerin üretiminde etkin şekilde kullanılmaktadır (Garcia-Tejedor et al. 2015; Giri et al. 2014, Lima et al. 2015). Diğer yandan, bakteri ve maya veya bakteri ve bakteri birlikte üretimi (Co-cultivation) ile peptid üretimlerinin arttığı bildirilmiştir (Bengoa et al. 2019). Fermentasyon sonucu elde edilen süpernatan içerisinde bulunan daha kısa yapılı peptid sekanslarının proteolitik enzimlerle hidroliz edilebileceği bildirilmiştir. Bu tür yöntemlerle üretilen peptitlerin, terapötik faydalarla birlikte daha yüksek düzeyde biyoaktivite sergiledikleri bildirilmiştir (Babini et al. 2017).

Peptidlerin Kullanıldığı Çeşitli Uygulamalar

Hesaplamalı yaklaşımlar, herhangi bir ana proteinden biyoaktif olduğu bildirilen herhangi bir spesifik amino asit dizisine ilişkin bilgilere erişmeyi mümkün kılan birçok protein dizisi bilgisi içeren veritabanlarını kullanır. Bilgisayar destekli bu çalışmalarda yeni protein kaynaklarından veya kullanıcı tanımlı sekanslardan elde edilen peptidlerin proteolitik aksiyonları simüle edilmektedir. Bu uygulamanın yardımıyla, bilinmeyen veya benzemeyen protein kaynaklarından bilinen peptidlerin eldesi mümkün olmaktadır. Yapılan araştırmalarda biyoaktif peptidlerin *in vitro* ve *in vivo* çalışmalarda tanımlanmasında bu yöntemin kullanıldığı bildirilmiştir (O'Brien et al. 2019; Tu et al. 2018).

Peptidlerin biyoaktivitesini ortaya çıkarmak için sadece bilgisayar destekli hesaplama yöntemlerinin kullanılması basit görünmektedir, ancak enzimatik sindirim simülasyonundan tahmin edilen tüm peptitler aktif olmayabilir veya *in vitro* veya *in vivo* test edildikten sonra istenen aktiviteyi sergileyemeyebilir. Bu nedenle birçok araştırmacı, test edilen kaynaktan daha az konsantre ancak güçlü peptitleri belirlemek için HPLC-MS verilerini farklı veritabanlarıyla karşılaştırır. Bu şekilde bilgisayar destekli uygulamalarla hibrit uygulamalar yaygın bir şekilde kullanılmaktadır (Sagardia et al. 2013).

Mikrobiyal Peptidlerin Terapötik Özellikleri

Uzun yıllardan beri biyolojik peptidler ilaç olarak kullanılmaktadır. Stabilitesi, spesifitesi ve nanomolar konsantrasyonlardaki fonksiyonlarına erişilebilirlik özellikleri nedeniyle klinik uygulamalarda biyoaktif peptid-

ler sıklıkla kullanılır (Gogineni and Hamann 2018). Amino asit kompozisyonu, hidrofobik ve hidrofilik karakteristikler N- ve C- terminal amino asit çeşidi, peptidin uzunluğu ve amino asit kapasitesi gibi özellikler bir peptidin karakteristik yapısını oluşturur (Cotter et al. 2013). Örneğin, düşük moleküler ağırlıklı peptidler (<1kDa), buğday proteinlerinin hidrolizasyonunda daha uzun peptid fraksiyonlarına göre önemli bir Fe+2 iyonunu şelatlama (kenetleme, bağlama) aktivitesi göstermektedir. Diğer yandan kasein hidrolizatlarının >3000kDa büyük fraksiyonlarından ortaya çıkan peptidlerin, *Lactobacillus bulgaricus* ve *Streptococcus thermophilus* türü bakterilerin prebiyotik etkisini zorlaştırdığı bildirilmiştir. Bir peptid sadece, fizyolojik düzeyde faydalı, ölçülebilir bir biyolojik etki sağladığında, biyoaktif olarak kabul edilir. Bununla birlikte, herhangi bir zararlı etki göstermemesi beklenmektedir (O'Loughlin et al. 2014; Zhang et al. 2011; Moller et al. 2008).

Prebiyotik ajanlar, sayısız probiyotik organizmanın gelişimini ve hayatta kalmasını düzenler (Yu et al. 2016). Mikroorganizmalardan elde edilen çeşitli biyoaktif peptidler ve proteinler bu etkilerini probiyotikler üzerinde göstermiştir (Ibrahim and Bezkorovainy 1994; Oda et al. 2013). Seçilmiş *Lactobacillus helveticus* suşları tarafından sütten salınan biyoaktif peptitler, sitokinlerin üretimi üzerinde pro- ve anti-inflamatuar etkilere sahip uyarıcı etki yaparak immünomodülatör etkilere neden olur (Elfahri et al. 2014). *Bacillus* sp. P7 tarafından sığır sütünden elde edilen hidrolizatlardaki biyoaktif peptidlerin antioksidan aktivite gösterdiği ve *Bacillus cereus, Corynebacterium fimi, Aspergillus fumigatus* ve *Penicillium expansum* üzerine antimikrobiyal aktivite gösterdiği bildirilmiştir (Correa et al. 2011).

Kızıl Deniz'de 1500-2500 m derinliklrden izole edilen *Chromohalobacter salexigens*, *Halomonas meridiana* (P3-37B), *Chromohalobacter israelensis* (K18), ve *Idiomarina loihiensis* (P3-37C) mikrobiyal ekstraklarında yapılan incelemeler neticesinde, *C. salexigens* ekstraktının apoptozu teşvik ettiği ve test edilen kanser hücrelerinin>%70 oranında yüksek apoptoz gösterdiği bildirilmiştir. Yapılan bir başka çalışmada 137 farklı laktobasil bakterisi izole edilmiş ve proteolitik aktiviteleri ile antibakteriyel aktiviteleri izlenmiştir. Sonuç olarak, elde edilen antibakteriyel aktivitelerin endüstride yaygın şekilde kullanıldığı bildirilmiştir (Sagar et al. 2013).

Fungal kaynaklardan elde edilen peptidlerin genellikle sitotoksik, antimikrobiyal ve antiviral aktiviteleri, anti-enflamatuvar özellikleri, antidiyabetik fonksiyonları ve lipid azaltıcı aktiviteleri araştırılmaktadır (Youssef et al. 2019). Deniz kaynaklı fungal mikroorganizmaların ürettiği biyoaktif peptidler ve proteinlerinin, sentetik yapıdaki ilaçlara oranla minimal insan toksisitesine ve yan etkilere sebep olduğu bildirilmiştir. Deniz kökenli (marine) funguslardan olan *Aspergillus terreus* türü fungusun

ürettiği «terrelumamid» adı verilen lumazin peptidlerinin H1N1 ve H3N2 domuz gribi virüsleri üzerine inhibitör etki oluşturduğu belirtilmiştir. Yine deniz kökenli bir fungus olan *Talaromyces* sp. Tarafından üretilen talarolid A-D peptidinin, antibakteriyel aktiviteye sahip olduğu bilinmektedir (You et al. 2015).

Mayalar, proteinden zengin yapıya sahip oldukları için biyoaktif peptid üretimi açısından önemli bir kaynaktır. Proteolitik aktiviteleri ile antimikrobiyal, aktioksidan ve ACE-inhibitör etkiye sahip peptidleri vardır (Mirzaei et al. 2021). Şeker kamışının ekmek mayası *Saccharomyces cerevisiae* tarafından enzimatik hidrolizi sonucunda (ticari adı Viscozyme) ve antianemik etkiye sahip demir bağlayıcı peptidlerin üretimi gerçekleştirilmektedir (De la Hoz et al. 2014).

1. Bakteriyel Peptidler

Prebiyotik ajanlar çeşitli probiyotik organizmanın gelişimini düzenler ve biyoaktif peptidlerle birlikte fonksiyonel etkilere sebep olur (Yu et al. 2016). Seçilmiş *Lactobacillus helveticus* suşları tarafından sütten salınan biyoaktif peptitler, sitokinlerin üretimi üzerinde pro- ve anti-inflamatuar etkilere sahip uyarıcı etki yaparak immünomodülatör etkilere neden olur (Elfahri et al. 2014).

Bakteriyosinler, benzer veya yakından ilişkili bakteri suşlarının büyümesini engelleyen, bakteriler tarafından üretilen ribozomal olarak sentezlenmiş antibakteriyel peptitlerdir. Çok çeşitli bakterilerden elde edilen çok sayıda bakteriyosin keşfedilmiş ve bunların farklı yapıları rapor edilmiştir. Bakteriyosinler, gıda ve ilaç endüstrilerinde gıda bozulmasını ve patojenik bakteri üremesini önlemek için etkili bir bileşik olarak kabul edilir. Bununla birlikte, biyosentezlerinin aydınlatılması, bakteriyosin kontrollü gen ekspresyon sistemlerinin ve bir bakteriyosin sınıfı olan lantibiyotiklerin biyosentetik enzimlerinin yeni peptidler tasarlama araçları olarak kullanılmasına yol açmıştır (Nishie et al. 2012). Klasik propionibakteriler, biyolojik aktiviteleri eşdeğer olmayan ve halka açık veritabanlarında homolog sekansları olmayan, genetik olarak benzersiz antimikrobiyal peptidler üretir. Propionisin T1 peptidi *Propionibacterium freudenreichii* dışında test edilen tüm propionibakteri türlerine karşı bakterisidal etki gösteren gerçek bir bakteriyosin örneğidir. Propionisin F, tür içi bir bakterisidal inhibisyon spektrumu sergileyen negatif yüklü bir bakteriyosindir (Faye et al. 2011).

Antibiyotiklerin geliştirilmesinde uygulanan mevcut yöntemler, antimikrobiyal direncin artmasıyla yetersiz kaldığından, bu zorluğun aşılması amacıyla yeni ve yenilikçi teknolojiler gereklidir. Bu bağlamda biyoaktif peptidlerin üzerine yapılan araştırmalar büyük önem taşımaktadır. Yapılan bir çalışmada, *Enterococcus faecalis* pPD1'den bakteriyosin Bac-21'in

tanımlanması yoluyla bakteri kaynaklı biyoaktif peptitlerin tespiti üzerine sonuçlar elde edilmiştir. Bakteri aşılanmış agar difüzyon deneylerinin uygulanması ve peptit kitaplıklarının isteğe bağlı sindirimi dahil olmak üzere bazı modifikasyonları yapılmıştır (Kirkpatrick et al. 2018). Farklı bir çalışmada bildirildiğine göre, Kızıl Deniz'de 1500-2500 m derinliklerden izole edilen *Chromohalobacter salexigens, Halomonas meridiana* (P3-37B), *Chromohalobacter israelensis* (K18), ve *Idiomarina loihiensis* (P3-37C) mikrobiyal ekstraklarında yapılan incelemeler neticesinde, *C. salexigens* ekstraktının apoptozu teşvik ettiği ve test edilen kanser hücrelerinin >%70 oranında yüksek apoptoz göstermiştir (Sagar et al. 2013). Bakterilerde mevcut antimikrobiyal moleküllere karşı direnç artmasıyla yeni antimikrobiyal moleküller geliştirilmekte ve araştırılmaktadır. Yeni nesil antibiyotik adayları olabilecek antimikrobiyal peptidler bu nedenle büyük önem taşımaktadır. Ökaryotlarda, bağışıklık sisteminin bir parçası olarak sentezlenirler (Yazici et al. 2018).

Staphylococcus warneri KL-1 ile yapılan bir araştırmada, çevresel parametrelerin antibakteriyel peptid üretimi üzerine etkileri incelenmiştir. Bu amaçla, bakterinin büyüme hızı ve besiyerinin havalandırma derecesinin peptid üretimi üzerine etkili olduğu bildirilmiştir. En yüksek antibakteriyel aktivitenin, beslemeli kesikli kültür ile gerçekleştirilen üretim sonucu elde edildiği tespit edilmiştir. Oluşan peptid molekülü üç boyutlu olarak incelenmiş ve moleküler yapısı gösterilmiştir. Sonuç olarak elde edilen peptidin bir Sınıf I lantibiyotik olduğu bulunmuştur (Polyudova et al. 2017).

Laktik asit bakterilerinden bakteriyosin üretimi, farklı endüstriyel uygulamalarda suşun faydasını arttırdığı için önemli olarak kabul edilmiştir. Bakteriyosin üreten laktik asit bakterilerinin, kendilerini hedef mikrobiyal nişe kolayca yerleştirebildikleri ve bu şekilde gıda fermantasyonu ve/veya probiyotik suşlarında daha etkili başlatıcı kültürler oldukları için daha yüksek bakteri uygunluğuna sahip oldukları düşünülmektedir. Yeni suşların ortak noktası, enerjilerini tüketmeden çok sayıda bakteriyosin üretme gibi olağanüstü bir başarıya ulaşmalarını sağlayan biyosentetik süreçteki bazı elementlerin dikkate değer bir şekilde paylaşılmasıdır. Biyosentetik enzimlerin aynı kökenli bakteriyosinlere özgü olduğu şeklindeki yaygın anlayışın aksine, çoklu bakteriyosin üreten suşlar, çoklu bakteriyosinleri arasında ortak biyosentetik elementler kullanır. Çekirdek algılayan üç bileşenli düzenleyici sistem, bakteriyosin olgunlaşması ve taşıma mekanizmaları, bu suşlardaki çoklu bakteriyosinler arasında paylaşılır. Bununla birlikte, yeni suşların uygulama potansiyellerinin yüksek olmaları sonucunda, potansiyel virülansları ve patojeniteleri açısından güvenliklerinin kapsamlı genotipik karakterizasyon yoluyla doğrulanması gerekir (Perez et al. 2022).

Çoklu ilaç kullanımında ortaya çıkan dirençli bakterilerin sebep olduğu enfeksiyonların tedavisinde uygulanan yöntemlerden olan antibiyofilm ve antibakteriyel bileşiklerinin izolasyonu üzerine yapılan bir araştırmada, topraktan izole edilen bakteriler tarafından sentezlenen pigmentlerin, antibakteriyel ve antibiyofilm aktiviteleri test edilmiştir. Bir Gram pozitif ve aerobik bakteri cinsi olan *Rhodococcus* sp. tarafınan üretilen pigmentlerin, patojenik bakteri türlerinden olan *P. aeruginosa* ve *E. coli* karşısında kuvvetli bir antibakteriyel ajan olarak etki gösterdiği bildirilmiştir (Cobanoglu and Yazici 2022).

2. Fungal peptidler

Fungal kaynaklardan elde edilen peptidlerin genellikle sitotoksik, antimikrobiyal ve antiviral aktiviteleri, anti-enflamatuvar özellikleri, antidiyabetik fonksiyonları ve lipid azaltıcı aktiviteleri araştırılmaktadır. Deniz kaynaklı fungal mikroorganizmaların ürettiği biyoaktif peptidler ve proteinlerinin, sentetik yapıdaki ilaçlara oranla minimal insan toksisitesine ve yan etkilere sebep olduğu bildirilmiştir (Youssef et al. 2019).

Kronik rahatsızlıkların başında gelen hipertansiyonun olumsuz etkilerinin azaltılması için diyet destekli yaşaklaşımlar sağlıklı bir hayat için kaçınılmazdır. Yapılan bir çalışmada, kuru kütlesinin %40'ı biyoaktif peptidlere hidrolize edilebilen kullanılmış bira mayasının, ACE inhibisyonu ve antioksidan aktivitesi hipertansif deney hayvanları üzerinde in vivo olarak araştırılmıştır. Elde edilen sonuçlar doğrultusunda, maya ekstraktının, antioksidan etki ile birlikte hipertansiyonun yönetimi ve tedavisi için nutrasötik veya fonksiyonel bir gıda bileşeni olarak potansiyel kullanımı vurgulanmıştır (Amorim et al. 2019).

Fungal peptidlerle ilgili diğer bir araştırmada, iki yeni lumazin içeren peptit olan Terrelumamides A (1) ve B (2), denizden türetilen *Aspergillus terreus* mantarının kültür sıvısından izole edilerek; kombine spektroskopik ve kimyasal analizlerin sonuçlarından, bu bileşiklerin yapılarının, 1-metillumazin-6-karboksilik asit, bir amino asit kalıntısı ve antranilik asit metil esterin peptit bağlarıyla bağlı doğrusal düzenekleri olduğu belirlenmiştir. Bu yeni bileşiklerin, insan kemik iliği mezenkimal kök hücreleri kullanılarak bir adipogenez modelinde değerlendirilen insülin duyarlılığını iyileştirerek farmakolojik aktivite sergilediği tespit edilmiştir. Ek olarak bileşikler, DNA'ya bağlandıklarında flüoresans değişiklikleri sergilediler ve bu da onların DNA dizisi tanımaya yönelik potansiyel uygulamalarını göstermiştir. Deniz kökenli (marine) funguslardan olan *Aspergillus terreus* türü fungusun ürettiği «terrelumamid» adı verilen lumazin peptidlerinin H1N1 ve H3N2 virüsleri üzerine inhibitör etki oluşturduğu belirtilmiştir (You et al. 2015).

Yapılan bir çalışmada bir Avustralya deniz tunikatından türetilen mantar, *Talaromyces* sp. CMB-TU011, kapsamlı bir şekilde N-metillenmiş 11-12 kalıntılı yeni bir lineer peptid sınıfı, talaropeptidler A-D (2-5) üretmeye yönelik koşulları ortaya çıkarmak için UHPLC-QTOF profiliyle desteklenen bir analitik mikrobiyoreaktör (MATRIX) yetiştirme programına tabi tutulmuştur. Mutlak konfigürasyonlar dahil olmak üzere 2-5 için yapılar, ayrıntılı spektroskopik ve kimyasal analizlerinin bir kombinasyonu ile belirlenerek, plazma stabilitesinin yanı sıra antibakteriyel, antifungal ve hücre sitotoksisitesi dahil olmak üzere 2-5'in biyolojik özellikleri bildirilmiştir. Talaropeptid mega ribozomal olmayan peptit sentetazı (NRPS), mantardan türetilen immünosüpresan siklosporin (11 kalıntılı, geniş ölçüde N-metillenmiş siklik peptit) için olandan sadece ikinci boyut olarak tarif edilmektedir (Dewapriya et al. 2018).

Fungusların farklı türlerinin antibiyofilm polipeptid üretim kapasitelerinin araştırılması amacıyla yapılan bir çalışmada, tarama amacıyla 120 adet fungus topraktan izole edilmiştir. İzolatlar arasında en yüksek antibiyofilm aktivitesine sahip olan türün *Aspergillus tubingensis* A01 olduğu tespit edilerek, elde edilen proteinin *S. aureus*'a karşı antimikrobiyal ve antibiyofilm aktivitesi gösterdiği kanıtlanmıştır. Çalışmadan elde edilen sonuçlar doğrultusunda, sitotoksisite eksikliği ile birlikte astusinin antimikrobiyal ve antibiyofilm aktivitesinin, onu tıpta uygulama için bir alternatif haline getirdiğini göstermiştir. Antibiyotiklere karşı mikroorganizmalar tarafından oluşturulan direnç, küresel bir sorundur ve antibiyotiğe dirençli bakterilerin ortaya çıkması mevcut tedavi yaklaşımlarının terapötik etkilerini azaltmaktadır. Bu bağlamda, antimikrobiyal peptitler, bakteriyel enfeksiyonlarla, özellikle biyofilmle ilişkili enfeksiyonlarla mücadelede potansiyel ajanlar olarak öne çıkmaktadır (Yazici et al. 2021).

Ribozomal olarak sentezlenmiş ve posttranslasyonel olarak modifiye edilmiş peptitler, güçlü biyolojik aktivitelere sahip doğal ürünlerdir. Bu peptidlerin çekirdek iskeleleri, proteinojenik amino asitlerden oluşmasına rağmen, öncü peptitlerin çeviri sonrası modifikasyon yöntemleri ile yapısal çeşitlilik üretilir. Amatoksinler ve omfalotinler, Basidiomycota mantarları tarafından üretilir. Bu bileşiklerin biyosentezinde sırasıyla prolil oligopeptidaz homologları tarafından makrosiklizasyon ve omurga amidlerinin N-metilasyonları karakterize edilmiştir. Ustiloksinler ve ilgili bileşikler, karakteristik makrosiklik eterlere sahip başka bir gruptur (Ozaki et al. 2023).

Yapılan bir çalışmada, yeni bir mantar kökenli ribozomal olmayan peptit-poliketid hibrit sentaz, yani CogA, *Cordyceps gunnii* mantarından genom madenciliği ile keşfedilmiştir. 4-hidroksil 2-pirolidinon alkaloidi (1) enzim katalizli olmayan N-1-C-2 kapatma yoluyla sentezleme yeteneği, *Aspergillus nidulans*'ta heterolog ekspresyonu ile doğrulanmıştır. Floro

ikameli 2-pirolidinon alka-loid analoglarının (4 ve 5) daha ileri düzeyde tasarlanmış biyosentezi de in vivo olarak gerçekleştirilmiştir (Rao et al. 2023).

Mayalar, proteinden zengin yapıya sahip oldukları için biyoaktif peptid üretimi açısından önemli bir kaynaktır. Yapılan araştırmalardan elde edilen bilgiler doğrultusunda maya orijinli peptidlerin, antioksidan, ACE inhibitörü, antidiyabetik, ayrıca kronik hastalıkların önlenmesi ve bağışıklık tepkilerinin sağlanması gibi fonksiyonlardan dolayı oldukça etkin bir yapıda olduğu bilinmektedir. Ayrıca maya hücrelerinin, fermantasyon süreçleri sırasındaki proteolitik aktiviteleri nedeniyle biyoaktif peptitlerin oluşumuna ve büyüme sırasında antimikrobiyal peptitlerin salınmasına katkıda bulunduğu bir gerçektir. Maya ekstraktının hazırlanması ve karakteristiğine ilişkin raporlar gün geçtikçe artmasına rağmen, biyoaktif peptidlerin içeriğine atfedilen maya ekstraktının fonksiyonel özellikleri ve üretim yöntemlerine ilişkin araştırmalar yeterli miktarda bulunmamaktadır. Maya hücrelerinin büyüme ve fermantasyon sürecinde biyoaktif peptitlerin üretimine katkısı üzerine yapılan araştırmalar mevcut durumda devam etmektedir. Bu bağlamda, elde edilen maya kökenli peptidler, üretim yöntemleri, biyoaktivite, etki mekanizması ve ayrıca yapı-işlev ilişkisi ve tanımlanan peptidlerin stabilitesi hakkındaki önceki çalışmalar, gelecek çalışmalara yön göstermektedir. Sonuç olarak, maya hücreleri ve maya ekstraktı, çoklu işlevselliklere sahip biyoaktif peptitler üretmek için büyük potansiyele sahiptir. Mayanın potansiyel sağlık yararına ilişkin mevcut bilimsel kanıtlar, peptitlerin üretim ve saflaştırma yöntemlerinden etkilenen biyoaktivitesi hakkında ek araştırmalara duyulan ihtiyacı vurgulamaktadır. Ayrıca, biyoinformatik araçlar, hayvan ve insan çalışmaları yardımıyla belirli işlevselliğe sahip yeni peptit dizilerinin tahmin edilmesi ve tasarlanması, bu bulguları pratik ve piyasa uygulamalarına etkili bir şekilde kazandıracağı düşünülmektedir (Mirzaei et al. 2021).

Yapılan bir çalışmada, şeker kamışının ekmek mayası olan *Saccharomyces cerevisiae* tarafından enzimatik hidrolizi sonucunda (ticari adı Viscozyme) ve antianemik etkiye sahip demir bağlayıcı peptidlerin üretimi gerçekleştirilmiştir. Çalışmada, demir şelatlayıcı peptitler, immobilize metal afinite kromatografisi kullanılarak izolasyon yapılmıştır. Elde edilen sonuçlara göre, orijinal hidrolizatlardan daha yüksek His, Lys ve Arg içeriği gösterdiği tespit edilmiştir. Zayıf demir çözünürlüğüne rağmen, Viscozyme'in hidrolizatları, diğer enzimlerinkinden daha yüksek demir diyalizlenebilirliği sağladığından; daha fazla demir şelatının veya kompleksinin oluştuğu ve bunların, demiri in vitro simüle edilmiş mide-bağırsak sindirimi sırasında sabit tutarak diyaliz edilebilirliğini geliştirdiği sonucu elde edilmiştir (De la Hoz et al. 2014).

Giri et al. (2012) tarafından yapılan bir çalışmada, *Aspergillus oryzae* inoküle edilen Japon kojisinin, fermentasyon süresi boyunca antioksidan aktivitesi ve hidrolize etme yeteneğinin değiştiği bildirilmiştir. Kullanılan *A. oryzae* küfünün fermentasyon yolu ile istavrit gibi daha az değerli olan balıklardan elde edilen balık misosunun antioksidan aktivitesinin artırılması ile daha yüksek besin değerine sahip olabildiği tespit edilmiştir. *A. oryzae* aynı zamanda Uzak Doğu yemek kültüründe pirinç, soya fasülyesi, patates ve tahıllardaki nişastayı şekere dönüştürerek sake, miso, soçu gibi ürünlerin üretiminde kullanılır (Goffeau 2005).

Mikrobiyal kökenli biyoaktif peptidlerin ticari üretimleri giderek artış göstermektedir. Farklı uygulamalarla geliştirilen etken maddelerden ve üretici mikroorganizmalardan bazıları aşağıdaki tabloda verilmiştir (Tablo 2). Mikrobiyal fermentasyon teknikleri ile gerçekleştirilen biyoaktif peptidlerin üretimi ve geliştirilmesi üzerine yapılan araştırmalar popüler hale gelmiştir.

Tablo 2. Mikroorganizma kökenli bazı biyoaktif peptidler ve fonksiyonları

Peptid	**Mikroorganizma**	**Fonksiyon**	**Kaynak**
Alternariasin A	*Alternaria alternata*	Antibakteriyel	Guo et al. 2021
Diaporone A	*Diaporthe* **sp.**	Antibakteriyel-sitotoksik etki	Guo et al. 2020
Iturin A-Basillomisin F	*Bacillus siamensis* JFL15	Antifungal	Xu et al. 2018
Saroclides A ve B	*Sarocladium kiliense* HDN11-112	Antiviral- yağ azaltıcı aktivite	Guo et al. 2018
Thiovarsolin	*Streptomyces varsoviensis* DSM40346	Sitotoksik	Santos-Aberturas et al. 2019
VLL-28	*Sulfolobus islandicus*	Antifungal-antibiyofilm	Roscetto et al. 2018

Günümüzde insanların daha az yapay ve işlenmiş gıdalara yönlenmesi ve daha az toksisite ve/veya yan etki gösteren terapötik ajanların kullanımına artan talep sonucunda, biyoaktif peptidler için büyüyen bir pazar söz konusu olmuştur. Doğal yollarla üretilen ve insan vücuduna zarar vermeyen proteinlerin alımı ile alerjik reaksiyonların oluşumunda azalma meydana gelmektedir (Korhonen and Pihlanto 2006). Gelecekte yapılması muhtemel araştırmalar neticesinde, biyoaktif peptidlerin farmakokinetik özelliklerinde iyileşme ve ilaç taşıma sistemlerinde hedef organa ulaşma konusunda daha başarılı hale getirilmeleri beklenmektedir.

Kaynaklar

1. Amorim, M., Marques, C., Pereira, J.O., Guardao, L., Martins, M.J., Osorio, H., Moura, D., Calhau, C., Pinheiro, H., Pintado, M., (2019). Antihypertensive effect of spent brewer yeast peptide. Process Biochemistry, 76, 213-218.

2. Aykut, M., Esen, Y. & Taşar, G. E. (2016). New host-parasite association of Acherontacarus rutilans (Acari, Hydrachnidia, Acherontacaridae) on Scarodytes halensis (Coleoptera: Dytiscidae). *International Journal of Acarology*, 42(5), 242-246.

3. Aykut, M., Tasar, G. E., & Ferry, H. (2018). Deronectes taron sp. n. from the eastern Anatolian region of Turkey (Coleoptera, Dytiscidae, Hydroporinae). *Zootaxa*, *4422*(3), 403–410.

4. Aykut, M., & Taşar, G. E. (2018). Contributions to the knowledge of Adep-hagan Fauna in Adıyaman Province, Turkey (Coleoptera: Dytiscidae, Gyrinidae, Haliplidae and Noteridae). *Munis Entomology & Zoology*, 13(1): 249-255.

5. Aykut, M., Taşar, G. E., & Fery, H. (2021). Bidessus anatolicus adiyaman ssp. n. from Adıyaman province, southern Turkey (Coleoptera, Dytiscidae, Bidessini). Zootaxa, 5027(4): 563-575.

6. Babini, E., Tagliazucchi, D., Martini, S., Dei Più, L., & Gianotti, A. (2017). LC-ESIQTOF- MS identification of novel antioxidant peptides obtained by enzymatic and microbial hydrolysis of vegetable proteins. *Food Chemistry*, 228, 186-196.

7. Beaumont, A. (1983). Putative Peptide Neurotransmitters: The Opioid Peptides, *Int Rev Exp Path,* 25, 279-305.

8. Bengoa, A.A., Iraporda, C., Garrote, G. L., & Abraham, A. G. (2019). Kefir micro-organisms: their role in grain assembly and health properties of fermented milk. *Journal of Applied Microbiology*, 126, 686-700.

9. Canli, O., Tasar, G. E., & Taskin, M. (2013). Inulinase production by Geotrichum candidum OC-7 using migratory locusts as a new substrate and optimization process with Taguchi DOE. *Toxicology and Industrial Health*, *29*(8), 704–710. https://doi.org/10.1177/0748233712442737

10. Canlı Taşar, Ö., & Taşar, G.E. (2023). Evaluation of an Edible İnsect (Locusta migratoria) as a Substrate for Microbial β-fructofuranosidase Production. *Journal of the Institute of Science and Technology*, 120–129. https://doi.org/10.21597/jist.1190049

11. Cobanoglu, S. and Yazici, A., (2022). Isolation, characterization, and antibiofilm activity of pigments synthesized by *Rhodococcus* sp. SC1. *Current Microbiology,* 79, 15.

12. Chabance, B., Marteau, P., Rambaud, J.C., Migliore-Samour, D., Boynard, M., Perrotin, P., Guillet, R., Jolles, P., Fiat, A.M. (1998). Casein peptide

release and passage to the blood in humans during digestion of milk or yogurt. *Biochimie,* 80:155-165.

13. Corrêa, A. P., Daroit, D. J., Coelho, J., Meira, S. M., Lopes, F. C., Segalin, J., Brandelli, A. (2011). Antioxidant, antihypertensive and antimicrobial properties of ovine milk caseinate hydrolyzed with a microbial protease. *Journal of the Science of Food and Agriculture*, 91(12), 2247-2254.

14. Cotter, P. D., Ross, R. P., & Hill, C. (2013). Bacteriocins A viable alternative to antibiotics? *Nature Reviews Microbiology*, 11, 95-105.

15. Çakıcı, İ., Ercan, Z.S., Kanzık, İ. (1987). Opioid peptidler, Pharmacia, JTPA, 27, 58 (1), 30-36.

16. Daliri, E. B. M., Lee, B. H., & Oh, D. H. (2018). Current trends and perspectives of bioactive peptides. *Critical Reviews in Food Science and Nutrition*, 58(13), 2273-2284.

17. De la Hoz, L., Ponezi, A. N., Milani, R. F., Nunes da Silva, V. S., De Souza, A. S., & Bertoldo-Pacheco, M. T. (2014). Iron-binding properties of sugar cane yeast peptides. *Food Chemistry*, 142, 166-169.

18. Descamps, H. C., Herrmann, B., Wiredu, D., & Thaiss, C. A. (2019). The path toward using microbial metabolites as therapies. In *EBioMedicine* (Vol. 44, pp. 747–754). Elsevier B.V. https://doi.org/10.1016/j.ebiom.2019.05.063

19. Dewapriya, P., Khalil, Z. G., Prasad, P., Salim, A. A., Cruz-Morales, P., Marcellin, E., &Capon, R. J. (2018). Talaropeptides A-D: Structure and biosynthesis of extensivelyN-methylated linear peptides from an Australian marine tunicate-derived Talaromyces sp. Frontiers in Chemistry, 6, 394.

20. Elfahri, K. R., Vasiljevic, T., Yeager, T., & Donkor, O. N. (2014). Potential of novel *Lactobacillus helveticus* strains and their cell wall bound proteases to release physiologically active peptides from milk proteins. International Dairy Journal, 38, 37-46.

21. Elfahri, K. R., Vasiljevic, T., Yeager, T., & Donkor, O. N. (2016). Anticolon cancer and antioxidant activities of bovine skim milk fermented by selected *Lactobacillus helveticus* strains. *Journal of Dairy Science*, 99, 31-40.

22. Erdmann, K., Grosser, N., Schipporeit, K., Schroder, H. (2006). The ACE inhibitory dipeptide Met-Tyr diminishes free radical formation in human endothelial cells via induction of heme oxygenase-1 and ferritin. *Journal of Nutrition*, 136:2148-2152.

23. Erman, Ö. K., Taşar, G. E., Aykut, M., Kurt, K. (2018). First Record of *Hydaticus histrio* Clark, 1864 (Coleoptera, Dytiscidae) from Turkey. Acta Biologica Turcica, 31(4), 174-177.

24. Faye, T., Holo, H., Langsrud, T., Nes, I.F., Brede, D.A. (2011). The unconventional antimicrobial peptides of the classical propionibacteria. Applied Microbiology and Biotechnology, 89, 3, 549-554.

25. García-Tejedor, A., Sánchez-Rivera, L., Recio, I., Salom, J. B., & Manzanares, P. (2015). Dairy Debaryomyces hansenii strains produce the antihypertensive caseinderived peptides LHLPLP and HLPLP. *LWT Food Science and Technology*, 61, 550-556.

26. Giri, A., Nasu, M., & Ohshima, T. (2012). Bioactive properties of Japanese fermented fish paste, fish miso, using koji inoculated with *Aspergillus oryzae*. *International Journal of Nutrition and Food Sciences*, 1, 13-22.

27. Goffeau, A. (2005). Multiple moulds. Nature, 438, 1092-1093.

28. Gogineni, V., & Hamann, M. T. (2018). Marine natural product peptides with therapeutic potential: Chemistry, biosynthesis, and pharmacology. *Biochimica et Biophysica Acta -General Subjects*, 1862(1), 81-196.

29. Gu, Y., Majumder, K., & Wu, J. (2011). QSAR-aided in silico approach in evaluation of food proteins as precursors of ACE inhibitory peptides. *Food Research International*, 44, 2465-2474.

30. Guo, W., Wang, S., Li, N., Li, F., Zhu, T., Gu, Q., Li, D. (2018). Saroclides A and B, cyclic depsipeptides from the mangrove-derived fungus *Sarocladium kiliense* HDN11-112. Journal of Natural Products, 81(4), 1050-1054.

31. Guo, L., Niu, S., Chen, S., & Liu, L. (2020). Diaporone A, a new antibacterial secondary metabolite from the plant endophytic fungus Diaporthe sp. The Journal of Antibiotics, 73 (2), 116-119.

32. Guo, Z., Huo, R., Niu, S., Liu, X., & Liu, L. (2021). Alternariasin A, new pentacyclic cytochalasin from the fungus Alternaria alternata. The Journal of Antibiotics, 74(9), 596-600.

33. Hartmann, R., & Meisel, H. (2007). Food-derived peptides with biological activity: from research to food applications. In *Current Opinion in Biotechnology* (Vol. 18, Issue 2, pp. 163–169). https://doi.org/10.1016/j.copbio.2007.01.013.

34. Hernandez-Ledesma, B., Davalos, A., Bartolome, B., Amigo, L. (2005). Preparation of antioxidant enzymatic hydrolysates from alpha-lactalbumin and beta-lactoglobulin. Identification of active peptides by HPLC-MS/MS. *J Agric Food Chem*, 53:588-593.

35. Horiguchi, N., Horiguchi, H., Suzuki, Y. (2005). Effect of wheat glüten hydrolysate on the immune system in healthy human subjects. *Biosci Biotechnol Biochem*, 69:2445-2449.

36. Hou, H., Li, B., Zhao, X., Zhang, Z., & Li, P. (2011). Optimization of enzymatic hydrolysis of Alaska pollock frame for preparing protein hydrolysates with low-bitterness. *Food Science & Technology*, 44, 421-428.

37. Houston, M. E., Jr., Campbell, A. P., Lix, B., Kay, C. M., Sykes, B. D., & Hodges, R. S. (1996). Lactam bridge stabilization of alpha-helices: The role of hydrophobicity in controlling dimeric vs monomeric alpha-helices. *Biochemistry*, 35(31), 10041-10050.

38. Ibrahim, S. A., & Bezkorovainy, A. (1994). Growth-promoting factors for Bifidobacterium longum. *Journal of Food Science*, 59, 189-191.

39. Jian, S., Yang, K., Zhang, L., Zhang, L., Xin, Z., Wen, C., He, S., Deng, J., & Deng, B. (2023). The modulation effects of plant-derived bioactive ingredients on chronic kidney disease: Focus on the gut–kidney axis. In *Food Frontiers*. John Wiley and Sons Inc. https://doi.org/10.1002/fft2.209

40. Kalibulla Syed Ibrahim, Karhika, R., Divyaa, N., Moniusha, J., Praveen, R. (2023). Peptides with therapeutic applications from microbial origin. Recent Advances and Future Perspectives of Microbial Metabolites*, Elsevier*, ISBN: 978-0-323-90113-0.

41. Kampa, M., Bakogeorgou, E., Hatzoglou, A., Damianaki, A., Martin, P.M., Castanas, E. (1997). Opioid alkaloids and casomorphin peptides decrease the proliferation of prostatic cancer cell lines (LNCaP, PC3 and DU145) through a partial interaction with opioid receptors. *Eur J Pharmacol*, 335:255-265.

42. Kirkpatrick, C.L., Parsley, N.C., Bartges, T.E., Wing, C.E., Kommineni, S., Kristich, C.J., Salzman, N.H., Patrie, S.M., Hicks, L.M., (2018). Exploring bioactive peptides from bacterial secretomes using PePSAVI-MS:identification and characterization of Bac-21 from *Enterococcus faecalis.* Microbial Biotechnology, 11, 5, 943-951.

43. Kitts, D.D. and Weiler, K. (2003). Bioactive proteins and peptides from food sources. Applications of bioprocesses used in isolation and recovery. Curr. Pharm. Des., 16, 1309-1323.

44. Knudsen, L. (2010). Liraglutide: The therapeutic promise from animal models. International Journal of Clinical Practice. *Supplement,* 64(167), 4-11.

45. Kodera T, Nio N., (2006). Identification of an angiotensin I-converting enzyme inhibitory peptides from protein hydrolysates by a soybean protease and the antihypertensive effects of hydrolysates in spontaneously hypertensive model rats. *J Food Sci*, 71:C164-C173.

46. Korhonen, H. And Pihlanto A. (2006). Bioactive peptides: Production and functionality. *International Dairy Journal,* 16, 945960.

47. Kumagai, H. (2010). Wheat proteins and peptides. In Y. Mine, E. Li-Chan, & B. Jiang (Eds.), Bioactive proteins and peptides as functional foods and nutraceuticals (pp. 289-303). Oxford, UK: Wiley-Blackwell.

48. Lafarga, T., Aluko, R. E., Rai, D. K., O'Connor, P., & Hayes, M. (2016). Identification of bioactive peptides from a papain hydrolysate of bovine serum albumin and assessment of an antihypertensive effect in spontaneously hypertensive rats. *Food Research International*, 81, 91-99.

49. Lassoued, I., Mora, L., Barkia, A., Aristoy, M. C., Nasri, M., & Toldrá, F. (2015). Bioactive peptides identified in thornback ray skin's gelatin hydrolysates by proteases from *Bacillus subtilis* and *Bacillus amyloliquefaciens*. *Journal of Proteomics*, 128, 8-17.

50. Lee, J.E., Bae, I.Y., Lee, H.G., Yang, C.B. (2006). Tyr-Pro-Lys, an angiotensin I-converting enzyme inhibitory peptide derived from broccoli (*Brassica oleracea* Italica). *Food Chem,* 99:143-148.

51. Levy, M., Kolodziejczyk, A. A., Thaiss, C. A., & Elinav, E. (2017). Dysbiosis and the immune system. In *Nature Reviews Immunology* (Vol. 17, Issue 4, pp. 219–232). *Nature Publishing Group*. https://doi.org/10.1038/nri.2017.7.

52. Lewis, R.V., Stern, A.S. (1983). Biosynthesis of the enchephalins and enchephalin containing polypeptides. *Ann Rev Phamacol Toxicol,* 23, 353-372.

53. Lima, C. A., Campos, J. F., Lima Filho, J. L., Converti, A., da Cunha, M. G. C., & Porto, A. L. (2015). Antimicrobial and radical scavenging properties of bovine collagen hydrolysates produced by Penicillium aurantiogriseum URM 4622 collagenase. *Journal of Food Science and Technology*, 52, 4459-4466.

54. Mandal, S., Xu, X., Jin, F., Panda, A., & Ibrahim, K. (Eds.). (2023). Recent Advances and Future Perspectives of Microbial Metabolites, *Elsevier*, ISBN: 978-0-323-90113-0.

55. McCann, K.B., Shiell, B.J., Michalski, W.P., Lee, A., Wan, J., Roginski, H., Coventry, M.J. (2006). Isolation and characterisation of a novel antibacterial peptide from bovine aS1-casein. *Int Dairy J*., 16:316-323.

56. Meinlschmidt, P., Ueberham, E., Lehmann, J., Schweiggert-Weisz, U., & Eisner, P. (2016). Immunoreactivity, sensory and physicochemical properties of fermented soy protein isolate. *Food Chemistry*, 205, 229-238.

57. Meisel H, Walsh DJ, Murray BA, FitzGerald RJ, (2006). ACE inhibitory peptides. In Nutraceutical Proteins and Peptides in Health and Disease. Edited by Mine V, Shahidi F. Taylor and Francis; 269-315.

58. Mine, Y., Kovacs-Nolan, J. (2006). New insights in biologically active proteins and peptides derived from hen egg. *Worlds Poult Sci J*, 62:87-95.

59. Mirzaei, M., Shavandi, A., Mirdamadi, S., Soleymanzadeh, N., Motahari, P., Mirdamadi, N., Goriely, S. (2021). Bioactive peptides from yeast: A comparative review on production methods, bioactivity, structure-function relationship, and stability. *Trends in Food Science and Technology*, 118, 297-315.

60. Mizushima, S., Ohshige, K., Watanabe, J., Kimura, M., Kadowaki, T., Nakamura, Y., Tochikubo, O., Ueshima, H. (2004). Randomized controlled trial of sour milk on blood pressure in borderline hypertensivemen. *Am J Hypertens,* 17:701-706.

61. Moller, N. P., Scholz-Ahrens, K. E., Roos, N., & Schrezenmeir, J. (2008). Bioactive peptides and proteins from foods: Indication for health effects. *European Journal of Nutrition*, 47, 171-182.

62. Murray, B.A. and FitzGerald, R.J., (2007). Angiotensin converting enzyme inhibitory peptides derived from food proteins: biochemistry, bioactivity and production. *Curr. Pharm. Des.*, 13, 8, 773-791.

63. Nagai T, Suzuki N, Nagashima T., (2006). Antioxidative activities and angiotensin I-converting enzyme inhibitory activities of enzymatic hydrolysates from commercially available Kamaboko species. *Food Sci Technol*, 12:335-346.

64. Nagaoka, S., Futamura, Y., Miwa, K., Awano, T., Yamuchi, K., Kanamaru, Y., Tadashi, K., Kuwata, T, (2001). Identification of novel hypocholesterolemic peptides derived from bovine milk betalactoglobulin. *Biochem Biophys Res Commun*, 281, 11-17.

65. Nishie, M., Nagao, J.I., and Sonomoto, K. (2012). Antibacterial Peptides "Bacteriocins": An Oveerview of Their Diveerse Characteristics and Applications. Biocontrol Science, 17, 1, 1-16.

66. Nishiwaki, T., Yoshimizu, S., Furuta, M., & Hayashi, K. (2002). Debittering of enzymatic hydrolysates using an aminopeptidase from the edible basidiomycete Grifola frondosa. *Journal of Bioscience and Bioengineering*, 93, 60-63.

67. O'Brien, K. T., Golla, K., Kranjc, T., O'Donovan, D., Allen, S., Maguire, P., Shields, D. C. (2019). Computational and experimental analysis of bioactive peptide linear motifs in the integrin adhesome. PLoS One, 14(1), e0210337.

68. Oda, H., Wakabayashi, H., Yamauchi, K., Sato, T., Xiao, J. Z., Abe, F., & Iwatsuki, K. (2013). Isolation of a bifidogenic peptide from the pepsin hydrolysate of bovine lactoferrin. *Applied and Environmental Microbiology*, 79, 1843-1849.

69. Okasha, H. (2020). Gene reports synthesis and molecular cloning of antimicrobial peptide chromogranin A N-46 gene using conventional PCR. *Gene Reports*, *18*(100571).

70. O'Loughlin, I. B., Murray, B. A., FitzGerald, R. J., Brodkorb, A., & Kelly, P. M. (2014). Pilot-scale production of hydrolysates with altered bio-functionalities based on thermally-denatured whey protein isolate. *International Dairy Journal*, 34, 146-152.

71. Ozaki, T., Minami, A., Oikawa, H., (2023). Recent advances in the biosynthesis of ribosomally synthesized and posttranslationally modified peptides of fungal origin. Journal of Antibiotics, 76, 1, 3-13.

72. Pan, J., Xu, H., Cheng, Y., Mintah, B. K., Dabbour, M., Yang, F., Chen, W., Zhang, Z., Dai, C., He, R., & Ma, H. (2022). Recent Insight on Edible Insect Protein: Extraction, Functional Properties, Allergenicity, Bioactivity, and Applications. In *Foods* (Vol. 11, Issue 19). MDPI. https://doi.org/10.3390/foods11192931.

73. Perez Espitia, P. J., de Fátima Ferreira Soares, N., dos Reis Coimbra, J. S.,

de Andrade, N. J., Souza Cruz, R., & Alves Medeiros, E. A. (2012). Bioactive peptides: Synthesis, properties, and applications in the packaging and preservation of food. *Comprehensive Reviews in Food Science and Food Safety*, 11, 187-204.

74. Perez, R.H., Zendo, T., Sonomoto, K. (2022). Multiple bacteriocin production in lactic acid bacteria. Journal of Bioscience and Bioengineering, 134, 4, 277-287.

75. Petersdorff, R.G., Adams, R.D., Braunwald, E., Isselbacher, K.J., Martin, J.J., Wilson, J.D. (1984). Harrison's Principles of International Medicine, Tenth Edition. Opiates and Synthetic Analgesics. Chapter 239. *McGraw-Hill Book Company.*

76. Polyudova, T.V., Lemkina, L.M., Likhatskaya, G.N., Korobov, V.P., (2017). Optimization of Production Conditions and 3-D Structure Modeling of Novel Antibacterial Peptide of Lantibiotic Family. Applied Biochemistry and Microbiology, 53, 1, 40-46.

77. Prakash Nirmal, N., Singh Rajput, M., Bhojraj Rathod, N., Mudgil, P., Pati, S., Bono, G., Nalinanon, S., Li, L., & Maqsood, S. (2023). Structural characteristic and molecular docking simulation of fish protein-derived peptides: Recent updates on antioxidant, anti-hypertensive and anti-diabetic peptides. In *Food Chemistry* (Vol. 405). Elsevier Ltd. https://doi.org/10.1016/j.foodchem.2022.134737

78. Quah, Y., Tong, S.-R., Bojarska, J., Giller, K., Tan, S.-A., Ziora, Z. M., Esatbeyoglu, T., & Chai, T.-T. (2023). Bioactive Peptide Discovery from Edible Insects for Potential Applications in Human Health and Agriculture. *Molecules*, *28*(3), 1233. https://doi.org/10.3390/molecules28031233.

79. Rai, A. K., Kumari, R., Sanjukta, S., & Sahoo, D. (2016). Production of bioactive protein hydrolysate using the yeasts isolated from soft chhurpi. *Bioresource Technology*, 219, 239-245.

80. Rao, L., Shi, H.C., Zou, Y. (2023). A fungal nonribosomal peptide-polyketide hybrid synthase synthezis 2- pyrrolidinone alkaloid. Tetrahedron, 125, 133060, eDOI: 10.1016/j.tet.2022.133060.

81. Roscetto, E., Contursi, P., Vollaro, A., Fusco, S., Notomista, E., & Catania, M. R. (2018). Antifungal and anti-biofilm activity of the first cryptic antimicrobial peptide from an archaeal protein against *Candida* spp. clinical isolates. Scientific Reports, 8(1), 17570.

82. Sable, R., Parajuli, P., & Jois, S. (2017). Peptides, peptidomimetics, and polypeptides from marine sources: A wealth of natural sources for pharmaceutical applications. *Marine Drugs*, *15*(4), 124.

83. Sagar, S., Esau, L., Holtermann, K., Hikmawan, T., Zhang, G., Stingl, U., Kaur, M. (2013). Induction of apoptosis in cancer cell lines by the Red Sea brine pool bacterial extracts. *BMC Complementary and Alternative Medicine*, 5(13), 344.

84. Sagardia, I., Iloro, I., Elortza, F., & Bald, C. (2013). Quantitative structure-activity relationship based screening of bioactive peptides identified in ripened cheese. International Dairy Journal., 33, 184-190.

85. Saleem, M., Ali, M., Hussain, S., Jabbar, A., Ashraf, M., & Lee YS. (2007). Marine natural products of fungal origin. *Natural Product Reports*, *24*, 1142–1152.

86. Sánchez, A., & Vázquez, A. (2017). Bioactive peptides: A review. *Food Quality and Safety*, *1*, 29–46.

87. Sanjukta, S., & Rai, A. K. (2016). Production of bioactive peptides during soybean fermentation and their potential health benefits. *Trends in Food Science and Technology*, 50, 1-10.

88. Santos-Aberturas, J., Chandra, G., Frattaruolo, L., Lacret, R., Pham, T. H., Vior, N. M., Truman, A. W. (2019). Uncovering the unexplored diversity of thioamidated ribosomal peptides in Actinobacteria using the RiPPER genome mining tool. Nucleic Acids Research, 47(9), 4624-4637.

89. Selamassakul, O., Laohakunjit, N., Kerdchoechuen, O., & Ratanakhanokchai, K. (2016). A novel multi-biofunctional protein from brown rice hydrolysed by endo/endo-exoproteases. *Food & Function*, 7, 2635-2644.

90. Souza, P. F. N., Marques, L. S. M., Oliveira, J. T. A., Lima, P. G., Dias, L. P., Neto, N. A. S., Lopes, F. E. S., Sousa, J. S., Silva, A. F. B., Caneiro, R. F., Lopes, J. L. S., Ramos, M. V., & Freitas, C. D. T. (2020). Synthetic antimicrobial peptides: From choice of the best sequences to action mechanisms. *Biochimie*, *175*, 132–145. https://doi.org/10.1016/j.biochi.2020.05.016.

91. Tadesse, S. A., & Emire, S. A. (2020). Production and processing of antioxidant bioactive peptides: A driving force for the functional food market. *Heliyon*, 6(8), e04765.

92. Takahashi, M., Moriguchi, S., Yoshikawa, M., Sasaki, R. (1994). Isolation and characterization of oryzatensin - a novel bioactive peptide with ileum-contracting and immunomodulating activities derived from rice albumin. *Biochem Mol Biol Int,* 33:1151-1158.

93. Tasar, G.E., (2014a). A Contribution to the knowledge of Turkish Dryopidae, Elmidae and Heteroceridae (Coleoptera: Byrrhoidea) Fauna. *Archives of Biological Sciences Belgrade.*, *66*(4), 1473–1478.

94. Taşar, G.E., Mascagni, A. (2014b). Checklist of Heteroceridae (Coleoptera) of Turkey. Pakistan Journal of Zoology, 46(6), 1685-1690.

95. Taşar, G.E., (2014c). The occurrence of the subgenus *Methydrus* Rey, 1885 in Turkey (Coleoptera: Hydrophilidae, *Enochrus*) with taxonomic and distributional notes. Munis Entomology & Zoology, 9(1), 478-482.

96. Tasar, G.E., (2017a). *Hydrochus adiyamanensis* sp. n. from Adıyaman Province in south-eastern Turkey (Coleoptera: Hydrochidae). *Zoology in the Middle East*, *63*(4), 356–361.

97. Taşar, G.E., (2017b). Hydrophiloidea (Coleoptera: Helophoridae, Hydrochidae and Hydrophilidae) Fauna of Adıyaman Province. KSU Journal of Naturel Sciences, 20(2): 103-110.

98. Tasar, G. E. (2018a). Contributions to the knowledge of Aquatic Coleoptera Fauna (Dryopidae, Helophoridae, Heteroceridae, Hydrochidae, Hydrophilidae, Gyrinidae, Haliplidae and Noteridae) of Diyarbakır, Mardin and Batman Provinces (Turkey). *Turkish Journal of Fisheries and Aquatic Sciences*, *18*, 927–936.

99. Taşar, G.E., (2018b). Investigations on the Hydrophiloidea (Coleoptera: Helophoridae, Hydrochidae and Hydrophilidae) Fauna of Şanlıurfa Province. KSU Journal of Agriculture and Nature, 21(2): 111-118.

100. Taşar, G. E. (2018c). Checklist of Dryopidae and Elmidae (Coleoptera: Byrrhoidea) of Turkey. Biharean Biologist, 12(1) 1-6.

101. Taşar, G.E., (2022a). Insac Scientific Researches in Natural and Engineering Sciences. Bölüm Adı: Sucul Böcekler, Yayın Yeri: Duvar Kitabevi, Editör: Yıldızel Sadık Alper, Ruşen Selmin Ener, Basım sayısı:1, Sayfa sayısı:284, ISBN:978-625-8261-13-4, Bölüm Sayfaları: 102-140.

102. Taşar, G. E. (2022b). Fen Bilimleri ve Matematik Alanında Güncel Tartışmalar. Bölüm Adı: Adıyaman İlinin (Türkiye) Sucul Böcek Çeşitliliği, Taşar Gani Erhan, Kızılkaya Murat, Kızılkaya Selda, Yayın Yeri: Duvar Kitabevi, Editör: Demirçalı Aykut, Basım sayısı:1, Sayfa sayısı:245, ISBN:978-625-8109-78-8, Bölüm Sayfaları:109-126.

103. Taşar, G.E., & Canlı Taşar, Ö. (2022). Yenilebilir Sucul Böcekler. Duvar Kitabevi, Editörler: Doç. Dr. Mustafa Tolga ÇÖĞÜRCÜ, Dr. Mehmet UZUN. Basım sayısı:1, Sayfa Sayısı 416, ISBN: 978-625-8109-01-6, Türkçe (Bilimsel Kitap). In *INSAC Natural and Technology Sciences*.

104. Thaiss, C. A., & Elinav, E. (2017). The remedy within: will the microbiome fulfill its therapeutic promise? In *Journal of Molecular Medicine* (Vol. 95, Issue 10, pp. 1021–1027). Springer Verlag. https://doi.org/10.1007/s00109-017-1563-z

105. Timmerman, P., Puijk, W. C., & Meloen, R. H. (2007). Functional reconstruction and synthetic mimicry of a conformational epitope using CLIPS technology. *Journal of Molecular Recognition*: JMR, 20, 283-299.

106. Tu, M., Cheng, S., Lu, W., & Du, M. (2018). Advancement and prospects of bioinformatics analysis for studying bioactive peptides from food-derived protein: Sequence, structure, and functions. TrAC Trends in Analytical Chemistry, 105, 7-17.

107. Uhlig, T., Kyprianou, T., Martinelli, F. G., Oppici, C. A., Heiligers, D., Hills, D., Verhaert, P. (2014). The emergence of peptides in the pharmaceutical business: From exploration to exploitation. *EuPA Open Proteomics*, 4, 58-69.

108. Vercruysse, L., Van Camp, J., Smagghe, G. (2005). ACE inhibitory pepti-

des derived from enzymatic hydrolysates of animal muscle protein: a review. *J Agr Food Che*, 53:8106-8115.

109. Walker, G., Cai, F., Shen, P., Reynolds, C., Ward, B., Fone, C., Honda, S., Koganei, M., Oda, M., Reynolds, E. (2006). Increased remineralization of tooth enamel by milk containing added casein phosphopeptide-amorphous calcium phosphate. *J Dairy Res*, 73:74-78.

110. Xu, B. H., Lu, Y. Q., Ye, Z. W., Zheng, Q. W., Wei, T., Lin, J. F., & Guo, L. Q. (2018). Genomics-guided discovery and structure identification of cyclic lipopeptides from the Bacillus siamensis JFL15. PLoS One, 13(8), e0202893.

111. Yada, R. Y. (2017). Plant proteases for bioactive peptides release: A review. Critical Reviews in Food Science and Nutrition, 8398, 2147-2163.

112. Yazici, A., Ortucu, S., Taskin, M., Marinelli, L., (2018). Natural-based antibiofilm and antimicrobial peptides from microorganisms. *Current Topics in Medicinal Chemistry*, 18, 24, 2102-2107.

113. Yazici, A., Ortucu, S., Taskin, M., (2021). Screening and characterization of a novel antibiofilm polypeptide derived from filamentous fungi. *Jounal of Proteomics,* 233, 104075.

114. You, M., Liao, L., Hong, S., Park, W., Kwon, D., Lee, J., Shin, J. (2015). Lumazine peptides from the marine-derived fungus *Aspergillus terreus*. *Marine Drugs*, 13, 1290-1303.

115. Youssef, F. S., Ashour, M. L., Singab, A., & Wink, M. (2019). A comprehensive review of bioactive peptides from marine fungi and their biological significance. *Marine Drugs*, 17, 559.

116. Yu, Y. J., Amorim, M., Marques, C., Calhau, C., & Pintado, M. (2016). Effects of whey peptide extract on the growth of probiotics and gut microbiota. *Journal of Functional Foods*, 21, 507-516.

117. Zhang, Q., Ren, J., Zhao, H., Zhao, M., Xu, J., & Zhao, Q. (2011). Influence of casein hydrolysates on the growth and lactic acid production of *Lactobacillus delbrueckii* subsp. *bulgaricus* and *Streptococcus thermophilus*. *International Journal of Food Science & Technology*, 46, 1014-1020.

118. Zhang, Q. T., Liu, Z. D., Wang, Z., Wang, T., Wang, N., Wang, N., Zhao, Y. F. (2021). Recent advances in small peptides of marine origin in cancer therapy. *Marine Drugs*, 19(2), 115.

119. Zhu KX, Zhou HM, Qian HF (2006). Antioxidant and free radicalscavenging activities of wheat germ protein hydrolysates (WGPH) prepared with alcalase. *Process Bioc*hemistry, 41:1296-1302.

120. Ziodrou, C, Streaty RA, Klee WA (1979). Opioid peptides derived from food proteins exorphins. Journal of Biological Chemistry, 254, 2446-2449.

BÖLÜM 4

CHAPTER 4

E_1^3 MINKOWSKI UZAYINDA SABİT ORANLI BAZI DÖNEL YÜZEYLER

Sezgin BÜYÜKKÜTÜK[1]

1 Kocaeli Üniversitesi Gölcük Meslek Yüksekokulu, Gölcük-Kocaeli, Türkiye (ORCID: 0000-0002-1845-0822) sezgin.buyukkutuk@kocaeli.edu.tr

GİRİŞ

Sabit oranlı yüzeyler ve sabit oranlı eğriler geçtiğimiz yirmi yıl içinde geometri alanında önemli sınıflandırmalar içinde yer almıştır [8,9,10]. Bu kavram ilk olarak Bang Yen Chen tarafından tanıtılmış, sonrasında ise özellikle sabit oranlı eğriler neredeyse tüm uzaylarda farklı çatılara göre çalışılmıştır [4, 5, 6, 7, 11, 12, 14, 19, 20].

$S:\varphi(x,y):(x,y)\in U\left(U\subset IE^2\right)$, n- boyutlu Minkowski uzayında bir yüzey olsun. Yüzeyin pozisyon vektörü S'nin teğetsel bileşeni ile S'nin normal bileşeninin toplamı olarak düşünülebilir:

$$\varphi=\varphi^T+\varphi^N \tag{1}$$

Eğer φ^T nin normu φ^N nin normu arasında bir oran var ise ele alınan $S:\varphi(x,y)$ yüzeyine sabit oranlı yüzey denir [8,9]. $\{v_1,v_2,...,v_n\}$, S yüzeyinin ortonormal çatısı olmak üzere, uzaklık fonksiyonu $d=\|\varphi\|$ nin gradiyenti

$$\operatorname{grad}(d)=\sum_{i=1}^{n}v_i(d)v_i \tag{2}$$

ile hesaplanır. Ayrıca $\langle\ ,\ \rangle_L$, IE_1^n de tanımlı Lorentz iç çarpımı olmak üzere

$$v_i(d)=\frac{\langle v_i,\varphi\rangle_L}{\|\varphi\|} \tag{3}$$

bağıntısını kullanarak (2) eşitliği

$$\operatorname{grad}(d)=\sum_{i=1}^{n}\frac{\langle v_i,\varphi\rangle_L}{\|\varphi\|}v_i \tag{4}$$

haline gelir. Dolayısıyla, grad(d) nin normu

$$\|\operatorname{grad}(d)\|^2=\sum_{i=1}^{n}\frac{\left(\langle v_i,\varphi\rangle_L\right)^2}{\|\varphi\|^2} \tag{5}$$

dir. Son eşitliğe göre, bir yüzeyin sabit oranlı olması demek

$$\operatorname{grad}(d)=\eta\ ,\quad \eta\in IR^+ \tag{6}$$

anlamına gelir.

Kanal yüzeyleri, tüp yüzeyleri, katenoid, açılabilir, regle yüzeyler gibi birçok yüzeyi içine alan Dönel yüzeyler, yüzeyleri karakterize etmede önemli bir role sahiptir. Özel olarak, katenoid yüzeyi minimal olan tek dönel yüzeydir. Ayrıca, bir açılabilir yüzey ise düz olan tek dönel dönel yüzeydir. Literatürde, bu tür yüzeylerle ilgili birçok çalışma mevcuttur [1,2,3,13,15,17].

Bu çalışmada, 3- boyutlu Minkowski uzayında sabit oranlı timelike dönel yüzeyleri ele aldık. İlk olarak Minkowski uzayında iki farklı dönmeye göre dönel yüzeylerin parametrizasyonunu verdik. Sonrasında, bu tip yüzeylerin sabit oranlı olması için gerek ve yeter koşulu elde ettik. Buna ek olarak, grad (d) = 0, grad (d) = 1 ve $\operatorname{grad}(d)=\eta$ sağlanma durumlarına göre yüzeyleri karakterize ettik. [16].

1.TEMEL KAVRAMLAR

3- boyutlu Minkowski uzayında, r_i, s_i, r ve s vektör alanlarının bileşenleri olmak üzere Loretziyen iç çarpım

$$\langle r, s\rangle_L = r_1 s_1 + r_2 s_2 - r_3 s_3 \tag{7}$$

ile verilir.

Keyfi seçilen bir vektör sırasıyla $\langle r, r\rangle_L$ nin sıfır, negatif ya da pozitif olmasına göre, null, timelike ya da spacelike olarak adlandırılır. $r \in IE_1^3$ nin boyunu veren bağıntı

$$\|r\|\sqrt{|\langle r, r\rangle|} \tag{8}$$

dir.

Ayrıca, r ve s nin vektör çarpımı

$$r \wedge q = \begin{vmatrix} i & j & -k \\ r_1 & r_2 & r_3 \\ s_1 & s_2 & s_3 \end{vmatrix} \tag{9}$$

ile hesaplanır.

3- boyutlu Minkowski uzayında, yukarıdaki tanımlamaya benzer şekilde, yüzeyler de null, timelike ve spacelike gibi üç farklı kategoriye ayrılır. Keyfi bir yüzey, teğetlerinden bir tanesi timelike olduğunda timelike yüzey olarak bilinir [18].

$S : \varphi(x, y) : (x, y) \in U \left(U \subset IE^2\right)$ Minkowski 3- uzayında bir timelike yüzey olsun. O halde, yüzeyi tanımlayan pozisyon vektörü (1)

eşitliğindeki gibi teğet ve normal kısımlara ayrılabilir. T(S) teğet uzayını üreten vektör alanları φ_x ve φ_y olmak üzere, birinci temel form katsayıları

$$E = \langle \varphi_x , \varphi_x \rangle_L$$

$$F = \langle \varphi_x , \varphi_y \rangle_L \qquad (10)$$

$$G = \langle \varphi_y , \varphi_y \rangle_L$$

olarak tanımlıdır. Böylece, birinci temel form

$$I = E\ dx^2 + 2F\ dxdy + G\ dy^2 \qquad (11)$$

olarak yazılır.

Yüzey timelike olduğundan, $EG - F^2 < 0$ olup E ya da G negatif olarak seçilir. Dolayısıyla, bundan sonraki kullanımlar için $W = \sqrt{F^2 - EG}$ olarak alalım. Buna ek olarak, φ_x ve φ_y dik (ortogonal) yani F=0 ise

$$v_1 = \frac{\varphi_x}{\sqrt{|E|}} \qquad (12)$$

$$v_2 = \frac{\varphi_y}{\sqrt{|G|}} \qquad (13)$$

şeklindedir.

IE_1^3 de sırasıyla (1,0,0) ve (0,0,1) tarafından üretilen spacelike ve timelike eksenlere göre iki farklı dönme karşımıza çıkar. Dönme matrisleri

$$R_1(y) = \begin{pmatrix} 1 & 0 & 0 \\ 0 & \cosh y & \sinh y \\ 0 & \sinh y & \cosh y \end{pmatrix} \qquad (14)$$

$$R_2(y) = \begin{pmatrix} \cos y & -\sin y & 0 \\ \sin y & \cos y & 0 \\ 0 & 0 & 1 \end{pmatrix} \qquad (15)$$

dir [16].

2.MINKOWSKI 3- UZAYINDA SABİT ORANLI YÜZEYLER

Tanım: $S:\varphi(x,y):(x,y)\in U\ (U\subset IE^2)$ 3- boyutlu Minkowski uzayında bir yüzey olsun. Eğer, $d=\|\varphi\|$ uzaklık fonksiyonunun gradiyenti,

$$\text{grad}\,(d)=\eta\ ,\quad \eta\in IR^+ \tag{16}$$

koşulunu sağlıyorsa, S yüzeyine IE_1^3 de sabit oranlı yüzey denir [9].

Tanımdan anlaşılacağı üzere, $\text{grad}\,(d)=\eta$ nin sağlanması için gerek ve yeter koşul

$$\|\varphi^T\|=\eta\|\varphi\| \tag{17}$$

dir. $\|\varphi^T\|\le\|\varphi\|$ nin sonucu olarak $\eta\le 1$ dir diyebiliriz.

$\{v_1,v_2,v_3\}$, S nin ortonormal çatısını temsil etsin. v_1, φ^T ye paralel olarak seçilebilir. Dolayısıyla

$$\varphi=\varphi^T+\varphi^N\ ,$$

$$\varphi^T=f\ v_1\ , \tag{18}$$

$$\varphi^N=g\ v_2$$

olarak yazılabilir. Eğer S sabit oranlı ise,

$$\|\varphi^T\|=\eta\|\varphi\| \tag{19}$$

dir. Böylece

$$f=\eta\,\|\varphi\|,\qquad g=\sqrt{1-\eta^2}\,\|\varphi\| \tag{20}$$

olur.

2.1.Sabit Oranlı Timelike 1 Tipinde Dönel Yüzeyler

Tanım: $\alpha:I\subset IR\to P$, Minkowski 3- uzayında $\alpha(x)=(w_1(x),w_2(x),0)$ ile verilen bir düzlem eğrisi ve L, (1,0,0) tarafından üretilen spacelike eksen olsun. Bu durumda α eğrisinin L ekseni etrafında dönmesiyle elde edilen S yüzeyine, IE_1^3 de 1 tipinde

dönel yüzey denir. Dolayısıyla (14) eşitliğindeki $R_1(y)$ dönme matrisini kullanarak, S yüzeyi

$$\varphi(x,y)=(w_1(x),\ w_2(x)\cosh y,\ w_2(x)\sinh y) \tag{21}$$

ile temsil edilir.

Teğet uzay,

$$\varphi_x=\left(w_1'(x),\ w_2'(x)\cosh y,\ w_2'(x)\sinh y\right) \tag{22}$$

$$\varphi_y=(0,\ w_2(x)\sinh y,\ w_2(x)\cosh y) \tag{23}$$

ile gerilir. Birinci temel form katsayıları

$$E=\left(w_1'\right)^2+\left(w_2'\right)^2$$

$$F=0 \tag{24}$$

$$G=-(w_2)^2$$

dir.

$EG-F^2=-\left(\left(w_1'\right)^2+\left(w_2'\right)^2\right)(w_2)^2$ olduğundan, S timelike yüzeydir. (22), (23) ve (9) eşitlikleri yardımıyla yüzeyin birim normali

$$n=\frac{1}{\sqrt{\left(w_1'\right)^2+\left(w_2'\right)^2}}\left(-w_2'(x),\ w_1'(x)\cosh y,\ w_1'(x)\sinh y\right) \tag{25}$$

olarak elde edilir.

Şimdi,

$$\varphi=f\ v_1+g\ v_3 \tag{26}$$

bağıntısını kullanalım. Birim vektör alanları $v_1=\frac{\varphi_x}{\sqrt{|E|}}$ ve $v_3=n$ ye denktir. (22) ve (25) ü (26) eşitliğinde yerine koyarak

$$(w_1(x), w_2(x)\cosh y, w_2(x)\sinh y) = \frac{f}{\sqrt{(w_1')^2 + (w_2')^2}}(w_1'(x), w_2'(x)\cosh y, w_2'(x)\sinh y) + \frac{g}{\sqrt{(w_1')^2 + (w_2')^2}}(-w_2'(x), w_1'(x)\cosh y, w_1'(x)\sinh y)$$

yazabiliriz. Bu eşitlikten,

$$w_2 \cosh y = \frac{f\, w_2' \cosh y + g\, w_1' \cosh y}{\sqrt{(w_1')^2 + (w_2')^2}},$$

$$w_2 \sinh y = \frac{f\, w_2' \sinh y + g\, w_1' \sinh y}{\sqrt{(w_1')^2 + (w_2')^2}},$$

$$w_1 = \frac{f\, w_1' - g\, w_2'}{\sqrt{(w_1')^2 + (w_2')^2}}$$

buluruz. Böylece f ve g fonksiyonlarını

$$f = \frac{w_1' w_1 + w_2' w_2}{\sqrt{(w_1')^2 + (w_2')^2}} \tag{27}$$

$$g = \frac{w_1' w_2 - w_2' w_1}{\sqrt{(w_1')^2 + (w_2')^2}} \tag{28}$$

olarak elde ederiz.

Teorem: S, (21) parametrizasyonu ile verilen bir dönel yüzey olsun. S, $\|\text{grad}(d)\| = 0$ olan bir sabit oranlı yüzeydir ancak ve ancak IE_1^3 de bir küreye karşılık gelir.

İspat: $S: \varphi(x, y)$, $\|\text{grad}(d)\| = 0$ 'ı sağlayan (21) parametrizasyonu ile verilen sabit oranlı dönel yüzey olsun. $\eta = 0$ olduğundan (20) eşitliğinden f=0 dır. O halde,

$$g = \sqrt{1-\eta^2}\,\|\varphi\| = \|\varphi\| = \sqrt{{w_1}^2 + {w_2}^2} = \text{sabit}$$

dir. (27) ve (28) yardımıyla,

$$w_1' w_1 + w_2' w_2 = 0$$

$$\frac{w_1' w_2 - w_2' w_1}{\sqrt{\left(w_1'\right)^2 + \left(w_2'\right)^2}} = c = \text{sabit}$$

olup bu diferansiyel denklem sistemi

$$w_1(x) = c\cos x$$

$$w_2(x) = c\sin x$$

çözümüne sahiptir. Sonuç olarak, S yüzeyi,

$$\varphi(x,y) = \left(c.\cos x,\, c.\sin x.\cosh y,\, c.\sin x.\sinh y\right)$$

parametrizasyonu ile verilen bir küreye karşılık gelir.

Teorem: S, IE_1^3 de (21) parametrizasyonu ile verilen bir dönel yüzey olsun. S, $\|\text{grad }(d)\| = 1$ olan bir sabit oranlı yüzeydir ancak ve ancak k bir reel sabit olmak üzere

$$\varphi(x,y) = \left(w_1(x),\, w_1(x)e^k.\cosh y, w_1(x)e^k.\sinh y\right)$$

parametrizasyonu ile verilen bir koniye karşılık gelir.

İspat: $S:\varphi(x,y)$, $\|\text{grad }(d)\| = 1$ 'ı sağlayan (21) parametrizasyonu ile verilen sabit oranlı dönel yüzey olsun. $\eta = 1$ olduğundan (20) eşitliğinden,

$$g = 0, \qquad f = \|\varphi\| = \sqrt{{w_1}^2 + {w_2}^2}$$

dir. (27) ve (28) yardımıyla,

$$\frac{w_1' w_1 + w_2' w_2}{\sqrt{\left(w_1'\right)^2 + \left(w_2'\right)^2}} = \sqrt{{w_1}^2 + {w_2}^2}$$

$$w_1' w_2 - w_2' w_1 = 0$$

olup bu diferansiyel denklem sistemi

$$w_2(x) = e^k \; w_1(x)$$

çözümüne sahiptir.

Örnek: Özel olarak, $w_1(x) = \exp(x) = e^x$ ve k=0 seçerek S yüzeyini Maple programında çizdirebiliriz.

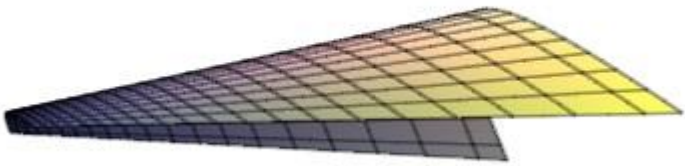

Şekil 1. Sabit oranlı timelike dönel yüzey

Teorem: S, IE_1^3 de (21) parametrizasyonu ile verilen bir dönel yüzey olsun. S, $\|\text{grad}\,(d)\| = \eta, \quad 0 < \eta < 1$ olan bir sabit oranlı yüzeydir ancak ve ancak

$$\varphi(x,y) = \left(w_1(x), \left(\int \sqrt{1 - \left(w_1'(x) \right)^2}\, dx \right).\cosh y, \left(\int \sqrt{1 - \left(w_1' \right)^2}\, dx \right).\sinh y \right)$$

parametrizasyonuna sahiptir.

İspat: $S : \varphi(x,y)$, $\|\text{grad}\,(d)\| = \eta$ 'ı sağlayan (21) parametrizasyonu ile verilen sabit oranlı dönel yüzey olsun. Bu durumda, S nin pozisyon vektörünün normu,

$$\|\varphi\| = \eta.x$$

bağıntısını sağlar. Bu denklem ve (17) yardımıyla,

$$\frac{\|\varphi^T\|}{\eta.x} = \eta,$$

$$f = \left\| \varphi^{T} \right\| = \eta^{2}.x \tag{29}$$

bulunur. (27), (28) ve (29) u birlikte ele alarak,

$$\frac{w_1' w_1 + w_2' w_2}{\sqrt{\left(w_1'\right)^2 + \left(w_2'\right)^2}} = \eta^{2}.x$$

olur ki bu,

$$d\left(\sqrt{w_1^{\,2} + w_2^{\,2}}\right) \frac{\sqrt{w_1^{\,2} + w_2^{\,2}}}{\sqrt{\left(w_1'\right)^2 + \left(w_2'\right)^2}} = \eta^{2}.x,$$

$$d(\eta.x) \frac{\eta.x}{\sqrt{\left(w_1'\right)^2 + \left(w_2'\right)^2}} = \eta^{2}.x,$$

$$\sqrt{\left(w_1'\right)^2 + \left(w_2'\right)^2} = 1$$

şeklinde bir çözüme sahiptir.

2.2.Sabit Oranlı Timelike 2 Tipinde Dönel Yüzeyler

Tanım: $\alpha : I \subset IR \to P$, Minkowski 3- uzayında $\alpha(x) = (w_2(x), 0, w_1(x))$ ile verilen bir düzlem eğrisi ve L, (0,0,1) tarafından üretilen timelike eksen olsun. Bu durumda α eğrisinin L ekseni etrafında dönmesiyle elde edilen S yüzeyine, IE_1^3 de 2 tipinde dönel yüzey denir. Dolayısıyla (15) eşitliğindeki $R_2(y)$ dönme matrisini kullanarak, S yüzeyi

$$\varphi(x, y) = (w_2(x)\cos y,\ w_2(x)\sin y,\ w_1(x)) \tag{30}$$

ile temsil edilir.

Teğet uzay,

$$\varphi_x = \left(w_2'(x)\cos y,\ w_2'(x)\sin y,\ w_1'(x)\right) \tag{31}$$

$$\varphi_y = (-w_2(x)\sin y,\ w_2(x)\cos y,\ 0) \tag{32}$$

ile gerilir. Birinci temel form katsayıları

$$E = \left(w_2'\right)^2 - \left(w_1'\right)^2$$

$$F = 0 \qquad (33)$$

$$G = {w_2}^2$$

dir.

S yüzeyini timelike seçeceğimiz için $W^2 = EG - F^2 = {w_2}^2\left(\left(w_1'\right)^2 - \left(w_2'\right)^2\right)$ olarak alalım. (31), (32) ve (9) eşitlikleri yardımıyla yüzeyin birim normali

$$n = \frac{1}{\sqrt{\left(w_1'\right)^2 - \left(w_2'\right)^2}}\left(w_1'(x)\cos y, w_1'(x)\sin y, w_2'(x)\right) \quad (34)$$

olarak elde edilir.

Şimdi, (26) bağıntısını kullanalım. (31) ve (34) ü burada yerine koyarak

$$\left(w_2(x)\cos y, w_2(x)\sin y, w_1(x)\right) = \frac{f}{\sqrt{\left(w_1'\right)^2 - \left(w_2'\right)^2}}\left(w_2'(x)\cos y, w_2'(x)\sin y, w_1'(x)\right) + \frac{g}{\sqrt{\left(w_1'\right)^2 - \left(w_2'\right)^2}}\left(w_1'(x)\cos y, w_1'(x)\sin y, w_2'(x)\right)$$

yazabiliriz. Bu eşitlikten,

$$w_2\cos y = \frac{f\,w_2'\cos y + g\,w_1'\cos y}{\sqrt{\left(w_1'\right)^2 - \left(w_2'\right)^2}},$$

$$w_2\sin y = \frac{f\,w_2'\sin y + g\,w_1'\sin y}{\sqrt{\left(w_1'\right)^2 + \left(w_2'\right)^2}},$$

$$w_1 = \frac{f\, w_1' + g\, w_2'}{\sqrt{\left(w_1'\right)^2 - \left(w_2'\right)^2}}$$

buluruz. Böylece f ve g fonksiyonlarını

$$f = \frac{w_1' w_1 - w_2' w_2}{\sqrt{\left(w_1'\right)^2 - \left(w_2'\right)^2}} \tag{35}$$

$$g = \frac{w_1' w_2 - w_2' w_1}{\sqrt{\left(w_1'\right)^2 + \left(w_2'\right)^2}} \tag{36}$$

olarak elde ederiz.

Teorem: S, (30) parametrizasyonu ile verilen bir dönel yüzey olsun. S, $\|\text{grad}\,(d)\| = 0$ olan bir sabit oranlı yüzeydir ancak ve ancak S nin parametrizasyonu

$$\varphi(x,y) = \left(\sqrt{w_1^2(x) + c}\cos y, \sqrt{w_1^2(x) + c}\sin y, w_1(x)\right), \quad c = \text{sbt.} \tag{37}$$

dir.

İspat: $S : \varphi(x,y)$, $\|\text{grad}\,(d)\| = 0$ 'ı sağlayan (30) parametrizasyonu ile verilen sabit oranlı dönel yüzey olsun. $\eta = 0$ olduğundan (20) eşitliğinden f=0 dır. O halde,

$$g = \sqrt{1-\eta^2}\,\|\varphi\| = \|\varphi\| = \sqrt{w_2^2 - w_1^2} = \text{sabit} \tag{38}$$

dir. (35), (36) ve (38) yardımıyla,

$$w_1' w_1 - w_2' w_2 = 0$$

$$\frac{w_1' w_2 - w_2' w_1}{\sqrt{\left(w_1'\right)^2 + \left(w_2'\right)^2}} = c = \text{sabit}$$

olup bu diferansiyel denklem sistemi

$$w_2^2(x) = w_1^2(x) + c$$

çözümüne sahiptir. Buradan istenilen sonuç elde edilir.

Teorem: S, IE_1^3 de (30) parametrizasyonu ile verilen bir dönel yüzey olsun. S, $\|\text{grad }(d)\| = 1$ olan bir sabit oranlı yüzeydir ancak ve ancak k bir reel sabit olmak üzere

$$\varphi(x,y) = w_2(x)(\cos y, \sin y, e^k)$$

parametrizasyonu ile verilen bir koniye karşılık gelir.

İspat: $S:\varphi(x,y)$, $\|\text{grad }(d)\| = 1$ 'ı sağlayan (30) parametrizasyonu ile verilen sabit oranlı dönel yüzey olsun. $\eta = 1$ olduğundan (30) eşitliğinden,

$$g = 0, \qquad f = \|\varphi\| = \sqrt{{w_2}^2 - {w_1}^2}$$

dir. (35) ve (36) yardımıyla,

$$\frac{w_1' w_1 - w_2' w_2}{\sqrt{(w_1')^2 - (w_2')^2}} = \sqrt{{w_2}^2 - {w_1}^2},$$

$$w_1' w_2 - w_2' w_1 = 0$$

olup bu diferansiyel denklem sistemi

$$w_1(x) = e^k \; w_2(x)$$

çözümüne sahiptir.

Teorem: S, IE_1^3 de (30) parametrizasyonu ile verilen bir dönel yüzey olsun. S, $\|\text{grad }(d)\| = \eta, \quad 0 < \eta < 1$ olan bir sabit oranlı yüzeydir ancak ve ancak

$$\varphi(x,y) = \left(\left(\int \sqrt{(w_1'(x))^2 - 1}\, dx\right).\cos y, \left(\int \sqrt{(w_1'(x))^2 - 1}\, dx\right).\sin y, w_1(x)\right)$$

parametrizasyonuna sahiptir.

İspat: $S:\varphi(x,y)$, $\|\text{grad}\,(d)\| = \eta$ 'ı sağlayan (30) parametrizasyonu ile verilen sabit oranlı dönel yüzey olsun. Bu durumda, (35) ve (29) eşitliklerinden

$$\frac{w_1' w_1 - w_2' w_2}{\sqrt{\left(w_1'\right)^2 - \left(w_2'\right)^2}} = \eta^2 . x$$

olur ki bu,

$$d\left(\sqrt{w_1^2 - w_2^2}\right)\frac{\sqrt{w_1^2 - w_2^2}}{\sqrt{\left(w_1'\right)^2 - \left(w_2'\right)^2}} = \eta^2 . x,$$

$$d(\eta . x)\frac{\eta . x}{\sqrt{\left(w_1'\right)^2 - \left(w_2'\right)^2}} = \eta^2 . x,$$

$$\sqrt{\left(w_1'\right)^2 - \left(w_2'\right)^2} = 1$$

şeklinde bir çözüme sahiptir

3. KAYNAKLAR

[1] Alegre, P., Arslan, K., Carriazo, A., Murathan, C. And Öztürk, G., Some special types of developable ruled surface, Hacet. J. Math. Stat., 2010, Vol. 39, 319–325.

[2] Althibany, N.M., Construction of developable surface with geodesic or line of curvature coordinates, Journal of New Theory, 2021, Vol. 36, 75–87.

[3] Blair, D.E., On a generalization of the Catenoid, Can. J. Math., 1975, Vol. 27(2), 231–236.

[4] Büyükkütük, S., Kişi İ., Öztürk G., A characterization of curves according to paralel transport frame in Euclidean n-space E^n, New Trends in Mathematical Science, 2017, Vol. 5,(2) 61-68.

[5] Büyükkütük, S., Kişi İ., Öztürk G., A characterization of non-lightlike curves with respect to paralel transport frame in Minkowski space-time, Malaysian Journal of Mathematical Sciences, 2018, Vol. 12(2), 223-234.

[6] Büyükkütük, S., Kişi İ., Öztürk G., Arslan, K., Some characterizations of curves in n-dimensional Euclidean space, Iğdır Üniversitesi Fen Bilimleri Dergisi, 2020, Vol. 10(2), 1273-1285.

[7] Büyükkütük, S., Kişi İ., Mishra, V.N., Öztürk G., Some characterizations of curves in Galilean 3-space G3, Facta Universitatis Series: Mathematics and Informatics, 2016, Vol. 31(2), 503-512.

[8] Chen, B.Y., Constant-ratio hypersurfaces, Soochow Journal of Mathematics, 2001, Vol. 27, 353-362.

[9] Chen,B. Y., More on convolution of Riemannian manifolds, Beitrage zur Algebra and Geometrie Contributions to Algebra and Geometry, 2003, Vol. 44, 9-24.

[10] Gürpınar, S., Arslan, K., Öztürk, G., A characterization of constant ratio curves in Euclidean 3-space, Acta Universtatis Apulensis, 2015, Vol. 44, 39–51.

[11] Kişi, İ., Büyükkütük, S., Öztürk, G., Constant ratio timelike curves in pseudo-Galilean 3-space G_1^3, Creative Mathematics and Informatics, 2018, Vol. 27(1), 57–62.

[12] Kişi, İ., Büyükkütük, S., Öztürk, G., Zor, A., A new characterization of curves on dual unit sphere, Journal of Abstract and Computational Mathematics, 2017, Vol. 2(1), 71-76.

[13] Kişi, İ., Öztürk, G., A new approach to canal surface with parallel transport frame, International Journal of Geometric Methods in Modern Physics, 2017, Vol. 14(2), 1750026.

[14] Kişi, İ., Öztürk, G., Constant ratio curves according to Bishop frame in Minkowski 3-space, Facta Universitatis Ser. Math. Inform., 2015, Vol. 30,

527–538.

[15] Kişi, İ., Öztürk, G., Tubular surface having pointwise 1-type Gauss map in Euclidean 4-space, International Electronic Journal of Geometry, 2019, Vol. 12(2), 202–209.

[16] Lee, S., Varnado, J.H., Timelike constant mean curvature surfaces of revolution in Minkowski 3- space, Differential Geometry and Dynamical Systems, 2007, Vol. 9, 82-102.

[17] Lee, T.U., Xie, Y.M., From ruled surfaces to elastica-ruled surfaces: New possibilities for creating architectural forms, Journal of the International Association for Shell and Spatial Structures, 2021, Vol. 62(4), 271-281.

[18] O'Neill, B., Semi-Riemannian Geometry with applications to relativity, Pure and Applied Mathematics, Academic Press, 1983.

[19] Öztürk,, G., Büyükkütük, S., Kişi, İ., A characterization of curves in Galilean 4-space G_4, Bulletin of Irannian Mathematical Society, 2017, Vol. 43(3), 771-780.

[20] Öztürk,, G., Kişi, İ., Büyükkütük, S., Constant ratio quaternionic curves in Euclidean spaces,Advances in Applied Clifford Algebras, 2017, Vol. 27(2), 1659-1673.

BÖLÜM 5

CHAPTER 5

SUPERNOVAE EXPLOSIONS AND THEIR EFFECTS ON EARTH

E. Nihal ERCAN[1]

1 Prof.Dr. Boğaziçi University, Physics Department

INTRODUCTION

A supernova is basically the greatest explosion in our universe. For us to understand this sentence, we should define what is an explosion. An explosion is an instant increment in volume with a highly great energy release of the material. Most of the explosions come up with the high energy flow inside the material.

As we can see in the name of supernovae, supernovae are 'supernovae and novae is a sudden increase in luminosity. It usually happens to faint stars. This increase in luminosity causes stars to explode and shine. While this event is happening, the faint unseen star happens to be visible to an observer. In this sense, this astronomical event is named novae which means "new" in Latin. Also, in supernovae eruption follows with an increase in luminosity but this increase is much greater than the novae. In the novae explosion after some time the star return to its initial structure and luminosity. But in the supernovae case, the star loses most of its mass during the eruption. Henceforth, supernovae destroy the star, but novae do not. In this work, other than the properties of novae and supernovae we will be focusing on near-earth supernovae. A near-earth supernova is a supernova that is sufficiently close to affecting Earth. Mostly released gamma radiation is responsible for this effect. Gamma radiation triggers the formation of nitrogen oxide in the Earth's biosphere. Also, there is a probability that near-earth supernovae have biological effects on Earth. Such researchers estimate that some evolutionary processes are caused by cosmic radiation. And the main output of cosmic radiation is supernovae. Therefore, this theory says that supernovae and evolution are somehow correlated. The aim of this study is to understand supernovae explosions and their effect on Earth. This understanding process needs to know other various astronomical terms. So, we include such concepts in this study. After the explanation of supernovae, we will examine the effects of near-earth supernovae with known theories and research.

NOVAE

A nova is a sudden increase in luminosity, the brightness of the star that slowly fades over in time. This fading process may be a couple of weeks or many months. All known novae are seen at white dwarf stars and in close binary systems. A white dwarf is a very dense star compared to the other star types. White Dwarves are considered to be the last stage of the one path of star evolution. They are located at the very bottom of the HR-Diagram. These binary systems in which novae occur usually contain a white dwarf and either a red giant, subgiant, or a main sequence star. For novae to start orbital period must decrease to one day or so. White dwarfs become so close to other stars that matter flows toward to white dwarf from

other stars to create a dense atmosphere. White Dwarf's thermal energy heats up the hydrogen in the atmosphere and eventually reaches a critical temperature to start runaway nuclear fusion. These reactions cause a massive increase in energy and therefore huge glow-up occurs in the binary system and initially faint white dwarf appears to be visible in the sky. The first observation of a nova was made by Tycho Brahe in the sixteenth century. He gave the name De nova stella in his book means concerning new star in Latin. But after the years' research shows that this event is actually not a nova but a supernova. Until the 1930's nova and a supernova were indistinguishable. In our times we call this type of nova a classical nova.

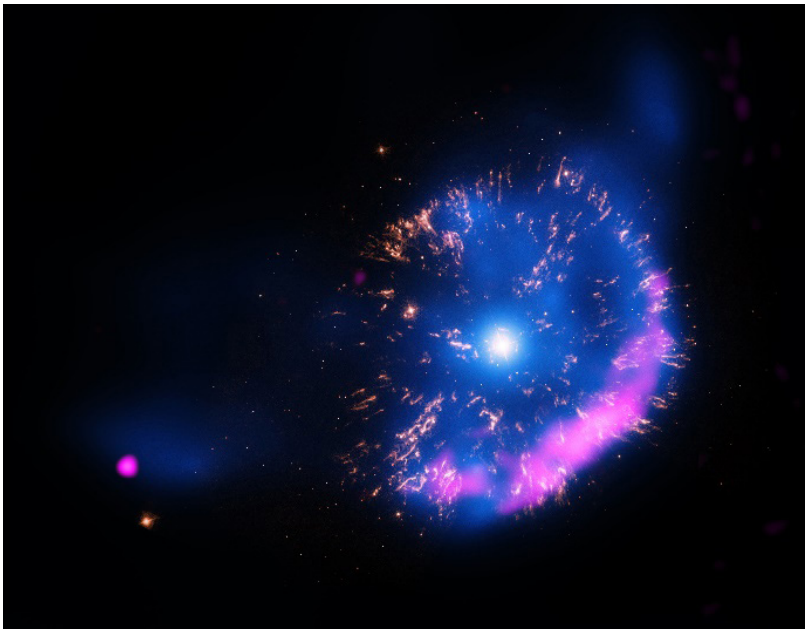

Figure 1. GK Persei: Nova of 1901

(For the whole figure captions please see the list at the end of the references part of this study)

SUPERNOVAE

A supernova can occur in two separate ways. The first one is the same case with the novae explosions. In a close binary system, a white dwarf pulls matter and then explodes this matter with its thermal energy output, or again in a close binary system stars are drawn to each other and collapse. The more complex and interesting one is the second case. A massive star's core experiences a gravitational collapse. Gravitational collapse is the shrinkage of the star due to its own gravitational force. This happens

when the star's nuclear pressure is not enough to balance its gravitation force. Although there are other cases and causes of supernovae, the main two classifications are these two.

Figure 2. supernova A type of Ia

DISCOVERY OF SUPERNOVAE

The first observation of the supernovae is possibly made by Indigenous observers in 4500 BC. There are many observations of supernovae in history that are recorded by astronomers, but I would like to jump to the main discovery process.

The first true observation of Nova was made by William Huggins in 1866. After that, in 1885 a nova-like explosion was observed in the direction of Andromeda galaxy. The reason behind the word nova-like is that in 1927 calculations showed this nova-like explosion had released much greater energy than an ordinary nova. The first research on this new type of nova was made by Walter Baade and Fritz Zwicky in 1931 and they gave the name supernova to this huge explosion.

HOW TO NAME A SUPERNOVA?

Names of supernovas consist of the SN abbreviation of supernova and year of discovery and finally a word that indicates the foundation order. First twenty-six supernova observations of the year followed by a letter

from a to z after that twenty-six we use aa, ab notation at the end of the name. For a better understanding, SN 2003b shows the second supernova discovered in 2003. For historical supernovae, we only use the foundation year afterward the SN, like SN 185.

SUPERNOVA CLASSIFICATION

Supernova classification is made by observing the optical spectra. Hydrogen presence in the optical spectra is the first separation of the supernovae. This first categorization was made by Rudolph Minkowski in 1941. If the absorption lines contain hydrogen, we call it Type II otherwise it is called Type I. In the 1980's this hydrogen-based categorizing was also sub-categorized by the presence of Silicon and Helium. Type 1a supernovae contain silicon absorption, type 1b does not contain silicon but contains helium, and type 1c does not contain either silicon or helium. In the first paragraph, we said that supernovae can happen in two separate ways. Type 1a is the result of a white dwarf containing a binary system and the other type is the result of core-collapse supernovae.

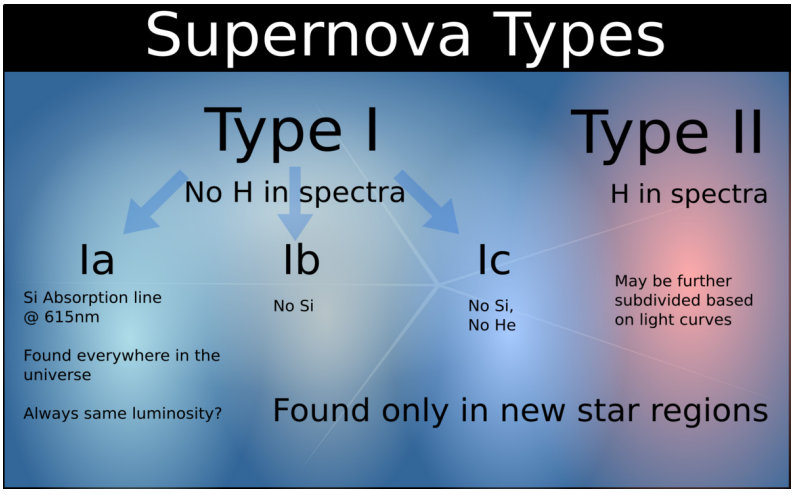

Figure 3. Supernova Types

TYPE I SUPERNOVAE

Type I supernovae are categorized by their optical spectra. If the spectra contain Si lines, we call that supernova Type 1a also If the spectra contain, He lines it is the Type 1b supernova but Type 1b does not contain Si absorption lines. There is one type called Type 1c lacking both He and Si

lines. The light curves of the Type I supernovae are generally the same. But the Type 1a supernova has the highest luminosity therefore brighter than the others.

TYPE II SUPERNOVAE

We said that Type II supernovae have hydrogen in their spectra. Most of the Type II supernovae have broad emission lines. Some of these types of supernovae have narrow features in their spectra, and we call them Type IIn and the n stands for the narrow. Some of the supernovae in type II have lines of helium that dominate the H-Balmer lines. We call such supernovas Type IIb and the name comes from the combination of Type Ib and Type II.

There is another sub-category in type II to identify lifetime hydrogen-dominant supernovae. This categorization is made by looking at the light curves. One sub-category is the "plateau" type. The light curve of this type of supernova remains relatively constant after the luminosity peak. This type is called Type II-p. The other is the Type II-L, the L stand for "linear." The light curve of this type is constantly decreasing, unlike type II-p. In the universe type, II-p is more common than type II-L.

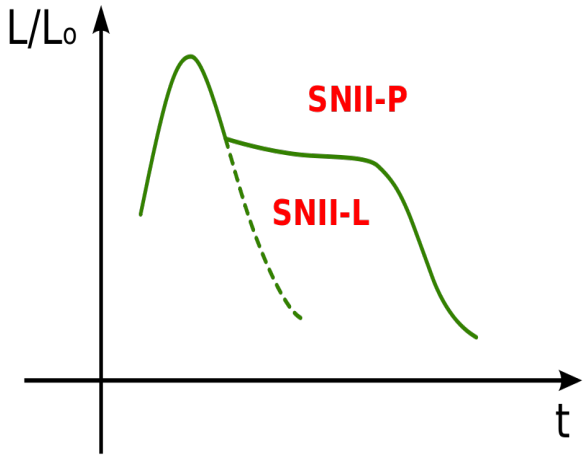

Figure 4. Supernova light-curves

THERMAL RUNAWAY

As we stated earlier Type Ia supernovae are the collapsing of a white dwarf star. This collapse is called a thermal runaway. Henceforth thermal

runaway is the process that type Ia supernova experiences.

In a closed binary system, White Dwarf's strong gravitational force is pulling material from the companion of the white dwarf, causing the white dwarf's mass to increase. Now we shall define the limit of the mass that a white dwarf can handle, astronomers call this Chandrasekhar Limit, named after S. Chandrasekhar. It is about 1.44 solar mass (2.765×10^{30} kg). If the increased mass is above the Chandrasekhar limit, the white dwarf begins to collapse (electron degeneracy pressure cannot balance the gravitational collapse). But in this case, the temperature raise is enough to star ignite carbon fusion in the core. Therefore, actually, the mass does not reach the limit, and a small portion of the white dwarf's mass is ejected during this process. We say that a supernova happens before a white dwarf turns into a neutron star. After a few seconds sudden nuclear fusion starts and releases enough energy to break the gravitational bound and the supernova happens. Matter flows outward with a velocity of %3 of the light speed and also luminosity increases, enormously increases.

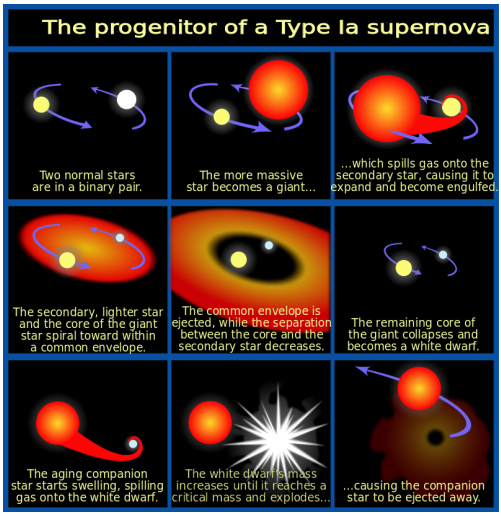

Figure 5. Schematic diagram of Type 1a supernova

CORE COLLAPSE

While Type Ia supernovae experience a nuclear explosion of a white dwarf, other types of supernovae experience core collapse. For massive stars (greater than 10 solar masses) fusion reactions do not end with an electron degenerate carbon core. It continues with carbon, neon, oxygen, and silicon burning. Eventually, these reactions end up with the most stable

element iron. Until this stage star's gravitational force is balanced with the energy of the fusion reactions. But iron cannot be fused without absorbing energy. Therefore, in this stage, there is not any energy to balance gravity and the star is to be ready to collapse. The remnant after the collapse is different from the mass of the core. While low-mass cores turn into neutron stars, high-mass cores will turn into black holes. After the collapse of the star, it begins to accelerate by beta decay, electron capture, and photodisintegration.

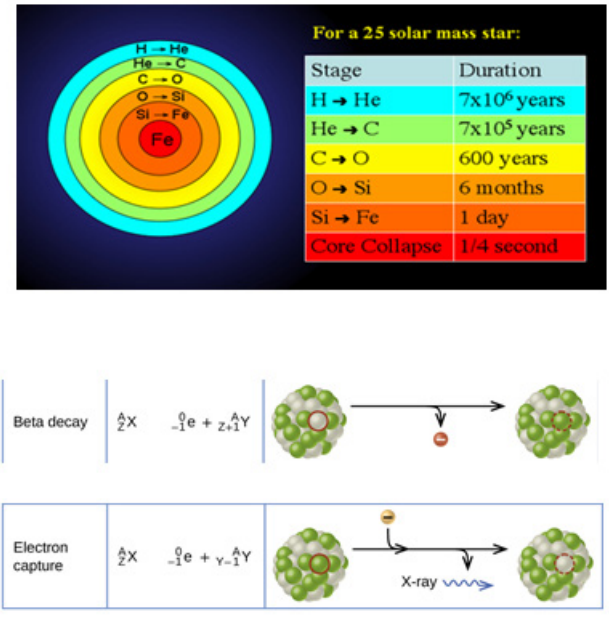

Figure 6. Nuclear reactions

Beta decay and electron capture causes neutrinos to spread and photodisintegration turns iron into helium and releases neutrons. These spreading neutrinos expand the inner core of the star and it becomes roughly 30km diameter. So that the density of the core becomes smaller. On the other hand, released neutrons try to balance collapse with neutron degeneracy pressure. If the mass of the core is greater than fifteen solar masses, neutron degeneracy pressure is not enough to stop core collapsing and the star ends up with turning into a black hole. In the lower mass cores, collapsing will stop, and new core consists of neutrons with high temperature. At this high temperature neutrinos and anti-neutrinos form thermal neutrinos and the density of these thermal neutrinos is greater than the electron capture neutrinos. About 10^{46} joules, approximately 10% of the star's rest mass, is converted into a

ten-second burst of neutrinos which is the main output of the event. The suddenly halted core collapse rebounds and produces a shock wave that stalls within milliseconds[2] in the outer core as energy is lost through the dissociation of heavy elements. A process that is not clearly understood is necessary to allow the outer layers of the core to reabsorb around 10^{44} joules from the neutrino pulse, producing the visible brightness.

DISTRIBUTION OF HEAVY ELEMENTS

Supernova explosions are the foundation of many elements in universe. Type Ia (nuclear expansion of the white dwarf) is mainly responsible for elements whose atomic mass is 56 (same with iron) and silicon. Types II, Ib, Ic also produce iron peak elements but less than the Type Ia plus they produce alpha elements and elements heavier than Zn up to Sr. This produce elements are distributed around via explosion and shock wave.

$$
\begin{aligned}
{}^{12}_{6}\mathrm{C} + {}^{4}_{2}\mathrm{He} &\longrightarrow {}^{16}_{8}\mathrm{O} + \gamma, \quad E = 7.16\ \mathrm{MeV}\\
{}^{16}_{8}\mathrm{O} + {}^{4}_{2}\mathrm{He} &\longrightarrow {}^{20}_{10}\mathrm{Ne} + \gamma, \quad E = 4.73\ \mathrm{MeV}\\
{}^{20}_{10}\mathrm{Ne} + {}^{4}_{2}\mathrm{He} &\longrightarrow {}^{24}_{12}\mathrm{Mg} + \gamma, \quad E = 9.32\ \mathrm{MeV}\\
{}^{24}_{12}\mathrm{Mg} + {}^{4}_{2}\mathrm{He} &\longrightarrow {}^{28}_{14}\mathrm{Si} + \gamma, \quad E = 9.98\ \mathrm{MeV}\\
{}^{28}_{14}\mathrm{Si} + {}^{4}_{2}\mathrm{He} &\longrightarrow {}^{32}_{16}\mathrm{S} + \gamma, \quad E = 6.95\ \mathrm{MeV}\\
{}^{32}_{16}\mathrm{S} + {}^{4}_{2}\mathrm{He} &\longrightarrow {}^{36}_{18}\mathrm{Ar} + \gamma, \quad E = 6.64\ \mathrm{MeV}\\
{}^{36}_{18}\mathrm{Ar} + {}^{4}_{2}\mathrm{He} &\longrightarrow {}^{40}_{20}\mathrm{Ca} + \gamma, \quad E = 7.04\ \mathrm{MeV}\\
{}^{40}_{20}\mathrm{Ca} + {}^{4}_{2}\mathrm{He} &\longrightarrow {}^{44}_{22}\mathrm{Ti} + \gamma, \quad E = 5.13\ \mathrm{MeV}\\
{}^{44}_{22}\mathrm{Ti} + {}^{4}_{2}\mathrm{He} &\longrightarrow {}^{48}_{24}\mathrm{Cr} + \gamma, \quad E = 7.70\ \mathrm{MeV}\\
{}^{48}_{24}\mathrm{Cr} + {}^{4}_{2}\mathrm{He} &\longrightarrow {}^{52}_{26}\mathrm{Fe} + \gamma, \quad E = 7.94\ \mathrm{MeV}\\
{}^{52}_{26}\mathrm{Fe} + {}^{4}_{2}\mathrm{He} &\longrightarrow {}^{56}_{28}\mathrm{Ni} + \gamma, \quad E = 8.00\ \mathrm{MeV}
\end{aligned}
$$

Figure 7. Alpha Process and Alpha Elements

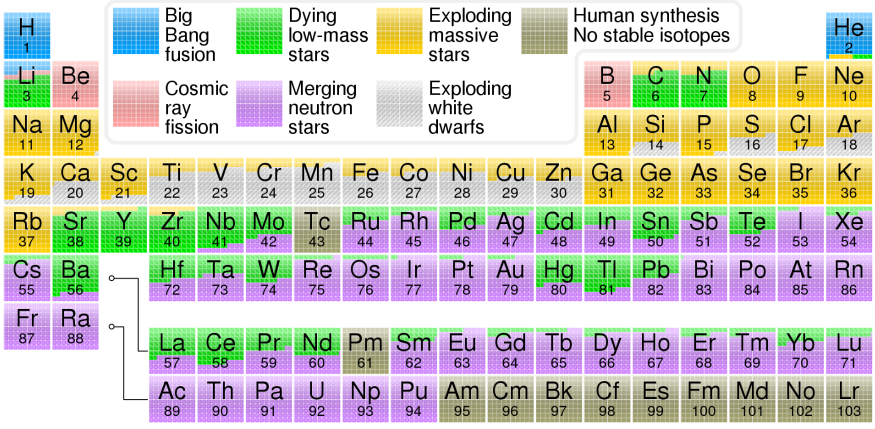

Figure 8. Periodic table and the stages of nuclear evolution

IMPACTS ON STELLAR EVOLUTION

As we mentioned earlier, supernovae produce heavier elements and distribute these elements through the interstellar medium. These free "heavier" elements eventually cool down and enrich star formation clouds. These enriched clouds tend to create different featured stars with different ratios of different elements. Also, there is one feature of supernovae that can influence star formation, the kinetic energy of the remnant of the supernova can start the star formation process by compressing the nearby molecular clouds.

SUPERNOVAE' EFFECTS ON EARTH

For a supernova to affect Earth, it must be close enough. We will call such supernovae near-earth supernovae in the preceding lines. The maximum distance for this case is 1000 light-years (300 pc). Of course, it depends on the type and the energy of the supernova. There exists an estimation that 20 supernovae happened nearby over 11 million years. Gamma rays from a supernova explosion are mostly responsible for the effects. Gamma rays happen to induce radiolysis of N_2 and O_2 in the biosphere. Radiolysis is the decomposition of the molecule into ions, atoms, or radicals. Decomposed nitrogen and oxygen molecules compose nitrogen oxides. These nitrogen oxides harm the ozone layer which causes to exposure solar radiation. Plankton families and reef communities are the most affected ones from this radiation. Hence the main effect of the near-earth supernova is disturbing the marine food chain.

Recently it has been shown that there is a close connection between the fraction of organic matter buried in sediments on Earth and changes in supernovae occurrence. This correlation is evident during the last 3.5 billion years and can be noticed in greater detail over the past 500 million years. This evidence indicates that supernovae have set essential conditions under which life on Earth had to exist. This is established in a new research article published in the scientific journal called 'Geophysical Research Letters' by Dr. H. Svensmark, DTU Space. According to the article, an explanation for the observed link between supernovae and life on Earth is that supernovae influence the Earth's climate. A high number of supernovae occurrences results in a cold climate with a temperature difference between the equator and polar regions. This results in strong winds and ocean mixing, which is vital for delivering nutrients to biological systems. High nutrient concentration leads to larger bio-productivity and a more extensive burial of organic matter in sediments. A warm climate has weaker winds and results in less mixing of the different oceans, a diminished supply of nutrients, a smaller bio-productivity, and less burial of organic matter. It has been noted that Photosynthesis produces oxygen and sugar from light, water, and CO_2. However, if organic material is not moved into

sediments, oxygen and organic matter become CO_2 and water. The burial of organic material prevents this reverse reaction. Therefore, supernovae indirectly control oxygen production, and oxygen is the foundation of all complex life. A measure of the concentration of nutrients in the ocean over the last 500 million years correlates with the variations in supernovae frequency. The concentration of nutrients in the oceans is observed by measuring trace elements in pyrite (FeS2) embedded in black shale, which is sedimented on the seabed. Estimating the fraction of organic material in sediments made it possible by measuring C-13 relative to C-12. Since life prefers the lighter carbon-12 atom, the amount of biomass in the world's oceans changes the ratio between carbon-12 and carbon-13 measured in marine sediments. Svensmark and colleagues have earlier also shown that ions help the formation and growth of aerosols, thereby influencing cloud fraction. As we know clouds can regulate the solar energy that reaches the Earth's surface, and the cosmic-ray-cloud link is important for climate. Empirical evidence shows that Earth's climate changes when the intensity of cosmic rays shifts. Supernovae' frequency can vary by several hundred percent on geological time scales, and as a result, climate changes become considerable. As Cosmic rays travel to the Solar system, some of them end their journey by colliding with the Earth's atmosphere where they are responsible for ionizing the atmosphere. A new NASA research has identified that supernovae could pose a threat to life on planets just like Earth. Chandra X-ray Observatory and other telescopes concluded that intense X-rays from exploded stars can affect planets over 100-light years away. A large dose of X-rays is produced when a supernova's blast wave infuses into dense gas surrounding the exploded star and they travel through the air for months, years, and even decades and can reach planets such as Earth, to trigger extinction events. However, even these alarming threats do not fully catalog the dangers in the wake of an exploded star. University of Illinois at Urbana-Champaign astronomer I. Brunton and his colleagues discovered that, in between these two previously identified dangers, lurks another. It has been indicated that if a torrent of X-rays sweeps over a nearby planet, the radiation would severely alter the planet's atmospheric chemistry as Dr. H. Svensmark also revealed. It can be said that the Earth is not in any danger from an event like this now, since there are no potential supernovae within the X-ray danger zone as claimed by Prof. Connor O'Mahoney, from the University of Illinois at Urbana-Champaign. However, it may be the case that such events played a role in Earth's past as it is revealed by his work. I recommend the reader watch the video through the link below

https://www.youtube.com/watch?v=Tpu1z6grJgc about the Biggest Supernova Ever Found Impacts Earth's Atmosphere. There are also plenty of links provided here at the end of the references list related to the text.

Figure 9. Illustration of an Earth-like exoplanet after X-ray radiation exposure. Image credit: NASA / CXC / M. Weiss.

BIOLOGICAL EFFECT PROBABILITIES

We know that supernovae are responsible for increasing radiation in the upper atmosphere. Considering the life on the Earth, the main effect of the increased radiation is mass extinction. Mass extinction is the extinction of at least half of the species on the Earth. Generally, we know the extinction of the dinosaurs could be a great example of a mass extinction event. Some of the investigations suggest that supernovae have caused the mass extinction of some animals.

It is possible to calculate the cosmic radiation flux received by Earth of the supernovae by looking at their remnants. Calculations made by Colgate and White (1966) found that Type II supernovae release 2 x 10^{51} ergs energy by cosmic rays. If we calculate the flux of the supernovae R light years away from earth's upper atmosphere, we get that $F = 9 \times 10^{13}/R^2$ erg cm^{-2} and the dose is $D = 3 \times 10^7/R^2$ roentgen. From these equations, we get that if there will be a smooth effect on Earth due to supernovae R must be less than a few hundred light years. Van Voeden (J. H. Oort, in Interstellar Matter in Galaxies, L. Woltjer) suggests that the number of Type II supernovae that occurred within R_0 and in t years is $N(R_0, t) = 2 \times 10^{-12} f t R_0^8$ where f is the frequency of the type II supernovae and is estimated like 0.02 per year. One can find that by the

equations driven the Earth receives 500 roentgens every 50 million years. By looking at the geological records in 600 million years one supernova with 2500 roentgens, four supernovae with 1000 roentgen, and ten or more supernovae with 500 roentgens happened. These doses would increase the mutation rate on Earth but cannot be the cause of any macroevolution. Therefore, if any biological effect of a supernova exists on Earth it would not be a macroevolution, but it can be a mass extinction.

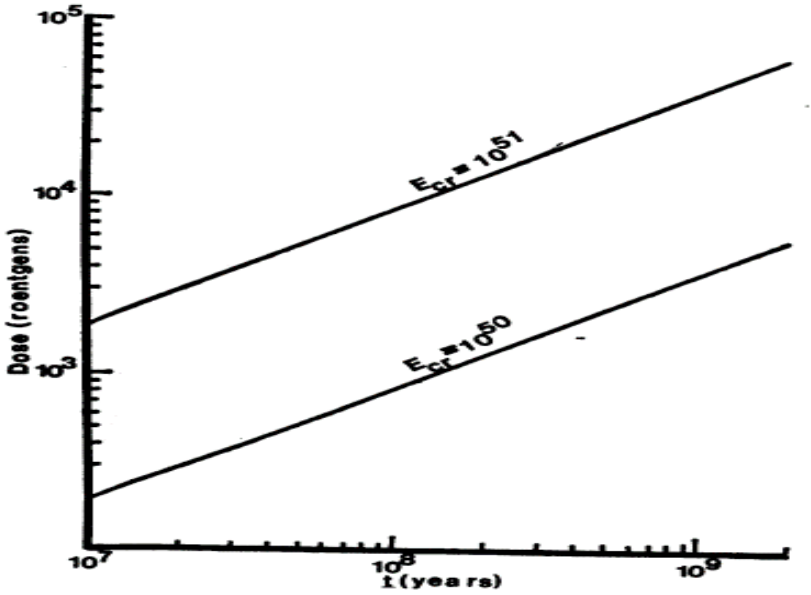

Figure 9. Cosmic radiation flux received by Earth

I would like to thank Taylan Yıldız, one of my undergraduate students for his help in preparing this short review.

1

REFERENCES related by the text:

https://en.wikipedia.org/wiki/Supernova

https://spaceplace.nasa.gov/supernova/en/

The Physics of Supernova Explosions S. E. Woosley and Thomas A. Weaver Annual Review of Astronomy and Astrophysics 1986 24:1, 205-253

https://en.wikipedia.org/wiki/Explosion

Theory of core-collapse supernovae Th. Jankaa, K. Langankebc, A. Mareka, G. Martínez-Pinedob, B. Müllera

https://en.wiktionary.org/wiki/influx

https://en.wikipedia.org/wiki/Nova

https://en.wikipedia.org/wiki/Near-Earth_supernova

https://en.wikipedia.org/wiki/White_dwarf

Biologic Effects of Supernovae K. D. TERRY AND W. H. TUCKER

https://www.sciencedirect.com/topics/physics-and-astronomy/gravitational-collapse

https://en.wikipedia.org/wiki/History_of_supernova_observation#Telescope_observation

https://www.universetoday.com/92173/supernova-alphabet-soup/

https://astronomy.swin.edu.au/cosmos/S/supernova+classification

https://www.ngawhetu.com/index.php/stellar-evolution-hdn?start=13

https://en.wikipedia.org/wiki/Chandrasekhar_limit

https://astronomy.swin.edu.au/cosmos/c/core-collapse

https://en.wikipedia.org/wiki/Photodisintegration

https://en.wikipedia.org/wiki/Alpha_process

https://en.wikipedia.org/wiki/Radiolysis

https://iopscience.iop.org/article/10.1086/346127/meta

https://www.amnh.org/exhibitions/dinosaurs-ancient-fossils/extinction/mass-extinction#:~:text=Mass%20extinctions%E2%80%94when%20at%20least,of%20all%20species%20went%20extinct.

CLARK, D., MCCREA, W. & STEPHENSON, F. Frequency of nearby supernovae and climatic and biological catastrophes. *Nature* **265,** 318–319 (1977).

https://arxiv.org/abs/astro-ph/9605128v1

Theory of core-collapse supernovae, H.-Th. Janka, K. Langanke, A. Marek, G. Martínez-Pinedo, B. Müller, Physics Reports, Elsevier, April 2007

J. H. Oort, in Interstellar Matter in Galaxies, L. Woltjer

S. Colgate and R. White, 1966 ,The Astrophysical Journal

Colgate, S. A. (1979). "Supernovae as a standard candle for cosmology".

Woosley, S. E.; Janka, H.-T. (2005). "The Physics of Core-Collapse Supernovae"

Barwick, S. W; Beacom, J. F; Cianciolo, V.; Dodelson, S.; Feng, J. L; Fuller, G. M; Kaplinghat, M.; McKay, D. W; Meszaros, P.; Mezzacappa, A.; Murayama, H.; Olive, K. A; Stanev, T.; Walker, T. P (2004). "APS Neutrino Study: Report of the Neutrino Astrophysics and Cosmology Working Group"

https://www.innovationnewsnetwork.com/supernovae-and-life-earth-are-seemingly-connected/16784/

https://interestingengineering.com/science/supernovae-pose-a-threat-to-life-on-earth-says-nasa-study

https://www.sci.news/astronomy/x-ray-luminous-supernovae-11849.html

https://www.universetoday.com/158316/how-dangerous-are-nearby-supernovae-to-life-on-earth/

https://astronomy.com/magazine/2019/07/how-supernovae-have-affected-life

https://www.space.com/new-supernova-type-destroy-planet-atmosphere

https://www.skyatnightmagazine.com/space-science/what-happen-supernova-close-to-earth/

https://www.space.dtu.dk/english/news/2022/01/supernovae-and-life-on-earth-appears-to-be-closely-connected?id=acf3fcac-075f-4e09-a3b6-a763305f1b84

https://www.popularmechanics.com/space/deep-space/a34686420/supernovas-change-earth-climate-tree-rings/

REFERENCES related with the Figures provided in the text.:

https://upload.wikimedia.org/wikipedia/commons/1/11/GKPersei-MiniSuperNova-20150316.jpg

https://commons.wikimedia.org/wiki/File:GKPersei-MiniSuperNova-20150316.jpg

https://en.wikipedia.org/wiki/File:SN1994D.jpg

http://large.stanford.edu/courses/2008/ph204/deaconu1/images/f1big.png

https://commons.wikimedia.org/wiki/File:SNIIcurva.svg

https://commons.wikimedia.org/wiki/File:Nucleosynthesis_periodic_table.svg

BÖLÜM 6

CHAPTER 6

THE STRUCTURAL, OPTICAL AND ELECTROCHEMICAL PROPERTIES OF UNDOPED AND Co DOPED NiO FILMS

Olcay GENÇYILMAZ[1]

1 Assoc. Prof., Çankırı Karatekin University, ORDIC ID: 0000-0002-7410-2937

1. Introduction

Nickel oxide is one of p-type semiconductors with stable wide band gap (3.6 - 4.0 eV) and it has 3d transition properties (Kunz, 1981). NiO is a well-studied material due to its use as the positive electrode in batteries, electrochromic devices, fuel cell electrodes, catalysis, gas sensors, and magnetic materials (Soleimanpour et al., 2012; Avendaño et al., 2016). In addition, NiO is the most important of the p-type metal oxides used in different applications due to its electronic band structure, high chemical stability, and electrochromic efficiency. NiO has the property of showing anodic electrochromic and can be colored with charge output. Because of these properties, it is used in areas such as medical, architectural, automotive and electrochromic devices. NiO films are also used in gas sensors, solar cells and fuel cells. The potential use of NiO films in these areas depends on the morphology, conductivity, transmittance and crystal structure of the films. One of the most important experimental parameters affecting these properties is the base used in NiO production. Therefore, ITO, FTO and glass substrates are generally preferred as substrates for the production of films.

NiO thin films are prepared by different physical and chemical methods like sputtering (Sato 1993), electrodeposition (Koussi-Daoud et al., 2016), sol- gel (Sreethawong et al., 2007) , chemical precipitation (Taşköprü et al., 2015), and spray pyrolysis (Yu and Kim, 2013). Among these techniques, spray pyrolysis has recently received attention. The spray technique is preferred more because of its economic, practicality, production on wide and different bases, and reproducibility. Also it is one of the most widely used techniques in the production of n-type and p-type thin films. This technique is suitable for thin film storage on different substrates such as FTO, ITO, glass. Another parameter that affects the physical and chemical properties of NiO films is doping. Doping is a fundamental technique to control the properties of semiconductors and to obtain new multifunctional technological materials.

Physical and chemical properties of NiO films strongly depend on doping elements. In order to provide some interesting properties, nickel oxide is doped by several elements such as lithium, cadmium, iron, magnesium, tungsten, manganese (Li et al., 2016; Taşköprü et al., 2015; Sharma et al., 2016; Yin, 2014). NiO and Co both have rock-salt structure, with lattice parameters 4.177 and 4.261 Å, respectively (Taşköprü et al., 2015). The lattice mismatch between them is 2 %. The crystal ionic radii of Co^{2+} (0.745 Å) and Ni^{2+} (0.69 Å) closely match each other. Thus, it is possible to dope NiO with relatively high amounts of Co without causing much lattice strain. Also, there are a few works on the effect of Co doping on structural, optical, morphological properties of NiO films deposited by spray pyroly-

sis technique (Bakr et al., 2015; Gençyılmaz, 2021; Sharma et al., 2014).

For these reasons, we produced the NiO film on the glass and FTO substrate, both without undoped and with Co doped by ultrasonic spray pyrolysis technique. We report the effect of Co doping on some optical parameters such as Urbach energy, refractive index, and dielectric constants, structural properties and electrochromic performance of NiO films.

2. Experimental procedures

2.1. Production of NiO films

Undoped and Co doped NiO films were deposited onto glass and FTO-coated glass substrates by ultrasonic spray pyrolysis technique. Nickel nitrate hexahydrate ($Ni(NO_3)_2 \cdot 6H_2O$) (0.01 M) and cobalt (II) nitrate hexahydrate ($Co(NO_3)_2 \cdot 6H_2O$) were used as source precursors for Ni and Co, respectively. The cobalt doping level was chosen at 3 % to avoid any disorder in NiO films.

Aqueous ammonia was added to the starting solution to adjust the value of pH= 9. Before the start of the deposition process, the substrates were cleaned thoroughly using warm acetone and methanol for 10 minutes. Finally, substrates were ultrasonically cleaned with deionized water.

The temperature of substrates was maintained at 450 °C using a temperature controller. The nozzle to substrate distance was fixed at 25 cm. The flow rate of solution and carrier gas pressure during spraying was held constant at 5 $ml.min^{-1}$ and 0.2 bars, respectively. Nitrogen was used as the carrier gas. The deposition time was 20 min. nickel nitrate hexahydrate solution was sprayed onto the glass and FTO-coated glass substrates.

When aerosol droplets come close to the substrates, highly adherent thin films were produced due to the pyrolytic process resulting in the formation NiO films according to the following reaction:

$$Ni(NO_3)_2.6H_2O \rightarrow NiO + 2NO_2 + 1/2O_2 + 6H_2O \qquad (1)$$

The samples were deposited on FTO-coated conducting glass substrates for electrochemical analysis. The colors of the undoped and Co doped NiO films were dark gray and brown. The change in color is attributed to the Co doping.

2.2. Characterization techniques

X-ray diffractometer (Bruker D8 Advance XRD) with *CuKα* line (λ=1.5406 Å) was used to analyze the crystal structure and calculated some structural parameters using XRD results. Raman spectra were obtained with a Bruker Senterra Dispersive Raman Microscope. A 3B diode

laser (532 nm) having 3-5 cm^{-1} resolution was used as excitation source at a power of 10 mW.

The morphological study was carried out using a field emission scanning electron microscopy (FESEM Zeiss Ultra Plus). The thicknesses of the NiO films were obtained by FESEM images from cross section views and found to be 396 nm in average.

Optical transmittance and the absorbance of films were carried out on UV-2550 UV–Vis spectrophotometer in the wavelength range 200–1000 nm.

The electrochemical properties of the films were characterized by cyclic voltammetry in a three-electrode arrangement using Electrochemical Quartz Potentiometer. Ag/AgCl was used as a reference electrode, a platinum wire as the counter electrode (anode) and NiO films deposited on FTO-coated glass substrate as the working electrode (cathode).

3. Results and discussions

The XRD patterns of the undoped and Co doped NiO films grown onto the glass and FTO-coated conducting glass substrates are shown in Figure 1. XRD pattern of undoped NiO film shows five peaks corresponding face centered cubic crystal structure with diffraction peaks at (111), (200), (220), (311), and (222) (Bunsenite, JCSPD 47-1049). In Figure 1(a), the XRD pattern of Co doped NiO film, the intensities of the crystal planes decrease and (311) peak disappeared. Also, it is observed that the peak positions of the (111) plane slightly change after doping, which implies that the structures have very small strain. Also, the unit cell value changes with Co doping. The slight shift in the peak position and the unit cell parameter may be attributed to the doped content, different ion radius (0.69 Å for Ni^{2+} ions and 0.745 Å for Co^{2+} ions) and the replacement of Ni^{2+} ions by Co^{2+} ions. There are no peaks related to other phases in XRD patterns which are related to low doping concentration (3 % at).

The films are deposited on FTO-coated glass substrates also have shown face cubic structure with (111), (200), and (220) diffraction planes (Figure 1(b)). Other peaks in the patterns belong to FTO. The deposited films on FTO-coated conducting glass substrates for electrochemical analysis have suitable structural properties.

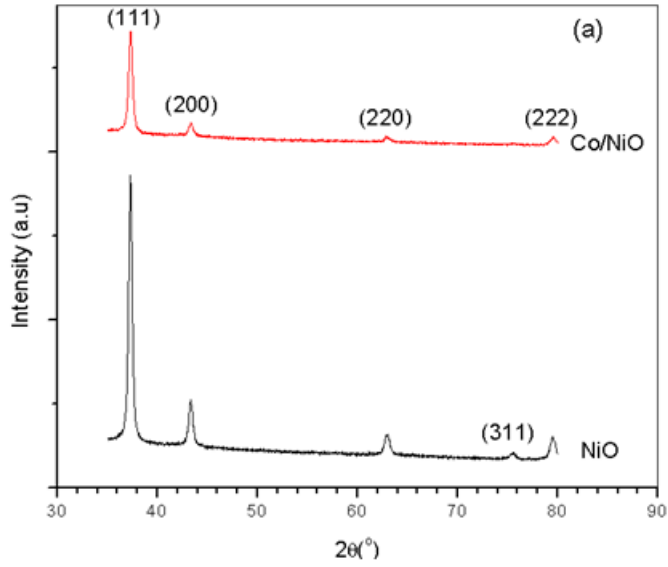

Figure 1. *The XRD patterns of the undoped and Co doped NiO films grown onto the (a) glass*

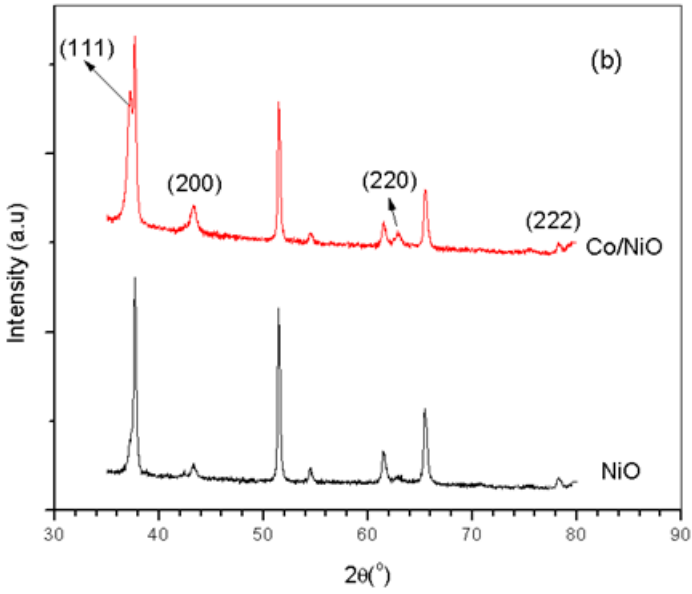

Figure 1. *The XRD patterns of the undoped and Co doped NiO films grown onto the (b) FTO-coated conducting glass substrates*

The texture coefficients (*TC*) have been determined using the equation below (Ghosh et al. 2004):

$$TC = \frac{I_{(hkl)}/I_{0(hkl)}}{\frac{1}{N}\sum_N I_{(hkl)}/I_{0(hkl)}} \quad (2)$$

where $I_{(hkl)}$ is the measured intensity, $I_{0(hkl)}$ is the standard intensity, and N is the number of diffraction peaks. This calculation is done to distinguish between dominant and preferential orientation. If $TC_{(hkl)}$ is greater than 1, we can say that atoms grow with a preferential orientation in this plane (Sharma et al. 2014).

The variation of $TC_{(hkl)}$ for prepared samples is shown in Figure 2. It is worth noting that the preferred orientation was affected by the doping process. We observed that while the undoped NiO films have two preferential growth along (111) and (222) planes, the Co-doped film has a preferential growth along (111) direction. Calculated $TC_{(hkl)}$ values for other planes are also listed in Table 1. The increase and decrease in the value of $TC_{(hkl)}$ are attributed to the reorientation effect of crystal in a given *(hkl)* direction due to the doping process.

The interplanar spacing d_{hkl} values of undoped and Co doped NiO films are calculated by using Bragg relation (Stock and Cullity, 2001):

$$2d_{hkl}sin\theta = n\lambda \quad (3)$$

where n is integer of diffraction and λ is the wavelength.

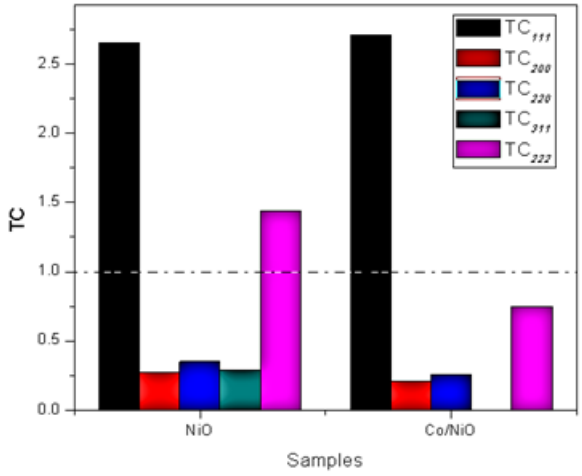

Figure 2. *The texture coefficient values of NiO films*

The lattice parameter is calculated using the following relation (Stock and Cullity, 2001):

$$d = \frac{a}{\sqrt{h^2+k^2+l^2}} \quad (4)$$

Table 2 summarizes the positions of (111) peak, the calculated values of $d_{(111)}$, which shows deviations from the standard value of the lattice parameters a= 4.1770 Å taken from JCPDS card file data. This could be an indication of strain in the films and interpreted as the unit cell of the samples undergoes contraction or expansion along a-axis.

The average crystallite size was calculated for (111) plane using the Scherrer formula (Stock and Cullity, 2001):

$$D = \frac{0.9\lambda}{\beta cos\theta} \quad (5)$$

where β is the broadening of diffraction line measured at half of its maximum intensity (FWHM). Comparing the FWHM values corresponding to (111) plane, the broadening of the diffraction peak is observed for the Co-doped film. The most probable explanation may be the increase in crystal defects. The average crystallite size of the samples was calculated in 22 and 20 nm for un-doped and Co- doped NiO films, respectively (Table 2).

Investigation of materials needs to the characterization of microstructure with an emphasis on the particle size and strain. The different doping elements may cause the lattice stress or strain in the material which dramatically affects optical and electrical properties of materials. The lattice strain and crystallite size are two independent factors that contribute to the total peak broadening. The total peak broadening is the sum of the contributions of crystallite size and strain present in the material. The crystallite size and strain (ε) in the films have been determined from the XRD measurements by using the Williamson–Hall equation (Gurumurugan et al., 1194) :

$$\beta = \frac{k\lambda}{Dcos\theta} - 4\varepsilon\, tan\theta \quad (6)$$

The term ($\beta cos\theta$) was plotted with respect to ($4sin\theta$) for the well-resolved peaks as seen in Figure 3. Accordingly, the slope and y-intersect of the fitted line represent strain and particle size, respectively. The estimated

strain and crystallite size values of the samples are listed in Table 2. The plots showed positive strain for the NiO film and negative strain for Co doped NiO film. The positive value of the strain indicates that the strain is tensile, and the negative value indicates that the strain is compressive (Ghosh et al., 2004).

Since the Raman scattering is very sensitive to the microstructure of nanocrystalline materials, it is also used to see the effect of Co doping in NiO structure. Figure 4 shows the Raman scattering spectra of the films.

Raman spectra show typical resonant Raman peaks located at 500 cm^{-1} and 1100 cm^{-1} could be assigned to first order longitudinal optical (LO) and second order longitudinal optical (2LO) phonon modes of NiO, respectively. The defect-induced LO mode occurred in NiO may be due to nickel vacancy defects (Taşköprü et al., 2015). It is obvious that the LO mode exhibits a blue shift with Co doping. It is attributed to the defects or impurity atoms (i.e., Co atoms) in the NiO film.

The FESEM images of the surface morphologies of samples were given in Figure 5. The surface morphology of the films has uniform grain distribution and small particle size. As a result of doping, different atomic clusters will form in the material, so the material may have a different crystal structure. In addition, the clusters of atoms formed in the material can also affect the grain size and shape. It was determined that the morphology of the Co-doped film was denser with the smaller particle size distribution. These results can be supported by XRD results.

Table 1. *The texture coefficients (TC) values of NiO films for dominant orientations*

Films	**$TC_{(hkl)}$**				
	$TC_{(111)}$	**$TC_{(200)}$**	**$TC_{(220)}$**	**$TC_{(311)}$**	**$TC_{(222)}$**
NiO/FTO	2.65	0.27	0.35	0.29	1.44
Co:NiO/FTO	2.71	0.21	0.26	-	0.75

Table 2. *Some structural parameters of NiO films*

Films	**$2\theta_{(111)}$ (°)**	**$d_{(111)}$ (Å)**	**a (Å)**	**D (nm)**	**DW-H**	**ε %**
NiO/FTO	37.177	2.4164	4.1870	20.2	27.6±1.1	0.095±0.015
Co:NiO/FTO	37.296	2.4090	4.1725	19.4	17.8±1.3	0.075±0.043

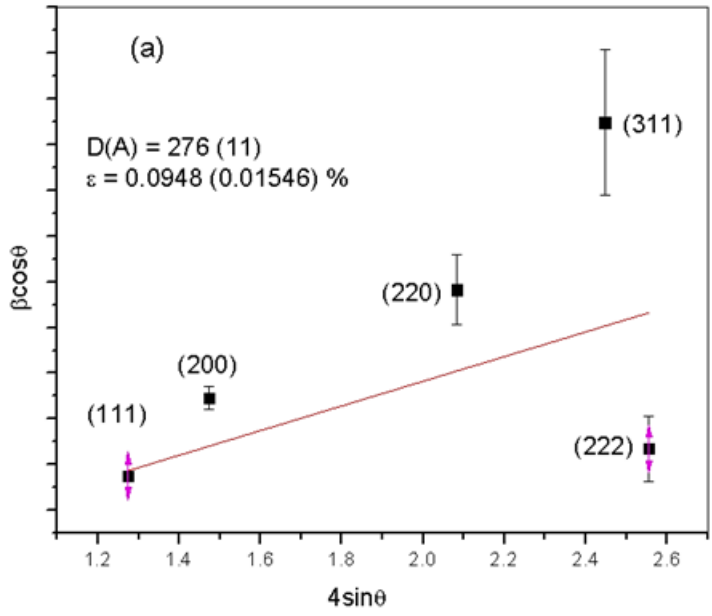

Figure 3. *The graph of the term (βcosθ) in relation to (4sinθ) of (a) NiO films*

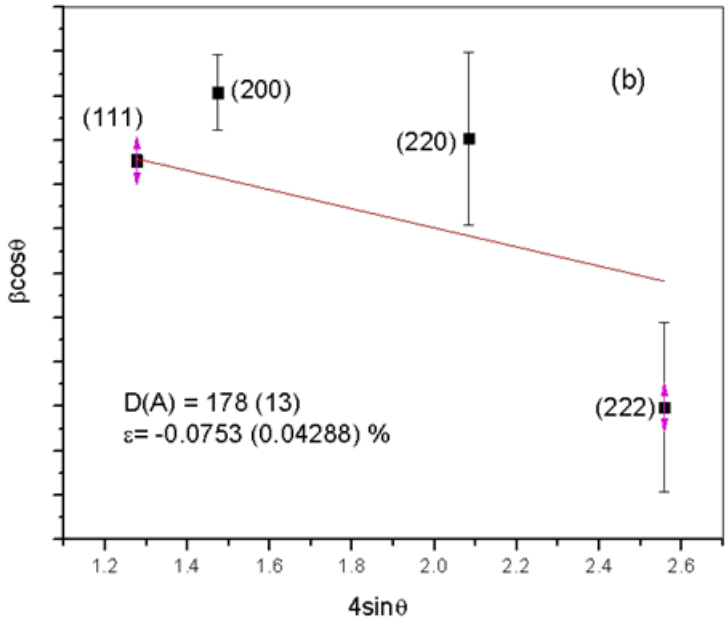

Figure 3. *The graph of the term (βcosθ) in relation to (4sinθ) of (b) Co:NiO films*

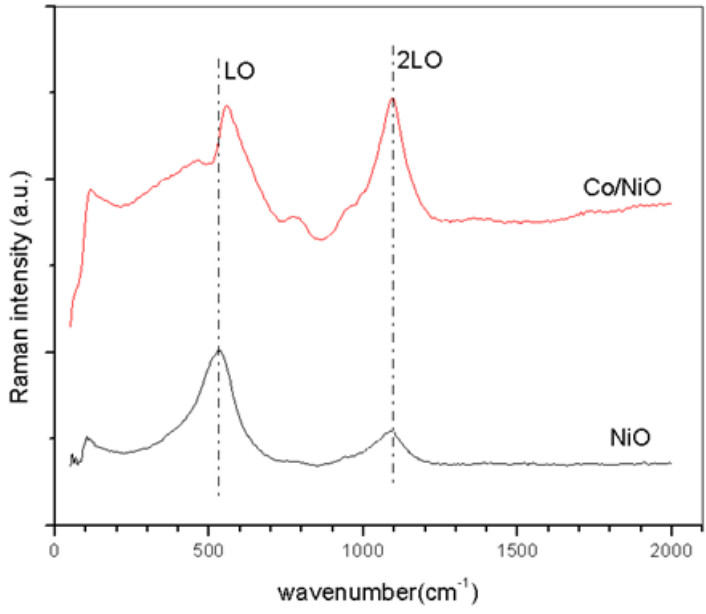

Figure 4. *The Raman scattering spectra of the NiO films*

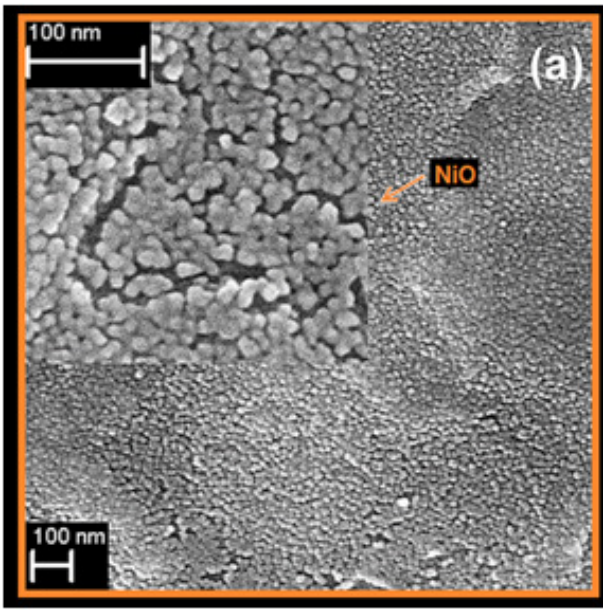

Figure 5. *The FESEM images of (a) NiO films*

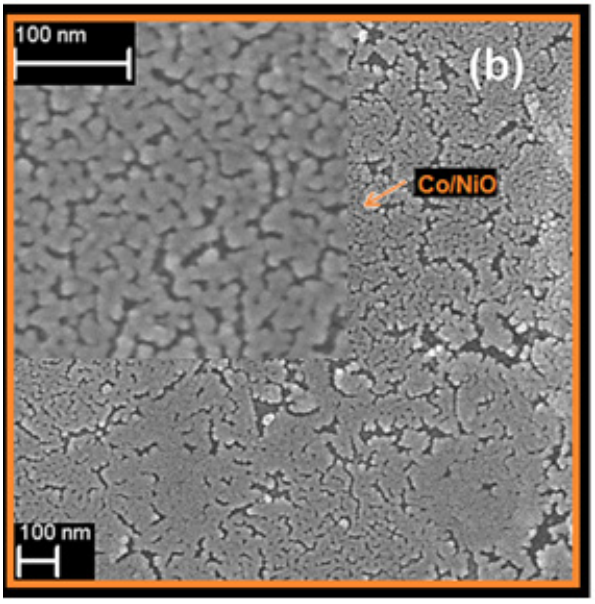

Figure 5. *The FESEM images of (b) Co:NiO films*

The optical properties of NiO films were studied to investigate the effect of the doping on the optical transmittance, band gap, and Urbach energy. The transmission spectra of the NiO films were taken in the wave-

length range of 300-900 nm at room temperature. Figure 6 shows the transmittance and the reflectance spectra of NiO samples. As seen in Fig. 6, the transmission and reflectance spectra of the films have been changed with Co doping. While the sharp absorption edge can be clearly observed for NiO film, the absorption edge shifts toward longer wavelength with Co doping which shows that the optical band gap of the films was shrunk with Co doping. We think that our Co-doped NiO film has deformation and defects near band edges due to the poor crystallinity (Umar and Hahn, 2009). This conclusion supports the XRD results. In addition, Co-doped NiO film exhibits lower optical transmittance. The similar results were observed by Predanocya et al. (Predanocy et al. 2017). This condition can be ascribed to the surface texture and decrease in roughness of film. Reflectance spectra of NiO films are shown in Figure 6b. It was determined that the average reflection value of NiO films is about 2 % in the visible region of the spectrum.

The band gaps of NiO films were determined using Tauc method. This method is associated absorption coefficient (α) and photon energy ($h\nu$) (Pankove, 1975):

$$\alpha h\nu = A(h\nu - E_g)^{1/2} \tag{7}$$

where A is the edge width parameter and E_g is the optical band gap. Fig. 7 shows the variation of $(\alpha h\nu)^2$ versus $h\nu$ for NiO films. The band gaps values were calculated 3.67 eV and 3.61 eV for undoped and Co doped films, respectively. It is clear that the band gap values are slightly decreased with Co doping. This may be due to the change in the crystallinity level in the film with the doping. This case attributes to the changes of crystallinity, surface morphological, film thickness, atomic distances, and the grain size gap, resulting in the reduction of the band gap (Patil et al., 2005; Gençyılmaz et al., 2015):

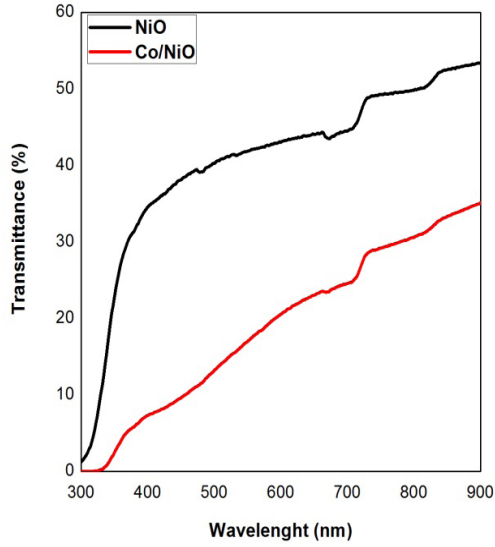

(a)

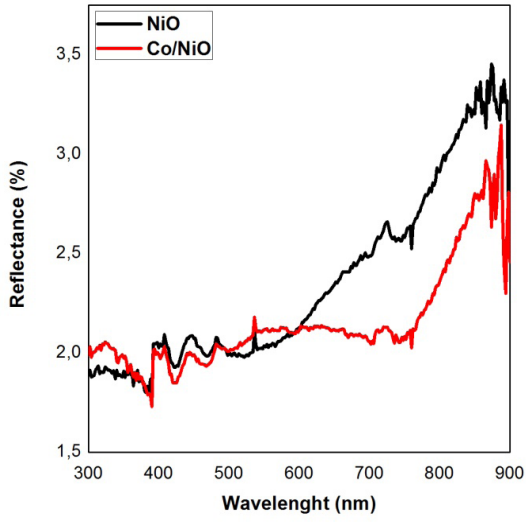

(b)

Figure 6. *(a) Transmittance and (b) reflectance spectra of NiO films*

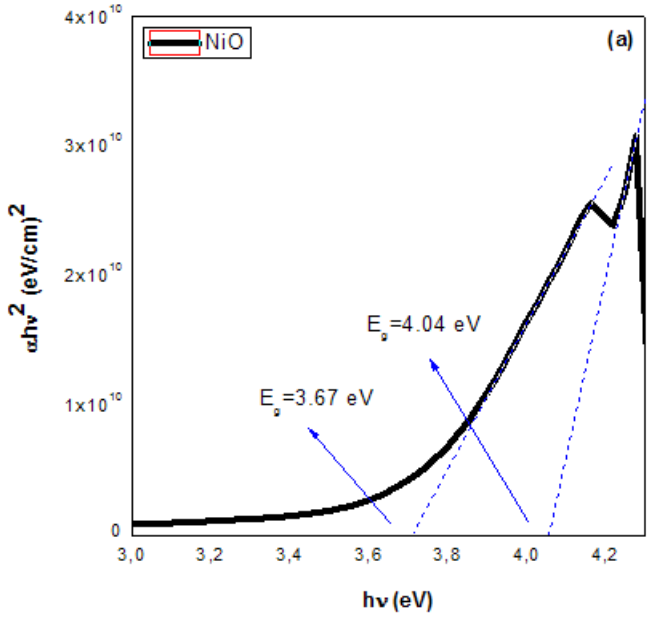

Figure 7. *The variation of* $(\alpha h\nu)^2$ *versus h (a) NiO films*

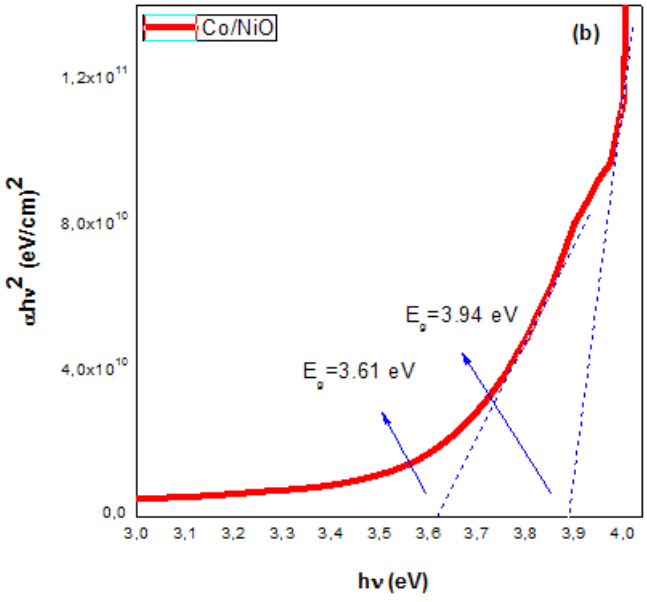

Figure 7. *The variation of* $(\alpha h\nu)^2$ *versus h (b) Co:NiO films*

The absorption coefficient (α) has been calculated from transmittance (*T*) and reflectance (*R*) data using the relation (Urbach, 1953):

$$\alpha = \frac{1}{d}.ln\left[\frac{(1-R)^2}{2T}\right] \quad (8)$$

where d is the film thickness. The spectral variation of α has been shown in Fig. 8.

While sharper absorption edge is observed near (~350 nm) for un-doped NiO film, the absorption edge of Co-doped NiO film shows a clear shift to longer wavelengths (red shift) that causes a decrease in the optical band gap. Generally, absorption changes as a function of crystalline properties (Sharma et al. 2016). The defect states inside the band gap make the optical absorption broad, while a rather sharp behavior is observed for the films with good crystalline quality. This decrease is attributed to Co^{+2} or Co^{+3} ions localized in the NiO lattice (Windisch et al., 2001).

The schematic band diagram of NiO film is shown in Figure 8. The valence band is formed in O^{2-} states. The Co^{+2} or Co^{+3} ions create additional energy levels in the band gap structure near the valence band. Since the band gap of CoO (1.67 eV for bulk crystals) is lower than that of NiO (3.67 eV for the present work), the band gap of Co-doped NiO should be lower than the band gap of un-doped NiO. The similar red shift off in the band gap of NiO film is discussed by various studies (Chia-Ching et al, 2013; Gençyılmaz et al., 2015; Şahin et al., 2014; Agrawal et al., 2017)

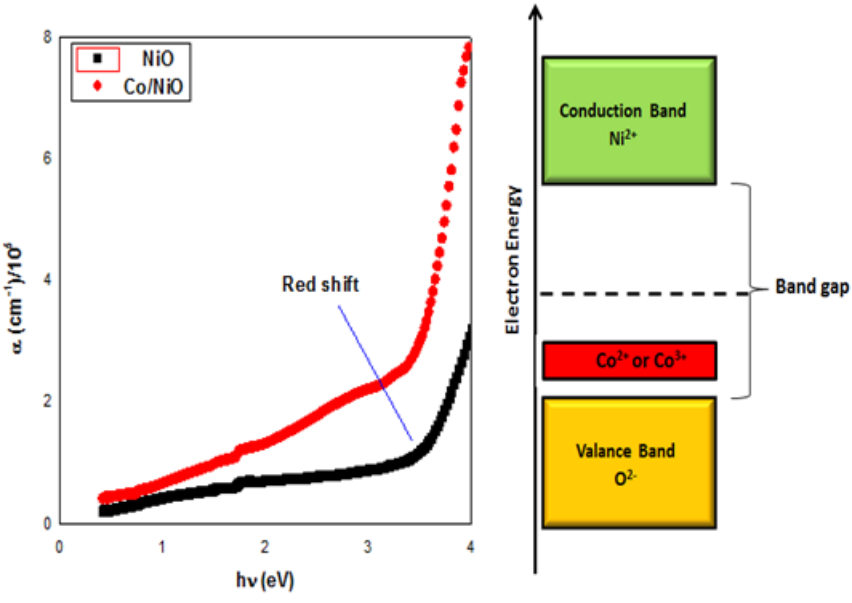

Figure 8. *The absorption coefficient (α) spectra of NiO films*

The Urbach energy is calculated with the following equation (Agrawal et al., 2017).

$$\alpha(h\nu) = \alpha_0 \exp(h\nu / E_u) \quad (9)$$

where α_0 is a constant, E_u is Urbach energy which corresponds to the width of the band tail and could be determined as the width of the localized states. Figure 9 shows the graph obtained with this relation. Usually, E_u depends on temperature and structural disorder describes the width of the localized states in the bandgap region (Boubaker, 2011). Figure 10 shows the changing of $ln\alpha$ vs. ($h\nu$) for the films.

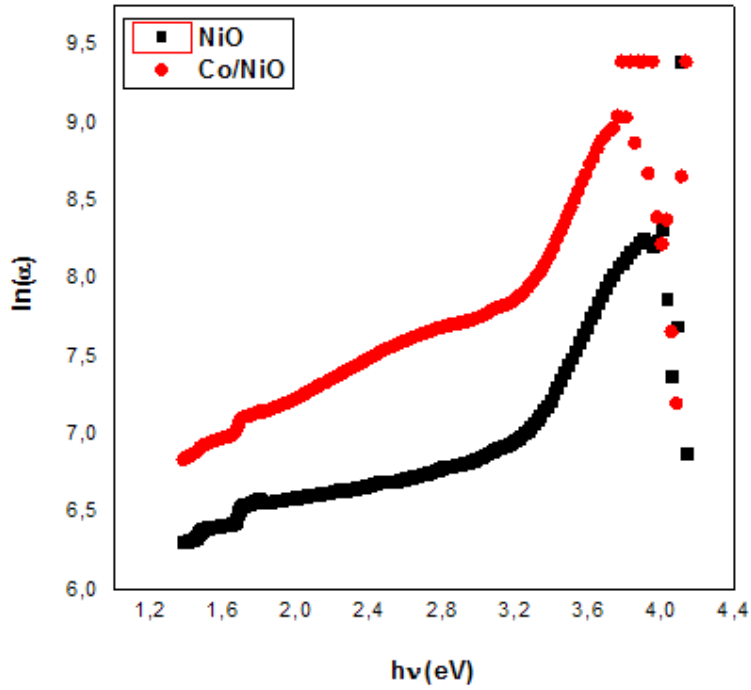

Figure 9. *The changing of lnα vs. (hν) for the NiO films*

To obtain the width of Urbach tail, a linear fit was established in the linear portions of the curves and the results were listed in Table 3. The steepness parameter, $s=kT/E_u$; characterizing the broadening of the optical absorption edge due to electron-phonon or exciton-phonon interactions (Mahr, 1962) was also determined taking T =300 K and given in Table 2.

E_u values change inversely with optical band gap. Also, the Urbach energy values give knowledge about local defects which create localized states in the bandgap region (Fterich et al., 2016). The refractive index (n) of the films was calculated using Herve-Vandamme and Moss relations (Mezrag et al., 2010; Akaltun et al., 2015; Hannachi and Bouarissa, 2015). Both methods present the relation between the refractive index and the band gap energy. Herve -Vandamme's method is;

$$n = \sqrt{1 + \left(\frac{A}{E_g + B}\right)^2} \quad (10)$$

where A and B are numerical constants with values of 13.6 and 3.4 eV, respectively. Also, Moss relation is presented;

$$n^4 = \frac{k}{E_g} \quad (11)$$

where k is a constant with a value of 108 eV. The calculated n values for un-doped and Co-doped NiO films are listed in Table 2. The n value increased with Co doping. It is attributed to the smaller optical band gap of Co-doped NiO film. Also, high frequency (ε_∞) and static (ε_o) dielectric constants were calculated using the following relations; $\varepsilon_\infty = n^2$ and $\varepsilon_o = 18.52 - 3.08E_g$, respectively. The calculated dielectric constants are listed in Table 2. High-frequency dielectric constant values changed according to used methods and Co-doping (Hannachi and Bouarissa, 2015).

Table 3. *Some optical parameters of NiO:Co/FTO films*

Films	**E_g (eV)**		**E_u (meV)**	**$\sigma x10^{-5}$**	**Herve-Vandemme**			**Moss Relation**		
	E_{g1}	**E_{g2}**			**n**	**ε_∞**	**ε_0**	**n**	**ε_∞**	**ε_0**
NiO	4.04	3.67	464	5.60	2.16	4.69	7.20	2.32	5.42	7.20
Co:NiO	3.94	3.61	412	6.13	2.18	4.75	7.37	2.33	5.46	7.37

The electrochemical properties of the NiO samples are characterized by cyclic voltammetry (CV), and coloration-bleaching cycling tests. The voltage ranges were 0.1-0.6 V for un-doped NiO film and -0.3- 0.8 V for Co-doped films. The voltage ranges were chosen in order to produce rapid degradation of the films. The electrolyte and sweep rate were 0.3 M KOH and 100 mV/s, respectively. Figure 10 presents the CV cycles of the samples at selected 1st, 25th and 50th cycles which show complete reversibility in the given voltage ranges. Both samples show good electrochemical stability during 50 cycles. It is clearly seen that the areas under anodic and cathodic curves are nearly identical which a sign of good reversibility.

The peaks associated with each cycle correspond to the oxidation and reduction process during the electrochemical experiment. There was one main oxidation peak (E_o) during the anodic scan and one reduction peak (E_R) during the reversed scan. The peaks E_o and E_R corresponded to reaction of Ni^{2+} to Ni^{3+} occurs on the surface of the NiO films according to the chemical reaction which is given by;

$$NiO + OH^- \rightleftarrows NiOOH + e^- \quad (12)$$

Potential and current density values for the anodic and cathodic peaks of the samples are presented in Table 4. The increase in the intensities of the cathodic and anodic peaks implies that in the first cycles there is a growth of charge capacity of the film which is attributed to the transformation of nickel oxide to nickel hydroxide. The higher value of the cathodic charge of Co doped NiO which is thought to be due to a more porous morphology of the un-doped NiO film. The calculated coulombic efficiency which is defined as the ratio of charge densities for the intercalation and deintercalation routes (Q_c/Q_a) is high, evidence of good reversibility for the intercalation–deintercalation reaction (Huang et al. 1998). On this basis, we calculate the coulombic efficiencies of about 63% and about 95% for un-doped and Co-doped NiO films, respectively. Since the electrochromic reactions that take place at the surface of NiO crystallites, The changes in electrochromic is attributed to the smaller grain size and clusters of grains which increases the effective surface area of NiO crystallites which resulted in an increase of electrochromic reactions (Xuping, and Guopin, 1997). It is noted that the anodic peaks shifted to more negative potentials for the Co-doped film. This shift of the anodic peaks could probably be attributed to the structural changes (Uplane et al., 2007). This argument is supported by examining the XRD and FESEM results shown in Figures 1 and 5.

Table 4. *Potential and current density values for the anodic and cathodic peaks of the NiO films*

Films	Cycle	E_o (V)	E_R (V)	I_o (10^{-4}mA)	I_R 10^{-4} (mA)	Q_o (10^{-4}mC)	Q_R (10^{-4}mC)	$\lvert Q_R/Q_o \rvert$
NiO	1st	0.495	0.248	12.4	-6.98	7.87	-4.16	0.53
	25th	0.487	0.242	13.6	-8.31	8.44	-5.08	0.60
	50th	0.487	0.24	13.7	-9.11	8.68	-5.47	0.63
Co/NiO	1st	0.434	-0.030	2.05	-1.66	2.39	-1.77	0.74
	25th	0.444	-0.033	2.16	-2.26	2.58	-2.07	0.80
	50th	0.448	-0.039	2.31	-2.85	2.97	-2.76	0.93

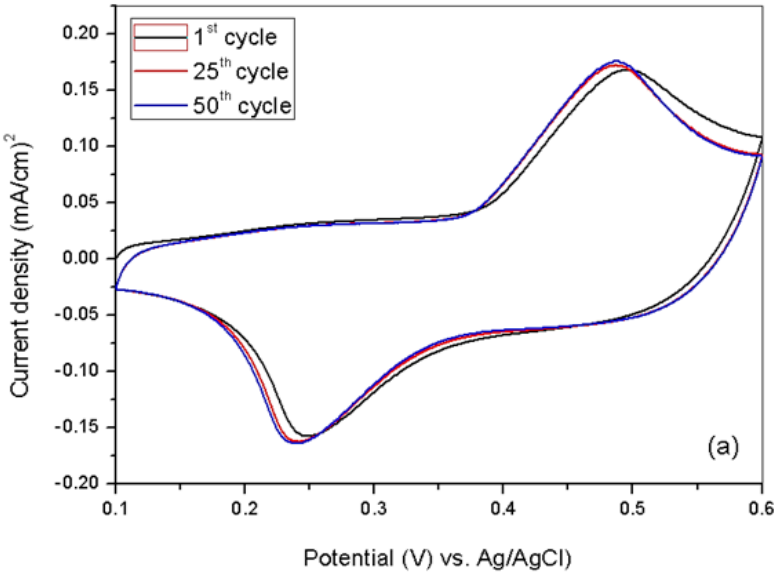

Figure 10. *The CV cycles of the (a) NiO films*

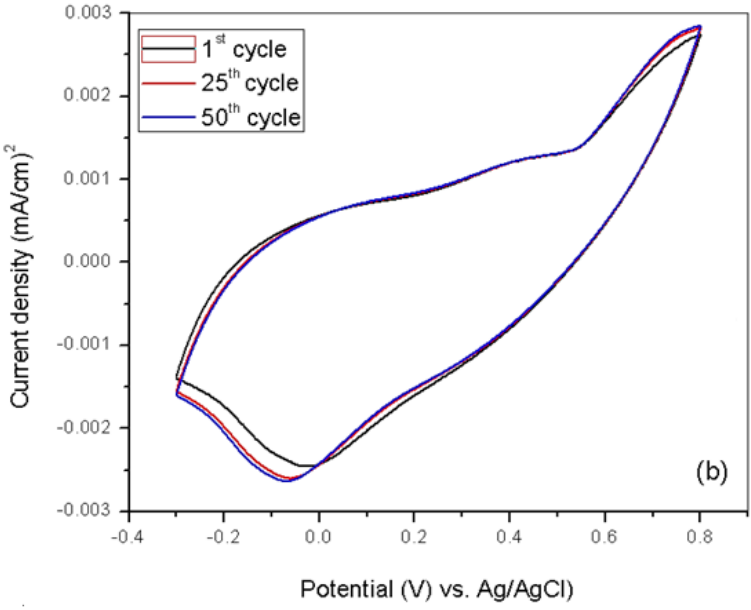

Figure 10. *The CV cycles of the (b) Co:NiO films*

4. Conclusions

Undoped and Co doped NiO films were successfully deposited by spray pyrolysis technique on glass and FTO-coated conducting glass substrates. The effect of Co doping on the structural, morphology, optical and electrochemical properties of the films was investigated. The analysis of XRD patterns revealed that all samples have face-centered cubic phase. The average crystallite size, lattice parameter, texture coefficient and micro-strain changed with Co doping, resulting in the structural variation. A blue shift was detected in LO mode in Raman spectrum of Co-doped NiO film. The optical transmittance measurement showed that films have low transparency and average transmittance values of NiO decreased with Co doping. The Co doping causes the red shift in optical absorption edge and decrease in band gap energy of NiO film. Electrochromic reversibility was found to be % 65 and % 93 for un-doped and Co-doped NiO films, respectively.

Acknowledgements

Authors are thankful to Prof. Dr. Evren TURAN and Prof. Dr. Ali Özcan Eskişehir Technical University for providing the facilities of production, XRD, FESEM, and electrochemical analysis.

References

Agrawal, S., PArveen, A., Azam, A. (2017), Microwave assisted synthesis of Co doped NiO nanoparticles and its fluorescence properties, Journal of Luminescence 184, 250-255.

Akaltun, Y., Çayir, T. (2015), Fabrication and characterization of NiO thin films prepared by SILAR method, Journal of Alloys Compounds 625, 144-148.

Avendaño, E., Berggren, L., Niklasson, G. A., Granqvist, C. G., Azens, A. (2006), Electrochromic materials and devices: Brief survey and new data on optical absorption in tungsten oxide and nickel oxide films, Thin Solid Films, 496, 30-36.

Bakr, N. A., Salman, S. A., Shano, A. M. (2015), International Letter Chemical Physics Astronomy, 41, 15-30.

Boubaker, K. (2011), Atomic structures beyond the spherical approximation along with PNC as conjectured explanations to Urbach tailing in neutral isolated ytterbium, The European Physical Journal B: Condensed Matter and Complex Systems, 84(2), 235-239.

Chia-ching, W., Cheng-fu, Y. (2013), Investigation of the properties of nanostructured Li-doped NiO films using the modified spray pyrolysis method, Nanoscale Research Letters, 8, 33.

Fterich, M., Nasr, F. B., Lefi, R., Toumi M., Guermazi, S. (2016), Effect of concentration of hexamethylenetetramine in structure,microstructure and optical properties of CuO nanoparticles synthesized by hydrothermal route, Material Science Semiconductor Processing, 43, 114-122.

Gençyilmaz, O. (2021), The Nanostructured CuO Films in The Different Thermal Oxidation Mediums: Production and XRD, UV-vis-NIR, FESEM and Raman Investigations, European Journal of Science and Technology, 32, S. 248-256.

Gençyilmaz, O., Taşköprü, T., Atay, F., Akyüz, I., (2015), Synthesis, characterization and ellipsometric study of ultrasonically sprayed Co_3O_4 films, Applied Physics A 121, 245-254.

Ghosh, R., BAsak, D., Fujihar, S., (2004), Effect of substrate-induced strain on the structural, electrical, and optical properties of polycrystalline ZnOZnO thin films, Journal of Applied Physics, 96, 2689.

Gurumurugan, K., Mangalaraj, D., NArayandass, S. K., Sekar, K., Girija C. P. Vallabhan, (1994), Characterization of transparent conducting CdO films deposited by spray pyrolysis, Semiconductor Science Technolony, 9, 1827-32.

Hannachi, L., Bouarissa, N. (2009), Band parameters for cadmium and zinc chalcogenide compounds, Physica B: Condensed Matter, 404, 3650-3654.

Huang, B., Jang, Y. I., Chiang, Y. M., Sadoway, D. R. (1998), Electrochemical evaluation of LiCoO2 synthesized by decomposition and intercalation of

hydroxides for lithium-ion battery applications, Journal of Applied Electrochemica, 28, 1365–1369.

Koussi-daoud, S., Majerus, O., Schaming, D., Pauporté, T. (2016), Electrodeposition of NiO films and ınverse opal organized layers from polar aprotic solvent-based electrolyte, Electrochimica Acta, 219, 638-646.

Kunz, A.B. J. (1981), Electronic structure of NiO,Journal of Physics C, 14L, 445.

Li, Y., Li, X. H., Wang, Z. X., Guo, H. J., Li, T. (2016), One-step synthesis of Li-doped NiO as high-performance anode material for lithium ion batteries, Ceramic International, 42, 14565-14572.

Mahr, H. (1962), Ultraviolet Absorption of KI Diluted in KCl Cryst als, Physical Review Journals Archive, 125, 1510.

Mezrag, F., Kara M. W., Bouarissa, N. (2010), The effect of zinc concentration upon optical and dielectric properties of Cd1−xZnxSe, Physica B: Condensed Matter, 405, 2272-2276.

Pankove, J. I., (1975), Optical Processes in Semiconductors, Dover Publication, New York.

Patil, P. S., Kawar R. K., Sadale S. B. (2005), Electrochromism in spray deposited iridium oxide thin films Electrochimica Acta, 50, 2527-2532.

Predanocy, M., Hotový, I., Čaplovičová, M. (2017), Structural, optical and electrical properties of sputtered NiO thin films for gas detection, Applied Surface Science, 395, 208-213.

Sato, H., Minami, T., Takata, S., Yamada, T. (1993), Study of Optical and Electrical Properties of Nickel Oxide (NiO) Thin Films Deposited by Using a Spray Pyrolysis Technique, Thin Solid Films 236, 27-31.

Sharma, R., Acharya, A. D., Moghe, S., Shrivastava, S. B., Gangrade, M., SHripathi, T., Ganesan, V. (2014), Effect of cobalt doping on microstructural and optical properties of nickel oxide thin films, Material Science Semiconductor Processing, 23, 42-49.

Sharma, R., Acharya, A. D., Shrivastava, S. B., Patidar, M. M., Gangrade, M., Shripathi, T., Ganesan, V. (2016), Fabrication, structural, optical, electrical, and humidity sensing characteristics of hierarchical NiO nanosheet/nanoballflower-like structure films, Optik 127, 4661-4668.

Soleimanpour, A. M., Jayatissa, A. H. (2012), Preparation of nanocrystalline nickel oxide thin films by sol–gel process for hydrogen sensor applications, Material Science Engineer C, 32, 2230-2234.

Sreethawong, T., Chavadej, S., Ngamsinlapasathian, S., Yoshikawa, S. (2007), A Modified sol–Gel Process-Derived Highly Nanocrystalline Mesoporous NiO with Narrow Pore Size Distribution, C Colloids and Surfaces A Physicochemical and Engineering Aspects296(1-3, (2007) 222-229.

Stock, S. R., Cullity, B.D. (2001), Elements of X-Ray Diffraction, Prentice-Hall Inc., New Jersey.

Şahin, B., Bayansal, F., Yüksel, M., Çetinkara H. A. (2014), Influence of annealing to the properties of un-doped and Co-doped CdO films, Materials Science in Semiconductor Processing, 18, 135-140.

Taşköprü, T., Bayansal, F., Şahin, B., Zor, M. (2015), Structural and optical properties of Co-doped NiO films prepared by SILAR method, Philosophical Magazine, 95, 32-40.

Taşköprü, T., Zor, M., Turan, E. (2015), Structural characterization of nickel oxide/hydroxide nanosheets produced by CBD technique, Material Research Bulletin, 70, 633-639.

Umar, A., Hahn, Y. B. (2010), Metal Oxide Nanostructures and Their Applications, American Scientific Publisher, California.

Uplane, M. M., Mujawar, S. H., Inamdar, A. I., Shinde, P. S., Sonavane, A., Patil P. S. (2007),Structural, optical and electrochromic properties of nickel oxide thin films grown from electrodeposited nickel sulphide, Applied Surface Science, 253, 9365-9371.

Urbach, F. (1953), The Long-Wavelength Edge of Photographic Sensitivity and of the Electronic Absorption of Solids, Physics Review, 92, 1324-1324.

Windisch, C., Exarhos, G., Ferris, K. , Engelhard, M., Stewart, D., (2001), Infrared transparent spinel films with p-type conductivity, Thin Solid Films 45, 398–399.

Xuping, Z., Guoping, C. (1997), The microstructure and electrochromic properties of nickel oxide films deposited with different substrate temperatures, Thin Solid Films 298, 53-56.

Yin, J. L., Park, J. Y. (2014), Electrochemical investigation of copper/nickel oxide composites for supercapacitor applications, International Journal of Hydrogen Energy, 39, 16562-16568.

Yu, J., Kim, D. (2013), The preparation of nano size nickel oxide powder by spray pyrolysis process, Powder Technology, 235, 1030-1037.

BÖLÜM 7

CHAPTER 7

GENERALIZED ADDITIVE MODELS FOR LOCATION, SCALE AND SHAPE: MODELING EUROPEAN UNION COVID-19 PANDEMIC DATA USING ZERO-TRUNCATED POISSON AND ZERO-TRUNCATED NEGATIVE BINOMIAL TYPE-I REGRESSION MODELS[1]

Mohamad ALNAKAWA[2], Neslihan İYİT[3]

1 Mohamad Alnakawa is Ph.D. student of the second author Assoc.Prof. Dr.Neslihan Iyit. This study is a part of Mohamad Alnakawa's Ph.D. Thesis entitled " Modeling Count Data Using Some Distributions from Generalized Additive Models with Applications in R-Programming" supervised by Assoc. Prof.Dr.Neslihan Iyit continuing in Selcuk University, Institute of Science, Statistics Department.

2 Ph.D Student, Department of Statistics, Faculty of Science, Selcuk University, Konya, Türkiye, ORCID ID: 0000-0001-7080-5005

3 Corresponding Author, Assoc.Prof.Dr., Department of Statistics, Faculty of Science, Selcuk University, Konya, Türkiye, niyit@selcuk.edu.tr, ORCID ID: 0000-0002-5727-6441

1.Introduction

There are many types of distributions that can be used in analyzing "count data". Some of these distributions belong to the "exponential family". To model these distributions from the "exponential family" in statistics, we use generalized linear model (GLM) approach considered as a generalization of the traditional linear model (Alnakawa, 2020; Özaltın and İyit, 2018; İyit, 2021; İyit et al., 2023). The GLM approach which is based on only the location parameter, ignoring the other parameters of the model leads to significant deficiencies in modeling of the data (Hilbe, 2011; İyit et al, 2016; İyit, 2018). Therefore, the GLMs are extended to "Generalized Additive Models for Location, Scale, and Shape (GAMLSS)" having the flexibility of modeling all parameters of any interested distribution regardless of whether it comes from the exponential family or not (Alnakawa and İyit, 2022). In this aspect, GAMLSS method is more effective and flexible than other methods in modeling count data. At this point, "count regression models" are statistical models used to analyze count data taking non-negative integer values. Count data are often utilized in various fields such as in energy (Catz, 1999), economics (Heberling et al., 2009), public health (Espinoza et al., 2021), criminology (Skardhamar et al., 2010), social sciences (Böhning et al., 1997), and etc. Count regression models are useful statistical tools in situations where the response variable is a count variable, and the explanatory variables are continuous, categorical or a combination of both.

There are several types of count regression models such as Poisson regression model, Negative Binomial regression model, Zero-inflated regression models, Hurdle regression models, truncated regression models, and etc. Truncated data occurs when some of the data in structure of the data is missing since it has been cut off or truncated beyond a

certain point (Kalbfleisch and Lawless, 1992). In order to better understanding, an example of truncated data in which zero cannot be occurred in the data structure is the number of days in which the carcasses of killed animals (snakes, birds, small mammals, and etc.) by hunters in the nature remain (Zuur et al. ,2009). There are different types of "truncated count data" such as left truncated, right truncated, and doubly truncated (Klein and Moeschberger, 2003). In this study, we will focus on "zero-truncated regression models" especially as "zero-truncated Poisson regression model", and "zero-truncated Negative Binomial Type-I regression model" with useful applications in R-Programme. Many researchers worked on zero-truncated Poisson regression model and zero-truncated Negative Binomial regression model are such as David and Johnson (1952), Tate and Goen (1958), Dahiya and Gross (1973), Bakouch et al. (2010), Athiany et al. (2020), Ridder (1955), Harteley (1958), Grogger and Carson (1991), Liu et al. (2013), Zaho et al. (2021), and etc.

2. Generalized Additive Models for Location, Scale and Shape (GAMLSS)

The generalized additive models for location, scale, and shape (GAMLSS) are flexible and efficient model family by modeling not only the linear relationships between the response variable and explanatory variables as "linear predictor" in GLMs, but the "linear predictor" between the response variable and explanatory variables are as in linear, nonlinear, parametric, and non-parametric smoothing functions.

The structure of the GAMLSS family has the following three components such as;

1- **The random component:** the probability distribution of the response variable coming from the continuous, discrete, and

mixture type of distributions from the exponential family or outside of it.

2- **Systematic Component:** describes the structure of the explanatory variables in the model.

3- **Link Function:** explains the form of how the random and systematic components are in related with together.

In this study, we will focus on the linear relationship between the linear predictor and the functions of the parameters in GAMLSS family.

2.1.Zero-truncated regression models

Let Y be a discrete random variable taking non-negative integer values such as 0,1,2,3,… that follows a Poisson distribution having equal values of the expected value and variance of the response variable, then the probability mass function (pmf) of this distribution with the location parameter μ is given as follows;

$$f\ (y\,;\mu) = \frac{\mu^{y} e^{-\mu}}{y\ !}$$

The pmf of the negative binomial (NB-1) distribution with the location parameter μ, and the scale parameter σ can be given as follows (Hilbe, 2011);

$$P(Y = y/\mu,\sigma) = \frac{\Gamma\left(y+\frac{1}{\sigma}\right)}{\Gamma\left(\frac{1}{\sigma}\right)\Gamma(1+y)}\left(\frac{\sigma\mu}{1+\sigma\mu}\right)^{y}\left(\frac{1}{1+\sigma\mu}\right)^{\frac{1}{\sigma}} \qquad (2)$$

where μ>0 , $\sigma > 0$ and $y = 0,1,2,3,.....$The expected value and variance of the response variable in NB-1 distribution are μ and $\mu + \sigma\mu^{2}$,respectively.

Let Y be a discrete random variable ($y = 0,1,2,3,4,.....$) having pmf (f (.)) and cdf(F(.)). Then the general formula of any truncated discrete distribution at point zero can be written as follows (Rose and Smith, 2002; Johnson, 2005);

$$f(Y = y \mid Y > 0) = \frac{f(Y = y)}{1 - F(Y = 0)} \tag{3}$$

Let Y be a random variable $y = 0,1,2,3,4,.....$ by using Eq (5), pmf of the zero-truncated Poisson distribution also called as positive Poisson distribution can be given as follows;

$$f(Y = y; \mu) = \frac{e^{-\mu}\mu^{y}}{y!(1 - e^{-\mu})} \tag{4}$$

where μ >0 and $y = 1,2,3,...$ By using Eq.(5), in the same manner, zero truncated NB-1 distribution can be given as follows;

$$P(Y = y/\mu,\sigma) = \frac{\dfrac{\Gamma\left(y + \dfrac{1}{\sigma}\right)}{\Gamma\left(\dfrac{1}{\sigma}\right)\Gamma(1+y)}\left(\dfrac{\sigma\mu}{1+\sigma\mu}\right)^{y}\left(\dfrac{1}{1+\sigma\mu}\right)^{\frac{1}{\sigma}}}{1 - \left(\dfrac{1}{1+\sigma\mu}\right)^{\frac{1}{\sigma}}} \tag{5}$$

where μ >0 , $\sigma > 0$, and $y = 1,2,3,...$

According to the structure of the GAMLSS family, zero-truncated Poisson regression model and zero-truncated NB-1 regression model can be obtained by adding the following default link function of the location parameter μ ;

$$\log(\mu) = \beta_0 + \beta_1 X_1 + \beta_2 X_2 + \cdots\cdots + \beta_n X_n \tag{6}$$

and by adding the following the default link function of the scale parameter σ ;

$$\log(\sigma) = \theta_0 + \theta_1 Z_1 + \theta_2 Z_2 + \cdots\cdots + \theta_n Z_n \qquad (7)$$

where $X_1, X_2, \cdots\cdots, X_n$ and $Z_1, Z_2, \cdots\cdots, Z_n$ are explanatory variables of the default link functions, and also $\beta_0, \beta_1, \beta_2, ..., \beta_n$ and $\theta_0, \theta_1, \theta_2, \cdots\cdots, \theta_n$ are regression models' coefficients .

3. Modeling European Union (EU) COVID-19 Pandemic Data Using Zero-truncated Poisson Regression Model and Zero-truncated Negative Binomial Type-I Regression Model

COVID-19 caused by the novel coronavirus SARS-CoV-2 was first identified in Wuhan, China in December 2019 and has since spread into a global pandemic all over the world. Symptoms of COVID-19 include fever, cough, shortness of breath, fatigue, body aches, and loss of taste or smell. Some people may experience more serious symptoms such as pneumonia, respiratory failure, or death. Preventive measures to limit the spread of COVID-19 include good hygiene such as washing hands frequently, wearing masks, avoiding large gatherings, practicing social distancing, and getting vaccinated. Treatment options vary depending on the severity of symptoms but may include supportive measures such as oxygen therapy or antiviral drugs. Infection rates with the COVID-19 virus which originated in the Wuhan province of China are increasing rapidly in the European continent. Therefore, European Union (EU) member countries had to impose sanctions in the form of strict measures, such as the closure of public areas. Concerns arising from the rapid spread of the pandemic in the EU member countries led to the rapid execution of vaccination campaigns, especially before winter and flu season. Certainly, these studies provide valuable insights into the impact

of the COVID-19 pandemic on various aspects in different countries in the European Union.

Some of the studies on the COVID-19 pandemic in EU in the literature can be given as follows; Largent et al. (2021) conducted survey to determine factors influencing hospital healthcare professionals' intentions to vaccinate against COVID-19 in France. Fisman et al. (2019) predicted the impact of closing on mortality from coronavirus disease. Loda (2020) highlighted influence of COVID-19 on medical education in Germany. Bohdan et al. (2021) determined the impact of COVID-19 pandemic on the Legal Migrant in Poland, Portugal, Latvia, and Belgium. Zavras (2021) studied the impact of COVID-19 on income in Greece. Chodkiewicz et al. (2021) focused on mental health during the COVID-19 pandemic's second wave. Edelhauser et al. (2021) attempted to assess the impact of one year of online education on the Romanian educational system. Chen et al. (2022) presented influence of COVID-19 pandemic on mental health and health behaviors in Swedish. Trifonova (2022) investigated Journalism's Challenges and Opportunities in Bulgaria's COVID-19 Communication Ecology.

3.1.Data Description of the European Union COVID-19 Pandemic

The data used in this study is available in https://github.com/owid/covid-19-data/tree/master/public/data/ and includes six different explanatory variables associated to the “total deaths attributed to the COVID-19 pandemic” from 26 EU member countries on February 1, 2020. EU member countries taken into the study are Cyprus, Luxembourg, Malta, Estonia, Slovenia, Denmark, Latvia, Switzerland, Netherlands, Slovenia, Austria, Lithuania, Belgium, Czech Republic, Portugal, Croatia, Hungary, Bulgaria, Romania, Sweden, Greece, Germany, Poland, France, Spain, and Italy as the subjects of this

study.The aim of this study is to determine the covariates influencing the total deaths of COVID-19 in the EU member countries on February 1, 2020 by using Poisson regression model, Negative Binomial Type I (NB-1) regression model, zero-truncated Poisson (ZTP) regression model, zero truncated negative Binomial Type I (ZTNB-1) regression model, with the log-link functions.

Table 1. Explanatory variables used in this study to model EU Member Countries COVID-19 Pandemic data by count regression models in the GAMLSS family.

Explanatory Variables	Descriptions of the Explanatory Variables
Male smokers	Share of men who smoke, most recent year available
GDP per capita	As gross domestic product at purchasing power parity, most recent year available
Aged 65 older	Share of the population that is 65 years and older, most recent year available
Hospital beds per thousand	Hospital beds per 1,000 people
Diabetes Prevalence	Diabetes prevalence (% of population aged 20 to 79)
Life Expectancy	Life expectancy at birth in 2019

Descriptive statistics and also skewness and kurtosis values of the response variable and the explanatory variables to model EU Member Countries COVID-19 Pandemic Data are represented in Table 2.

Table 2. Descriptive statistics and measures of the shape of the distributions of the response variable and the explanatory variables to model EU Member Countries COVID-19 Pandemic Data

Variables	Min.	Median	Mean	Max.	Skewness	Kurtosis
Total COVID-19 deaths	551	16906	34686	146925	1.45	3.77
Male smokers	18.80	32.25	33.64	52.70	0.53	2.89
Log (GDP per capita)	4.26	4.52	4.55	4.97	0.68	3.51

Aged 65 older	13.42	19.31	18.84	23.02	-0.91	3.49
Hospital beds per thousand	2.22	4.61	4.97	8.00	0.09	1.78
Diabetes prevalence	3.28	5.78	6.15	9.85	0.53	2.35
Life expectancy	75.05	81.44	80.42	83.78	-0.73	2.21

Gamlss.tr library in R is used to create zero truncated distributions and then to construct zero-truncated regression models used in this study. Maximum likelihood (ML) method is used for estimating parameters of the Poisson regression model, NB-1 regression model, zero truncated Poisson regression model, and zero truncated NB-1 regression model. The results of the count regression models in the GAMLSS family to model EU Member Countries COVID-19 Pandemic Data are given in Table 3, respectively.

Table 3. Count regression models in the GAMLSS family to model EU Member Countries COVID-19 Pandemic Data

Poisson Regression model

```
Type of Mu link function:  log

Mu Coefficients:
                    Estimate   Std. Error    t value  Pr(>|t|)
(Intercept)        8.2236148  0.0579701     141.86   <2e-16 ***
age65older         0.0676922  0.0006926     97.74    <2e-16 ***
diabetes          -0.1164823  0.0006940    -167.85   <2e-16 ***
male smokers      -0.0685843  0.0002340    -293.12   <2e-16 ***
hospital beds      0.6112040  0.0010707     570.84   <2e-16 ***
life expectancy    0.4863635  0.0009570     508.22   <2e-16 ***
log(GDP)          -8.4930828  0.0194767    -436.06   <2e-16 ***

Signif. codes:  0 '***' 0.001 '**' 0.01 '*' 0.05 '.' 0.1 ' ' 1
```

Negative Binomial Type I Regression model

```
Type of Mu link function:  log
Mu Coefficients:
                     Estimate    Std. Error    t value   Pr(>|t|)
(Intercept)          -13.85242   5.29613      -2.616     0.01616 *
diabetes              0.21512    0.03783       5.687     1.21e-05 ***
hospital beds         0.73911    0.10861       6.805     9.94e-07 ***
life expectancy       0.42773    0.06418       6.664     1.35e-06 ***
log(GDP)             -3.41967    1.18332      -2.890     0.00876 **


Type of Sigma link function:  log
Sigma Coefficients:
                    Estimate    Std. Error     t value    Pr(>|t|)
(Intercept)         -55.7535    13.3437        -4.178     0.000424 ***
life expectancy      0.6868     0.1645          4.175     0.000428 ***
```

Zero Truncated Poisson Regression model

```
Type of Mu link function:  log
Mu Coefficients:
                      Estimate  Std. Error   t value  Pr(>|t|)
(Intercept)          8.2117460  0.0579666    141.66   <2e-16 ***
age65older           0.0676052  0.0006926    97.61    <2e-16 ***
diabetes            -0.1162129  0.0006939   -167.48   <2e-16 ***
male smokers        -0.0685404  0.0002340   -292.94   <2e-16 ***
hospital beds        0.6112054  0.0010707    570.87   <2e-16 ***
life expectancy      0.4863064  0.0009570    508.13   <2e-16 ***
log(GDP)            -8.4897725  0.0194760   -435.91   <2e-16 ***

Signif. codes:  0 ‘***’ 0.001 ‘**’ 0.01 ‘*’ 0.05 ‘.’ 0.1 ‘ ’ 1
```

Zero Truncated Negative Binomial Type I Regression model

```
Type of Mu link function:  log

Mu Coefficients:
                    Estimate    Std. Error   t value    Pr(>|t|)
(Intercept)          4.42758    4.93468      0.897      0.3808
diabetes             0.19634    0.03250      6.041      8.23e-06 ***
hospital beds        0.52675    0.08502      6.195      5.94e-06 ***
male smokers         0.03377    0.01188     -2.842      0.0104 *
life expectancy      0.33238    0.04166      7.978      1.75e-07 ***
log(GDP)            -5.26950    0.76986     -6.845      1.57e-06 ***


Type of Sigma link function:  log

Sigma Coefficients:
                    Estimate   Std.Error    t value     Pr(>|t|)
(Intercept)        -54.5137    8.1608      -6.680      2.18e-06 ***
life expectancy      0.9441    0.1225       7.704       2.92e-07 ***
log(GDP)            -4.8245    1.8680      -2.583       0.0182 *
---
Signif. codes:  0 ‘***’ 0.001 ‘**’ 0.01 ‘*’ 0.05 ‘.’ 0.1 ‘ ’ 1
```

The link function of the Poisson regression model belonging to the EU Member Countries COVID-19 Pandemic Data is given as follows;

$$\log(\hat{\mu}) = 8.22 + 0.06(age\,65\,older) - 0.11(diabetes) - 0.06(male\,smo\,\ker s) \\ +0.61(hospital\,beds) + 0.48(life\ \exp ectancy) - 8.49(\log(GDP)) \quad (8)$$

The link functions of the NB-1 regression model belonging to the EU Member Countries COVID-19 Pandemic Data is given as follows;

$$\log(\hat{\mu}) = -13.85 + 0.21(diabetes) + 0.73(hospital\,beds) \\ +0.42(life\exp ectancy) - 3.41(\log(GDP)) \quad (9)$$

$$\log(\hat{\sigma}) = -55.75 + 0.68(life\exp ectancy) \quad (10)$$

The link functions of the zero-truncated Poisson regression model belonging to the EU Member Countries COVID-19 Pandemic Data is given as follows;

$$\log(\hat{\mu}) = 8.211 + 0.06(age65older) - 0.11(diabetes) - 0.06(malesmokers) + 0.61(hospitalbeds) + 0.48(lifeexpectancy) - 8.48(\log(GDP)) \quad (11)$$

The link functions of the zero-truncated NB-1 regression model belonging to the EU Member Countries COVID-19 Pandemic Data is given as follows;

$$\log(\hat{\mu}) = 0.19(diabetes) + 0.03(male\ smokers) + 0.52(hospital\ beds) + 0.33(lifeexpectancy) - 5.26(\log(GDP)) \quad (12)$$

$$\log(\hat{\sigma}) = -54.51 + 0.94(lifeexpectancy) - 4.82(\log(GDP)) \quad (13)$$

Information criteria (IC) as Akaike information criteria, Bayesian information criteria, generalized Akaike information criteria, and also log-likelihood value to compare count regression models in GALMSS family to determine the most appropriate model belonging to the EU Member Countries COVID-19 Pandemic data are given in Table 4.

Table 4. Information criteria to compare count regression models in GALMSS family belonging to the EU Member Countries COVID-19 pandemic data.

Type of count regression models in GALMSS family	**Information criteria**			
	AIC	**BIC**	**Log-likelihood**	**GAIC**
Poisson	613491.09	613500.42	-306738.5	613491.09
NB-1	624.91	**634.23***	-305.54	624.91
Zero truncated Poisson	613491.10	613500.41	-306738.6	613491.10
Zero truncated NB-1	**623.08***	635.07	**-302.54***	**623.08***

The smallest information criteria values given in Table 4 count regression models in GALMSS family belonging to the EU Member Countries COVID-19 pandemic data indicate the most appropriate model as the "zero truncated NB-1 regression model". On the other hand, BIC showed a discrimination problem to determine the best model with a small deviation.

Residual plots for the zero truncated NB-1 regression model as the most appropriate model belonging to the EU Member Countries COVID-19 Pandemic data are given in Figure 1. Summary of the Quantile Residuals for the zero truncated NB-1 regression model in the GAMLSS family to model EU Member Countries COVID-19 Pandemic Data are given in Table 5. As seen from Table 5, the mean is close to zero, variance is close to one, coefficient of skewness is close to zero, and coefficient of kurtosis is close 2.6. As seen from Figure 1 and Table 5, this model's residuals exhibit good behavior. In addition, the negative value of the coefficient of skewness indicates that there is a longer left tail than the right tail.

Figure 1. Residual plots for the zero truncated NB-1 regression model in the GAMLSS family to model EU Member Countries COVID-19 Pandemic Data

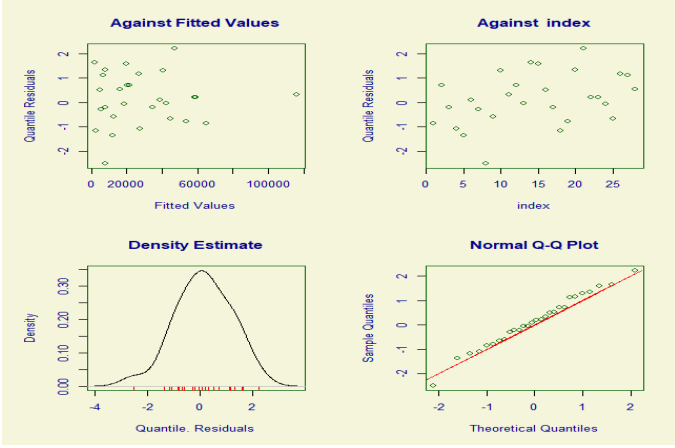

Table 5. Summary of the Quantile Residuals for the zero truncated NB-1 regression model in the GAMLSS family to model EU Member Countries COVID-19 Pandemic Data

Summary of the Randomized Quantile Residuals	
Mean	0.135
Variance	1.125
Coefficient of skewness	-0.221
Coefficient of kurtosis	2.688

4.Conclusion

As a main conclusion of this study, the expected value of the location parameter of the zero truncated NB-1 regression model for the "new COVID-19 deaths" data according to the EU Member Countries on February 1, 2020

increases $e^{0.03} = 1.03$ times by 1% change in male smokers,

decreases $e^{-5.26} = 0.005$ times by 1 unit change by log(GDP per capita),

increases $e^{0.52} = 1.68$ times by per thousand hospital beds,

increases $e^{0.19} = 1.20$ times by 1% change in diabetes prevalence,

increases $e^{0.33} = 1.39$ times by life expectancy at birth.

The expected value of the scale parameter of the zero truncated NB-1 regression model for the "new COVID-19 deaths" data according to the EU Member Countries on February 1, 2020

increases $e^{0.94} = 2.55$ times by life expectancy at birth.

decreases $e^{-4.82} = 0.008$ times by 1 unit change by log(GDP per capita)

Acknowledgement

The authors would like to thank the "Türkiye Scholarships Program" for providing scholarships to the first author of this paper during his Ph.D. thesis study, and also Mr. Mehmet ŞAVATA (Association for Solidarity with Asylum Seekers and Migrants-Kayseri Branch Manager) and Mr. Faruk Yavuz TEMÜR (Migration Health Unit-Kayseri Coordinator) for their moral support.

References

1) Alnakawa, M. (2020). An Application Based on Zero-inflated Poisson and Negative Binomial Regression Models (Master's thesis, Fen Bilimleri Enstitüsü).

2) İyit, N., Sevim, F., & Kahraman, Ü. M. (2023). Investigating the impact of CO2 emissions on the COVID-19 pandemic by generalized linear mixed model approach with inverse Gaussian and gamma distributions. Open Chemistry, 21(1), 20220301.

3) Özaltın, Ö., and İyit, N. (2018). Modelling the US diabetes mortality rates via generalized linear model with the Tweedie distribution. Int. J. Sci. Res, 7(2), 1326-1334.

4) İyit, N., Yonar, H., and Yonar, A. (2021). An Application of Generalized Linear Model Approach on Econometric Studies. Research & Reviews in Science and Mathematics-II, Gece Publishing, 175-188.

5) Iyit, N. (2018). Modelling world energy security data from multinomial distribution by generalized linear model under different cumulative link functions. Open Chemistry, 16(1), 377-385.

6) İyit, N., Yonar, H., and Genç, A. (2016). Generalized linear models for European Union countries energy data. Acta Physica Polonica A, 130(1), 397-400.

7) Alnakawa, M., and İyit, N. (2022). Usage of Generalized Additive Models for Some Discrete Distributions in Modelling Bangladesh's Enterprises Count Data in the Field of Business Administration. Academic Studies in Social, Human, and Administrative Science, Gece Publishing, 195-215.

8) Athiany, H., Wanjoya, A., Orwa, G. and Mwalili, S. (2020) Bayesian Analysis of Zero-Truncated Poisson Model: Application to the Self-Controlled Case-series Design, International Journal of Data Science and Analysis, 6(6), 170-182.

9) Bakouch, H. S. and Ristić, M. M. (2010). Zero truncated Poisson integer-valued AR (1) model. Metrika, 72, 265-280.

10) Bohdan, A., Maziarz, B. and Dornfeld-Kmak, A. (2021). Impact of the COVID-19 pandemic on the legal migrant in Poland, Portugal, Latvia, and Belgium.

11) Böhning, D., Dietz, E. and Schlattmann, P. (1997). Zero-inflated count models and their applications in public health and social science. Applications of latent trait and latent class models in the social sciences, 333-344.

12) Catz, H. (1999). Energy data book. France in the world.

13) Chen, T. and Lucock, M. (2022). The mental health of university students during the COVID-19 pandemic: An online survey in the UK. PloS one, 17(1), e0262562.

14) Chodkiewicz, J., Miniszewska, J., Krajewska, E. and Biliński, P. (2021).

Mental health during the second wave of the COVID-19 pandemic—Polish studies. International journal of environmental research and public health, 18(7), 3423.

15) Dahiya, R. C. and Gross, A. J. (1973). Estimating the zero class from a truncated Poisson sample. Journal of the American Statistical Association, 68(343), 731-733.

16) David, F. N. and Johnson, N. L. (1952). The truncated poisson. Biometrics, 8(4), 275-285.

17) Edelhauser, E. and Lupu-Dima, L. (2021). One year of online education in COVID-19 age, a challenge for the Romanian education system. International Journal of Environmental Research and Public Health, 18(15), 8129.

18) Fisman, D. N., Bogoch, I., Lapointe-Shaw, L., McCready, J. and Tuite, A. R. (2020). Risk factors associated with mortality among residents with coronavirus disease 2019 (COVID-19) in long-term care facilities in Ontario, Canada. JAMA network open, 3(7), e2015957-e2015957.

19) Ghitany, M. E., Al-Mutairi, D. K. and Nadarajah, S. (2008). Zero-truncated Poisson–Lindley distribution and its application. Mathematics and Computers in Simulation, 79(3), 279-287.

20) Grogger, J. T. and Carson, R. T. (1991). Models for truncated counts. Journal of applied econometrics, 6(3), 225-238.

21) Hartley, H. O. (1958). Maximum likelihood estimation from incomplete data. Biometrics, 14(2), 174-194.

22) Heberling, M. T. and Templeton, J. J. (2009). Estimating the economic value of national parks with count data models using on-site, secondary data: the case of the Great Sand Dunes National Park and Preserve. Environmental Management, 43, 619-627.

23) Hilbe, J. M. (2011). Negative binomial regression. Cambridge University Press.

24) COVID-19 Data. [Online]. Available https://github.com/owid/covid-19-data/tree/master/public/data/

25) Irshad, M. R., Chesneau, C., Shibu, D. S., Monisha, M. and Maya, R. (2022). Lagrangian Zero Truncated Poisson Distribution: Properties Regression Model and Applications. Symmetry, 14(9), 1775.

26) Johnson, D. (2005). Two-wave panel analysis: Comparing statistical methods for studying the effects of transitions. Journal of Marriage and Family, 67(4), 1061-1075.

27) Johnson, N. L., Kemp, A. W. and Kotz, S. (2005). Univariate discrete distributions. John Wiley&Sons.

28) Jollant, F., Blanc-Brisset, I., Cellier, M., Ambar Akkaoui, M., Tran, V. C., Hamel, J. F., Aude Piot, M., Nourredine, M., Nisse, P., The French Poison Center Control Research Group, Hawton, K.,Descatha, A. and Vodovar,

D. (2022). Temporal trends in calls for suicide attempts to poison control centers in France during the COVID-19 pandemic: a nationwide study. European journal of epidemiology, 37(9), 901-913.

29) Kalbfleisch, J. D. and Lawless, J. F. (1992). Some useful statistical methods for truncated data. Journal of Quality Technology, 24(3), 145-152.

30) Klein, J. P. and Moeschberger, M. L. (2003). Survival analysis: techniques for censored and truncated data (Vol. 1230). New York: Springer.

31) Largent, E. A. and Miller, F. G. (2021). Problems with paying people to be vaccinated against COVID-19. Jama, 325(6), 534-535.

32) Lim, K. K. (2023). Analysis of Railroad Accident Prediction using Zero-truncated Negative Binomial Regression and Artificial Neural Network Model: A Case Study of National Railroad in South Korea. KSCE Journal of Civil Engineering, 27(1), 333-344.

33) Liu, X., Saat, M. R., Qin, X. and Barkan, C. P. (2013). Analysis of US freight-train derailment severity using zero-truncated negative binomial regression and quantile regression. Accident Analysis & Prevention, 59, 87-93.

34) Rose, C. and Smith, M. D. (2002). Mathematical Statistics with Mathematica. Springer.

35) Rose, C. and Smith, M. D. (2002). Mathematical statistics with Mathematica (Vol. 1). New York: Springer.

36) Shanker, R. and Shukla, K. K. (2017). Zero-truncated Poisson-Garima distribution and its applications. Biostat Biometrics Open Access Journal, 3(1), 555605.

37) Skardhamar, T., Schweder, T. and Schweder, S. G. (2010). Modelling'crime-proneness'. A comparison of models for repeated count outcomes (No. 611). Discussion Papers.

38) Stasinopoulos, M. D., Rigby, R. A. and Bastiani, F. D. (2018). GAMLSS: A distributional regression approach. Statistical Modelling, 18(3-4), 248-273.

39) Stasinopoulos, M. D., Rigby, R. A., Heller, G. Z., Voudouris, V. and De Bastiani, F. (2017). Flexible regression and smoothing: using GAMLSS in R. CRC Press.

40) Tate, R. F. and Goen, R. L. (1958). Minimum variance unbiased estimation for the truncated Poisson distribution. The Annals of Mathematical Statistics, 755-765.

41) Trifonova Price, L. and Antonova, V. (2022). Challenges and Opportunities for Journalism in the Bulgarian COVID-19 Communication Ecology. Journalism Practice, 1-18.

42) Winkelmann, R. (2008). Econometric analysis of count data. Springer Science & Business Media.

43) Zavras, D. (2021). A cross-sectional population-based study on the influence of the COVID-19 pandemic on incomes in Greece. AIMS Public Health, 8(3), 376.

44) Zhao, S., Shen, M., Musa, S. S., Guo, Z., Ran, J., Peng, Z., Zhao, Y., MarcK.C.,Y., Daihai He, C. and Wang, M. H. (2021). Inferencing superspreading potential using zero-truncated negative binomial model: exemplification with COVID-19. BMC Medical Research Methodology, 21, 1-8.

45) Zuur, A. F., Ieno, E. N., Walker, N., Saveliev, A. A., Smith, G. M. and Smith, G. M. (2009). Zero-truncated and zero-inflated models for count data. Mixed effects models and extensions in ecology with R, 261-293.

BÖLÜM 8

CHAPTER 8

RECENT PROGRESS ON

POLY(LACTIC-CO-GLYCOLIC ACID) MICRO AND NANOPARTICLES

Gülce TAŞKOR ÖNEL[1]

1 Asst. Prof., Erzincan Binali Yıldırım University, Faculty of Pharmacy, Dept. of Analytical Chemistry, ORCID: 0000-0002-9375-2329, gulce.onel@erzincan.edu.tr, gulcetaskor@gmail.com

INTRODUCTION

Poly(lactic-*co*-glycolic acid) (PLGA), which has been widely researched for therapeutic purposes recently, is a synthetic biopolymer in polyester structure approved by US Food and Drug Administration (FDA) and European Medicine Agency (EMA). Excellent biocompatibility and controlled biodegradability of PLGA have given very effective properties for therapy in the medical related field such as drug/gene delivery, biomaterials, etc. For instance, a new nanomedicine approach was presented with the design of catalase&imiquilod-encapsulated PLGA nanoparticles that increase the effectiveness of radiotherapy by Chen et al. A PLGA nanoparticular system was prepared that modulates the tumor microenvironment and induces a strong antitumor immune response. The PLGA nanoparticle system also created a long-term immunological memory and created the synergy of preventing metastasis. (Chen et al., 2019)

PLGA micro (MPs) and nanoparticles (NPs) can be prepared in a matrix (capsule) or core-shell (sphere) morphology in sizes of 1-1000 μm (Mishra & Singh, 2020) and 1-1000 nm (Zielińska et al., 2020), respectively, according to their areas of use. Polysorbate-80 coated PLGA nanoparticle formulations loaded with the anti-cancer drug rapamycin, which has a classic water solubility problem, have been investigated for the treatment of glioma. Nanoparticles showing promise for advanced treatments demonstrated good results in the in vitro drug release behavior, storage stability, and in vitro anti-glioma activity. (Escalona-Rayo et al., 2019) In another study, two synthetic controlled-release biomaterials, hydrogel/PLGA MP vaccine delivery system were developed to activate immune cells as vaccine adjuvants. With this study, the successful results of hydrogel/PLGA MPs that prevent type 1 diabetes were shown by explaining their mechanisms. (Yoon et al., 2015) Saleh et all. explained that chlorogenic acid (CGA) isolated from *Euphorbia milii* flowers was an effective phytochemical against respiratory tract infections. The phytochemical was nano-formulated into the PVA/PLGA polymeric matrix by the electrospray technique. They reported that CGA PVA/PLGA nanoparticles had antiviral activity on coronavirus (HCoV-229E) and (Middle East respiratory syndrome coronavirus (MERS-CoV), NRCEHKU270), which were global problems during the pandemic. (Saleh et al., 2023)

In this chapter, as described with a few examples above, it was aimed to summarize the considerable literature regarding recent progress in the PLGA micro- and nanoparticles. Special focuses would be on the novel properties, preparation methods, characterization, pharmaceutical formulations, loading methods, and release mechanisms of macro and nanoparticles as well as radiotherapy, chemo-chemodynamic therapy, stem/stromal cell therapeutics, regenerative medicine, gene therapy, and vaccine systems.

OVERVIEW OF THE PLGA

Biocompatible and biodegradable polymer research, the bioavailability of which has been developed for biomedical, nanomedicine, tissue engineering, drug delivery, and health chemistry applications, has been increasing rapidly over the past 20 years. (Aksoy, Taskor, Gultekinoglu, Kara, & Ulubayram, 2018; Taşkor Önel, 2023) PLGA is one of the trendy biocopolymers in this field. Two types of PLGA synthesis methods have been widely reported in the literature. The first and most popular is the ring-opening polymerization method of lactide and glycolide structures. (Taşkor Önel, 2023) The second method is the direct condensation reaction of lactic acid and glycolic acid and is less preferred. (Gentile, Chiono, Carmagnola, & Hatton, 2014) It is synthesized on a wide range of molecular weight depending on different ratios of monomers. Depending on the molecular weight and monomer ratios of the synthesized PLGA, polydispersity, crystallinity, tacticity, pH, biological conditions, hydrophilic & hydrophobic functional groups, stereo sequence, bioavailability, biodegradation, and biocompatibility have been changing. (J. Li, Stayshich, & Meyer, 2011; Shaver & Cameron, 2010; Zolnik & Burgess, 2007)

Differentiation of catalyst and initiator ratios in PLGA synthesis a research article has been reported in which its effects on the molecular weight, monomer transformation, and thermal properties of the polymer have been determined by Little et al. Increasing the reaction temperature from 130°C to 205 °C significantly reduced the time required for high monomer transformations, while reducing the amount of catalyst used resulted in a longer reaction time and a higher temperature needed to complete the reaction. (Little et al., 2021) In the study of Dai et al., they stated that lactic acid, which is revealed as a result of the degradation of PLGA, causes inflammation. They synthesized the cross-linked crystal structure of PLGA to prevent inflammation. Because of PLGA has controllable crystallinity, the biodegradability property has also been controllable. They explained that crystal PLGA, whose hydrolysis results are also supported by cell culture studies, is an ideal biomaterial for tissue engineering studies. (Dai, Liang, Zhang, Bernaerts, & Zhang, 2021)

The preparing a large number of different biomaterials such as micro/nanoparticles, fibers, composites, lipid hybrid structures, gels, sponges, scaffolds, and implants with PLGA biopolymer offers an increasing research area every day. (Ghitman, Biru, Stan, & Iovu, 2020; Pandey & Jain, 2015; Sarkar et al., 2022) The most cited PLGA publications are on explaining the chemical and physical properties of PLGA and clarifying the production methods of drug carrier systems such as PLGA micro/nanoparticles, which is the most basic field of the application when examined. (Danhier et al., 2012; Makadia & Siegel, 2011) When current publications

were examined, more detailed publications such as the study of the effect of particle size on water solubility and the preparation of PLGA hybrid systems for increasing stability and bioavailability were reflected in the literature. (Sher, Zahoor, Shah, & Khan, 2023; Yuan et al., 2023)

Articular cartilage, which is a very special tissue for living things, provides a smooth surface for joint movement and load transmission, and it is a big problem for tissue engineering because its regeneration is limited. In the study, dental follicle mesenchymal stem cells (Mscs) had ideal properties for cell formation, proliferation, and differentiation on the scaffold prepared from PCL/PLGA (80:20) mixture, and their ability to differentiate into chondrocytes was reported. (González-González et al., 2023) The fact that PLGA-containing biopolymers have nontoxic properties and exhibit cellular integration in the cartilage region shows that they are ideal biomaterials for clinical treatments. Research that attracts attention about PLGA micro and nanoparticles in the literature is detailed under the following headings.

PLGA MICRO AND NANOPARTICLES

PLGA micro and nanoparticles have excellent cellular compatibility, biodegradation profiles, and adjustable drug release properties are traditional information. (Guo et al., 2023) Aseptic loosening and periprosthetic infections at the interface between inert ceramic implants and body tissues are important complications. In order to prevent these complications, PLGA nanoparticles loaded with gentamicin and bacitracin antibiotics and calcium phosphate-coated implants have been prepared. Thus, a new generation of implants with antimicrobial properties with increased bioactivity was prepared with PLGA nanoparticles. It had been observed that implants inhibited bacterial activity for 1 month owing to controlled drug release and support excellent behavior showing the homogeneous distribution of cells. (Desante et al., 2023)

The drug afatinib is widely used for the treatment of lung cancer. The PLGA nanoparticle formulation of afatinib was often preferred because of increasing the bioavailability of the drug. (Elbatanony et al., 2021) In the research of Vanza et al., afatinib PLGA NPs formulation was switched to dry powder form by lyophilization technique. They reported that afatinib PLGA in this powder forum penetrates deeper areas of the lung as a result of being delivered to the lung by inhaler method with NPs. They also observed that *in vitro* experiments with the A549 adenocarcinoma cell line showed better inhibition of nanoformulation compared to pure drug. (Vanza, Lalani, Patel, & Patel, 2023)

Cheng et al. obtained PLGA orthoester functionality with polyethylene glycol methyl ether and made the polymer sensitive to acid in order

to accelerate drug release. In addition, hemin&cisplatin were loaded onto the prepared PLGA nanoparticles, and active targeting with phenylboronic acid was used in the design. It has been found that this hybrid nanosystem effectively improves blood stability and circulation time with PEG coating, and efficiently increases cellular uptake after reaching tumor areas with a phenyl boronic acid targeting agent. Furthermore, hemin, which was capsulated with PLGA nanoparticles, increased the formation of oxygen, and this was reported to significantly increased the release rate because it stimulated biodegradation. As a result, hybrid PLGA nanoparticles were reported to effectively inhibit the increase of drug-resistant A549 lung cancer cells with chemotherapy and chemodynamic combination therapy. (Cheng et al., 2023)

CONTROLLED/SUSTAINED-RELEASE DRUG DELIVERY SYSTEMS

Numerous studies have been reported on controlled drug release studies of PLGA or hybrid formulations of PLGA in literature. (Han, Thurecht, Whittaker, & Smith, 2016; Hines & Kaplan, 2013; Yoo & Won, 2020) In a newly published study, bionic red blood cell (RBC)-like Fe_3O_4@PLGA-PEG-PLGA microparticles were prepared by one step-double-needle electrospray method. It was found that the hydrophilicity of MPs was increased with the PLGA-PEG-PLGA block copolymer, supported the proliferation of human umbilical vein endothelial cells and adhesion proteins, and significantly improved cell affinity. The results also demonstrated that RBC-like MPs could provide magnetic targeting to drug delivery systems with their magnetic property, and particles can also be monitored by bioimaging techniques with their luminescence ability. (Xu et al., 2023)

The release rate of drugs depends on many parameters such as the shape of particles, size, molecular weight of the polymer, functional groups, branching, crystallinity, and tacticity. (Son, Lee, & Cho, 2017) In this study, which examines the effect of drugs itself on drug release rate, donepezil was loaded into PLGA microspheres and in vitro and in vivo release rates were compared. PLGA microspheres, which were loaded with donepezil in amorphous form, were found that polymers' molecular weight and end group did not affect the in vitro and in vivo performance. However, as a result of the basic catalysis effect induced by the biodegradation effect of donepezil on PLGA microspheres, it was found that the molecular weight with GPC fell sharply to 11,000 Da within the first three days. Moreover, a correlation was observed between in vitro release and in vivo absorption. (Quan, Guo, LinYang, Cun, & Yang, 2023)

REGENERATIVE MEDICINE APPLICATIONS

PLGA micro and nanoparticles are successful biodegradable biomaterials due to their hydrophilicity and were studied widely due to their ability to repair or replace cells and tissues that have been impacted by illness, age, or injuries, and also to normalize congenital abnormalities in regenerative medicine. (Sharma et al., 2023) The wound-healing process in diabetes patients is a chronic problem. (Spampinato, Caruso, De Pasquale, Sortino, & Merlo, 2020) Mesenchymal stem cells were reported to improve diabetic wound healing, so PLGA nanoparticles encapsulated with the anti-inflammatory and angiogenic cytokine IL-8 were prepared to improve proliferation, differentiation, and anti-apoptosis ability. These PLGA nanoparticles integrated into the intracellular dermal matrix in the cutaneous wounds of diabetic mice were observed to effectively induce capillary structure, collagen accumulation, and wound healing. Furthermore, advanced immunofluorescence analysis showed that proangiogenic factors (VEGF and α-SMA) were upcoordinated in the regenerated tissue when examined. (Zhang et al., 2023)

When a different diabetic wound healing study was examined, Human beta defensin-2 loaded PLGA nanoparticles impregnated in collagen/chitosan composite scaffolds were formulated for the accelerated healing of diabetic wounds. *In vitro* studies on biodegradable cross-linked scaffolds have shown that the structure was biocompatible for cell development, and angiogenesis and had optimal porosity for drug release. *In vivo* studies indicate that the group treated with scaffolds containing PLGA nanoparticles accelerated recovery compared to control groups. The accelerated recovery in the group treated with this hybrid scaffold was reported to be due to the synergistic effects of PLGA, angiogenic effect, and collagen synthesis; Human beta defensin-2 having anti-inflammatory, anti-bacterial, positive angiogenic effect, cell proliferation and migration; collagen establishing wound healer and stabilizer as well as chitosan having anti-bacterial activity. (Sanapalli et al., 2023)

NEXT-GENERATION VACCINES

In recent years, the importance of vaccines has attracted attention again with the COVID-19 pandemic. Encapsulation of mRNA-based covid-19 vaccines with lipid nanoparticles has accelerated research on the development of new-generation vaccines. (Schoenmaker et al., 2021) In a recent study, the autoinducer *N*-octanoyl-*L*-homocerinehomocerine lactone (C8-HSL), one of the adjuvants that increased the level of immune response to the antigen and modulate the stability and immunogenicity of vaccine antigens, had formulated a PLGA microparticle for next generation vaccines. The results of *in vitro* immunogenicity tests of C8-HSL PLGA microparti-

cles showed that they were as immunogenic as FDA-approved adjuvants. It had been reported by researchers that C8-HSL adjuvants formulated with PLGA microparticles could increase the immunogenicity of both bacterial and viral vaccines. (Shah, Joshi, Chbib, Roni, & Uddin, 2023)

Gu et al. investigated how the surface charge and antigen loading mode of nanoparticles affect immune responses in the PLGA nanoparticle vaccine delivery systems research they developed. In this study, three ovalbumin-loaded PLGA nanoparticles with different surface charges and antigen loading modes were developed and the nanoparticles were designed as negatively charged Angelica sinensis polysaccharide-encapsulated antigen, polyethyleneimine-coated encapsulated antigen, and adsorbed antigen on polyethyleneimine-coated. According to the results of in vivo experiments, it was observed that positively charged polyethyleneimine-coated PLGA nanoparticles had the potential to induce stronger and longer-lasting humoral and cellular immune responses, as they supported antigen escape from the endosome, which led to cytoplasmic antigen transmission. (Gu et al., 2019)

SOME THERAPEUTIC TECHNOLOGIES

Therapeutic systems, which pave the way for the field of personalized treatment, focus on the development of biomaterials in accordance with needs. (Chandrasekaran, Capozza, & Wong, 1978) Acute liver failure occurs with symptoms of hepatocellular necrosis, inflammation, and increased oxidative stress. (Blackmore & Bernal, 2015) It was developed a hybrid system consisting of versatile biomimetic copper oxide nanozymes loaded PLGA nanofibers and decellularized extracellular matrix hydrogels for delivery of human adipose-derived mesenchymal stem/stromal cells-derived hepatocyte-like cells for the treatment of acute liver failure. It was reported that with this hybrid PLGA nanofiber structure, results were observed that clear the accumulation of oxidative stress at the initial stage of acute liver failure and reduce the accumulation of large pro-inflammatory cytokines, effectively preventing the deterioration of hepatocellular necrosis. In addition, it was stated that the cytoprotection effect on the transplanted hepatocyte-like cells of PLGA nanofibers was observed in vivo conditions. (Jin et al., 2023)

Cancer cells sometimes need non-essential biomolecules for survival, growth, and proliferation. (Schiliro & Firestein, 2021) Enzyme-based therapeutics are the ideal approaches for the inhibition of these biomolecules. (Chandan et al., 2023) Silica-coated PLGA nanoparticles encapsulating these enzymes were proposed for cancer therapy by Gustafson et al. They reported that the ideal therapeutics were silica-coated PLGA nanoparticles encapsulated with enzymes that supported the long-term and controlled release to cancer cells under in vivo conditions. (Gustafson et al., 2023)

GENE DELIVERY

Lipid micro and nanoparticles are popular with their easy production methods, but they have stability problems due to their easy and quick aggregation. Whereas, hybrid nanoparticle formulations with lipid, PLGA-PEG polymers were proposed as newly developed systems for transporting genetic materials. It was observed that when DNA and mRNA were loaded into lipid-modified PLGA-PEG nanoparticles and examined in vitro and in vivo, the genetic material was stored for at least 12 months at -20° C after lyophilization without losing its transfection efficiency. In addition, it was reported that this hybrid material offers improved transfection efficiency, sustained gene release behavior, and excellent stability for gene therapy. (Z. Li et al., 2022)

Not only PLGA but also block copolymers of PLGA are often used for gene and drug carrier systems. (Adams, Lavasanifar, & Kwon, 2003; Jeong, Kim, & Park, 2004) In a newly published study, amphiphilic 4-arm star-shaped and linear polylactide-*b*-poly[(oligoethylene glycol)methylether acrylate] and PLGA-*b*- polylactide-*b*-poly[(oligoethylene glycol) methylether acrylate] biodegradable block copolymers were synthesized by ring-opening polymerization and radical polymerization. It was reported that micro and nanoparticles prepared using these polymers tended to form spontaneously, and were new biomaterials with biocompatible and biodegradable properties. (Oliveira et al., 2023)

CONCLUSION AND FUTURE OUTLOOK

With this review study, which aims to provide some new ideas for PLGA micro nanoparticles for widespread application areas in the future, a perspective on clinical treatments and future research areas was presented. PLGA micro nanoparticles are currently being designed according to specific application areas and research is being intensified in the direction of preparing hybrid formulations with other biomaterials. PLGA, an ossified biomaterial for drug carrier systems, is now also participating in hybrid formulations for gene therapy. The use of PLGA as an encapsulation material and stabilizer in vaccines based on genetic material, which came to the fore with the COVID-19 pandemic, attracts attention. In addition, PLGA is often preferred as a wound-healing biomaterial loaded with active substances in tissue engineering applications. In the new generation of hybrid therapeutic systems, PLGA also appears in the role of increasing bioavailability. Considering the speed of PLGA-based research, it is inevitable that PLGA micro-nanoparticles, nano-vaccines, regenerative biomaterials, next-generation therapeutic systems, and drug/gene delivery systems will become more effective and widespread in the next decade.

REFERENCES

Adams, M. L., Lavasanifar, A., & Kwon, G. S. (2003). Amphiphilic block copolymers for drug delivery. *Journal of Pharmaceutical Sciences, 92*(7), 1343-1355. doi:https://doi.org/10.1002/jps.10397

Aksoy, E. A., Taskor, G., Gultekinoglu, M., Kara, F., & Ulubayram, K. (2018). Synthesis of biodegradable polyurethanes chain-extended with (2S)-bis(2-hydroxypropyl) 2-aminopentane dioate. *Journal of Applied Polymer Science, 135*(5), 45764. doi:https://doi.org/10.1002/app.45764

Blackmore, L., & Bernal, W. (2015). Acute liver failure. *Clin Med (Lond), 15*(5), 468-472. doi:10.7861/clinmedicine.15-5-468

Chandan, G., Saini, A. K., Kumari, R., Chakrabarti, S., Mittal, A., Sharma, A. K., & Saini, R. V. (2023). The exploitation of enzyme-based cancer immunotherapy. *Human Cell, 36*(1), 98-120. doi:10.1007/s13577-022-00821-2

Chandrasekaran, S. K., Capozza, R., & Wong, P. S. L. (1978). Therapeutic systems and controlled drug delivery. *Journal of Membrane Science, 3*(2), 271-286. doi:https://doi.org/10.1016/S0376-7388(00)83027-6

Chen, Q., Chen, J., Yang, Z., Xu, J., Xu, L., Liang, C., . . . Liu, Z. (2019). Nanoparticle-Enhanced Radiotherapy to Trigger Robust Cancer Immunotherapy. *Advanced Materials, 31*(10), 1802228. doi:https://doi.org/10.1002/adma.201802228

Cheng, X., Wang, L., Liu, L., Shi, S., Xu, Y., Xu, Z., . . . Li, C. (2023). A sequentially responsive cascade nanoplatform for increasing chemo-chemodynamic therapy. *Colloids and Surfaces B: Biointerfaces, 222*, 113099. doi:https://doi.org/10.1016/j.colsurfb.2022.113099

Dai, J., Liang, M., Zhang, Z., Bernaerts, K. V., & Zhang, T. (2021). Synthesis and crystallization behavior of poly (lactide-co-glycolide). *Polymer, 235*, 124302. doi:https://doi.org/10.1016/j.polymer.2021.124302

Danhier, F., Ansorena, E., Silva, J. M., Coco, R., Le Breton, A., & Préat, V. (2012). PLGA-based nanoparticles: An overview of biomedical applications. *Journal of Controlled Release, 161*(2), 505-522. doi:https://doi.org/10.1016/j.jconrel.2012.01.043

Desante, G., Pudełko, I., Krok-Borkowicz, M., Pamuła, E., Jacobs, P., Kazek-Kęsik, A., . . . Schickle, K. (2023). Surface Multifunctionalization of Inert Ceramic Implants by Calcium Phosphate Biomimetic Coating Doped with Nanoparticles Encapsulating Antibiotics. *ACS Applied Materials & Interfaces, 15*(17), 21699-21718. doi:10.1021/acsami.3c03884

Elbatanony, R. S., Parvathaneni, V., Kulkarni, N. S., Shukla, S. K., Chauhan, G., Kunda, N. K., & Gupta, V. (2021). Afatinib-loaded inhalable PLGA nanoparticles for localized therapy of non-small cell lung cancer (NSCLC)-development and in-vitro efficacy. *Drug Deliv Transl Res, 11*(3), 927-943. doi:10.1007/s13346-020-00802-8

Escalona-Rayo, O., Fuentes-Vázquez, P., Jardon-Xicotencatl, S., García-Tovar, C. G., Mendoza-Elvira, S., & Quintanar-Guerrero, D. (2019). Rapamycin-loaded polysorbate 80-coated PLGA nanoparticles: Optimization of formulation variables and in vitro anti-glioma assessment. *Journal of Drug Delivery Science and Technology, 52*, 488-499. doi:https://doi.org/10.1016/j.jddst.2019.05.026

Gentile, P., Chiono, V., Carmagnola, I., & Hatton, P. V. (2014). An overview of poly(lactic-co-glycolic) acid (PLGA)-based biomaterials for bone tissue engineering. *Int J Mol Sci, 15*(3), 3640-3659. doi:10.3390/ijms15033640

Ghitman, J., Biru, E. I., Stan, R., & Iovu, H. (2020). Review of hybrid PLGA nanoparticles: Future of smart drug delivery and theranostics medicine. *Materials & Design, 193*, 108805. doi:https://doi.org/10.1016/j.matdes.2020.108805

González-González, A. M., Cruz, R., Rosales-Ibáñez, R., Hernández-Sánchez, F., Carrillo-Escalante, H. J., Rodríguez-Martínez, J. J., . . . Ludert, J. E. (2023). In Vitro and In Vivo Evaluation of a Polycaprolactone (PCL)/Polylactic-Co-Glycolic Acid (PLGA) (80:20) Scaffold for Improved Treatment of Chondral (Cartilage) Injuries. *Polymers, 15*(10). doi:10.3390/polym15102324

Gu, P., Wusiman, A., Zhang, Y., Liu, Z., Bo, R., Hu, Y., . . . Wang, D. (2019). Rational Design of PLGA Nanoparticle Vaccine Delivery Systems To Improve Immune Responses. *Molecular Pharmaceutics, 16*(12), 5000-5012. doi:10.1021/acs.molpharmaceut.9b00860

Guo, X., Zuo, X., Zhou, Z., Gu, Y., Zheng, H., Wang, X., . . . Wang, F. (2023). PLGA-Based Micro/Nanoparticles: An Overview of Their Applications in Respiratory Diseases. *International Journal of Molecular Sciences, 24*(5). doi:10.3390/ijms24054333

Gustafson, K. T., Mokhtari, N., Manalo, E. C., Montoya Mira, J., Gower, A., Yeh, Y.-S., . . . Fischer, J. M. (2023). Hybrid Silica-Coated PLGA Nanoparticles for Enhanced Enzyme-Based Therapeutics. *Pharmaceutics, 15*(1). doi:10.3390/pharmaceutics15010143

Han, F. Y., Thurecht, K. J., Whittaker, A. K., & Smith, M. T. (2016). Bioerodable PLGA-Based Microparticles for Producing Sustained-Release Drug Formulations and Strategies for Improving Drug Loading. *Frontiers in Pharmacology, 7*. doi:10.3389/fphar.2016.00185

Hines, D. J., & Kaplan, D. L. (2013). Poly(lactic-co-glycolic) acid-controlled-release systems: experimental and modeling insights. *Crit Rev Ther Drug Carrier Syst, 30*(3), 257-276. doi:10.1615/critrevtherdrugcarriersyst.2013006475

Jeong, J. H., Kim, S. W., & Park, T. G. (2004). Biodegradable Triblock Copolymer of PLGA-PEG-PLGA Enhances Gene Transfection Efficiency. *Pharmaceutical Research, 21*(1), 50-54. doi:10.1023/B:PHAM.0000012151.05441.bf

Jin, Y., Zhang, J., Xu, Y., Yi, K., Li, F., Zhou, H., . . . Li, M. (2023). Stem cell-derived hepatocyte therapy using versatile biomimetic nanozyme incorporated nanofiber-reinforced decellularized extracellular matrix hydrogels for the treatment of acute liver failure. *Bioactive Materials, 28*, 112-131. doi:https://doi.org/10.1016/j.bioactmat.2023.05.001

Li, J., Stayshich, R. M., & Meyer, T. Y. (2011). Exploiting Sequence To Control the Hydrolysis Behavior of Biodegradable PLGA Copolymers. *Journal of the American Chemical Society, 133*(18), 6910-6913. doi:10.1021/ja200895s

Li, Z., Zhang, X.-Q., Ho, W., Bai, X., Jaijyan, D. K., Li, F., . . . Xu, X. (2022). Lipid-Polymer Hybrid "Particle-in-Particle" Nanostructure Gene Delivery Platform Explored for Lyophilizable DNA and mRNA COVID-19 Vaccines. *Advanced Functional Materials, 32*(40), 2204462. doi:https://doi.org/10.1002/adfm.202204462

Little, A., Wemyss, A. M., Haddleton, D. M., Tan, B., Sun, Z., Ji, Y., & Wan, C. (2021). Synthesis of Poly(Lactic Acid-co-Glycolic Acid) Copolymers with High Glycolide Ratio by Ring-Opening Polymerisation. *Polymers, 13*(15). doi:10.3390/polym13152458

Makadia, H. K., & Siegel, S. J. (2011). Poly Lactic-co-Glycolic Acid (PLGA) as Biodegradable Controlled Drug Delivery Carrier. *Polymers, 3*(3), 1377-1397. doi:10.3390/polym3031377

Mishra, B., & Singh, J. (2020). Chapter 4 - Novel drug delivery systems and significance in respiratory diseases. In K. Dua, P. M. Hansbro, R. Wadhwa, M. Haghi, L. G. Pont, & K. A. Williams (Eds.), *Targeting Chronic Inflammatory Lung Diseases Using Advanced Drug Delivery Systems* (pp. 57-95): Academic Press.

Oliveira, A. S. R., Pereira, P., Mendonça, P. V., Fonseca, A. C., Simões, S., Serra, A. C., & Coelho, J. F. J. (2023). Novel degradable amphiphilic 4-arm star PLA-b-POEOA and PLGA-b-POEOA block copolymers: synthesis, characterization and self-assembly. *Polymer Chemistry, 14*(2), 161-171. doi:10.1039/D2PY01216B

Pandey, A., & Jain, D. S. (2015). Poly Lactic-Co-Glycolic Acid (PLGA) Copolymer and Its Pharmaceutical Application. In *Handbook of Polymers for Pharmaceutical Technologies* (pp. 151-172).

Quan, P., Guo, W., LinYang, Cun, D., & Yang, M. (2023). Donepezil accelerates the release of PLGA microparticles via catalyzing the polymer degradation regardless of the end groups and molecular weights. *International Journal of Pharmaceutics, 632*, 122566. doi:https://doi.org/10.1016/j.ijpharm.2022.122566

Saleh, A., Abdelkader, D. H., El-Masry, T. A., Eliwa, D., Alotaibi, B., Negm, W. A., & Elekhnawy, E. (2023). Antiviral and antibacterial potential of electrosprayed PVA/PLGA nanoparticles loaded with chlorogenic acid for the management of coronavirus and Pseudomonas aeruginosa lung infection. *Artificial Cells, Nanomedicine, and Biotechnology, 51*(1), 255-267. doi:10

.1080/21691401.2023.2207606

Sanapalli, B. K. R., Yele, V., Singh, M. K., Thumbooru, S. N., Parvathaneni, M., & Karri, V. V. S. R. (2023). Human beta defensin-2 loaded PLGA nanoparticles impregnated in collagen-chitosan composite scaffold for the management of diabetic wounds. *Biomedicine & Pharmacotherapy, 161*, 114540. doi:https://doi.org/10.1016/j.biopha.2023.114540

Sarkar, C., Kommineni, N., Butreddy, A., Kumar, R., Bunekar, N., & Gugulothu, K. (2022). PLGA Nanoparticles in Drug Delivery. In *Nanoengineering of Biomaterials* (pp. 217-260).

Schiliro, C., & Firestein, B. L. (2021). Mechanisms of Metabolic Reprogramming in Cancer Cells Supporting Enhanced Growth and Proliferation. *Cells, 10*(5). doi:10.3390/cells10051056

Schoenmaker, L., Witzigmann, D., Kulkarni, J. A., Verbeke, R., Kersten, G., Jiskoot, W., & Crommelin, D. J. A. (2021). mRNA-lipid nanoparticle COVID-19 vaccines: Structure and stability. *International Journal of Pharmaceutics, 601*, 120586. doi:https://doi.org/10.1016/j.ijpharm.2021.120586

Shah, S. M., Joshi, D., Chbib, C., Roni, M. A., & Uddin, M. N. (2023). The Autoinducer N-Octanoyl-L-Homoserine Lactone (C8-HSL) as a Potential Adjuvant in Vaccine Formulations. *Pharmaceuticals, 16*(5). doi:10.3390/ph16050713

Sharma, D., Rout, S. R., Kenguva, G., Khatravath, M., Jain, G. K., Aggarwal, G., . . . Dandela, R. (2023). Chapter 12 - PLGA-based nanoparticles as regenerative medicine. In P. Kesharwani (Ed.), *Poly(lactic-co-glycolic acid) (PLGA) Nanoparticles for Drug Delivery* (pp. 335-356): Elsevier.

Shaver, M. P., & Cameron, D. J. A. (2010). Tacticity Control in the Synthesis of Poly(lactic acid) Polymer Stars with Dipentaerythritol Cores. *Biomacromolecules, 11*(12), 3673-3679. doi:10.1021/bm101140d

Sher, M., Zahoor, M., Shah, S. W. A., & Khan, F. A. (2023). Is particle size reduction linked to drug efficacy: an overview into nano initiatives in pharmaceuticals. doi:doi:10.1515/zpch-2023-0221

Son, G.-H., Lee, B.-J., & Cho, C.-W. (2017). Mechanisms of drug release from advanced drug formulations such as polymeric-based drug-delivery systems and lipid nanoparticles. *Journal of Pharmaceutical Investigation, 47*(4), 287-296. doi:10.1007/s40005-017-0320-1

Spampinato, S. F., Caruso, G. I., De Pasquale, R., Sortino, M. A., & Merlo, S. (2020). The Treatment of Impaired Wound Healing in Diabetes: Looking among Old Drugs. *Pharmaceuticals (Basel), 13*(4). doi:10.3390/ph13040060

Taşkor Önel, G. (2023). Synthesis and Characterization of Poly(lactic-co-glycolic acid) Derived with LGlutamic Acid and L-Aspartic AcidSynthesis and Characterization of Poly(lactic-co-glycolic acid) Derived with LGlutamic Acid and L-Aspartic Acid. *Erzincan Üniversitesi Fen Bilimleri Enstitüsü*

Dergisi, 16, 155-168. doi:10.18185/erzifbed.1235522

Vanza, J. D., Lalani, J. R., Patel, R. B., & Patel, M. R. (2023). DOE supported optimization of biodegradable polymeric nanoparticles based dry powder inhaler for targeted delivery of afatinib in non-small cell lung cancer. *Journal of Drug Delivery Science and Technology, 84*, 104554. doi:https://doi.org/10.1016/j.jddst.2023.104554

Xu, J., Cui, Y., Liu, M., An, Z., Li, K., Gu, X., . . . Fan, Y. (2023). Enhanced hydrophilicity of one-step electrosprayed red blood cell-like PLGA microparticles by block polymer PLGA-PEG-PLGA with excellent magnetic-luminescent bifunction and affinity to HUVECs. *European Polymer Journal, 191*, 112040. doi:https://doi.org/10.1016/j.eurpolymj.2023.112040

Yoo, J., & Won, Y.-Y. (2020). Phenomenology of the Initial Burst Release of Drugs from PLGA Microparticles. *ACS Biomaterials Science & Engineering, 6*(11), 6053-6062. doi:10.1021/acsbiomaterials.0c01228

Yoon, Y. M., Lewis, J. S., Carstens, M. R., Campbell-Thompson, M., Wasserfall, C. H., Atkinson, M. A., & Keselowsky, B. G. (2015). A combination hydrogel microparticle-based vaccine prevents type 1 diabetes in non-obese diabetic mice. *Scientific Reports, 5*(1), 13155. doi:10.1038/srep13155

Yuan, J., Guo, M., Zhao, S., Li, J., Wang, X., Yang, J., . . . Song, X. (2023). Core-shell lipid-polymeric nanoparticles for enhanced oral bioavailability and antihypertensive efficacy of KY5 peptide. *Chinese Chemical Letters, 34*(4), 107943. doi:https://doi.org/10.1016/j.cclet.2022.107943

Zhang, Y., Jiang, W., Kong, L., Fu, J., Zhang, Q., & Liu, H. (2023). PLGA@IL-8 nanoparticles-loaded acellular dermal matrix as a delivery system for exogenous MSCs in diabetic wound healing. *International Journal of Biological Macromolecules, 224*, 688-698. doi:https://doi.org/10.1016/j.ijbiomac.2022.10.157

Zielińska, A., Carreiró, F., Oliveira, A. M., Neves, A., Pires, B., Venkatesh, D. N., . . . Souto, E. B. (2020). Polymeric Nanoparticles: Production, Characterization, Toxicology and Ecotoxicology. *Molecules, 25*(16). doi:10.3390/molecules25163731

Zolnik, B. S., & Burgess, D. J. (2007). Effect of acidic pH on PLGA microsphere degradation and release. *Journal of Controlled Release, 122*(3), 338-344. doi:https://doi.org/10.1016/j.jconrel.2007.05.034

BÖLÜM 9

CHAPTER 9

MYXOMYCETES OF THE GENUS *FULIGO* HALLER (PHYSARALES, MYXOMYCETES) IN TURKEY

Hasan AKGÜL[1], Celal BAL[2], Emre Cem ERASLAN[3], Mustafa SEVİNDİK[4]

1 Department of Biology, Faculty of Science, Akdeniz University, 07100, Antalya, Turkey.
2 Oguzeli Vocational High School, Gaziantep University, 27900, Gaziantep, Turkey.
3 Department of Food Processing, Bahçe Vocational School of Higher Education, Osmaniye Korkut Ata University, Osmaniye 80500, Turkey.
4 Department of Biology, Facult of Science and Literature, Osmaniye Korkut Ata University, 80500, Osmaniye, Turkey.

Introduction

Myxomycetes are known as true slime molds, plasmodial slime molds or Myxogastrea. Myxomycetes are multinuclear single-celled organisms that can produce one or more spores (Stephenson & Stempen, 1994; Baba and Sevindik, 2018; Sevindik et al., 2018). Myxogastrea species are abundant in cool, moist and shaded areas such as rotten tree trunks, branches, alive or dead bark, decayed fruit or fruit scraps, decayed leaves and leaf debris. Myxomycetes live in the environment by feeding on other microorganisms (bacteria, yeasts, fungus hyphae, blue-green bacteria and green algae) (Farr, 1981; Sevindik and Akgül, 2019). Myxogastrea fruitbodies could develop spontaneously in the nature. Furthermore, especially after identification with the moist chamber technique, they could be detected especially on plant surfaces (Härkönen & Ukkola, 2000). The number of known Myxomycetes species is 1088 taxa globally (Lado, 2023). 309 taxa were identified in Turkey (Baba and Sevindik, 2019; Baba and Atay, 2019; Baba et al., 2018; Ocak and Konuk, 2018; Baba et al., 2019; Baba and Sevindik, 2020a; Baba et al., 2020a; Baba et al., 2020b; Sesli et al., 2020; Baba, 2021; Baba and Sevindik, 2021; Baba et al., 2021a; Baba et al., 2021b; Baba et al., 2021c; Eroğlu, 2021; Baba and Sevindik, 2022a; Baba and Sevindik, 2022b; Baysal and Eroğlu, 2022).

In Order Physarales: Fruiting bodies with granular or crystalline calcareous deposits on some of their structures, calcium in the peridium, stalk, or capillitium. Columella present or absent. Capillitium always present, filamentous or tubular, sometimes provided with calcareous nodules. Spores black, dark purple or purplish brown in mass, dark purple to purplish brown under the microscope. Plasmodium of the phaneroplasmodium type. The distinguishing characteristic of the Physarales is the presence of lime (calcium carbonate) in some parts of the fruiting bodies, either in stalk, peridium or capillitium.

Family Physaraceae: Fruiting bodies sessile or stalked, sporocarpic or plasmodiocarpic, rarely aethalioid, with calcareous deposits in some parts of their structure, without oil or wax. Peridium usually with granular calcareous deposits, the wall a thin membrane, usually with an outer layer of minute roundish granules of lime. Stipe present or often absent, seldom prolonged within the sporangium as a columella. Columella absent, rarely present, sometimes with a calcareous pseudocolumella. Capillitium a network of hyaline tubules connecting calcareous nodes, sometimes with branched threads or simple and unbranched peridial outgrowths. Consisting of slender tubules, which branch repeatedly in every direction and anastomose to form an intricate network, the extremities attached on all sides to the wall of the sporangium. The tubules more or less expanded at the angles of the network and inclosing minute roundish granules of

lime, these granules either aggregated into nodules with intervening empty spaces or more rarely distributed throughout their entire length. Spores globose, very rarely ellipsoidal, violaceous.

Material and methods

Two species are obtained by Baba and his friends were collected from the natural environment or obtained in the laboratory using by moist chamber technique. Natural myxomycete samples were collected from natural area. On different substrates, cortex, woods, barks, leaf, debris, organic plants and animal material samples were transported to the laboratory in small carton boxes. Furthermore, after the field studies, myxomycete fructifications were obtained from the moist chamber culture in laboratory. For moist chamber culture; live or dead plant materials (forest floor litter, aerial litter, wood and bark from living or dead trees) were obtained at a number of localities. Moist chambers cultures consisted of disposable plastic petri dishes lined with filter paper. The sample material in each dish was moistened with distilled water. After a period of approximately 24 -48 hours (in summer 48 hours, in winter 24 hours), excess water in each dish was removed. Cultures were kept at room temperature (24ºC) in diffuse daylight (Baba et al., 2021b). Examined with a stereomicroscope on a regular basis for a period of up to two months in order to detect plasmodia or fruiting bodies. When necessary, a small amount of water was added to each culture to maintain moist conditions. The moist chamber with the developing myxomycete samples was allowed to dry and the myxomycetes were dried for one week. Myxomycete plasmodia or fruiting bodies were noted and recorded. Each time the cultures were checked. All fruiting bodies were removed. Air-dried and glued in small pasteboard boxes for permanent storage. The samples were photographed and identified.

The samples were identified under stereomicroscope and light microscopy. General structure, plasmodium type, fructification type, shape, colour, macroscopic measurements, the presence or absence of lime or the color and shape of the samples were examined with the stereomicroscope. In light microscopy, the capillitium, spore, shape, color, size, ornamentation, branching shape, features was observed. Capillitium, pseudo-capillitium and columella or pseudo-columella, capillitium formation, shape and size, condition of columella (free or attached) were examined with light microscopy. Furthermore, the shape, color, size and ornamentation of the spores were examined. For every species recognized, the most typical specimens were used for providing descriptions. Species descriptions were used to define the genus and to provide a dichotomous key to the species. Spore colors were obtained in 10% NH3 solution. The myxomycete samples were identified based on a variety of digital and printed sources (Nomen.eumycetozoa.com; Martin and Alexopoulos, 1969; Farr, 1976;

1981; Thind, 1977; Martin et al., 1983; Stephenson and Stempen, 1994; Ing, 1994; Neubert et al., 2000; Alexopoulos et al., 1996; Lado and Pando, 1997; de Haan et al., 2004; Stephenson and Rojas, 2017; Baba and Dogan, 2018; Baba and Er, 2018; Zümre et al., 2019). Samples were arranged as fungarium material and kept in the Biology Department's laboratory of Hatay Mustafa Kemal University Hatay-Turkey. The list below includes the recorded myxomycetes, arranged alphabetically, taxonomic treatment includes a key to species, generic and specific descriptions, photos, habitat data and comments.

Results and discussion

Eukaryota

Protista

Mycetozoa

Myxomycetes

Physarales

Physaraceae

Genus Fuligo Haller, Hist. stirp. Helv. 3:110 (1768)

Synonyms:

Lignydium Link, Ges. Naturf. Freunde Berlin Mag. Neuesten Entdeck. Gesammten Naturk. 3(1):24 (1809)

Aethalium Link, Ges. Naturf. Freunde Berlin Mag. Neuesten Entdeck. Gesammten Naturk. 3(1):24 (1809)

Aethaliopsis Zopf, in Schenk, Handb. Bot. 3(2):149 (1885)

Erionema Penz., Myxomyc. Fl. Buitenzorg 36 (1898)

Fuligo subg. Erionema (Penz.) Y. Yamam.,

Description; Fructification aethalioid, occasionally subplasmodiocarpous, consisting of interwoven and poorly defined tubes. Sporotheca elongate, branched, and interwoven, combined to form a pulvinate aethalium, outer portion sterile, barren and forming a fragile cortex, charged with deposits of lime granules and without spores sometimes nearly lacking. Basal layer a membranous hypothallus, the intermediate portion containing spores, capillitium, and limy walls derived from the plasmodial tubes. Lime present on the peridium and in the capillitum, of rounded granules. Columella none. Capillitium a network of limeless tubules with connected calcareous nodes at many or all the junctions, hyaline, tubular threads connecting the lime-knots, forming a net-work of irregular meshes, more or

less expanded at the angles, the tubules containing in greater or less abundance irregular nodules of lime, often rather scanty. Spores dark in mass. Spores globose or sometimes ellipsoidal, violaceous.

Comments: Fuligo, genus of true slime molds (class Myxomycetes) whose large fruiting body (compound sporangia), 5 centimetres or more long and about half as wide, occur commonly on decaying wood. The component sporangia branching and anastomosing in every direction, complicate and grown together consisting of interwoven and poorly defined tubes each with a calcareous. The sporangia, on bursting, release fine black spores. Fuligo septica, the best-known species, is also called "flowers of tan," from the frequent appearance of its yellow fruiting body in tan bark bits used for tanning hides. According to the literature only 10 species are recognized all over the World (Lado, 2005-2023).

Distribution: 10 species are recognized all over the world, *Fuligo aurea* (Penz.) Y. Yamam., *Fuligo cinerea* (Schwein.) Morgan*, Fuligo intermedia* T. Macbr., *Fuligo laevis* Pers., *Fuligo leviderma* H. Neubert, Nowotny & K. Baumann, *Fuligo licentii* Buchet, *Fuligo luteonitens* L.G. Krieglst. & Nowotny., *Fuligo megaspora* Sturgis, *Fuligo muscorum* Alb. & Schwein., *Fuligo septica* (L.) F.H. Wigg.

Turkey: 2 species of them are recorded in Turkey, *Fuligo cinerea* (Schwein.) Morgan and *Fuligo septica* (L.) F.H. Wigg.

Key to the species of Fuligo in Turkey

1. Spores larger than 10 µm, spherical or ellipsoid 2

1'. Spores 6-9 µm in diameter, fructification aethalioid, aethalium usually yellow, sometimes white, greyish, pale rose to lemon-yellow, violet; lime nodes small, fusiform, the aethalial wall with an irreular, foam-like surface ….…..….. *Fuligo septica*

2. Fructification from aethalioid to subplasmodiocarps in small groups, pulvinate, hypothallus developed, membranous, cream or whitish, cortex thick, lime nodes connected by hyaline threads, lime nodes large, angular or irregular in shape, spores from spherical to ellipsoid, spinulose, spinules often connected by narrow ridges into a broken reticulum, 13-14 µm ……. .....*Fuligo cinerea*

Description and other information about the Fuligo species detected in Turkey is given below;

1. *Fuligo cinerea* (Schwein.) Morgan, J. Cincinnati Soc. Nat. Hist. 19(1):33 (1896)

Synonyms: *Enteridium cinereum* Schwein.,

Lachnobolus cinereus Schwein.,

Badhamia coadnata Rostaf.,

Physarum ellipsosporum Rostaf.,

Fuligo ellipsospora (Rostaf.) Lister,

Lignydium ellipsosporum (Rostaf.) Kuntze,

Aethaliopsis stercoriformis Zopf,

Fuligo stercoriformis (Zopf) Racib.,

Description; Aethalia often in small groups, slightly oblate, flat, low pulvinate or irregular, bent brain-like and coalescing into an aethalium of irregular shape, sessile on a broad base, pale grey or white, 0.5-6 cm across and up to 0.5 cm thick, cortex brittle and crumbling irregularly, smooth or rough, rarely absent. Sporangia variously contracted and grown together, forming a dense reticulum. Hypothallus membranous, often consisting of several perforated layers, encrusted with white lime, often protruding outside the aethalium. Peridium persistent, white to pale lilac, fragmented and impregnated with white lime; component tubules, as far as recognisable, confluent. Capillitium tubules colourless, connected at each end to peridium, branched or unbranched and sometimes forming a net, with a variable number of large or small fusiform or irregular, lime nodes containing white lime, the nodes sometimes merged into a pseudocolumella in the middle of the tubes. Spore-mass black. Spores rather dark purple-brown, mostly oval, (10-)13-14(-15) µm diam., verruculose (rarely spinulose), some having a paler area, slightly elliptical, these often united by narrow ridges into a broken reticulum. Plasmodium translucent white.

Comments: *Fuligo cinerea* sporocarps aethalium to subplasmodiocarps, usually in small groups, scattered to very gregarious, usually slender and protruding, sometimes elongated to pulvinate. Peridium rind, hard, usually smooth and thick, but sometimes underdeveloped or more or less curved gray or beige. The capillitium consists of interconnected hyaline filaments and white, large, irregular nodules that sometimes form a pseudocolumella.

Distribution: Czech Republic, Finland, Papua New Guinea, Peru, Taiwan, USA,

Turkey: Ocak, 2015; Baba and Atay, 2019.

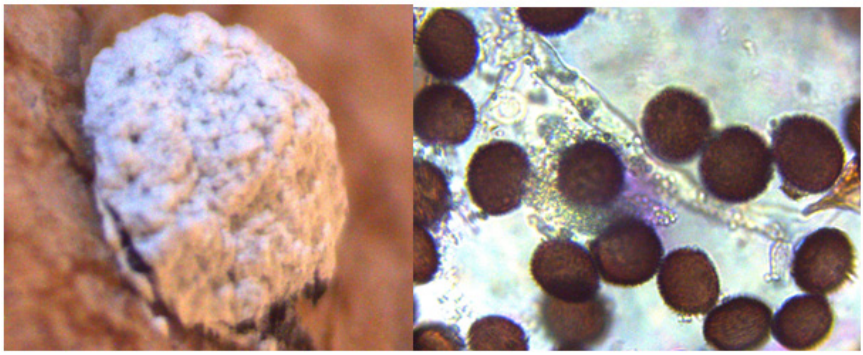

Figüre 1. ***Fuligo cinerea*** *sporocarp, capillitium and spores*

2. ***Fuligo septica*** (L.) F.H. Wigg., Prim. fl. holsat. 112 (1780)

Synonyms: *Mucor septicus* L.,

Reticularia septica (L.) With.,

Fuligo septica (L.) J.F. Gmel.,

Aethalium septicum (L.) Fr.,

Mucor mucilago Scop.,

Mucor ovatus Schaeff.,

Reticularia ovata (Schaeff.) With.,

Fuligo ovata (Schaeff.) T. Macbr.,

Reticularia lutea Bull.,

Reticularia hortensis Bull.,

Fuligo hortensis (Bull.) Duby,

Aethalium rufum (Pers.) Wallr.,

Aethalium rufum (Pers.) Alexandrovicz,

Fuligo flava Pers.,

Aethalium flavum (Pers.) Link,

Aethalium septicum var. *flavum* (Pers.) Fr.,

Fuligo septica var. *flava* (Pers.) Lázaro Ibiza,

Fuligo septica f. *flava* (Pers.) Y. Yamam.,

Fuligo rufa Pers.,

Reticularia rufa (Pers.) Schwein.,

Aethalium septicum var. *rufum* (Pers.) Fr.,
Fuligo septica var. *rufa* (Pers.) Lázaro Ibiza,
Fuligo septica f. *rufa* (Pers.) Y. Yamam.,
Fuligo vaporaria Pers.,
Reticularia vaporaria (Pers.) Chevall.,
Aethalium vaporarium (Pers.) Becker,
Aethalium septicum var. *vaporarium* (Pers.) Rabenh.,
Fuligo septica var. *vaporaria* (Pers.) Lázaro Ibiza,
Fuligo candida Pers.,
Aethalium candidum (Pers.) Schltdl.,
Fuligo septica var. *candida* (Pers.) R.E. Fr.,
Fuligo septica f. candida (Pers.) Meyl.,
Fuligo pallida Pers.,
Reticularia cerea Sowerby,
Fuligo carnea Schumach.,
Fuligo flavescens Schumach.,
Reticularia carnea (Schumach.) Fr.,
Fuligo cerebrina Brond.,
Fuligo varians Sommerf.,
Aethalium septicum var. *cinnamomeum* Fr.,
Aethalium ferrincola Schwein.,
Licea lindheimeri Berk.,
Tubulina lindheimeri (Berk.) Massee,
Tubifera lindheimeri (Berk.) E. Sheld.,
Fuligo varians f. ecorticata Rostaf.,
Fuligo varians var. ecorticata (Rostaf.) Cooke,
Fuligo tatrica Racib.,
Fuligo candida Jahn,
Fuligo septica var. *cinnamomea* R.E. Fr.,
Fuligo septica f. corticata Meyl.,

Fuligo septica var. *rosea* Nann.-Bremek.,

Fuligo candida f. persicina Y. Yamam.,

Fuligo septica var. *lapislazulicolor* H.Marx & A. Kuhnt,

Description: Fructifications aethaloid, aethalia small or large, irregular, pulvinate, subplasmodiocarpous, 2-13 cm long and 0.5-3 cm thick (Aethalia can be much larger). Peridium inside the aethalia white or colourless, grayish white, black when moist, often encrusted with globular lime and in that case brittle, usually fragmentary, sometimes the tubes in places with small spaces between them. Cortex thick, calcareous, fragile, dehiscence irregular, lemon-yellow, pale yellow green-yellow or ochraceous, spongy, brittle, rough on the outside and fragile, crumbling away. Hypothallus membranous, often consisting of several perforated layers, white and containing a little coloured lime, usually protruding somewhat outside the aethalium. Capillitium colourless, pale yellow lime connected by hyaline threads, hyaline with yellow nodes, nodes large, abundant or sparse, tubules with many or few anastomoses, if abundant then protruding elastically, the tubules with few or many small fusiform or branched white lime nodes, internodes small hyaline, non calcareous. Spore-mass black, dark brown. Spores pale lilac-grey or lilac- brown, violaceous brown, almost spherical, globose, 7-10 µm diam., minutely spiny, minutely spinulose, verruculose. Plasmodium yellow.

Comments: Very variable species that some authors, depending on colour of capillitium, consider varieties or different species. Pulvinated aethalium, yellow, 3mm to 5mm high and 20mm to 45mm thick; calcium-encrusted cortex, yellow; hypothallus white, well developed, irregular, membranous, calcareous; abundant capillitium, hyaline filaments, calcareous nodules irregular, yellow; spore blackish-brown; spore globose, with tiny warts, pale brown under light transmitted.

Distribution: Czech Republic, Finland, Papua New Guinea, Peru, Taiwan, USA

Turkey: Ergül and Gücin, 1994; Ergül and Dülger, 2000d, 2002c; Ergül et al., 2005a, 2005b; Ocak and Hasenekoğlu, 2005; Oran et al., 2006; Yağız and Afyon, 2007b; Baba and Tamer, 2008a; Ergül and Akgül, 2011; Eroğlu and Kaşık, 2013a; Ocak, 2015; Baba, 2017; Baba and Doğan, 2018; Baba and Atay, 2019; Baba et al., 2020; Baba et al., 2021b.

Figüre 2. Fuligo septica sporocarps, capillitium and spores

Conclusion

With this study 2 species of Fuligo genus recorded from Turkey. *Fuligo cinerea* (Schwein.) Morgan and *F. septica* (L.) F.H. Wigg. *F. septica* has proven to be the most common species of this genus in Turkey, *Fuligo cinerea* is less common from Turkey.

References

Adamonyte G, (2007). Myxomycetes of the Genus Clastoderma in Lıthuanıa. Botanica Lithuanica, 13(1): 27–32.

Alexopoulos CJ, Mims CW, Blackwell M (1996). Introductory Mycology, 4.th Edition, John Wiley and Sons Inc., New York.

Baba H and Atay M (2019). Myxomycetes of Kumlu and Reyhanlı districts of Hatay/Turkey province. Biological Diversity and Conservation, ISSN 1308-8084 Online; ISSN 1308-5301 Print 12/2 41-50.

Baba H and Doğan Y (2018). Investigation of Myxomycetes (Myxomycota) in South Amanos Mountains (Hatay-Turkey). Celal Bayar Univ. J. Sci., 14: 277–284.

Baba H and Sevindik M (2019). Mycetozoa of Turkey (Checklist), Mycopath 17(1):1-14.

Baba H and Sevindik M (2020a). Myxomycetes of Eşmişek Plateau (Kırıkhan-Hatay). KSÜ Tarım ve Doğa Derg KSU J. Agric Nat 23(4): 917-923, 2020

Baba H and Sevindik M (2021). A New Myxomycetes record (Myxogastria) from Turkey: Didymium listeri Massee. KSU J. Agric Nat 24 (4): 820-823.

Baba H and Sevindik M (2022a). Myxomycetes diversity in Adana Province (Turkey) with two new records. Phytotaxa 547 (1): 031–042.

Baba H and Sevindik M (2022b). New Records of Myxogastria (Mycetozoa) from the Eastern Mediterranean Region of Turkey. ISSN 1062-3590, Biology Bulletin, Vol. 49, No. 2, pp. 85–94.

Baba H and Tamer AÜ (2007). A study on the Myxomycetes in Manisa. Herb J. Syst. Bot., 14:179–196.

Baba H, Altaş B and Sevindik M (2021b). Myxomycetes Diversity of Batman Province and Hasankeyf District. KSÜ Tarım ve Doğa Derg 24 (2): 435-441.

Baba H, Cennet E, Sevindik M (2019). Investıgatıon of Myxomycetes (Myxomycota) in Kırıkhan (Hatay Provınce). Commun. Fac. Sci. Univ. Ank. Series C Volume 29, Number 2, Pages 160-169.

Baba H, Er A, Sevindik M (2020). Myxomycetes Diversity of Belen Region of Hatay Province (Turkey). Kastamonu Univ., Journal of Forestry Faculty, 20(2): 86-96.

Baba H, Gelen M, Sevindik M (2018). Taxonomic investigation of myxomycetes in Altınözü, Turkey. Mycopath, 16(1): 23–31.

Baba H, Gündoğdu F and Sevindik M (2021a). Myxomycetes biodiversity in Gaziantep Province (Turkey) with four new records. Phytotaxa 478 (1): 105–118.

Baba H, Sevindik M, Dogan M, Akgül H (2020b). Antıoxıdant, antımıcrobıal actıvıtıes and heavy metal contents of some Myxomycetes. Fresenius Environmental Bulletin Volume 29 – No. 09/2020 pages 7840-7846.

Baba H, Sevindik M, Er A, Atay M, Doğan Y, Altaş B and Akgül A (2021c). New four Mycetozoa records from South East Anatolia-Turkey. Fresenius Environmental Bulletin Volume 30 – No. 04 pages 3565-3574.

Baba, H. (2021). Five new myxomycetes (Myxogastria) records from Turkey. Phytotaxa, 507(2), 131-143.

Baba, H., & Doğan, Y. (2018). Investigation of Myxomycetes (Myxomycota) in South Amanos Mountains (Hatay-Turkey). Celal Bayar University Journal of Science, 14(3), 277-284.

Baba, H., & Er, A. (2018). Craterium dictyosporum: A new record of Myxomycetes from Hatay, Turkey. Acta Biologica Turcica, 31(1), 33-35.

Baba, H., & Sevindik, M. (2018). The roles of myxomycetes in ecosystems. J Bacteriol Mycol Open Access, 6(3), 165-166.

Baysal R and Eroğlu G (2022). Diversity of myxomycete on Konya-Beyşehir highway route. Anatolian Journal of Botany 6(1): 55-61.

Ergül CC and Akgül H (2011). Myxomycete diversity of Uludağ National Park, Turkey. Mycotaxon, 116: 479.

Ergül CC and Dülger B (2000d). Myxomycetes of Turkey. Karstenia, 40: 39–41.

Ergül CC and Dülger B (2002c). New records for the myxomycetes flora of Turkey. Turk. J. Bot., 26: 277–280.

Ergül CC and Gücin F (1994). A new record for Turkish myxomycetes: (Fuligo septica (L.) Wiggers). In: Aktaç N. et al., (eds). XII. Ulusal Biyoloji Kongresi, Trakya Üniversitesi, Edirne. 157–159 (In Turkish).

Ergül CC, Dülger B, Akgül H (2005a). Myxomycetes of Mezit Stream valley of Turkey. Mycotaxon, 92: 239–242.

Ergül CC, Dülger B, Oran RB, Akgül H (2005b). Myxomycetes of the western Black Sea Region of Turkey. Mycotaxon, 93: 269–272.

Eroğlu G (2021). Cribraria lepida, Physarum dictyosporum, P. diderma, and P. spectabile newly recorded from Turkey. ISSN (print) 0093-4666 (online) 2154-8889 Mycotaxon, Volume 136, pp. 853–863.

Eroğlu G and Kaşık G (2013a). Myxomycete of Hadim and Taşkent districts (Konya/Turkey) and their ecology. Biodivers. Conserv., 6: 120–127.

Farr ML (1976). Flora Neotropica. Monograph No. 16. New York Botanical Garden Press.

Farr ML (1981). True Slime Molds. Dubuque Iowa: Wm. C. Brown Comp.

Harkönen M and Ukkola T (2000). Conclusions on myxomycetes compiled over

twenty-five years from 4793 moist chamber cultures. Stapfia 73, zugleich Kataloge des OO. Landesmuseums, Neue Folge Nr. 155: 105-112.

Ing B (1994). The phytosociology of myxomycetes. New Phytologist 126: 175–201.

Lado C (2005–2023). An on line nomenclatural information system of Eumycetozoa. Real Jardín Botánico, CSIC. Madrid, Spain. http://www.nomen.eumycetozoa.com. Last updated April 25, 2023.

Lado C and Pando F (1997). Flora Mycologica Iberica, Madrid, Spain: CSIC, vol. 2.

Martin GW and Alexopoulos CJ (1969). The Myxomycetes. Iowa City, Univeristy of Iowa Press.

Martin GW, Alexopoulos CJ, Farr ML (1983). The Genera of Myxomycetes. Univ. of Iowa Pres., Iowa City.

Neubert H, Nowotny W, Baumann K, Marx H (2000). Die Myxomyceten (Band III). Karlheinz Baumann Verlag Gomaringen.

Ocak İ (2015). Seasonal distribution of field-collected myxomycete in the Köroğlubeli Forest, Afyonkarahisar, Turkey. Ekoloji, 24: 48–56.

Ocak İ and Hasenekoğlu İ (2005). Myxomycetes from Trabzon and Giresun Provinces (Turkey). Turk. J. Bot., 29: 11–21.

Ocak İ and Konuk M (2018). Diversity and ecology of Myxomycetes from Kütahya and Konya (Turkey) with four new records. Mycobiology, 46: 215-223.

Oran RB, Ergül CC, Dülger B (2006). Myxomycetes of Belgrad Forest (Istanbul). Mycotaxon, 97: 183–187.

Sesli E, Asan A, Selçuk F. (edlr.) Abacı Günyar Ö, Akata I, Akgül H, Aktaş S, Alkan S, Allı H, Aydoğdu H, Berikten D, Demirel K, Demirel R, Doğan HH, Erdoğdu M, Ergül CC, Eroğlu G, Giray G, Halikî Uztan A, Kabaktepe Ş, Kadaifçiler D, Kalyoncu F, Karaltı İ, Kaşık G, Kaya A, Keleş A, Kırbağ S, Kıvanç M, Ocak İ, Ökten S, Özkale E, Öztürk C, Sevindik M, Şen B, Şen İ, Türkekul İ, Ulukapı M, Uzun Ya, Uzun Yu, Yoltaş A. 2020. Türkiye Mantarları Listesi. Ali Nihat Gökyiğit Vakfı Yayını. İstanbul.

Sevindik, M., & Akgul, H. (2019). Fruiting bodies structures of myxomycetes. Journal of Bacteriology & Mycology, 7(6), 144-148.

Sevindik, M., Baba, H., Bal, C., Colak, O., & Akgul, H. (2018). Antioxidant, oxidant and antimicrobial capacities of Physarum album (Bull.) Chevall. JBMOA, 6(6), 317-320.

Stephenson SL and Rojas C (2017). Myxomycetes: Biology, Systematics, Biogeography and Ecology. London, Academic Press. p. 299-332.

Stephenson SL and Stempen H (1994). Myxomycetes: A Handbook of Slime Molds. Portland, USA: Tımber Press.

Thind KS (1977). The Myxomycetes of India, New Delhi: I.C.A.R.

Yağız D and Afyon A, 2007b. The ecology and chorology of myxomycetes in Turkey. Checklist to Mycotaxon, 101: 279–282.

Zümre, M., Baba H, & Sevindik, M. (2019). Investigation of myxomycetes in Selcen Mountain (Turkey) and its close environs. Eurasian Journal of Forest Science, 7(3), 284-292.

BÖLÜM 10

CHAPTER 10

PROBABILITY OF RUIN: A SIMULATION STUDY ON DIFFERENT RUIN SCENARIOS

Demet SEZER[1], Fahreddin KALKAN[2], İsmail Hakkı KINALIOĞLU[3], İsmail KINACI[4]

1 Asst. Prof. Dr., Department of Actuarial Sciences, Faculty of Science, Selcuk University, Konya, Türkiye. ORCID ID: 0000-0002-0680-948X
2 Res. Asst., Department of Actuarial Sciences, Faculty of Science, Selcuk University, Konya, Türkiye.ORCID ID: 0000-0002-1175-5359
3 Asst. Prof. Dr., Department of Actuarial Sciences, Faculty of Science, Selcuk University, Konya, Türkiye. ORCID ID: 0000-0001-7445-3510
4 Prof. Dr., Department of Actuarial Sciences, Faculty of Science, Selcuk University, Konya, Türkiye.ORCID ID: 0000-0002-0992-4133

1. INTRODUCTION

The probability of ruin is a value that insurance companies wonder about, and it is also very meaningful in determining premium strategies. Of course, for the ruin probability to be meaningful, the claim frequency and size must be modeled correctly, which are components of the risk process. While discrete distributions are used for claim frequency, continuous distributions are generally used for claim size, but discrete distributions can also be used. The reason for using discrete distribution instead of continuous distribution for claim size is the difficulty of obtaining the aggregate claim size distribution.

2. CLAIM SIZE DISTRIBUTIONS

In actuarial studies, probability distributions are often used when evaluating the probabilities of future events. These distributions are used to describe the probability of a particular event and the extent of risk. Some important distributions for claim size in insurance are Pareto, lognormal and Weibull distributions. These distributions are frequently preferred for modeling claim size due to their flexibility and long tail characteristics. While flexibility provides the ability to model loss sizes with different characteristics, long tailing enables insurance companies to determine a cautious premium policy against the risks that will arise. Here, some distributional properties are mentioned about them.

2.1. Lognormal Distribution

The lognormal distribution is a probability distribution that is frequently used in many actuarial areas such as cost projections, premium estimations, and modeling of investment returns. The lognormal distribution is useful for modeling values greater than zero. Lognormal distribution is frequently used especially in financial markets and insurance premium estimations. The lognormal distribution represents situations where the natural logarithm of a variable is normally distributed. Thanks to this feature, it allows the use of statistical methods based on normal distribution. The lognormal distribution does not have a symmetrical structure like the normal distribution. This reflects the fact that most financial data sets are unsymmetrical and skewed to the right. It is important to consider this unsymmetrical structure in actuarial analysis. These features of the lognormal distribution make it easy to assess risk and uncertainty in actuarial analysis and to predict the probabilities of future events. Actuaries can make reliable estimates in many areas such as insurance premiums, risk reserves and future cost projections using the lognormal distribution.

The probability density function, expected value and variance for a

lognormal random variable X with parameters $\mu \in \square$ and $\sigma > 0$ are given respectively in Equations (1)-(3):

$$f\left(x|\mu,\sigma\right) = \frac{1}{\sqrt{2\pi}\sigma x}\exp\left\{-\frac{\left(\log x-\mu\right)^2}{2\sigma^2}\right\},\ x>0 \tag{1}$$

$$E\left(X\right) = \exp\left\{\mu+\frac{\sigma^2}{2}\right\} \tag{2}$$

$$V\left(X\right) = \exp\left\{2\mu+\sigma^2\right\}\left(\exp\left\{\sigma^2\right\}-1\right) \tag{3}$$

2.2. Pareto Distribution

The Pareto distribution, like the lognormal distribution, is a frequently used probability distribution in the actuarial field. The importance of the Pareto distribution can be explained in the following ways: The Pareto distribution is useful for modeling extreme events. It is important to analyze risks that are rare in actuarial studies but have major implications. For example, the Pareto distribution can be used to understand the effects of a major natural disaster on insurance companies. The Pareto distribution has a long-tailed distribution structure. This indicates that there are rare events queuing towards higher values. In actuarial analysis, such extreme events and tail risk are important considerations in calculating risk reserves, determining insurance premiums, and capital adequacy analysis. The Pareto distribution is used when modeling rare values with large effects. For example, the Pareto distribution may be a suitable choice when modeling the wealth distribution or the costs of major accidents. In actuarial studies, it is important to estimate the parameter values that best fit the data and to analyze using an appropriate Pareto distribution. The probability density function, expected value and variance for a Pareto random variable X with parameters $\alpha > 0$ and $\beta > 0$ are respectively given in Equations (4)-(6):

$$f\left(x|\alpha,\beta\right) = \frac{\alpha\beta^{\alpha}}{\left(\beta+x\right)^{\alpha+1}},\ x>0 \tag{4}$$

$$E\left(X\right) = \frac{\beta}{\alpha-1},\ \alpha>1 \tag{5}$$

$$V\left(X\right) = \frac{\alpha\beta^2}{\left(\alpha-1\right)^2\left(\alpha-2\right)},\ \alpha>2 \tag{6}$$

2.3. Weibull Distribution

In the actuarial field, the Weibull distribution plays an important role in the risk assessment and risk analysis processes. In many actuarial applications, the Weibull distribution is used to provide information about the time it takes for an expected event to occur or the probability of a particular event. It is an important tool in risk management processes and affects issues such as insurance premium determination, reserve estimates and capital adequacy analyses. The Weibull distribution can also be used in life analysis and in the creation of life tables. The probability density function, expected value and variance for a Weibull random variable X with parameters $k > 0$ and $\theta > 0$ are respectively as in Equations (7)-(9):

$$f\left(x|k,\theta\right) = \frac{k}{\theta}\left(\frac{x}{\theta}\right)^{k-1} \exp\left\{-\left(\frac{x}{\theta}\right)^{k}\right\},\ x > 0 \tag{7}$$

$$E\left(X\right) = \theta\Gamma\left(1+\frac{1}{k}\right) \tag{8}$$

$$V\left(X\right) = \theta^{2}\left[\Gamma\left(1+\frac{2}{k}\right) - \Gamma^{2}\left(1+\frac{1}{k}\right)\right] \tag{9}$$

3. INSURANCE RISK and RUIN

Insurance risk and ruin are important concepts in the insurance industry. Insurance risk refers to the risk undertaken by insurance companies. Insurance companies assume a certain risk in exchange for premiums paid by policyholders. This risk refers to the amount that the insurance company must pay in case of events covered by insurance policies. Insurance risk includes the financial consequences of unexpected events such as natural disasters, accidents, health problems. Insurance companies correctly determine premiums for risk management and resort to methods such as reinsurance when necessary. Ruin means that a company is unable to meet its financial obligations. Insurance companies may also face the risk of ruin. Ruin of insurance companies can cause significant financial problems for policyholders and other interested parties. In case of ruin, the insurance company cannot pay the indemnities specified in the contracts to the policy holders and the coverage of the insured risks is disrupted. In this case, insurance regulators and other relevant organizations take various measures to ensure the protection of policyholders in the event of ruin.

Factors such as risk management, capital adequacy, reserve estimates,

reinsurance are very important in minimizing the risk of ruin of insurance companies and protecting policyholders. Insurance companies analyze risks, monitor their financial soundness and aim to reduce the risk of ruin by taking appropriate action. In addition, insurance regulatory authorities evaluate the financial soundness of insurance companies and make the necessary regulations.

The first general ideas and mathematical conslusions about the probability of ruin were presented by Lundberg (1903, 1926) and Cramer (1930). Risk (or ruin, or surplus) process in insurance is defined as in Equation (10):

$$U_t = u + c\,t - \sum_{i=1}^{N_t} X_i,\ t > 0 \tag{10}$$

where, $t \in N$ denotes the periods, N_t is the number of claims until time t, X_i is the ith claim size, c is premium rate or obtained premium for a unit time period and u is the initial capital or capital at time $t = 0$ (for more details, see: Dickson (1996), Mikosch (2009), Sundt (1993), Tse (2009)).

The random variables defined as in Equations (11)-(14),

$$T_1 = \inf\left\{t : U_t < 0,\ t \le t_0\right\} \tag{11}$$

$$T_2 = \inf\left\{t : U_{t-m+1}, U_{t-m+2}, \ldots, U_t < 0,\ t \le t_0\right\} \tag{12}$$

$$T_3 = \inf\left\{t : \sum_{i=1}^{t} I_{(-\infty,0)}\left(U_i\right) \ge m,\ t \le t_0\right\} \tag{13}$$

$$T_4 = \inf\left\{t : \sum_{i=(t-\delta)+1}^{t} I_{(-\infty,0)}\left(U_i\right) \ge 2,\ t \le t_0\right\} \tag{14}$$

denote the ruin times for four ruin scenarios when the initial surplus is u. At the first scenario, the ruin occurs at the first negative surplus, at the second scenario, the ruin occurs at the m th consequtive negative surplus, at the third scenario, the ruin occurs at the m th negative surplus, at the last scenario, the ruin occurs when the period between two consequtive negative surplus is less than $\delta \in$ □. Then the finite time ruin probability for any scenario can be expressed in terms of T_i, $i = 1, 2, 3, 4$ as in Equation (15),

$$\psi\left(u,t_0\right)=P\left(T_i<t_0\right). \tag{15}$$

Calculating the probability of ruin of insurance companies can be difficult because the insurance industry is complex and many variables interact. Factors such as uncertainties, long- term liabilities, reinsurance effect, financial market conditions, regulation and auditing make the calculation of the ruin probability a complex process. In addition, the probability of ruin based on the ruin process given in Equation (10) cannot be obtained analytically, depending on the distributions of random variables N_t and X.

4. SIMULATIONS FOR RUIN PROBABILITY

In this study, simulation study is performed to investigate how effect ruin scenarios to ruin probability. We consider two mean claim sizes (mcs) such as 5 and 10, three distributions such as Pareto, Lognormal and Weibull as claim size distribution and homogeneous Poisson process as claim count process. The Monte Carlo simulation results for four different ruin scenarios are presented via plots given in Figures (1)-(12). In simulations, the parameters β,α and θ in the claim size distributions Pareto $(\alpha=4,\beta)$, lognormal $(\mu=1,\sigma)$ and Weibull $(k=0.7,\theta)$ are chosen to be 5 and 10 on mean. Expected premium principle with loading factor $g=0,0.1,0.2$ is used to determine $c=\left(1+g\right)\left(mcs\right)\lambda$ for the risk process in Equation (10).

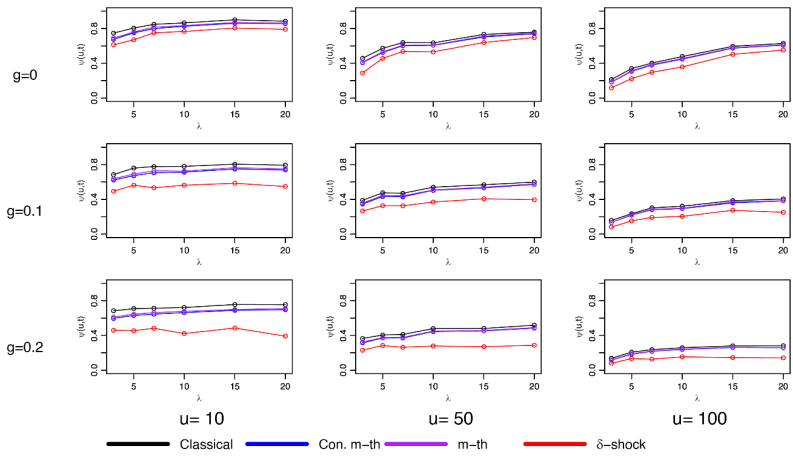

Figure 1. *Ruin probabilities according to* λ *for Pareto distribution with mean 5*

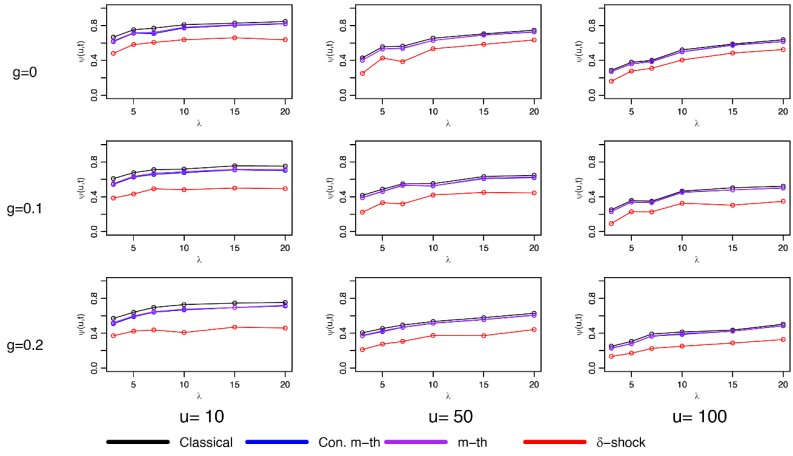

Figure 2. *Ruin probabilities according to* λ *for lognormal distribution with mean 5*

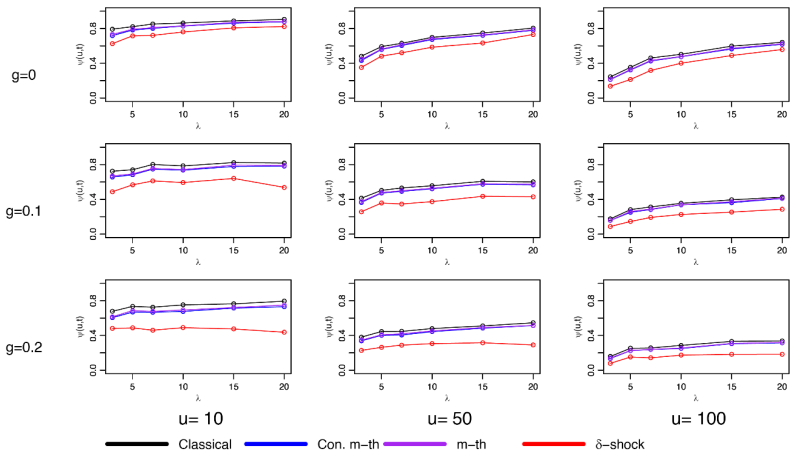

Figure 3. *Ruin probabilities according to* λ *for Weibull distribution with mean 5*

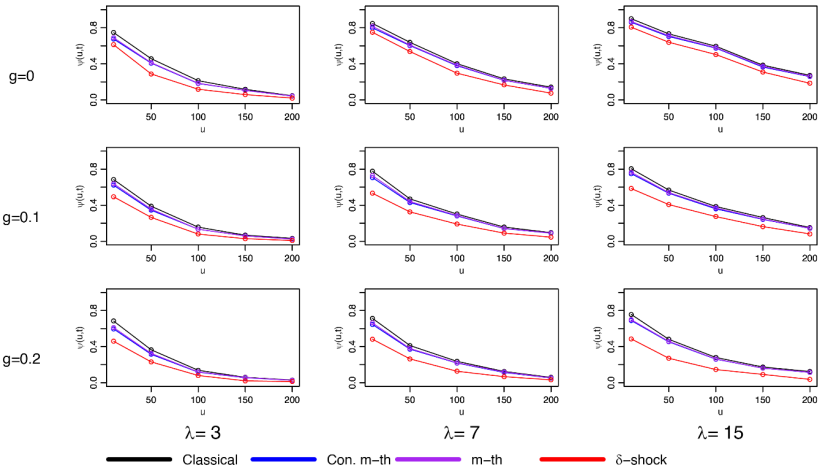

Figure 4. *Ruin probabilities according to* u *for Pareto distribution with mean 5*

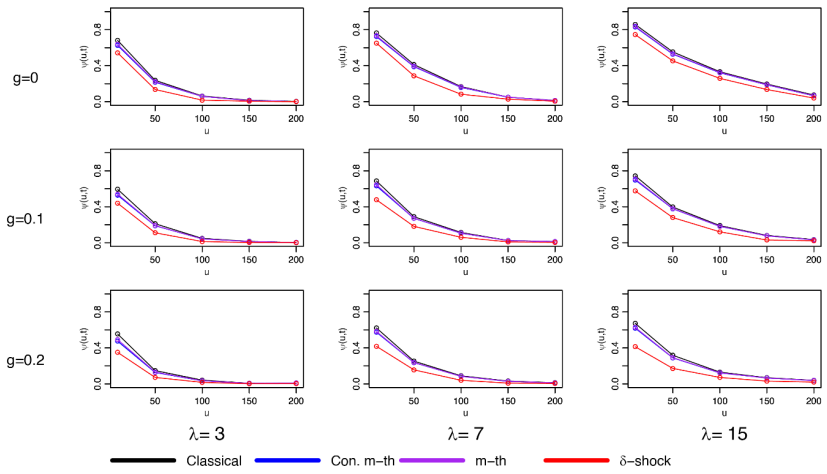

Figure 5. *Ruin probabilities according to* u *for lognormal distribution with mean 5*

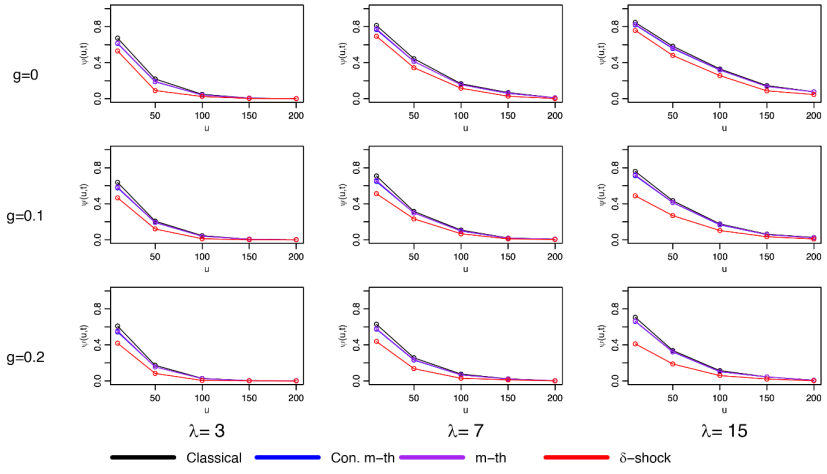

Figure 6. *Ruin probabilities according to* u *for Weibull distribution with mean 5*

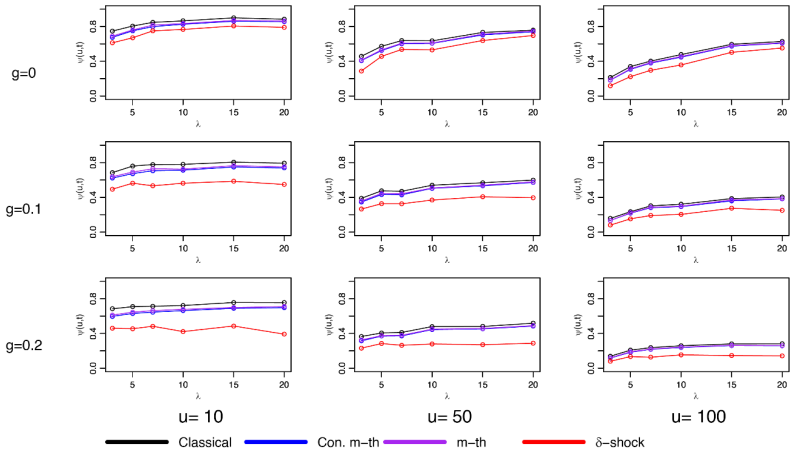

Figure 7. *Ruin probabilities according to* λ *for Pareto distribution with mean 10*

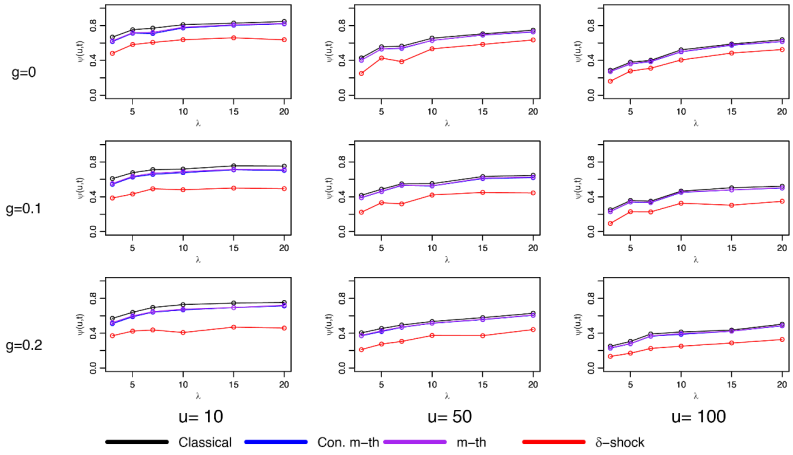

Figure 8. *Ruin probabilities according to* λ *for lognormal distribution with mean 10*

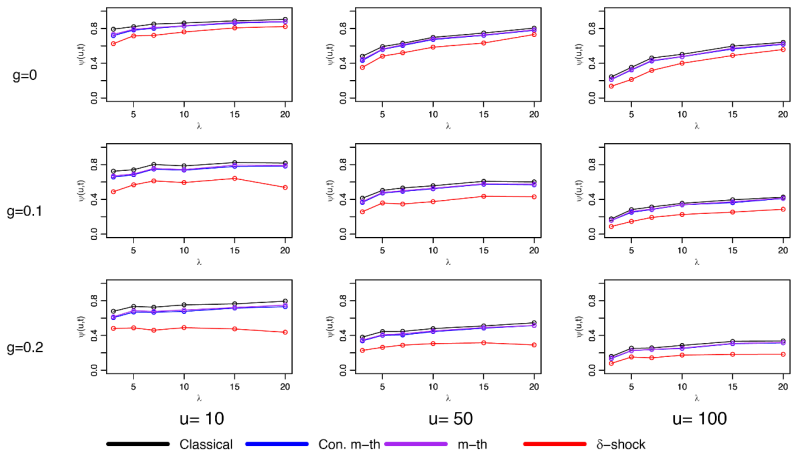

Figure 9. *Ruin probabilities according to* λ *for Weibull distribution with mean 10*

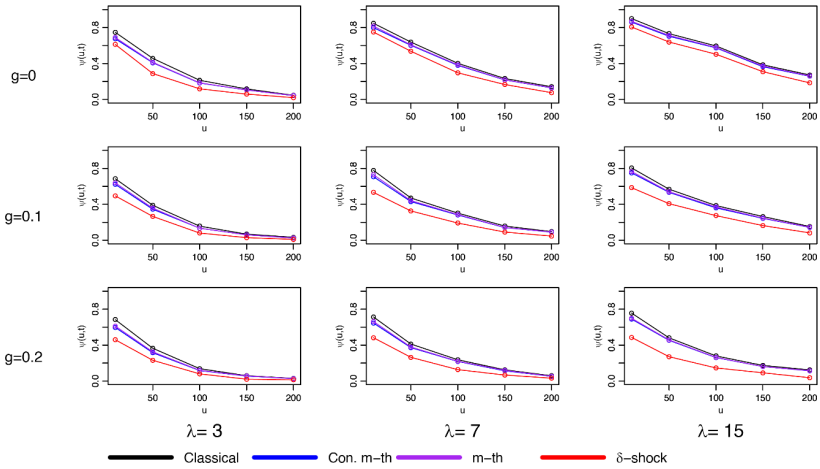

Figure 10. *Ruin probabilities according to* u *for Pareto distribution with mean 10*

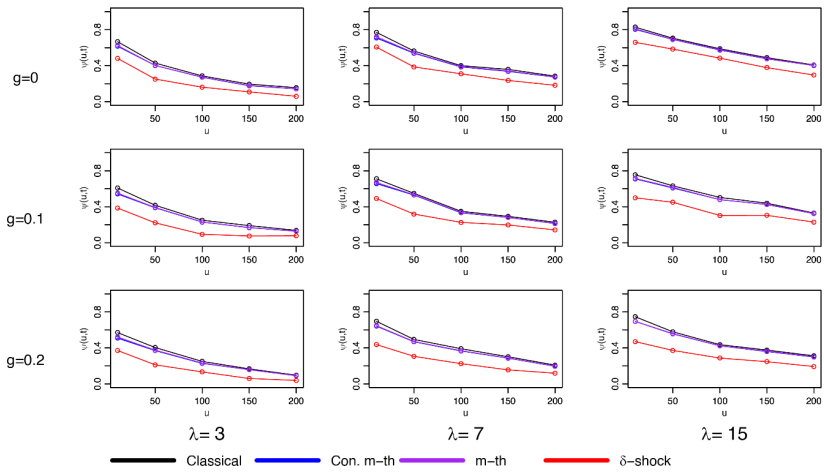

Figure 11. *Ruin probabilities according to* u *for lognormal distribution with mean 10*

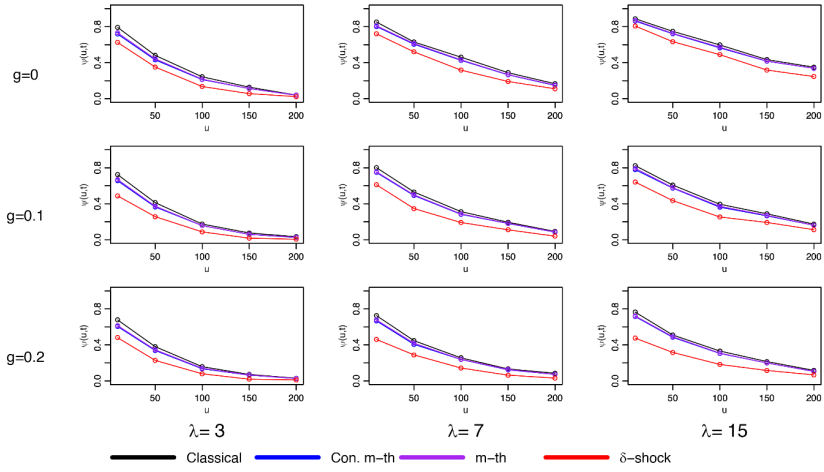

Figure 12. *Ruin probabilities according to* u *for Weibull distribution with mean 10*

5. CONCLUSION

One can see from the plots above for Pareto, lognormal and Weibull distributions that:

• when the premium loading increases from 0 to 0.2, the ruin probabilities are slightly but not much reduce.

• the minimum ruin probability is belong to ruin scenario based on

$\delta - shock$ with $\delta = 3$.

• when the parameter λ in Poisson claim count process increases, the ruin probabilities slightly but not much increase.

• when the initial capital u increases, the ruin probabilities reduce.

REFERENCES

1) Cramer, H. (1930), On the Mathematical Theory of Risk. Skandia Jubilee Volume, Stockholm.

2) Dickson, D. C. M. (1996), Insurance Risk and Ruin, Second Edition, Cambridge University Press.

3) Lundberg, F. (1903), I Approximerad Framstdllning av Sannolikhetsfunktionen. II Aterforsdkring av Kollektivrisker . Almqvist & Wiksell, Uppsala.

4) Lundberg, F. (1926), Forsdkringsteknisk Riskutjdmning. F. Englunds Boktryckeri AB, Stockholm.

5) Mikosch, T. (2009), Non-life Insurance Mathematics: An introduction with the Poisson process, Second Edition, Springer.

6) Sundt, B. (1993), An Introduction to Non-life Insurance Mathematics, VVW.

7) Tse Y. K. (2009), Nonlife Actuarial Models: Theory, Methods and Evaluation. International

Series on Actuarial Science, 1st edition. Cambridge University Press.

BÖLÜM 11

CHAPTER 11

A STUDY OF THE GENUS OLIGONEMA ROSTAF. (TRICHIALES, MYXOMYCETES) IN TURKEY

Hayri BABA[1], Hasan AKGÜL[2]

1 Department of Biology, Faculty of Science and Art, Hatay Mustafa Kemal University, Hatay 31060, Turkey. hayribaba_68@hotmail.com
2 Department of Biology, Faculty of Science, Akdeniz University, Antalya 07058, Turkey.

Introduction

Myxomycetes are known as true slime molds, plasmodial slime molds or Myxogastrea. Myxomycetes are multinuclear single-celled organisms that can produce one or more spores (Stephenson & Stempen, 1994). Myxogastrea species are abundant in cool, moist and shaded areas such as rotten tree trunks, branches, alive or dead bark, decayed fruit or fruit scraps, decayed leaves and leaf debris. Myxomycetes live in the environment by feeding on other microorganisms (bacteria, yeasts, fungus hyphae, blue-green bacteria and green algae) (Farr, 1981; Baba and Sevindik, 2018). Myxogastrea fruitbodies could develop spontaneously in the nature. Furthermore, especially after identification with the moist chamber technique, they could be detected especially on plant surfaces (Härkönen & Ukkola, 2000). The number of known Myxomycetes species is 1088 taxa globally (Lado, 2023). 309 taxa were identified in Turkey (Sevindik et al., 2018; Baba and Sevindik, 2019; Baba and Atay, 2019; Baba et al., 2019; Sevindik and Akgul, 2019; Baba and Sevindik, 2020a; Baba et al., 2020a; Baba et al., 2020b; Baba, 2021; Baba and Sevindik, 2021; Baba et al., 2021a; Baba et al., 2021b; Baba et al., 2021c; Baba and Sevindik, 2022a, Baba and Sevindik, 2022b, Baysal and Eroğlu, 2022; Eroğlu, 2021; Ocak and Konuk, 2018; Sesli et al., 2020).

In Trichiales order; Stipitate or sessile sporophores, greater than 500 μm in total height, with ornate capillitium and without columella. Peridium persistent, at least at the base of the sporotheca. Capillitium generally ornamented with warts, spines, teeth, semi-rings, rings or spirals. Trichiaceae family has tubular capillitium, ornamented with spiral bands, elateriform. Oligonema genus has tubuler capillitium with well-defined spiral bands (with very vague bands, almost smooth tubules, and with warts or rings in.

The genus Oligonema was published in 1875 by Rostafinski. It belongs to the family Trichiaceae of the Order Trichiales. Rostafinski distinguished the new taxon from the Trichia and Perichaena genera by the differences in capillitium ornamentation, as well as peridium and sporocarp characteristics. Recently, based on the analyses of two genes (SSU rRNA, elongation factor 1-alpha), Fiore-Donno et al. (2013) proposed that members of this taxon such as *O. schweinitzii* may in fact be aberrant forms of Trichia and suggested further studies to clarify their distinction at the genus level (Cavalcanti et al., 2015). Capillitial tubules simple or little branched, not matted, sometimes smooth or with warts or rings between the whorls. According to the literature only 11 species are recognized all over the World (Lado, 2023), *Oligonema affine* (de Bary) García-Cunch., J.C. Zamora & Lado, *O. aurantium* Nann.-Bremek., *O. dancoii* Aramb. & Spinedi, *O. favogineum* (Batsch) García-Cunch., J.C. Zamora & Lado, *O. flavidum* (Peck) Peck, *O. fulvum* Morgan, *O. intermedium* Haan, *O. oe-*

donema Yu Li, Shuang L. Chen & H.Z. Li, *O. persimile* (P. Karst.) García-Cunch., J.C. Zamora & Lado, *O. schweinitzii* (Berk.) G.W. Martin, *O. verrucosum* (Berk.) García-Cunch., J.C. Zamora & Lado. 6 species of them are recorded in Turkey, *Oligonema affine, O. favogineum, O flavidum, O. persimile, O schweinitzii* and *O. verrucosum*.

Material and methods

Detailed information on Oligonema species that were not collected by us were taken from the articles of the researchers (Härkönen, 1988; Ergül and Dülger, 2000d; Ergül and Dülger, 2002c; Ocak and Hasnekoğlu 2003b; Ergül et al., 2005a; Ocak and Hasenekoğlu, 2005; Yağız and Afyon, 2005; Oran et al., 2006; Ergül and Akgül, 2011; Eroğlu and Kaşık, 2013a; Ocak, 2015). Species obtained by Baba and his friends were collected from the natural environment or obtained in the laboratory using by moist chamber technique (Baba and Tamer, 2008a; Baba et al., 2013; Baba et al., 2015; Baba et al., 2016; Baba and Arslan, 2017b; Baba and Doğan, 2018; Baba et al., 2018; Zümre et al., 2019).

Natural myxomycete samples were collected from natural area. On different substrates, cortex, woods, barks, leaf, debris, organic plants and animal material samples were transported to the laboratory in small carton boxes. Furthermore, after the field studies, myxomycete fructifications were obtained from the moist chamber culture in laboratory. For moist chamber culture; live or dead plant materials (forest floor litter, aerial litter, wood and bark from living or dead trees) were obtained at a number of localities. Moist chambers cultures consisted of disposable plastic petri dishes lined with filter paper. The sample material in each dish was moistened with distilled water. After a period of approximately 24 -48 hours (in summer 48 hours, in winter 24 hours), excess water in each dish was removed. Cultures were kept at room temperature (24ºC) in diffuse daylight (Baba et al., 2021b). Examined with a stereomicroscope on a regular basis for a period of up to two months in order to detect plasmodia or fruiting bodies. When necessary, a small amount of water was added to each culture to maintain moist conditions. The moist chamber with the developing myxomycete samples was allowed to dry and the myxomycetes were dried for one week. Myxomycete plasmodia or fruiting bodies were noted and recorded. Each time the cultures were checked. All fruiting bodies were removed. Air-dried and glued in small pasteboard boxes for permanent storage. The samples were photographed and identified.

The samples were identified under stereomicroscope and light microscopy. General structure, plasmodium type, fructification type, shape, colour, macroscopic measurements, the presence or absence of lime or the color and shape of the samples were examined with the stereomicroscope.

In light microscopy, the capillitium, spore, shape, color, size, ornamentation, branching shape, features was observed. Capillitium, pseudo-capillitium and columella or pseudo-columella, capillitium formation, shape and size, condition of columella (free or attached) were examined with light microscopy. Furthermore, the shape, color, size and ornamentation of the spores were examined. For every species recognized, the most typical specimens were used for providing descriptions. Species descriptions were used to define the genus and to provide a dichotomous key to the species. Spore colors were obtained in 10% NH3 solution (de Haan et al., 2004). The myxomycete samples were identified based on a variety of digital and printed sources (Nomen.eumycetozoa.com; Martin and Alexopoulos, 1969; Farr, 1976; 1981; Thind, 1977; Martin et al., 1983; Stephenson and Stempen, 1994; Ing, 1994; Neubert et al., 1995; 2000; Alexopoulos et al., 1996; Lado and Pando, 1997; de Haan et al., 2004; Stephenson and Rojas, 2017). Samples were arranged as fungarium material and kept in the Biology Department's laboratory of Hatay Mustafa Kemal University Hatay-Turkey. The list below includes the recorded myxomycetes, arranged alphabetically, taxonomic treatment includes a key to species, generic and specific descriptions, photos, habitat data and comments.

Results and discussion

Eukaryota

Protista

Mycetozoa

Myxomycetes

Trichiida

Trichiaceae

Genus Oligonema Rostaf. Sluzowce monogr. 291 (1875);

Description; Fructification: sporangiate, the sporangia densely crowded, scattered or in close clusters. They tend to develop in loose to dense colonies, sometimes in combination with some solitary sporocarps. The colour is always yellow to orange with or without green to brown hues. Sporotheca: subglobose, more or less irregular, sessile or stipitate, never with cell-like bodies in the stalk. Peridium: sometimes single or double, with granular outermost layer, membranous internal layer, infrequently simple, membranous, bright, with irregular dehiscence. The peridium is a yellowish, smooth and shining, the wall thin, transparent membranous, sometimes iridescent and often with small warts or papillae on the inner side. Capillitium: of short or long, simple or branched yellow elaters, nearly smooth or obscurely sculptured with spirals and sometimes with spines,

papillae, warts or rings or faint spiral bands. These spirals are never as well developed and regular as in many species of the genus Trichia Haller. Capillitium is elastic; hollow filaments, simple or branched, smooth or slightly wrinkled. The elaters can have one branch, their extremities are mostly round, blunt and clavate, with one or two spines, sometimes with a ring-shaped enlargement at the base of the apex. Spore mass are viewed in yellow, orange or reddish-brown, yellow by transmitted light. The spores are yellow to orange, their shape is globose or subglobose, globose to irregularly elliptical; they are ornamented with warts or a reticulate. verrucose, spiny or with reticulate bands that are sometimes incomplete.

Comments: The species of the genus Oligonema seem to have the same preferences as to their habitat. They are found in very moist environments. Most collections were made in the summer and autumn. The species of this genus are usually very easy to distinguish from the other species in the family Trichiaceae (Order Trichiales). Their mostly smaller fructifications are sessile sporocarps and in some cases short plasmodiocarps, grouped to overlapping in dense groups, occasionally scattered (de Haan et al., 2004).

Distribution: 11 species are recognized all over the world, *Oligonema affine*, *O. aurantium O. dancoii*, *O. favogineum*, *O. flavidum*, *O. fulvum*, *O. intermedium*, *O. oedonema*, O. persimile, O. schweinitzii *O. verrucosum*.

Turkey: 6 species of them are recorded in Turkey, *Oligonema affine, O. favogineum, O flavidum, O. persimile, O schweinitzii* and *O. verrucosum*.

Key to the species of Oligonema Rost. in Turkey

1. Sporophore sessile ……..….. 2

1. Sporophore stalked, Stalk longitudinally grooved, 0.8–1.2 mm yellow, reddish brown Elaters with short tapered ends. Spores coarsely reticulate, bands of reticulation pitted, 12-16 µm diam ……..***O verrucosum***

2. Elaters has clearly visible spiral bands ….....…… 3

2. Elaters almost invisible spirals, ….…….....….***0. schweinitzii***

3. Sporocarps subglobose, globose, obovoid…….…… 4

3. Sporocarps higher than wide, clustered in one layer, in close groups but not superimposed, 0.2 - 0.5 mm wide and 0.4 - 1.0 mm high..... .....***O. flavidum***

4. Spores with a wide-meshed net-ornamentation, the meshes themselves formed by rows of fine meshes, ……..……
…….....…...……5

4. Spores net-ornamentation mostly rather complete, ocasionally with meshes formed from simple ridges bright yellow. Elaters with smooth sparal bands or with only few small spines……
.....……..……..……..***O. affine***

5. Sporocarps ± spherical. Elaters 4-6 µm bro
ad…….....…….....……6

5. Sporocarps higher than wide. Elaters 6-8 µm broad, smooth. Spores coarsely reticulate, bands of reticulation pitted, 12-15 µm diam …….. ***O. favogineum***

6**.** Elaters with spinulose spiral bands. Spores ochraceous, net-ornamentation often irregular, occasionally with broad groups of small meshes Spore-bands pitted .....***O. persimile***

Description and other information about the Oligonema species detected in Turkey is given below in alphabetical order;

1. Oligonema affine (de Bary) García-Cunch., J.C.Zamora & Lado, in García-Cunchillos, Zamora, Ryberg & Lado, Mol. Phylogenet. Evol. 177:107609, 15 (2022).

Synonyms: *Trichia affinis* de Bary

Hemitrichia helvetica Meyl.

Description; Sporophores: obovoid to oblong, subglobose to globose sessile, rarely short plasmodiocarp. Plasmodiocarps, crowded on a common hypothallus, 0.8-1 mm diam in height, 0.4-0.5 mm in diameter, shining lemon-yellow to golden-yellow (Figure 1). Hypothallus: confluent, membranous. Peridium: thin, membranous, shining, marked with irregular stripes, brittle, persistent at the base and with irregular dehiscence. Capillitium: of golden-yellow or lemon-yellow elaters, elastic tubular elaters, 4-6 µm diam., marked with 4-5 spiral bands, most of them broken and revealing the abundant bright yellow capillitium usually spinulose, rarely smooth, sometimes with longitudinal striae, with short, pointed free ends of 5–10 µm in length. Spore mass: lemon-yellow. Spores: very pale yellow, 11-15 µm diam, ornamented with a broad, irregular and sometimes fragmented reticulum, coarsely banded-reticulate with 3-5 meshes to the hemisphere. The broad bands are up to 1 µm in height, which themselves are formed by a reticulum with numerous little holes. Plasmodium: white.

Comments: This species is characterized by sessile yellowish sporocarps. The capillitium is composed of narrow elaters. Spore ornamentation

has a net of variable morphology. The reticulum consists of wide discontinuous bands which form a broken mesh. The bands also are composed of a reticulum with smaller meshes. The diameter of the capillitium is a good character to separate *O. favogineum* (8–10 µm diam.) from *O. affine* and *O. persimile* (4–6 µm diam.). Without this additional diagnostic character the separation of these latter two species can be difficult. For *O. affine*, the presence of a capillitium with smooth or with small spines, spiral bands and spores with a broken reticulum is characteristic, while for *O. persimile*, the presence of a capillitium with spiny spiral bands, and spores with a reticulum in the form of islets or patches of reticulum are typical. Also *O. affine* differs from *O. favogineum* in that the latter does not have globose sporocarps, they are cylindrical and the spores are larger (13–15 µm diam. (Moreno et al., 2022).

Distribution: Argentina, Australia, Chile, Cuba, Ecuador, New Zealand.

Turkey: Ergül and Dülger, 2002c; Ergül et al., 2005a; Oran et al., 2006.

Figüre 1. Oligonema affine opened sporocarps

2. O. favogineum (Batsch) García-Cunch., J.C.Zamora & Lado, in García-Cunchillos, Zamora, Ryberg & Lado, Mol. Phylogenet. Evol. 177:107609, 15 (2022).

Synonyms: *Lycoperdon favogineum* Batsch,

Stemonitis favoginea (Batsch) J.F. Gmel.,

Trichia favoginea (Batsch) Pers.,

Sphaerocarpus chrysospermus Bull.,

Trichia chrysosperma (Bull.) Lam. & DC.,

Trichia jackii Rostaf.,

Trichia affinis var. *jackii* (Rostaf.) L.F. Celak.,

Trichia abrupta Cooke,

Hemitrichia persimilis var. *abrupta* (Cooke) Torrend,

Trichia proximella P. Karst.,

Trichia balfourii Massee,

Trichia sulphurea Massee,

Trichia intermedia Massee,

Hemitrichia persimilis var. *intermedia* (Massee) Torrend,

Trichia kalbreyeri Massee,

Trichia pulchella Rex,

Trichia drakei Lodhi,

Description: Sporocarps sessile, clustered, taller than wide, yellow, smooth and shining up to 2 mm tall, 0.6-0.7 mm wide crowded on a well-developed hypothallus (Figure 2). Hypothallus membranous, colourless, marked with vein-like brown deposits. Peridium membranous, thin, transparent, opening irregularly above ochraceous to olivaceous brown, shining, dehiscence mostly by rupturing of the peridium, the inside marked with irregular stripes. Capillitium golden yellow, escaping entirely from the peridia and forming woolly masses above them, 6-8 µm diam., with 4-5 spiral bands separated by longitudinal striae, normally smooth but sometimes with occasional spines, the tips short-tapered and ending in a smooth point. Spore-mass ochraceous, yellow. Spores pale yellow, 13-15 µm diam., with a coarse reticulation of tall bands, 3-5 meshes to the hemisphere, bordered in optical section to 2 µm high. Plasmodium white, yellow.

Comments: The diameter of the capillitium is a good character to separate *O. favogineum* (8–10 µm diam.) from *O. affine* and *O. persimile* (4–6 µm diam.). Without this additional diagnostic character the separation of these latter two species can be difficult. For *O. affine*, the presence of a capillitium with smooth or with small spines, spiral bands and spores with a broken reticulum is characteristic, while for *O. persimile*, the presence of a capillitium with spiny spiral bands and spores with a reticulum in the

form of islets or patches of reticulum are typical. Also *O. affine* differs from *O. favogineum* in that the latter does not have globose sporocarps, they are cylindrical and the spores are larger (13–15 µm diam.) (Moreno et al., 2022). This is a common species occurring mostly in autumn in Europe, but occasionally it can also be found close to melting snow in spring. In Spain, the species is more frequent in the North (Lado & Pando 1997).

Distribution: China, Costa Rica, Cuba, Europe, Japan, New Zealand, Spain, Taiwan.

Turkey: Härkönen, 1988; Ergül and Dülger, 2000d; Ergül et al., 2005a; Ocak and Hasenekoğlu, 2005; Yağız and Afyon, 2005; Baba and Tamer, 2008a; Ergül and Akgül, 2011; Baba et al., 2016; Baba and Doğan, 2018.

Figüre 2. O. favogineum sporocarp, capillitium and spores

3. O. flavidum (Peck) Peck, Annual Rep. New York State Mus. 31:42 (1878)

Synonyms: *Perichaena flavida* Peck,

Oligonema brevifilum Peck,

Oligonema flavidum var. *brevifilum* (Peck) Torrend,

Oligonema minutulum Massee,

Description: Sporocarps sessile, clustered in one layer, rarely loosly heaped, ovoid to cylindrical, subglobose when isolated, densely clustered, becoming obpyriform or subcylindric when massed, higher than wide, 0.2 - 0.5 mm wide and 0.4 - 1.0 mm high, yellow to orange, bright yellow, later on with ochre to brown hue. Peridium single, membranous, smooth to somewhat wrinkled, shining, rarely dull; yellow, transparent, with few wrinkles, inner side densely covered with small warts, some forming rows giving the whole a marble-like aspect; and with few scattered, larger

warts. Hypothallus inconspicuous, colourless, glossy, transparent, membranous. Capillitium usually sparse, of short to moderately long elaters, 10-300 µm long and 3-5 µm diam. in thickness, irregular, swollen in places and occasionally branched, sculpured with minute warts arranged in indistinct spirals, the apices generally blunt, sometimes ending in one or more points. The threads are longer than in any other species, and not infrequently branched, smooth, or more commonly, very distinctly minutely spinulose throughout, no trace of rings or relief sculpture of any sort, the spirals, that are to be expected, very imperfect, if discernible at all. With light microscope covered with small warts and papillae, in some places arranged in rows which tend to look like weak spirals, with SEM irregular fingerlike papillae; round, blunt, clavate apex, sometimes rostrate, with few branches and swellings in some places, thin warts or faint spirals on the surface and rounded ends. Spore-mass yellow dark ochraceous, Spores pale yellow, irregularly globose to ellipsoid, (10 -) 13-15 (- 16) µm diam., with a coarse-meshed, often irregular but usually complete reticulum of narrow pitted bands, ornamentation 0.5 - 2 µm high; irregular reticulum, sometimes incomplete, the walls of the larger meshes consist of very small meshes; usually with complete reticulum, (3) 4–5 (6) meshes per hemisphere, often irregular, with border of 1–1.5 µm thickness and some meshes are observed with faint reticulation at centre yellow. Plasmodium watery white, later yellow.

Comments: Characteristics such as the often larger sporocarps than in the other species and the typical short cylindrical shape of the sporocarps grouped in an upright position, allow generally easy recognition in the field. On some occasions the sporocarps can be small and rather globose, and they can be confused with other Oligonema species. The microscopical traits are also very typical. For example, the elaters with warts are unique. In some places warts are arranged as if they were spirals, but under immersion their true nature becomes apparent. *Oligonema flavidum* resembles *O. schweinitzii*, differentiated only by the peridium granulation, capillitium ornamentation and the type of spore reticulation. Occurrence time is summer and early autumn. The capillitum, which is scant in the specimen, is covered only with warts along its entire length while in other collections the warts can form thickened bands, in places resembling rings or spirals (de Haan et al., 2004; Salamaga, 2013; Cavalcanti et al., 2015).

Distribution: Africa, Algeria, Argentina, North America and South America, Asia, Brazil, Belgium, Estonia, Europe, Germany, Holland, Hungary, Poland, Ukraine, United States, and India

Turkey: Ocak, 2015.

4. O. persimile (P.Karst.) García-Cunch., J.C.Zamora & Lado, in García-Cunchillos, Zamora, Ryberg & Lado, Mol. Phylogenet. Evol. 177:107609, 15 (2022).

Synonyms: *Trichia persimilis* P. Karst.,

Trichia favoginea var. *persimilis* (P. Karst.) Y. Yamam.,

Description: Sporocarps sessile, clustered, subglobose, globose, obovoid or irregularly spherical,0.5-0.8 mm diam, shining ochraceous to yellow-brown, seated on a common, yellow-brown hypothallus (Figure 3). Hypothallus thin, but usually very distinct. Peridium membranous, shining, the inside marked with rows of warts which are often arranged in lines. Capillitium of ochraceous-yellow elaters, 4-6 µm diam., marked with 4-5 closely-set spiral bands and studded with short spines, longitudinal striae inconspicuous. Spore-mass ochraceous yellow. Spores pale yellow, 11-14 µm diam., marked with a broken banded reticulation of small meshes, the non-reticulate areas covered with large warts, border incomplete in optical section. Plasmodium white.

Comments: The diameter of the capillitium is a good character to separate *O. persimile* (4–6 µm diam.) from *O. favogineum* (8–10 µm diam.) and *O. affine*. Without this additional diagnostic character the separation of these latter two species can be difficult. For *O. affine*, the presence of a capillitium with smooth or with small spines, spiral bands and spores with a broken reticulum is characteristic, while for *O. persimile*, the presence of a capillitium with spiny spiral bands, and spores with a reticulum in the form of islets or patches of reticulum are typical (Moreno et al., 2022).

Distribution: China, Malta, New Zealand.

Turkey: Baba et al., 2015; Baba and Doğan, 2018.

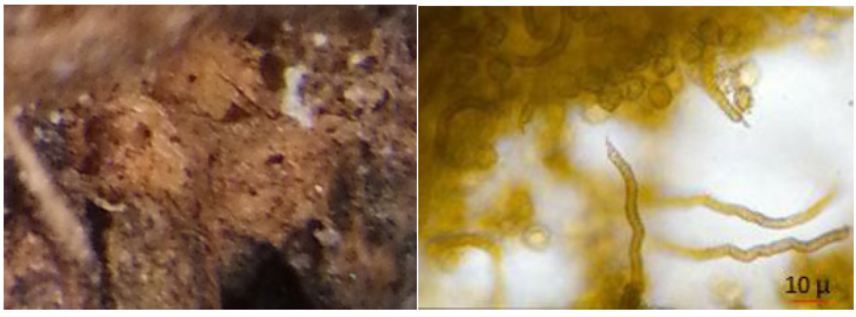

Figüre 3. O. persimile sporocarps, capillitium and spores

5. O. schweinitzii (Berk.) G.W. Martin, Mycologia 39(4):460 (1947)

Synonyms: *Physarum schweinitzii* Berk.,

Trichia nitens Lib.,

Oligonema nitens (Lib.) Rostaf.,

Cornuvia nitens (Lib.) Rostaf

Trichia kickxii Rostaf.,

Trichia bavarica Thüm.,

Oligonema bavaricum (Thüm.) Balf.f. & Berl.,

Trichia pusilla J. Schröt.,

Oligonema nitens var. *anomalum* A. Pouchet,

Description: Sporocarps sessile, mostly tightly clustered, heaped, very irregular in shape and size, spherical, pulvinate, pyramidal to short-vermiculate plasmodiocarpic, often angular with flattened sides, 0.2 - 0.7 mm wide; golden-yellow to yellow-orange, later with ochre to brown hue (Figure 4). Peridium single, membranous, smooth to plicate, internally papillose, shining, sometimes iridescent, rarely dull, with light microscope yellow, transparent, inner side smooth or with minute lines and covered in some places with small warts, thus having a rougher appearence; with few scattered, larger warts; with SEM smooth to minutely wrinkled, in some places covered with irregularly shaped, small warts. Hypothallus inconspicuous, colourless, shining, transparent, membranous. Capillitium not abundant, yellow, mostly of short elaters, 20-100 µm long, 2-6 µm wide, sometimes branched, with narrow rings or vesiculous enlargements; with light microscope ornamented with clearly visible to almost invisible spirals, sometimes with minute warts; with SEM the spirals mostly smooth but sometimes roughened, in some places covered with warts; round, blunt, clavate apex, with one or two spines, also with a ring shaped enlargement at the base of the apex. Spore-mass yellow. Spores yellow, 12-16 µm diam., marked with an incomplete reticulation of large and small meshes, with a wide border in optical section. Spores globose to elliptical, angular; ornamentation 1 - 2 µm high; reticulum irregular, sometimes incomplete, the walls of the large meshes consisting of very small meshes, frequently with a group of smaller meshes in the centre of the large meshes; with SEM the ornamentation in the centre of the large meshes lower, about 0.5 tm; pale yellow. Plasmodium white or yellow.

Comments: The Sporocarps are densely grouped and ornamentation of most elaters is very tenuous, with faint spirals; spores have incomplete reticulation with broad meshes, about 4 by hemisphere. With worldwide

distribution, *O. schweinitzii* is recorded in many countries in Africa, the Americas, Asia, Europe and Australia, especially in the northern hemisphere. Time of occurrence: late summer and autumn, with exceptions. Habitat: rotten wood of broad-leaved trees in almost dried up ponds or marshes, also on mosses and mud (Ndiritu et al. 2009). The sporocarps of *0. intermedium* seem similar to those of *0. schweinitzii*. But the microscopy is different of *0. intermedium*. and *0. schweinitzii*. This species has larger, regularly shaped sporocarps, 0.5 - 1.0 mm high, which are grouped in one layer. The elaters are typical Trichia-like, abundant with regular, very distinct spirals and an always pointed apex (de Haan et al., 2004; Cavalcanti et al., 2015).

Distribution: Argentina, Australia, Brazil, Europe, Mexico, North America, North Africa, Japan, Puerto Rico, Russia.

Turkey: Ocak and Hasnekoğlu 2003b; Baba et al., 2013; Eroğlu and Kaşık, 2013a.

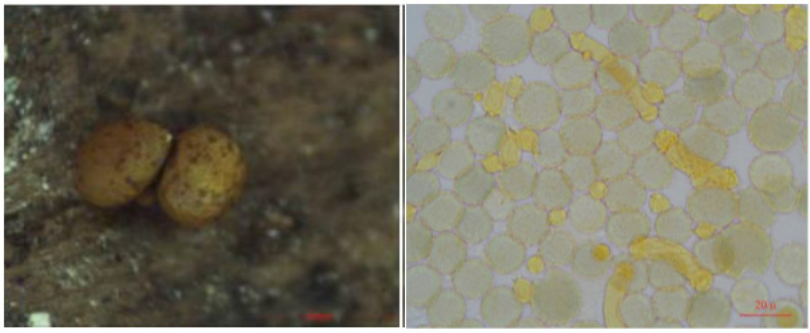

Figüre 4. O. schweinitzii sporocarps, capillitium and spores

6. O. verrucosum (Berk.) García-Cunch., J.C.Zamora & Lado, in García-Cunchillos, Zamora, Ryberg & Lado, Mol. Phylogenet. Evol. 177:107609, 15 (2022).

Synonyms: *Trichia verrucosa* Berk.,

Trichia superba Massee,

Description: Sporocarps aggregated, stalked, usually several sporocarps united by the stalks, 1.6–2.6 mm in total height. rarely sessile. Sporothecae pyriform or obovoid, often clustered on united stalks, bright ochraceous, yellow to orange yellow up to 0.8 mm wide and 4 mm tall (Figure 5). Hypothallus membranous, common to a group of sporocarps, effuse, opaque. Stalk weak, often flattened, simple or consolidated with others, weak, inclined, or procumbent twice the height of the spore-case, longitudinally grooved, 0.8–1.2 mm long, 0.1–0.15 mm wide, yellow, red-

dish brown each bearing 5–9 yellow sporothecae. Peridium pale yellow, membranous, translucent, papillose within, often somewhat thickened by granular deposits, single, partially evanescent, remaining at the basal part as a calyculus, thin, fragile, the inner side papillate, dehiscence irregular. Capillitium of long, cylindric elaters, bearing 3-5 spirals, these smooth or bearing a few scattered spines, with short, tapered tips. elastic network of threads arising from the base of the sporotheca, threads of 5–7 µm in diameter, yellow, flexuous, scarcely branched, with acute free ends of 10–12.5 µm long, ornamented with 4 or 5 spiral bands. Spore-mass pale yellow, ochraceous yellow. Spores free, bright yellow, coarsely and prominently reticulate, the bands narrow, minutely pitted and 1 µm high, 10-14 µm diam, 12-16 µm including the ridges. Plasmodium white.

Comments: The examined specimen is characteristic and agrees well with the concept of the species. Sporocarps of *O. verrucosum* with confluent stalks are very characteristic. Species with similar spore ornamentation are *O. affine* and *O. favogineum* they both are never stalked and generally possess larger spores. Although rather widely distributed in the world, the species does not appear to be frequent. *O. verrucosum* is usually found sporulating on dead wood, particularly of coniferous trees (Adamonyte, 2007).

Distribution: Australia, Austria, Argentina, Brasil, Canary Islands, China, Chile, Costa Rica, Cuba, Dominica, Jamaica, Denmark, France, Germany, Great Britain, Japan, New Zealand, Phillipines, Poland, Portugal, Russia, Taiwan, Thailand, Tasmania, Mexico, USA.

Turkey: Oran et al., 2006; Baba and Tamer, 2008a; Baba et al., 2013, 2015; Baba and Arslan, 2017b; Baba and Doğan, 2018; Baba et al., 2018; Zümre et al., 2019.

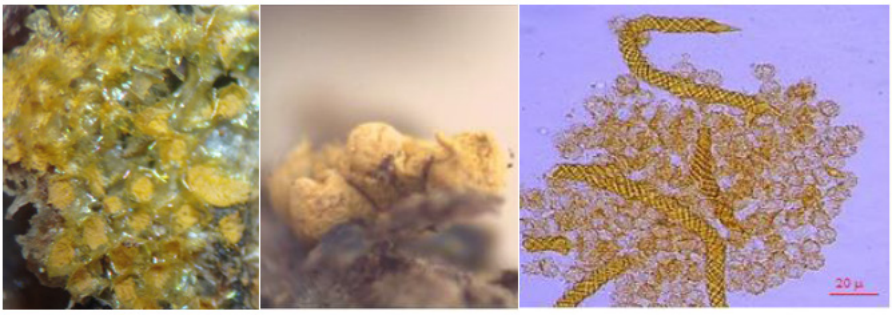

Figüre 5. O. verrucosum sporocarps, capillitium and spores

Morphological comparison of *Oligonema* species

Species	Sporocarp	Stalk	Peridium	Capillitium	Spore	Plasmodium
Oligonema affine	Obovoid to oblong, yellow, 0.8-1 mm	Sessile	Membranous shining, thin, irregular stripes	4-6 µm, 4-5 spiral bands	Banded-reticulate, pale yellow, 11-15 µm	White,
Oligonema favogineum	Taller than wide, yellow 2 mm	Sessile	Membranous, shining, thin, opening irregularly	6-8 µm, 4-5 spiral bands	With a coarse reticulation, pale yellow, 13-15 µm	White, yellow
Oligonema flavidum	Ovoid to cylindrical, subglobose, yellow, 0.4 - 1 mm	Sessile	Single, membranous, smooth to somewhat wrinkled	3-5 µm, longer, warts or faint spirals	Coarse-meshed, often irregular but usually complete reticulum, pale yellow, 13-15 (- 16) µm	Watery white, later yellow
Oligonema persimile	Subglobose, globose, obovoid, yellow, 0.5-0.8 mm	Sessile	Membranous, shining	4-6 µm marked with 4-5 spiral bands	Broken banded reticulation, non-reticulate areas covered with large warts, pale yellow 11-14 µm	White
Oligonema schweinitzii	Spherical, pyramidal to short-vermiculate plasmodiocarpic, yellow, 0.2 - 0.7 mm	Sessile	Single, membranous, smooth to plicate	2-6 µm clearly visible to almost invisible spirals	Marked with an incomplete reticulation, yellow, 12-16 µm	White or yellow
Oligonema verrucosum	Sporothecae pyriform or obovoid, often clustered on united stalks 1.6–4 mm	Stalkedlongitudinally grooved, 0.8–1.2 mm yellow, reddish brown	Membranous, translucent, dehiscence irregular	5–7 µm, cylindric elaters, 3-5 spiral bands	Reticulate, the bands narrow, bright yellow 10-14 µm	White

Conclusion

With this study 6 species of Oligonema genus recorded from Turkey. *Oligonema favogineum* and *O. verrucosum* has proven to be the most common species of this genus in Turkey, *Oligonema affine, O. persimile* and *O. schweinitzii* is less common and *O flavidum* is the rarest. *Oligonema aurantium O. dancoii, O. fulvum, O. intermedium* and *O. oedonema*, are not yet reported from Turkey.

References

Adamonyte G, (2007). Myxomycetes of the Genus Clastoderma in Lıthuanıa. Botanica Lithuanica, 13(1): 27–32.

Alexopoulos CJ, Mims CW, Blackwell M (1996). Introductory Mycology, 4.th Edition, John Wiley and Sons Inc., New York.

Baba H (2021). Five new Myxomycetes (Myxogastria) records from Turkey. Phytotaxa 507 (2): 131–143.

Baba H, Altaş B, Sevindik M (2021b). Myxomycetes Diversity of Batman Province and Hasankeyf District. KSÜ Tarım ve Doğa Derg 24 (2): 435-441.

Baba H, Arslan Ç (2017b). Myxomycetes of North Amanos Mountains (Hatay/Turkey). Biological Diversity and Conservation, 10: 88-95.

Baba H, Atay M (2019). Myxomycetes of Kumlu and Reyhanlı districts of Hatay/Turkey province. Biological Diversity and Conservation, ISSN 1308-8084 Online; ISSN 1308-5301 Print 12/2 41-50.

Baba H, Cennet E, Sevindik M (2019). Investıgatıon of Myxomycetes (Myxomycota) in Kırıkhan (Hatay Provınce). Commun. Fac. Sci. Univ. Ankara Series C Volume 29, Number 2, Pages 160-169.

Baba H, Doğan Y, (2018). Investigation of Myxomycetes (Myxomycota) in South Amanos Mountains (Hatay-Turkey). Celal Bayar Univ. J. Sci., 14: 277–284.

Baba H, Er A, Sevindik M (2020b). Myxomycetes diversity of Belen Region of Hatay province (Turkey). Kastamonu Univ., Journal of Forestry Faculty, 20(2): 86-96.

Baba H, Gelen M, Sevindik M (2018). Taxonomic investigation of myxomycetes in Altınözü, Turkey. Mycopath, 16(1): 23–31.

Baba H, Gündoğdu F, Sevindik M (2021a). Myxomycetes biodiversity in Gaziantep Province (Turkey) with four new records. Phytotaxa 478 (1): 105–118.

Baba H, Kolukırık M, Zümre M (2015). Differentiation of some myxomycetes species by ITS sequences. Turkish Journal of Botany, 39: 377-382. doi:10.3906/bot-1405-12.

Baba H, Sevindik M (2019). Mycetozoa of Turkey (Checklist). Mycopath 17(1):1-14.

Baba H, Sevindik M (2020a). Myxomycetes of Eşmişek Plateau (Kırıkhan-Hatay). KSÜ Tarım ve Doğa Derg KSU J. Agric Nat 23(4): 917-923.

Baba H, Sevindik M (2021). A New Myxomycetes record (Myxogastria) from Turkey: *Didymium listeri* Massee. KSU J. Agric Nat 24 (4): 820-823.

Baba H, Sevindik M (2022a). Myxomycetes diversity in Adana Province (Turkey) with two new records. Phytotaxa 547 (1): 031–042.

Baba H, Sevindik M (2022b). New Records of Myxogastria (Mycetozoa) from

the Eastern Mediterranean Region of Turkey. ISSN 1062-3590, Biology Bulletin, Vol. 49, No. 2, pp. 85–94.

Baba H, Sevindik M, Dogan M, Akgül H (2020a). Antıoxıdant, antımıcrobıal actıvıtıes and heavy metal contents of some Myxomycetes. Fresenius Environmental Bulletin Volume 29 – No. 09/2020 pages 7840-7846.

Baba H, Sevindik M, Er A, Atay M, Doğan Y, Altaş B, Akgül A (2021c). New four Mycetozoa records from South East Anatolia-Turkey. Fresenius Environmental Bulletin Volume 30 – No. 04 pages 3565-3574.

Baba H, Tamer AÜ (2008a). A study on the Myxomycetes in Manisa. The Herb Journal of Systematic Botany, 14(2): 179–196.

Baba H, Zumre M, Gelen M, (2016). An Investigation on North Adana (Turkey) Myxomycetes. Chiang Mai J. Sci., 43: 54-67.

Baba H, Zümre M, Gelen M (2013). Biodiversity of Kuseyr Plateau Myxomycetes (Hatay-Turkey). Journal of Selcuk University, Natural and Applied Science, Part 1: 669–683.

Baba, H., & Sevindik, M. (2018). The roles of myxomycetes in ecosystems. J Bacteriol Mycol Open Access, 6(3), 165-166.

Baysal R, Eroğlu G (2022). Diversity of myxomycete on Konya-Beyşehir highway route. Anatolian Journal of Botany 6(1): 55-61.

Cavalcanti LH, Costa AAA, Barbosa DI, Agra LANN, Bezerra ACC (2015). Distribution and occurrence of Oligonema (Trichiales, Myxomycetes) in Brazil. Braz. J. Bot (2015) 38(1):187–191. doi 10.1007/s40415-014-0107-9.

De Haan M, De Pauw S, Bogaerts A (2004). A study of the genus Oligonema (Myxomycota) in Belgium. Syst Geogr Plants 74:251–260.

Ergül CC, Akgül H (2011). Myxomycete diversity of Uludağ National Park, Turkey. Mycotaxon, 116: 479.

Ergül CC, Dülger B (2000d). Myxomycetes of Turkey. Karstenia, 40: 39–41.

Ergül CC, Dülger B (2002c). New records for the myxomycetes flora of Turkey. Turk. J. Bot., 26: 277–280.

Ergül CC, Dülger B, Akgül H (2005a). Myxomycetes of Mezit Stream valley of Turkey. Mycotaxon, 92: 239–242.

Eroğlu G (2021). *Cribraria lepida, Physarum dictyosporum, P. diderma,* and *P. spectabile* newly recorded from Turkey. ISSN (print) 0093-4666 (online) 2154-8889 Mycotaxon, Volume 136, pp. 853–863.

Eroğlu G, Kaşık G (2013a). Myxomycete of Hadim and Taşkent districts (Konya/Turkey) and their ecology. Biodivers. Conserv., 6: 120–127.

Farr ML (1976). Flora Neotropica. Monograph No. 16. New York Botanical Garden Press.

Farr ML (1981). True Slime Molds. Dubuque Iowa: Wm. C. Brown Comp.

Härkönen M (1988). Some additions to the knowledge of Turkish myxomycetes. Karstenia, 27: 1–7.

Harkönen M, Ukkola T (2000). Conclusions on myxomycetes compiled over twenty-five years from 4793 moist chamber cultures. Stapfia 73, zugleich Kataloge des OO. Landesmuseums, Neue Folge Nr. 155: 105-112.

https://doi.org/10.1111/j.1469-8137.1994.tb03937.x

Ing B (1994). The phytosociology of myxomycetes. New Phytologist 126: 175–201.

Ing B (1999). The Myxomycetes of Britain and Ireland. The Richmond Publishing Co.

Lado C (2005–2023). An on line nomenclatural information system of Eumycetozoa. Real Jardín Botánico, CSIC. Madrid, Spain. http://www.nomen.eumycetozoa.com. Last updated April 25, 2023.

Lado C, Pando F (1997). Flora Mycologica Iberica, Madrid, Spain: CSIC, vol. 2.

Li Y, Chen SL, Li HZ (1992). Myxomycetes from China VIII. The Genus Oligonema New to China with a New Spe- cies. Mycosystema 1992: 171-173.

Martin GW, Alexopoulos CJ (1969). The Myxomycetes. Iowa City, Univeristy of Iowa Press. Nannenga-Bremekamp NE (1974). De Nederlandse myxomyceten. Kon. Nederl. Natuurhist. Verenig.

Martin GW, Alexopoulos CJ (1969). The Myxomycetes. Univ. of Iowa Pres., Iowa City.

Martin GW, Alexopoulos CJ, Farr ML (1983). The Genera of Myxomycetes. Univ. of Iowa Pres., Iowa City.

Moreno G, Castillo A, Thüs H (2022). Critical revision of Trichiales (Myxomycetes) at the Natural History Museum London (BM). Phytotaxa 567 (1): 001–020. https://doi.org/10.11646/phytotaxa.567.1.1

Ndiritu GG, Winsetti KE, Spiegel FW, Stephenson SL (2009). A checklist of African myxomycetes. Mycotaxon 107:353–356.

Neubert H, Nowotny W, Baumann K (1993). Die Myxomyceten (Band I). Karlheinz Baumann Verlag Gomaringen.

Ocak İ (2015). Seasonal distribution of field-collected myxomycete in the Köroğlubeli Forest, Afyonkarahisar, Turkey. Ekoloji, 24: 48–56.

Ocak İ, Hasenekoğlu İ (2003b). Four new records of myxomycetes from Turkey. Turk. J. Bot., 27: 333–337.

Ocak İ, Hasenekoğlu İ (2005). Myxomycetes from Trabzon and Giresun Provinces (Turkey). Turk. J. Bot., 29: 11–21.

Ocak İ, Konuk M (2018). Diversity and ecology of Myxomycetes from Kütahya and Konya (Turkey) with four new records. Mycobiology, 46: 215-223.

Oran RB, Ergül CC, Dülger B (2006). Myxomycetes of Belgrad Forest (Istanbul).

Mycotaxon, 97: 183–187.

Salamaga A (2013). *Oligonema flavidum* (Myxomycetes): a species new to Poland. Pol Bot J 58:747–749.

Sesli E, Asan A, Selçuk F. (edlr.) Abacı Günyar Ö, Akata I, Akgül H, Aktaş S, Alkan S, Allı H, Aydoğdu H, Berikten D, Demirel K, Demirel R, Doğan HH, Erdoğdu M, Ergül CC, Eroğlu G, Giray G, Halikî Uztan A, Kabaktepe Ş, Kadaifçiler D, Kalyoncu F, Karaltı İ, Kaşık G, Kaya A, Keleş A, Kırbağ S, Kıvanç M, Ocak İ, Ökten S, Özkale E, Öztürk C, Sevindik M, Şen B, Şen İ, Türkekul İ, Ulukapı M, Uzun Ya, Uzun Yu, Yoltaş A. 2020. Türkiye Mantarları Listesi. Ali Nihat Gökyiğit Vakfı Yayını. İstanbul.

Sevindik, M., & Akgul, H. (2019). Fruiting bodies structures of myxomycetes. Journal of Bacteriology & Mycology, 7(6), 144-148.

Sevindik, M., Baba, H., Bal, C., Colak, O., & Akgul, H. (2018). Antioxidant, oxidant and antimicrobial capacities of Physarum album (Bull.) Chevall. JBMOA, 6(6), 317-320.

Stephenson SL, Rojas C (2017). Myxomycetes: Biology, Systematics, Biogeography and Ecology. London, Academic Press. p. 299-332.

Stephenson SL, Stempen H (1994). Myxomycetes: A Handbook of Slime Molds. Portland, USA: Tımber Press.

Thind KS (1977). The Myxomycetes of India, New Delhi: I.C.A.R.

Yağız D, Afyon A (2005). A study on the myxomycetes of Seydişehir (Konya) District. Afyon Kocatepe Üniversitesi Fen Bilimleri Dergisi, 5: 55–60 (In Turkish).

Zümre M, Baba H, Sevindik M (2019). Investigation of myxomycetes in Selcen Mountain (Turkey) and its close environs. Eurasian Journal of Forest Science. 7(3): 284-292.